Univerza v Ljubljani
Fakulteta za elektrotehniko

Janez Jamšek

Spektri višjih redov kardiovaskularnih signalov na osnovi transformacije z valčki

Doktorska disertacija

Mentorica: doc. dr. Aneta Stefanovska

Ljubljana, 2005

University of Ljubljana
Faculty of Electrical Engineering

Janez Jamšek

High-order Spectra of Cardiovascular Signals Based on Wavelet Transform

Dissertation

Ljubljana, 2005

University of Ljubljana
Faculty of Electrical Engineering

Janez Jamšek

High-Order Spectra of Cardiovascular Signals Based on Wavelet Transform

Dissertation

Mentor: doc. dr. Aneta Stefanovska

Ljubljana, 2005

To my parents

ACKNOWLEDGEMENTS

I would like to thank my mentor, doc. dr. Aneta Stefanovska, for showing me the way into the world of cardiovascular dynamics, and for all the invaluable expert knowledge, support, perfection convergence, science intuition, and not to mention, for all the Saturdays, Sundays, and holidays spent discussing cardiovascular matter.

This work would not be the same without the influence of Lancaster University, where professor Peter V.E. McClintok, hosted me in his Nonlinear Group. I am grateful to him for all of his Cambridge perfection that has influenced me. His supervision was, by all means, most pleasurable.

I have met many great scientists, but above all, I have met great people. Mitya D.G. Luchinsky showed me that science can be a real pleasure, and that social life must not be neglected, but rather accomplished in synchronization. "Start always from zero, rather than think twice about it, and there is always a way around it", is Mitya's inheritance. To Igor A. Khovanov, whom knowing was productive and problem-goal oriented. To Andriy Bandrivskyy, with whom we improvised a relaxation oscillatory kind of sport events after serious studying hours. Many thanks for all his help and valuable advice whenever needed, and to Stefano Beri, whom it was a pleasure to study and socialize.

To Alan Bernjak and Bojan Musizza, co-workers in the Group of Nonlinear Dynamics and Synergetic.

I'am grateful to Alenka Flander, for all her advices and help just when I needed it.

For all of their careful reading, I would like to thank Jožica Gračarin, Vesna Habinc, Bojan Ilich and Marko Mlakar.

At last, I am grateful to my parents, Bernardka and Miroslav Jamšek for all of their kind support and patience during my long studies.

SPEKTRI VIŠJIH REDOV KARDIOVASKULARNIH SIGNALOV NA OSNOVI TRANSFORMACIJE Z VALČKI

RAZŠIRJENI POVZETEK

Ritmi so med najbolj očitnimi lastnostmi živih sistemov. Pojavljajo se na vseh nivojih bioloških organizacij, od enoceličnih do večceličnih organizmov, s periodami od dela sekunde do leta. Tako srčna in dihalna funkcija kot circadianov ritem[1] v spanju in pri zavesti do ključnih periodičnih procesov za ohranjanje človeškega življenja. Kljub veliki navezavi s fiziologijo periodični pojavi niso omejeni le na žive sisteme. Primer so kemične reakcije, ki so jih prvi odkrili Bray leta 1921, Belousov in Zabotinski leta 1959 oziroma leta 1964 in drugi.

KARDIOVASKULARNI SISTEM

Kardiovaskularni sistem je eden od osnovnih sistemov človeškega organizma. Vsem celicam organizma neprestano dovaja energijo in snovi, ki so potrebne za njihovo normalno delovanje, hkrati pa iz celic odnaša snovi, ki nastanejo z metabolizmom. Sestavljata ga srce in ožilje (arterije, kapilare in vene). Pretok, ki je enak celotnemu volumnu krvi (t.j. 4 l – 6 l oziroma 7 % - 8 % telesne teže), sklene pot pri sproščenem, zdravem človeku po ožilju povprečno v eni minuti [55]. Tako dinamiko kardiovaskularnega sistema preučujemo na časovni osi okoli ene minute. Srce ima vlogo črpalke, ki poganja kri po sklenjenem krogu elastičnih žil. Pljuča lahko gledamo kot generator pritiska [55]. Krvni pretok, pritisk ter aktivnost pljuč in srca določajo dinamiko sistema krvnega obtoka. Raziskave so pokazale [8, 9, 10, 110-112, 117], da izmerjeni signali krvnega pretoka vsebujejo deterministično dinamiko, kar pomeni, da je sistem krvnega obtoka izid končnega števila podsistemov (avtonomnih oscilatorjev), med katerimi ima vsak svojo značilno frekvenco. Pri regulaciji krvnega pretoka in pritiska sodeluje pet podsistemov: srčni, respiratorni, miogeni, nevrogeni in metabolični sistem.

Vsi ti sistemi so tudi pri zdravih ljudeh v mirovanju med seboj rahlo sklopljeni, zato njihove značilne frekvence niso stalne, temveč se spreminjajo s časom, njihove amplitude pa so modulirane [6, 7, 110, 111]. Med posameznimi oscilatorji lahko nastanejo fazne sklopitve in sinhronizacija, ki se pokažejo v

[1] L. *circa* = okoli; *dies* = dan.

obliki povezav med njihovimi frekvencami in fazami [9, 79, 94, 97, 113, 114]. Fazna sklopitev je torej pojav določenih relacij med fazami medsebojno delujočih sistemov, medtem ko ni nujno, da med amplitudami obstaja korelacija.

Sklopitve omogočajo izmenjavo informacije med procesi in so tako temelj za pravilno delovanje sistema krvnega obtoka. Frekvenca in amplituda vsake opazovane oscilacije nam priča o aktivnosti oscilatorja in učinku vseh sklopitev. Dobro je raziskana frekvenčna modulacija srčnega ritma v ritmu dihanja, znana pod imenom respiratorna sinusna aritmija [18, 34]. Bivariatna analiza v časovnem prostoru, ki je bila pred kratkim razvita za analizo sinhronizacije ali posplošene sinhronizacije pri kaotičnih in šumnih oscilatorjih, je pokazala, da obstaja sinhronizacija srčnega in respiratornega oscilatorja [3, 23, 112, 117].

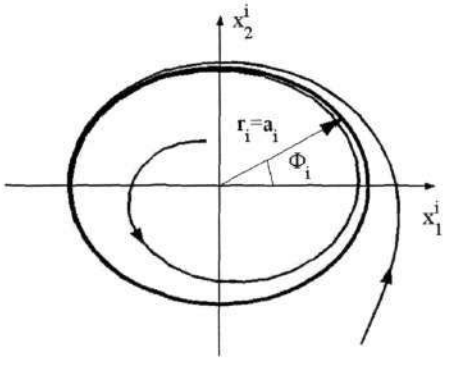

Slika 1: Rešitev enačbe (1) v faznem prostoru za osnovni oscilator. Stabilni limitni cikel je $r_i = a_i$ s fazo $\phi_i = 2\pi f_i t$, če je $\phi_i = 0$ pri $t = 0$.

Sklopitve med podsistemi sistema krvnega obtoka obstajajo, narava njihovega delovanja pa je še nepojasnjena. Model kardiovaskularnega sistema lahko tako predstavimo s sistemom enačb petih sklopljenih podsistemov, od katerih lahko vsak avtonomno oscilira [115, 116]. Osnovna enota je preprost oscilator z limitnim ciklom, ki ga je opisal Poincaré [128]

$$\frac{dx_1^i}{dt} = \alpha_i x_1^i (a_i - r_i) - 2\pi f_i x_2^i, \qquad (1)$$

$$\frac{dx_2^i}{dt} = \alpha_i x_2^i (a_i - r_i) + 2\pi f_i x_1^i,$$

kjer je $r_i = \sqrt{x_1^{i\,2} + x_2^{i\,2}}$. Oscilator vsebuje strukturno stabilnost in robustnost, ki ju določata fiziološko razumevanje in analiza izmerjenih signalov. Spremenljivki stanja x_1^i in x_2^i opisujeta pretok in hitrost

pretoka *i*-tega oscilatorja. Vsak oscilator je določen s frekvenco f_i in amplitudo a_i, konstanta α_i pa določa hitrost, s katero se vektor stanj približuje limitnemu ciklu, slika 1.

Ker podsistemov ne moremo obravnavati ločeno, je proučevanje njihove narave in lastnosti posameznih medsebojnih sklopitev oscilatorjev zelo težko. Zanima nas narava in pomen faznih zvez med posameznimi avtonomnimi oscilatorji, ki lahko v primeru nelinearne sklopitve povzročijo novo odvisno komponento pri modulirani frekvenci, ki je vsota osnovnih frekvenc sklopljenih oscilatorjev. Sklopitve so torej ključnega pomena za razumevanje kardiovaskularnega in morda tudi celotnega človeškega sistema.

Biološki signali so običajno pomešani s šumom. Za izločitev informacije o faznih, frekvenčnih in amplitudnih sklopitvah uporabljamo zapletene transformacije, ki poudarijo njihovo vsebino.

METODA

Bispektralna analiza spada v skupino tehnik, zasnovanih na statistiki višjih redov, ki se lahko uporabljajo za analiziranje neGaussovih signalov, za pridobivanje fazne informacije, zmanjševanje Gaussovega šuma neznanih spektralnih oblik ter odkrivanje in določevanje nelinearnosti signalov [60, 68, 69]. V sledečem besedilu razširjamo bispektralno analizo za določanje uporabnih lastnosti iz nestacionarnih podatkov in demonstriramo spremenjeno tehniko z uporabo na testnih signalih sklopljenih oscilatorjev.

Bispekter vsebuje statistiko tretjega reda. Ocenjevanje spektrov je osnovano na konvencionalnem Fourierevem tipu direktnega pristopa z izračunom momentov tretjega reda, ki so v primeru statistike tretjega reda enaki kumulantom tretjega reda [60, 66-69].

Klasično oceno bispektra dobimo kot povprečje ocenjenih momentov tretjega reda za vsak segment, na katere je razdeljen signal, in sicer zaradi zagotovitve statistične stabilnosti [67]. Moment tretjega reda je enak trojnemu produktu diskretne Fouriereve transformiranke pri diskretnih frekvencah k, l in $k+l$ [69]

$$B(k,l) = X(k)X(l)X^*(k+l). \tag{2}$$

Bispekter $B(k, l)$ je kompleksor, določata ga amplituda A in faza ϕ

$$B(k,l) = |B(k,l)|e^{j\angle B(k,l)} = Ae^{j\phi}. \quad (3)$$

Za vsako bifrekvenco (k, l) ga lahko predstavimo kot točko v kompleksnem prostoru $\Re[B(k, l)]$ proti $\Im[B(k, l)]$, kar določa vektor. Njegova amplituda (dolžina) je imenovana tudi biamplituda. Faza, ki se v primeru bispektra imenuje bifaza, je določena s kotom med vektorjem in pozitivno realno osjo. Algoritem za izračun ocene bispektra je podrobno opisan v [39].

Kot je podrobno obravnavano v [39], bispekter meri razmerje med osnovnimi oscilatornimi komponentami opazovanega signala. Še posebno bispekter določa razmerje med oscilacijami osnovnih dveh frekvenc k in l ter harmonični komponenti pri frekvenci $k + l$. Te tri frekvence tvorijo tako imenovano trojico (k, l, $k + l$). Za vsako trojico podaja bispekter $B(k, l)$ vrednost, ki vsebuje informacijo o fazi in jakosti sklopitve. Velika amplituda bispektra pri bifrekvenci (k, l) nakazuje vsaj frekvenčno sklopitev v trojici frekvenc k, l, in $k \pm l$. Močne sklopitve nakazujejo, da imata lahko oscilatorni komponenti pri k in l skupnega povzročitelja. Takšni komponenti lahko povzročita nastanek nove komponente pri sestavljeni frekvenci $k \pm l$, če je prisotna kvadratična nelinearnost.

Klasična bispektralna metoda je primerna za študijo stacionarnih signalov, katerih frekvenčna vsebina se časovno ohranja. Da bi vsebovali časovno odvisnost v bispektralni analizi, analogno kot v primeru kratkočasovne Fourierevе transformacije (KČFT), premikamo časovno okno $w(n)$ dolžine M preko signala $x(n)$ in računamo diskretno Fourierevo transformiranko za vsako pozicijo okna [81]

$$X(k,n) \cong \frac{1}{M}\sum_{n=0}^{M-1} x(n)w(n-\tau)e^{-j2\pi nk/M}, \quad (4)$$

kjer pomeni τ časovni premik. Izbira dolžine okna M je kompromis med doseganjem optimalne frekvenčne ločljivosti in detekcije časovne spremenljivosti. Trenutno bifazo izračunamo kot

$$\phi(k,l,n) = \phi_k(n) + \phi_l(n) - \phi_{k+l}(n). \quad (5)$$

Če sta dve frekvenčni komponenti k in l frekvenčno in fazno sklopljeni, $\phi_{k+l} = \phi_k + \phi_l$, potem velja, da je bifaza enaka 0 (2π) radianov. V našem primeru je fazna sklopitev manj stroga, ker so lahko odvisne frekvenčne komponente fazno zamaknjene. Za fazno sklopitev smatramo, če je bifaza konstantna (ni nujno enaka 0 radianom) za vsaj nekaj period nižje frekvenčne komponente bifrekvence. Istočasno opazujemo trenutno biamplitudo, ki lahko podaja relativno jakost sklopitve

$$A(k,l,n) = \left| X_k(n) X_l(n) X^*_{k+l}(n) \right|. \tag{6}$$

Na ta način želimo opazovati prisotnost in trajanje sklopitev med oscilatorji.

Zaradi simetrije močnostnega spektra pri frekvenci vzorčenja $f_s/2$ ima bispekter veliko simetrij v k, l področju [77, 78]. V primeru realnih signalov ima bispekter 12 simetričnih področij. Bispekter je potrebno izračunati le za neredundantno ali glavno področje. To je sestavljeno iz notranjega in zunanjega trikotnika, v katerih ima bispekter različne lastnosti [32, 33, 105]. V tej nalogi se bomo omejili na določanje bispektra v notranjem trikotniku.

Da lahko dobljene rezultate med seboj primerjamo, je potrebno izvesti normalizacijo. Bispekter normaliziramo z vrednostjo povprečnega bispektra preko celega področja notranjega trikotnika [25, 69]. Kritična vrednost za oceno bispektra in biamplitude je normalizirana na 1. Oceno jemljemo za veljavno, če je višja od povprečne vrednosti bispektra na področju notranjega trikotnika. Kritična vrednost je tista vrednost, ki presega efekt razlivanja (Fourierева transformacija), šumno ozadje (različno od Gaussa) in zaokrožitvene napake.

ANALIZA SKLOPITEV

Ilustracijo in preskus bispektralne metode ponazorimo na primeru generičnega modela medsebojnega vplivanja sistemov, katerih osnovna enota je Poincaré oscilator [128]:

$$\begin{aligned} \dot{x}_i &= -x_i q_i - \omega_i y_i + g_{x_i}, \\ \dot{y}_i &= -y_i q_i + \omega_i x_i + g_{y_i}, \\ q_i &= \alpha_i (\sqrt{x_i^2 + y_i^2} - a_i). \end{aligned} \tag{7}$$

Kjer sta x in y vektorja spremenljivk stanj oscilatorja, so α_i, a_i ter ω_i konstante, $g_x(x)$ in $g_y(y)$ pa vektorja sklopitve. Aktivnost posameznega sistema opišemo z dvema spremenljivkama stanja x_i in y_i, kjer $i = 1,..., N$ določa podsistem.

Različne načine medsebojnega vpliva med podsistemi, kot so linearna, kvadratična sklopitev in parametrična frekvenčna modulacija, proučujemo s signali, dobljenimi s predlaganim modelom. Za bolj realistične razmere proučujemo signale z ali brez dodanega osrediščenega belega Gaussovega

šuma. V vseh primerih analiziramo spremenljivko x_1 prvega oscilatorja. Najprej izračunamo klasični bispekter. Bifrekvence, kjer se pojavijo vrhovi zaradi možnih frekvenčnih interakcij, proučujemo naprej z izračunom biamplitude in bifaze v odvisnosti od časa.

Linearna sklopitev. V primeru linearne sklopitve med dvema oscilatorjema (i = 1, 2) je termin sklopitve v modelu (7) enostranski in linearen

$$g_{x_1} = \eta_2 x_2, g_{y_1} = \eta_2 y_2. \tag{8}$$

V glavnem področju bispektra se nahaja le vrh pri samosklopitveni bifrekvenci prvega oscilatorja s frekvenco f_1. Bispektralna analiza namreč ugotavlja razmerje med osnovnima frekvenčnima komponentama oscilatorjev f_1 in f_2 ter modulacijsko komponento pri frekvenci $f_1 \pm f_2$, ki pa ni prisotna v močnostnem spektru signala. Metoda kot takšna je nezmožna ugotoviti prisotnost linearne sklopitve med oscilatorjema. Bispektralna analiza je prvenstveno namenjena za ugotavljanje nelinearne kvadratične sklopite in frekvenčne modulacije, ker imata obe za posledico frekvenčne komponente pri vsoti in razliki karakterističnih frekvenc vzajemno delujočih oscilatorjev. Da lahko ugotovimo linearno sklopitev z bispektralno metodo, je potrebno metodo prilagoditi v smislu spremembe frekvenčnega razmerja

$$B_a(k,l) = E\left[X(k)X(l)X^*(2k-l)\right], \tag{9}$$

prav tako se ustrezno spremeni fazno razmerje

$$\phi_a(k,l) = \phi_k + \phi_l - \phi_{2k-l} - \phi_c. \tag{10}$$

Prilagojeni bispekter $|B_a|$ signala pokaže vrh, ki se nahaja na bifrekvenci (f_1, f_2). Ta je naše primarno zanimanje. Vrh namiguje, da gre vsaj za linearno frekvenčno sklopitev med frekvencama f_1 in f_2, kar je zadosten razlog za nastop vrha. Fazno sklopitev ugotovimo šele z izračunom bifaze, ki je konstantna v času trajanja linearne sklopitve.

Kvadratična sklopitev. Predpostavimo, da sta dva Poincaré oscilatorja sklopljena nelinearno; sklopitveni člen v modelu (7) ustrezno spremenimo

$$g_{x_1} = \eta_2 (x_1 - x_2)^2, g_{y_1} = \eta_2 (y_1 - y_2)^2. \tag{11}$$

Tako dobljeni signal je prikazan na sliki 2 (a). Kvadratična nelinearna sklopitev povzroči nastop višjih harmonskih komponent poleg karakterističnih frekvenc [69], kot je prikazano na sliki 2 (b). Bispekter, slika 2 (c) in (d), prikazuje značilen razpored vrhov. Ko je kvadratična sklopitev prisotna, je biamplituda različna od nič in bifaza konstantna, slika 2 (e). Močnejša ko je sklopitev, višja je biamplituda, slika 2 (f). Rezultati so enaki kot v primeru brez šuma, iz česar lahko sklepamo, da je metoda robustna na šum.

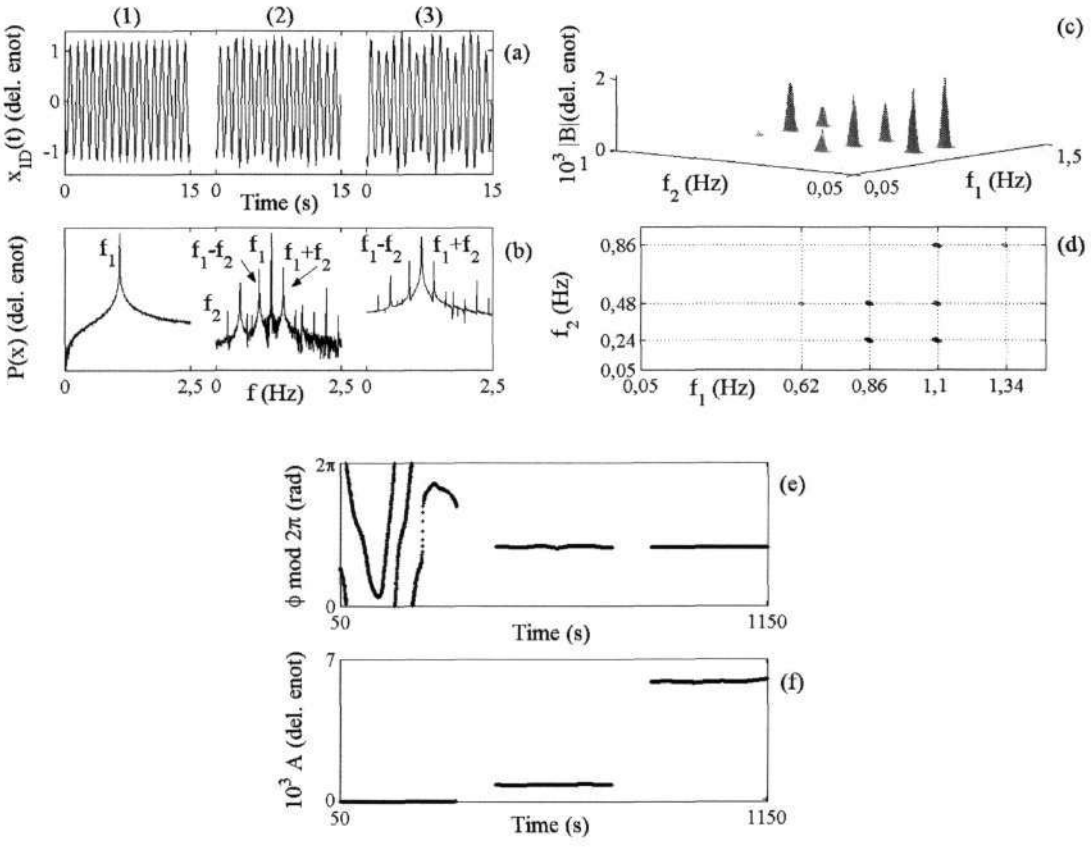

Slika 2: Rezultati v primeru kvadratične sklopitve z dodanim šumom. (a) Testni signal x_{1D}, spremenljivka x_1 prvega oscilatorja s karakteristično frekvenco f_1 = 1,1 Hz. Karakteristična frekvenca drugega oscilatorja je f_2 = 0,24 Hz. Oscilatorja sta sklopljena enosmerno kvadratično s tremi različnimi stopnjami jakosti sklopitve: η_2 = 0,0 (1); 0,05 (2); in 0,1 (3). Vsaka sklopitev traja 400 s in je vzorčena z vzorčno frekvenco f_s = 10 Hz. Za vsak primer je prikazan signal za prvih 15 s. (b) Močnostni spekter. (c) Bispekter $|B|$ izračunan iz K = 33 segmentov, s 66 % prekrivanjem in z uporabo Blackmanovega okna za zmanjšanje razlivanja in (d) njegov nivojni prikaz. Del bispektra nad f_2 > 1,0 Hz je odrezan, ker trojica (1,1 Hz, 1,1 Hz, 1,1 Hz) povzroči visok vrh, ki je fizično nepomemben. (e) Bifaza ϕ in (f) biamplituda A za bifrekvenco (1,1 Hz, 0,24 Hz) z 0,3 s časovnim korakom in 100 s dolgim oknom za oceno diskretne Fourierove transformiranke in uporabo okna Blackman.

Frekvenčna modulacija. Z bispektrom želimo ugotoviti tudi parametrično frekvenčno modulacijo in jo razlikovati od kvadratične. Parametrična modulacija povzroči nastanek frekvenčnih komponent pri vsoti in razliki karakteristične frekvence prvega oscilatorja in frekvence modulacije drugega

oscilatorja. Obe komponenti bi bili lahko tudi posledica nelinearne kvadratične sklopitve. Enačbo prvega oscilatorja modela (7) ustrezno spremenimo

$$\begin{aligned} \dot{x}_1 &= -x_1 q_1 - y_1(\omega_1 + \eta_m x_2) + \xi(t), \\ \dot{y}_1 &= -y_1 q_1 + x_1(\omega_1 + \eta_m y_2), \\ q_1 &= \alpha_1(\sqrt{x_1^2 + y_1^2} - a_1). \end{aligned} \tag{12}$$

Bispekter se razlikuje od tistega v primeru kvadratične sklopitve. Pri bifrekvenci (f_1, f_2) dobimo vrh, čeprav komponente drugega oscilatorja f_2 (ena komponenta trojice) ni prisotne v močnostnem spektru signala, je vrednost različna od nič zaradi šuma. Bifaza ne kaže razdobja konstantne bifaze. V primeru močnejše modulacije je ta manj spremenljiva in ni pogostih faznih 2π skokov, kar je samo dodatna indikacija, da gre za primer modulacije.

SRČNO-RESPIRATORNA SKLOPITEV

V raziskavi je sodelovalo šest moških starih od 25 - 27 let, brez evidence o srčni bolezni. Pred začetkom meritve je vsak ležal sproščeno 15 minut. En nabor meritev je bil izmerjen v normalnem sproščenem stanju pri spontanem dihanju ter nadaljnja dva do trije nabori meritev pri različnem enakomernem dihanju (počasnejšem/hitrejšem od spontanega). Meritve so trajale 20 minut pri spontanem in 12 minut pri enakomernem dihanju. Merili smo krvni pretok na štirih različnih mestih s podobnimi lastnostmi krvožilnega sistema: na obeh rokah (levo in desno zapestje) in obeh nogah (levem in desnem gležnju) z vzorčno frekvenco 40 Hz. Istočasno smo merili tudi električno aktivnost srca (EKG) in dihanja z vzorčno frekvenco 400 Hz. Pri vsaki meritvi je tako nastala podatkovna datoteka, ki je vsebuje 7 signalov. Tehnika zajema podatkov je opisana v [112]. Vse skupaj je bilo zajetih 22 podatkovnih datotek.

Signale krvnega pretoka smo predhodno obdelali. Odstranili smo zelo nizke in zelo visoke frekvence z uporabo oken z drsečim povprečjem; dolžine 200 s za trend in 0,2 s za visoke frekvence, hkrati pa smo jih prevzorčili na 10 Hz. Tako smo se izognili problemom prekrivanja [81]. Signale smo normalizirali med nič in ena in jim odstranili srednjo vrednost. Določili smo karakteristično srčno f_1 in dihalno f_2 frekvenco ter komponente pri njunih harmoničnih pozicijah. Slika 3 levo prikazuje časovni potek tako obdelanih signalov za primer enakomernega dihanja, počasnejšega kot v primeru spontanega dihanja, in desno detekcijo frekvenčnih komponent v močnostnem spektru.

Sledil je izračun normaliziranega bispektra kot povprečje preko več segmentov, ki smo jim vsakokrat odšteli povprečno vrednost signala. Za ugotavljanje nelinearne kvadratične sklopitve smo za vsak signal obdelali 8 vrhov, kot so našteti v preglednici 1.

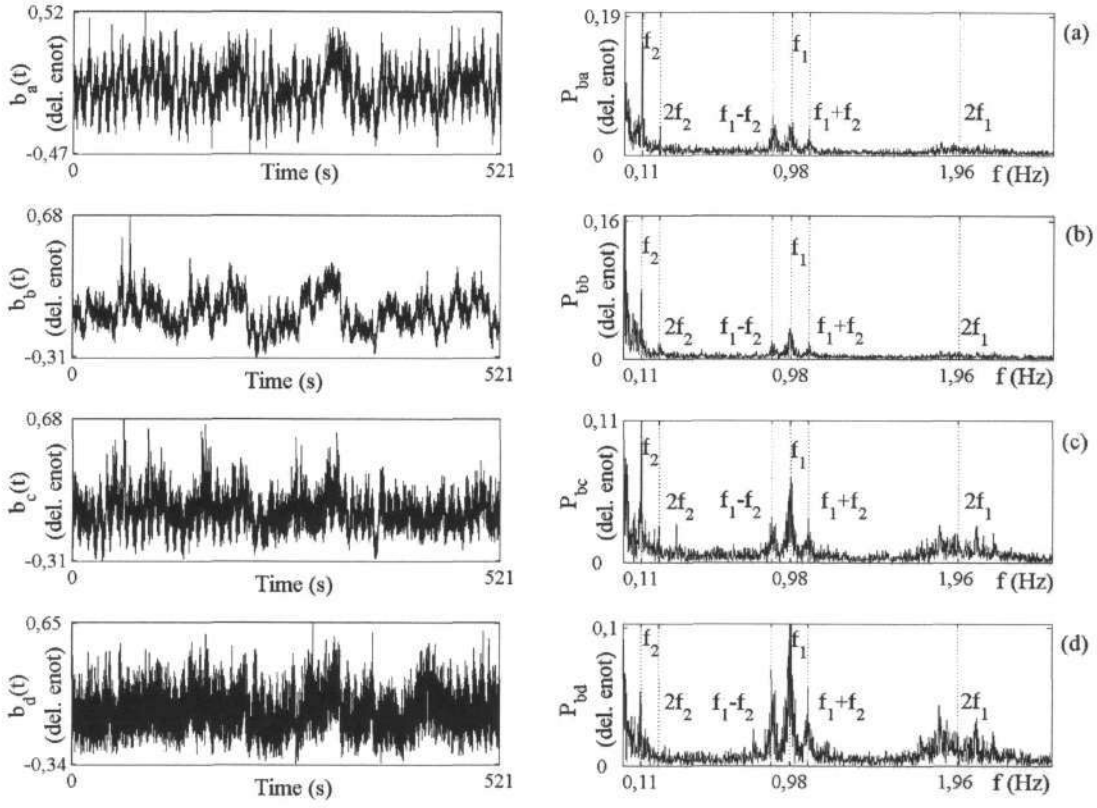

Slika 3: Signal krvnega pretoka $b(t)$, merjen istočasno na štirih različnih mestih. Vsakemu je odstranjen trend in visoke frekvence ter je prevzorčen, normaliziran in osrediščen. Signali so dolgi 521 s in prevzorčeni na vzorčno frekvenco $f_s = 10$ Hz. (a) Signal, izmerjen na desnem zapestju $b_a(t)$ in njegov močnostni spekter; (b) levo zapestje $b_b(t)$ in njegov močnostni spekter; (c) desni gleženj $b_c(t)$ in njegov močnostni spekter; (d) levi gleženj $b_d(t)$ in njegov močnostni spekter.

Za vsak vrh smo izračunali bifazo in biamplitudo. Frekvenčno ločljivost smo nastavili tako, da je bila vsaj 1/10 najnižje dihalne frekvence. Uporabili smo okno, dolgo 100 s za izračun bispektra, biamplitude in bifaze. Uporabljeno okno določa tudi časovno ločljivost. Za izključitev ugotovitve naključnih sklopitev smo se osredotočili na tiste, ki so trajale vsaj 10 period počasnejše - dihalne frekvence, to je približno 100 s ali krajše. Ker je hkratna frekvenčna in časovna ločljivost izključujoča po Heisenbergovem principu nedoločenosti [43], je izbor možnosti omejen in potreben je kompromis. Okno smo premikali vzdolž časovne vrste s korakom 0,1 s = $(1/f_s)$. Kritično vrednost za oceno biamplitude smo postavili v vseh primerih na 2, to je dvakrat več kot je povprečna vrednost bispektra v tako imenovanem notranjem trikotniku bifrekvenčne domene.

Da bi lahko sklepali na kvadratično sklopitev, smo določili potrebne pogoje: (i) Konstantna bifaza vsaj 10 period počasnejše sklopitvene komponente; (ii) Istočasno prisoten plato bifaze za vseh šest (osem) vrhov; (iii) V času sklopitve ni nobenih faznih skokov in bifazne spremembe so znotraj intervala π radianov (šum); (iv) Biamplituda mora biti nad določeno kritično vrednostjo.

Preglednica 1: Vrhovi in pripadajoče bifrekvence v bispektru kot posledica nelinearne kvadratične sklopitve med dvema oscilatorjema s karakterističnima frekvencama f_1 in f_2.

Vrh	Bifrekvenca
1	(f_1, f_2)
2	$(f_1\text{-}f_2, f_2)$
3	$(f_1\text{-}f_2, 2f_2)$
4	$((f_1, 2f_2)$
5	$(f_1, f_1\text{-}f_2)$
6	$(f_1\text{+}f_2, f_1\text{-}f_2)$
7	(f_2, f_2)
8	(f_1, f_1)

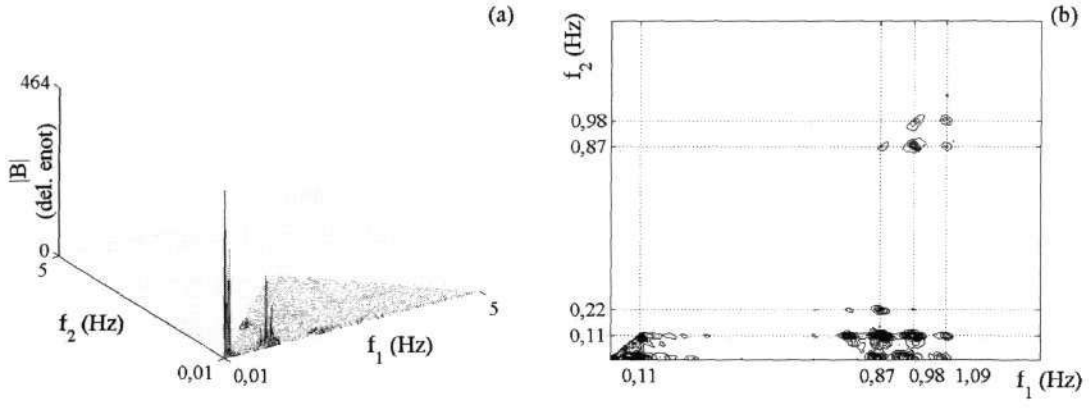

Slika 4: (a) Bispekter $|B|$ signala b_a, izračunan iz K = 33 segmentov, 87 % prekrivanjem in Blackmanovim oknom za zmanjševanje razlivanja. (b) Nivojni prikaz dela bispektra $f_1, f_2 < 1{,}4$ Hz, ki nas zanima.

Primer tipičnega bispektra za celotno frekvenčno področje prikazuje slika 4 (a). Razvidnih je več vrhov. Področje našega interesa je srčno-respiratorna sklopitev, področje okoli bifrekvence (f_1, f_2), ki je podrobnejše prikazano na sliki 4 (b). Pri nižjih frekvencah so razvidne sklopitve, ki so lahko posledica sklopitev med miogenim in nevrogenim oscilatorjem. Teh v tem delu ne obravnavamo. Natančna analiza pokaže, da se v bispektru nahajajo vsi vrhovi, našteti v preglednici 1. Izračun bifaz in biamplitud za vse vrhove pa razkrije, da so v določenem časovnem intervalu T_{qc} izpolnjeni vsi pogoji za nelinearno kvadratično sklopitev. Primer vrhov, biamplitud in bifaz za vrhova ena in dva

prikazuje slika 5. Povzetek analize vseh signalov, v katerih je bila ugotovljena nelinearna sklopitev, pa je podan v preglednici 2. Čeprav so bili signali izmerjeni na šestih osebah, so v preglednici 2 podatki samo za pet oseb. Tudi pri šesti osebi smo ugotovili nelinearne sklopitve, vendar niso izpolnjevale zahtevanega časa trajanja. Samo za en primer spontanega dihanja so bili izpolnjeni vsi pogoji za nastop nelinearne sklopitve. Pri spontanem dihanju so epizode sklopitev kratke in fazni preskoki pogostejši.

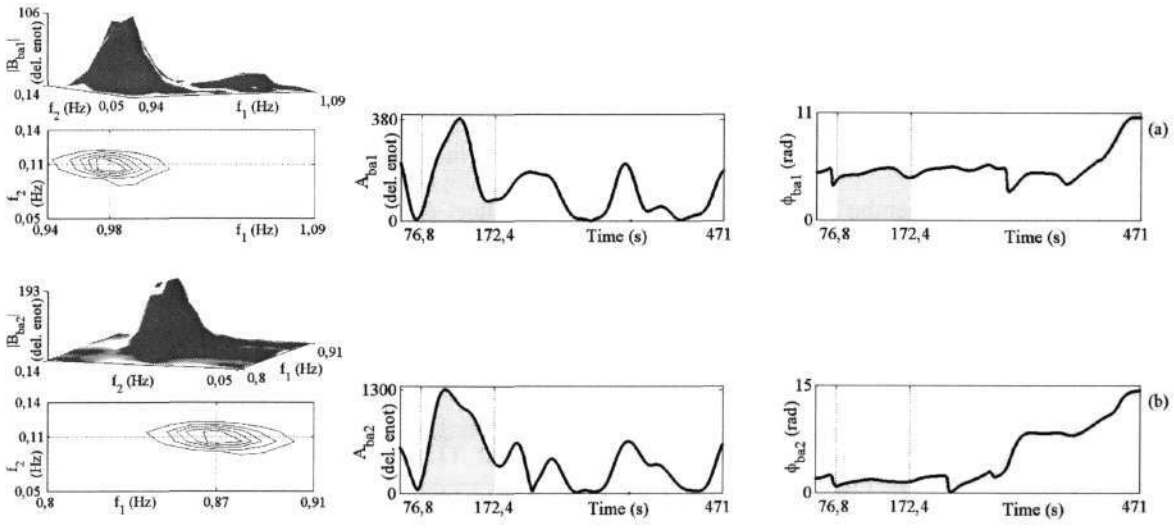

Slika 5: Analiza krvnega pretok signala $b_a(t)$, izračunanega iz $K = 33$ segmentov, 87 % prekrivanjem, z 0,1 s časovnim korakom in 100 s dolgim oknom za izračun diskretne Fourierjeve transformiranke z uporabo Blackmanovega okna za zmanjševanje razlivanja za vrhova (a) 1 in (b) 2; levi stolpec, bispekter $|B_{ba}|$ s pripadajočim nivojnim prikazom; sredinski, biamplituda A_{ba}; in desni, bifaza ϕ_{ba}.

Vprašanje, ali kardiovaskularni sistem vsebuje deterministično dinamiko, je bilo že predmet številnih raziskav [6, 8, 109, 110, 112]. Številni rezultati potrjujejo, da je sistem, ki regulira krvni pretok, deterministično. Ali so rezultati bispektralne analize posledica deterministične ali stohatične komponente v signalih krvnega pretoka, preverimo z uporabo surogatov [102, 106]. V ta namen uporabimo metodo surogatov naključne faze [44, 102, 106, 123, 124]. Tako dobljeni signali imajo podobne spektralne lastnosti kot originalni signali krvnega pretoka, to je enako povprečno vrednost, enako varianco, enako avtokorelacijsko funkcijo in posledično enak močnostni spekter s to razliko, da ni faznih povezav, oziroma so rezultat linearnega Gaussovega procesa. Z bispektralno analizo ne ugotovimo nelinearnih sklopitev v surogatih signalov krvnih pretokov. Zaključimo lahko, da so fazne informacije vsebovane v kardiovaskularnem signalu krvnega pretoka deterministične narave.

Aktivnost srca se izraža v vsaki krvni žili in je prisotna tudi v mikrocirkulaciji kapilarnega omrežja. Periferni krvni pretok regulirata zunanji (centralni) in notranji (lokalni) mehanizem in mora tako

odražati aktivnost obeh [6, 7, 9, 108, 110]. Signali krvnega pretoka odražajo centralne in lokalne mehanizme regulacije v kardiovaskularnem sistemu. Signali, zajeti na različnih, med seboj precej oddaljenih mestih, so lahko zelo podobni. Čeprav odražajo pretok v kapilarni mreži, vsi vsebujejo informacijo o prostorsko invariantni periodični aktivnosti centralno generiranih srčnih in dihalnih signalov. Jakost periodičnih komponent v perifernem krvnem pretoku se spreminja s premerom žil in gostote omrežja, to je z lokalno upornostjo pretoka.

Preglednica 2: Nelinearna kvadratična sklopitev zaznana v signalih krvnega pretoka. Za vsako meritev so bili istočasno izmerjeni krvni pretoki na štirih različnih mestih, kanali a-d. T_{qc} je interval, v katerem z bispektralno analizo ugotovimo, da sta srčni oscilator f_{hr} in respiratorni oscilator f_{res} lahko nelinearno sklopljena. Produkt $T_{qc} \times f_{res}$ določa trajanje sklopitve. Za časa T_{qc} smo izračunali najvišjo biamplitudo za vrh 1, ki je našega osnovnega zanimanja, največjo spremembo bifaze $\Delta\phi$, njeno povprečno vrednost $\overline{\phi}$ in standardno deviacijo σ_ϕ.

Oseba	Dihanje	Kanal	f_{hr} (Hz)	f_{res} (Hz)	T_{qc} (s)	$T_{qc} \times f_{res}$	A_{1max} (arb. units)	$\Delta\phi$ (rad)	$\overline{\phi}$ (rad)	σ_ϕ (rad)
1	enakomerno	a	1,08	0,11	105,7	11,6	190	1,11	8,92	0,20
1	enakomerno	d	1,00	0,23	56,8	13,1	62	0,92	10,93	0,29
1	enakomerno	b	0,97	0,34	18,9	6,4	50	0,84	0,47	0,28
2	spontano	a	1,16	0,14	82,0	11,5	352	1,87	32,68	0,47
2	enakomerno	c	1,05	0,10	89,5	9,0	122	1,48	4,05	0,34
2	enakomerno	a	0,98	0,11	95,6	10,5	383	1,47	3,22	0,42
3	enakomerno	d	1,08	0,13	56,5	7,3	334	1,29	2,21	0,48
3	enakomerno	c	1,10	0,26	52,4	13,6	52	0,46	4,96	0,10
4	enakomerno	d	1,01	0,10	105,6	10,6	407	2,47	0,58	0,18
4	enakomerno	d	0,99	0,11	95,6	10,5	219	2,19	-6,51	0,76
5	enakomerno	d	1,20	0,10	57,5	5,8	1009	2,05	5,88	0,67

Čeprav so bili izmerjeni signali krvnega pretoka zajeti na različnih, med seboj oddaljenih mestih (kanal a-d), vsi odražajo enake karakteristične srčne in respiratorne frekvence. Z bispektralno analizo signalov krvnega pretoka smo za vsako meritev dobili enake rezultate za vse signale, istočasno izmerjene na različnih mestih (kanal a-d) in tako potrdili, da se informacija o faznem razmerju ohranja, kar je v skladu s predhodnimi raziskavami.

Bispekter, definiran kot (2), je poseben primer križnega spektra, ko so vsi trije signali enaki. Imenujemo ga tudi avto bispekter. Poleg signalov krvnega pretoka smo istočasno merili tudi signal EKG, signal dihanja in signal krvnega pritiska. Z uporabo križnega bispektra preverimo srčno-respiratorno sklopitev z uporabo bivariatnih podatkov. Križni bispekter definiramo kot [69]

$$B_{XYY}(k,l) = X(k)Y(l)Y^*(k+l), \tag{13}$$

kjer sta X in Y diskretni Fourierevi transformiranki dveh različnih signalov $x(t)$ in $y(t)$ pri diskretnih frekvencah k, l in $k+l$. Izračunali smo križne spektre B_{cebb} (kjer c pomeni križni, e signal $e(t)$ in b signal $b(t)$), za primer, ko je $x(t)$ signal EKG $e(t)$ in $y(t)$ signal krvnega pretoka $b_a(t)$. Signal EKG nam primarno govori o srčni električni aktivnosti. Fazo prve, srčne komponente f_1, v trojici (f_1, f_2, $f_1 + f_2$) dobimo tako neposredno iz EKG signala, dihalno komponento f_2 in komponento pri harmonski poziciji $f_1 + f_2$ pa iz signala krvnega pretoka. Na podoben način kot (13) definiramo še križni bispekter $B_{\text{XYX}}(k, l)$ in ga izračunamo za dva različna primera: (i) B_{cbrb}, kjer je $x(t)$ signal krvnega pretoka $b_a(t)$ in $y(t)$ signal dihanja $r(t)$. Signal $r(t)$ najbolj direktno opisuje aktivnost respiratornega oscilatorja (ii) B_{cprp}, kjer je $x(t)$ signal krvnega pritiska $p(t)$ in $y(t)$ signal dihanja $r(t)$.

Z izračunom križnih bispektrov ugotovimo, da je informacija o sklopitvi med srčnim in respiratornim oscilatorjem neodvisna od signala, oziroma da je prisotna tudi v drugih kardiovaskularnih signalih. Križne spektre smo izračunali tudi za primer surogatov signalov $e(t)$, $r(t)$ in $p(t)$ z naključno fazo. V tem primeru nismo ugotovili faznih sklopitev.

Nelinearna sklopitev ali linearna sklopitev močno nelinearnih oscilatorjev. Naša študija je zasnovana na predpostavki, da sta srčni in respiratorni proces opisana kot šibki nelinearni oscilator in da so sklopitve med njima šibke [116]. Prikladno se je vprašati, kaj se zgodi, če predpostavke niso izpolnjene. Odgovor na to vprašanje smo poiskali na dva različna načina, z analitično aproksimacijo in digitalno simulacijo.

V analizi v prilogi B obravnavamo generiranje harmonikov paroma sklopljenih šibko nelinearnih oscilatorjev. Ta potrjuje, da pri šibki sklopitvi nastopijo dodatne harmonične komponente pri $2\omega_2$, $2\omega_1$, $\omega_1 \pm \omega_2$, $2\omega_1 \pm 2\omega_2$, $3\omega_1 \pm \omega_2$, ki jih lahko povežemo s kvadratično sklopitvijo. Če gre za zadosti nelinearen oscilator in zadosti močno sklopitev, se lahko v principu pojavijo te in ostale kombinatorne frekvence kot posledica efekta drugega reda tudi v primeru linearne sklopitve. Vendar pa nastop teh kombinatornih frekvenc sam po sebi ni zadosten za izpolnitev pogojev za nastop nelinearne sklopitve v bispektru. Za to pri šibko do srednje močnih sklopitvah lahko vedno zanesljivo določimo, da gre za nelinearno sklopitev. Ko so nelinearnosti posebno močne ne moremo vedno pričakovati, da bo bispektralni pristop razkril zanesljivo informacijo o naravi sklopitve.

Analiza je dopolnjena z digitalno simulacijo, s katero ugotavljamo področje ekstremnih pogojev, kjer pričakujemo, da bo bispektralni pristop neuspešen. Za generičen model izberemo van der Polov oscilator z dodatno nelinearnostjo, vsiljen z drugim relaksacijskim van der Polovim oscilatorjem v

smislu aditivne sklopitve z dodanim Gaussovim šumom. Analiziramo podroben nabor parametrov za primera: (i) ko sta dva oscilatorja močno nelinearna, vendar linearno sklopljena; in (ii) ko sta nelinearna in nelinearno sklopljena. V najbolj ekstremnem primeru zelo močne linearne sklopitve in zelo močne dodane nelinearnosti ne moremo več razlikovati med močno nelinearnostjo oscilatorjev in močno nelinearno sklopitvijo. V tem primeru bispektralna metoda odpove.

Kljub temu pa je več argumentov, ki podpirajo domnevo, da sta srčni in dihalni podsistem šibka nelinearna oscilatorja, ki sta šibko sklopljena. (i) Pri spontanem dihanju zdravih ljudi se pojavljajo le *občasne* in *kratke* epizode sinhronizacije [10, 99-101], kar nakazuje na relativno šibke sklopitve. (ii) Sinusna respiratorna aritmija je šibka pri spontanem dihanju in le malo močnejša pri zelo nizkih dihalnih frekvencah [23], kar ponovno podpira šibko sklopljen opis. (iii) Sklopitve lahko včasih popolnoma izginejo, kot je to pri komi [112]. Brez sklopitev se dinamika drastično poenostavi s popolno odsotnostjo sinhronizacije in modulacije. Dejstvo, da kljub majhni amplitudni spremenljivosti zaradi notranjega šuma ni opažene nobene spremembe naravnih frekvenc, nakazuje, da so sami oscilatorji kvečjemu šibko nelinearni. (iv) Če bi bili oscilatorji močno nelinearni in močne sklopitve (linearne), bi opazili veliko kombinatornih komponent okoli srčne frekvence.

Analizirano pretirano močno sklopitveno področje je tako irelevantno za srčno-respiratorno sklopitev, ki jo ugotavljamo v tem delu.

Razmerje do sinhronizacije. Dejstvo da lahko notranje sklopitve med oscilatorjema privedejo do sinhronizacije kot tudi do modulacije, je imelo za posledico veliko študij faznega razmerja med srčnim in respiratornim oscilatorjem [10, 24, 42, 46, 52, 71, 92, 95, 97, 100, 101, 113, 114, 118]. Prav možnost sinhronizacije nas je motivirala, da smo razvili nova orodja za nadaljnje raziskovanje sklopitev med sistemi: smer, jakost in še posebej naravo sklopitev. Informacijo o sklopitvah lahko dobimo s pomočjo bivariatnih podatkov (signal dihanja in EKG signal), z uporabo nedavno razvitih metod za analizo sinhronizacije, ali s posplošeno sinhronizacijo med kaotičnimi in/ali šumnimi sistemi (glej [72] in reference, ki so tam navedene). Tu nas zanima, ali se sinhronizacija pojavi ali ne, v pogojih, ko jasno zaznamo sklopitev. Z uporabo sinhrograma ugotovimo obstoj frekvenčne modulacije, ne pa sinhronizacije v primeru enakomernega nizkofrekvenčnega dihanja. Bispektralna analiza podaja drugačno informacijo kot jo dobimo iz sinhrograma. Razmerje do sinhronizacije v širšem smislu podrobneje podajamo v naslednjem poglavju.

Vsiljen oscilator. Z uporabo novih razvitih tehnik za analizo smeri sklopitve [72, 93, 94, 103] je bilo pokazano [73, 117], da sta srčni in respiratorni sistem *sklopljena obojesmerno*. Vendar pa je vpliv dihanja prevladujoč (vodilni sistem) pri vseh dihalnih frekvencah, spontanih ali enakomernih [73,

117]. Sklopitev med srčnim in respiratornim oscilatorjem lahko tako vidimo kot enosmerno: respiratorni sistem vodi srčnega. Poseben primer je enakomerno dihanje. Čeprav je med enakomernim dihanjem dihalna frekvenca konstantna, se primer razlikuje od primera vsiljenega oscilatorja (kjer je srčni oscilator vsiljen in respiratorni vodilo). Primer ponazorimo z generičnim modelom skoraj periodičnega Poincaré oscilatorja, vsiljenega s periodično šibko zunanjo silo. Srčno-respiratorna sklopitev je bolj kompleksna kot vzeti primer, ki ne more povzročiti frekvenčnih komponent, ki jih opazimo pri srčno-respiratorni sklopitvi. Eksperiment enakomernega dihanja lahko razumemo kot sistem dveh sklopljenih oscilatorjev, čeprav je frekvenca enega vsiljena in konstantna (respiratorni sistem) sklopitev med obema spontana.

RAZMERJE MED BISPEKTRI IN SINHRONIZACIJO

Sinhronizacija je osnovni pojav v fiziki, ki ga je v začetku moderne dobe znanosti prvič odkril Huygens [37]. V klasičnem smislu pomeni sinhronizacija nastavitev frekvenc oscilatorjev zaradi šibkih medsebojnih vplivov [2, 4, 30]. Ne obstaja enotna definicija za sinhronizacijo. Najbolj osnovni sta frekvenčna in fazna sinhronizacija. Ti dve definiciji sta bili generalizirani na pojav sinhronizacije dveh ali več oscilatorjev, ki so periodični, šumi ali kaotičnih oscilatorji [79, 90, 91, 96]. V najbolj enostavnem primeru dveh periodičnih oscilatorjev je fazna sinhronizacija definirana kot sklopitev faz [79]

$$|n\phi_1 - m\phi_2 - \delta| < const., \tag{14}$$

kjer sta n in m celi števili, ki opisujeta sklopitveno razmerje, ϕ_1 in ϕ_2 fazi oscilatorjev in δ nek začetni fazni premik. Enačba (14) v ožjem smislu velja samo za kvaziperiodične oscilatorje. Za periodične oscilatorje je pogoj za fazno sklopitev ekvivalenten pogoju za frekvenčno sklopitev $nf_1 = mf_2$, kjer sta f_1 in f_2 karakteristični frekvenci oscilatorjev.

Kadar opazujemo sinhronizacijo v prisotnosti šuma, sinhronizacijo kaotičnih sistemov ali oscilatorjev z moduliranimi lastnimi frekvencami, fazna in frekvenčna sklopitev nista več ekvivalentni [101]. Kadar je šum močan, lahko pride do faznih preskokov in vidi se le težnja k sinhronizaciji. Fazno sinhronizacijo lahko razumemo kot pojav vrha v porazdelitvi ciklične relativne faze

$$\Psi_{n,m} = \phi_{n,m} \bmod 2\pi \tag{15}$$

in si jo razlagamo kot obstoj preferenčne stabilne vrednosti fazne razlike $\phi_{1,2}$ med dvema oscilatorjema. V takih primerih ne moremo enoumno odgovoriti na vprašanje o sinhronizaciji sistema, nanjo lahko gledamo le v statističnem smislu.

Pri kardiovaskularnem sistemu s časovno spremenljivimi karakterističnimi frekvencami se lahko fazna sinhronizacija pojavi, za frekvence pa ni nujno, da so povezane. Držimo se zapisa (14) za fazno sinhronizacijo, v besedilu uporabljamo skrajšano sinhronizacija.

Že odprto vprašanje razmerja bispektrov do sinhronizacije podrobnejše obdelamo na primeru signalov podgan med splošno anestezijo. Signali so bili že obdelani z metodami za analizo sinhronizacije [63]. Iz signalov smo izbrali in analizirali z bispektri dva signala, za katera dobimo v sinhrogramu zelo jasno izraženo epizodo sinhronizacije.

Za podgane med splošno anestezijo smo merili električno aktivnost srca (EKG), dihanje, EEG in temperaturo. Izmerjenih je bilo 21 podgan, težkih 250 g, večina jih je bilo samcev. Prvih 11 smo uporabili za testiranje in umerjanje merilnih naprav ter za določanje kvalitete signalov. Z meritvijo smo začeli 4-7 minut po vbrizgu anestetika in končali, ko so se podgane začele spontano gibati. Meritve so trajale ~70 min, vzorčna frekvenca je bila 1000 Hz. Med meritvijo so podgane ležale na trebuhu v Faradayevi kletki [63, 64].

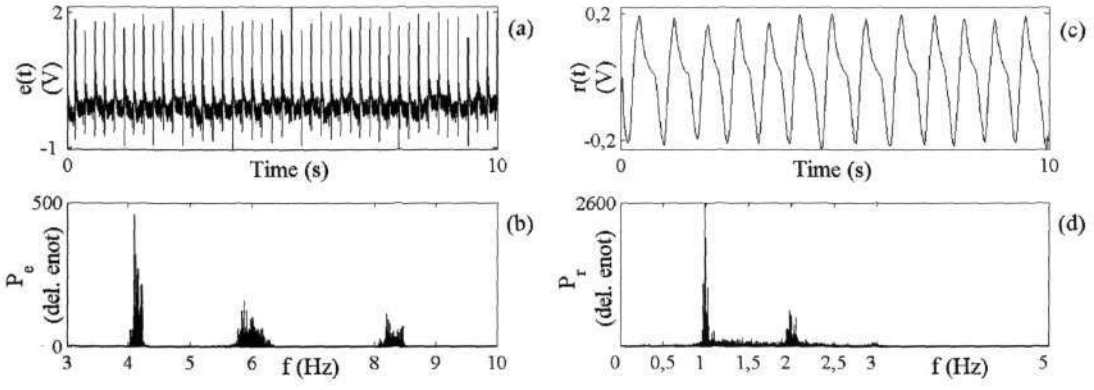

Slika 6: 10 s detrendiranega, prevzorčenega, normaliziranega in osrediščenega signala (a) EKG $e(t)$ in (c) dihanja $r(t)$ signala rat20 med splošno anestezijo, ~72 min dolg, vzorčen s f_s = 50 Hz in njuna močnostna spektra (b) in (d). Vrh pri 6 Hz v močnostnem spektru $e(t)$ nastopi, ko se podgana začne zbujati iz anestezije, strm prehod v trenutni srčni frekvenci okoli 40 minute, slika 7 (a).

Za obe podgani smo izračunali križne bispektre B_{cere}, kjer pomeni c križni, e signal $e(t)$ in r signal $r(t)$. Signale EKG in dihanja smo predhodno obdelali. Odstranili smo zelo nizke in zelo visoke frekvence z uporabo oken z drsečim povprečjem; dolžine 200 s za trend in 0,04 s za visoke frekvence, hkrati pa

smo jih prevzorčili na 50 Hz. Tako smo se izognili problemom prekrivanja [81]. Signale smo normalizirali med nič in ena in jim odstranili srednjo vrednost. Primer tako obdelanih signalov EKG $e(t)$ in dihanja $r(t)$ in njunih močnostnih spektrov za podgano rat20 je prikazan na sliki 6. Za oba signala smo najprej izračunali trenutno srčno in respiratorno frekvenco ter njuno razmerje in sinhrogram, ki so za podgano rat20 prikazani na sliki 7. Sledil je izračun križnih bispektrov in za prve štiri vrhove iz preglednice 1 še izračun biamplitude in bifaze.

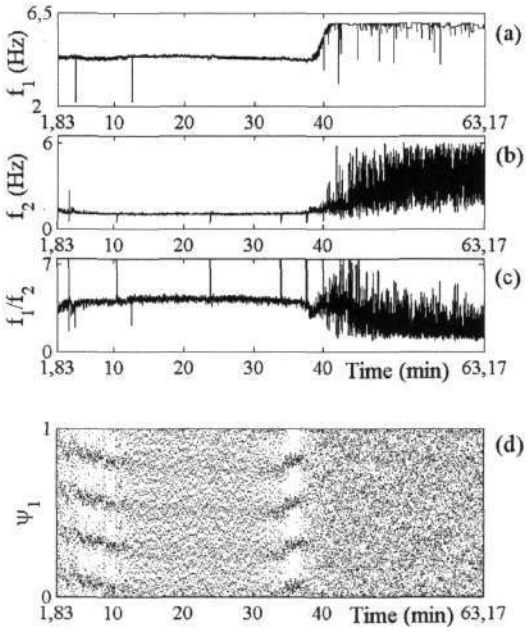

Slika 7: (a) Trenutna srčna (b) dihalna frekvenca in (c) njuno frekvenčno razmerje za podgano rat20 med splošno anestezijo. (d) Srčno-respiratorni sinhrogram za podgano rat20.

Frekvenčno ločljivost smo nastavili na 1/20 najnižje respiratorne frekvence, ki je bila okoli 1 Hz (potrebno je 20 s dolgo okno). Opazovali smo sklopitve, ki so trajale vsaj 10 period nižje sklopitvene frekvence, 10 krat $(1/f_2) = 10$ s. Glede na Heisenbergov princip nedoločenosti [43] smo zadovoljili potrebo po frekvenčni ločljivosti in izbrali 20 s dolgo okno za izračun bispektra, biamplitude in bifaze. Okno smo premikali vzdolž časovne vrste s korakom 0,1 s. Kritično vrednost smo za vse primere postavili na 2, to je dvakratno vrednost povprečne vrednosti bispektra na področju notranjega trikotnika.

Križni bispektri razkrijejo nastanek in trajanje sinhronizacije, kot je prikazano na sliki 8. Ugotovimo tudi pojav nelinearnih sklopitev. Relacijo do sinhronizacije dopolnimo še z generičnim modelom. Pojav sinhronizacije lahko spremlja modulacija. V poglavju „Analiza sklopitev" smo pokazali primer modulacije brez sinhronizacije. Iz sinhrograma težko ugotovimo prisotnost modulacije, možno je le v primeru, da je ta zelo močna. Z generičnim modelom pa ugotavljamo zmožnosti bispektralne analize v

primeru, da istočasno nastopita sinhronizacija in modulacija. Uporabimo skoraj periodični vsiljen Poincaré oscilator, ki ga periodično vodi šibka zunanja sila z dodano frekvenčno modulacijo. Njuno frekvenčno razmerje namenoma vzamemo za celoštevilsko; tako dobimo s sinhrogramom sinhronizacijo tudi, ko med njima ni sklopitve.

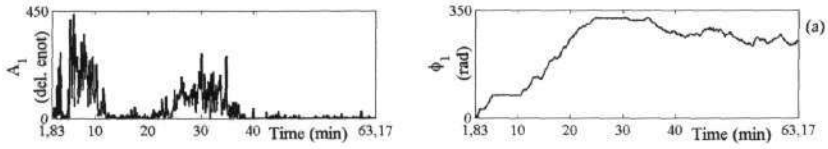

Slika 8: Bifaza ϕ in biamplituda A za vrh 1 (4,3 Hz, 1,05 Hz), izračunani z 0,1 časovnim korakom in 20 s dolgim oknom za oceno diskretne Fourierove transformiranke in uporabo Blackmanovega okna.

Pri močni sinhronizaciji sta uspešna oba, sinhrogramom in bispekter. V bispektru opazujemo vrh 1 in obdobje konstantne bifaze, če je biamplituda nad kritično vrednostjo. Šibka sinhronizacija je težko zaznavna s sihrogramom, v bispektru pa je bifaza manj konstantna z več faznimi preskoki. Če sinhronizacije ni, potem ni vodoravnih črt v sinhrogramu, v bispektru pa vrha 1. Sinhrogram nas lahko zavede v primeru, da sklopitve med sistemoma ni, je pa njuno frekvenčno razmerje konstantno. V primeru sinhronizacije se lahko pojavi tudi nelinearna sklopitev, to pa ne velja nujno tudi v obratni smeri. Med njima ni enostavne povezave. Samo prisotnost modulacije lahko ugotovimo z bispektrom, zavede pa nas lahko hkratna prisotnost modulacije in linearne sklopitve. V tem primeru je potrebno analizirati več vrhov. Pomagamo si lahko z opazovanjem poteka faz frekvenčnih komponent v trojici. Skupni nastop močne nelinearne sklopitve in močne modulacije ni mogoče razločiti.

Bispektralna analiza je bolj občutljiva na sklopitve med sistemi kot sinhrogram. Ugotovimo lahko tudi nastanek sinhronizacije, vendar v splošnem ne podaja enake informacije kot sinhrogram.

SPEKTRI VIŠJIH REDOV NA OSNOVI TRANSFORMACIJE Z VALČKI

Fouriereva transformacija je zasnovana na predpostavki (a) periodičnosti signala in (b) neskončno dolgih časovnih vrst [57, 58]. Ker nobena od predpostavk ni strogo izpolnjena za izmerjene signale, je določitev posameznih frekvenc v sistemu, ki vsebuje močne sklopitve, zelo zahtevna. Še težje je v nizkofrekvenčnem področju, ki nas še posebej zanima, saj je karakteristične frekvence še težje ločiti. Princip nedoločenosti Fouriereve transformacije omejuje zmožnosti ločevanja harmoničnih

komponent v frekvenčnem področju bispektra [20, 69]. To lahko povzroči težave pri ugotavljanju nelinearne kvadratične sklopitve, ko je frekvenčni par blizu skupaj. Da lahko zagotovimo dobro ločljivost nizkih frekvenc, potrebujemo daljše odseke za izračun diskretnih Fourierevih transformirank. To hkrati zniža število odsekov in poslabša oceno bispektralnih mer. Daljši signali pa vodijo v nestacionarnost in varianca postane še večja [69].

Pomagamo si lahko s transformacijo z valčki (TV), ki je v nekem smislu posplošena Fouriereva transformacija [43] z dodano časovno ločljivostjo na bolj osnoven način, kot je to dovoljeno s KČFT [81]. TV je že bila uspešno uporabljena za obdelavo kardiovaskularnih signalov [3, 5]. Posplošitev bispektra na TV lahko omogoči ugotavljanje začasnih sprememb v faznih sklopitvah ali kratkotrajne sklopitve. Prav tako pričakujemo, da bo uspešna pri ločevanju širokih in sovpadajočih vrhovih na račun povečane časovne ločljivosti.

VT preslika signal iz časovnega prostora v prostor čas-skala. Signal $g(t)$ razstavi na družino v splošnem neortogonalnih funkcij $\Psi_{s,t}$, ki jih dobimo s premikanjem in skaliranjem osnovnega valčka $\psi(u)$. Valčna transformiranka $W_g(s, t)$, ki jo je prvi vpeljal Morlet [28], je definirana kot [43]

$$W_g(s,t) = \int_{-\infty}^{+\infty} \Psi^*\left(\frac{\tau - t}{s}\right) g(\tau) d\tau \,. \tag{16}$$

Osnovni valček mora biti omejen tako v časovnem kot v frekvenčnem prostoru. Za analizo kardiovaskularnih signalov je najbolj primeren Morletov valček, ki je Gaussova funkcija, modulirana s sinusnim valom [6, 8]. Poenostavljena oblika v časovnem prostoru je

$$\psi(u) = \pi^{-1/4} e^{-j2\pi f_0 u} e^{-\frac{u^2}{2}} \,. \tag{17}$$

Razmerje med skalo s in frekvenco f je $f = f_0/s$, kjer s f_0 določimo število period sinusa v oknu. Frekvenčna ločljivost se tako spreminja s skalo (frekvenco) - pri nizkih je boljša kot pri visokih, medtem ko je časovna ločljivost boljša pri visokih kot pri nizkih frekvencah.

Valčni bispekter *WB* definiramo analogno v skladu s Fourierevo definicijo bispektra kot

$$WB(s_1, s_2) = \int_T W_g(s_1, \tau) W_g(s_2, \tau) W_g^*(s, \tau) d\tau, \tag{18}$$

kjer velja

$$\frac{1}{s_1}+\frac{1}{s_2}=\frac{1}{s}. \tag{19}$$

Valčni bispekter meri vrednost fazne sklopitve, ki nastopi med valčnimi transformirankami pri skalah s_1, s_2 in s signala $g(t)$ na intervalu T, tako da je pravilo vsote skal (frekvenc) (19) izpolnjeno.

Valčni bispekter WB je kompleksor, določata ga amplituda A in faza ϕ

$$WB(s_1,s_2)=\left|WB(s_1,s_2)\right|e^{j\angle WB(s_1,s_2)}=Ae^{j\phi}. \tag{20}$$

Za vsako biskalo (s_1, s_2) ga lahko predstavimo kot točko v kompleksnem prostoru $\Re$[WB(s_1, s_2)] proti $\Im$[WB(s_1, s_2)], kar določa vektor. Njegova amplituda (dolžina) je biamplituda, bifaza pa je določena s kotom med vektorjem in pozitivno realno osjo. Trenutno bifazo izračunamo analogno kot v primeru (5)

$$\phi(s_1,s_2,t)=\phi_{s_1}(t)+\phi_{s_2}(t)-\phi_s(t). \tag{21}$$

Če sta dve skalni komponenti s_1 in s_2 skalno in fazno sklopljeni, $\phi_s = \phi_{s1} + \phi_{s2}$, potem velja, da je bifaza enaka 0 (2π) radianov. V našem primeru je fazna sklopitev manj stroga, ker so lahko odvisne skalne komponente fazno zamaknjene. Za fazno sklopitev smatramo, če je bifaza konstantna (ni nujno enaka 0 radianom) za vsaj nekaj period višje skalne komponente biskale (s_1, s_2). Istočasno opazujemo trenutno biamplitudo, ki lahko podaja relativno jakost sklopitve

$$A(s_1,s_2,t)=\left|WB(s_1,s_2,t)\right|. \tag{22}$$

V skladu s Fourierevo definicijo križnega bispektra lahko definiramo analogno križni valčni bispekter kot

$$WB_{cfgg}(s_1,s_2)=\int_T W_f(s_1,\tau)W_g(s_2,\tau)W_g^{*}(s,\tau)d\tau. \tag{23}$$

Da lahko zadostimo frekvenčnemu pogoju vsote (19) pri visokih frekvencah, je potrebna višja frekvenčna ločljivost. Dosežemo jo tako, da Morletov valček spremenimo

$$\psi(u) = a_m \cdot c_n \cdot e^{-i2\pi f_0 u} e^{-\frac{u^2}{2d}}. \tag{24}$$

Faktor d določa eksponentno upadanje Morletovega valčka. Večji kot je počasneje upada Gaussova funkcija in boljša je frekvenčna ločljivost ob hkratnem zmanjšanju časovne ločljivosti. Ustrezno frekvenčno ločljivost pri visokih frekvencah lahko zagotovimo tudi s faktorjem a_m, s katerim dosežemo, da širina okna ne upada hiperbolično, temveč počasneje. Za višje frekvence lahko uporabimo tudi konstantno širino valčka. S konstanto c_n dosežemo normalizacijo, da transformacija ohranja energijo (moč). Za analizo kardiovaskularnih signalov izberemo $f_0 = 1$, da je razmerje med frekvenco in skalo $f = 1/s$, in lažje interpretacije valčnih bispektrov.

Na sliki 9 (a) in (b) je prikazan valčni bispekter za testni primer nelinearne kvadratične sklopitve med dvema Poincaré oscilatorjema z dodanim Gaussovim šumom, signal x_{1D}, slika 2 (a).

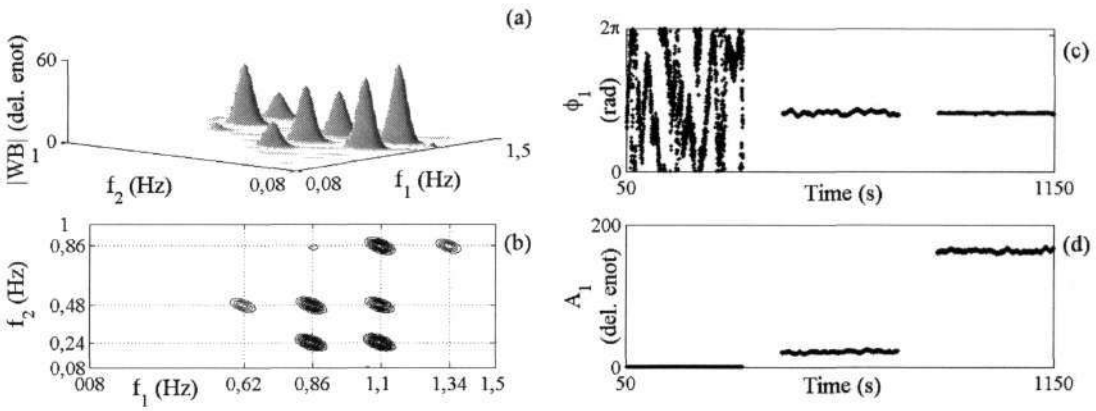

Slika 9: Rezultati za kvadratično sklopitev v prisotnosti aditivnega Gaussovega šuma, testni signal x_{1D}, dobljen z valčnim bispektrom. (a) Valčni bispekter $|WB|$, izračunan iz $K = 33$ segmentov, 66 % prekrivanjem, T_m[2] = 8 s, G_e[3] = 0,001 in z uporabo Morletovega valčka s konstantno dolžino $T_{HF} = 40$ s za izračun visokih frekvenc in (b) njegov nivojski prikaz. Del valčnega bispektra nad $f_2 > 1{,}0$ Hz je odrezan, ker trojica (1,1 Hz, 1,1 Hz, 1,1 Hz) povzroči visok vrh, ki je fizično nepomemben. (c) Bifaza ϕ in (d) biamplituda A za bifrekvenco (1,1 Hz, 0,24 Hz), z 0,1 s časovnim korakom.

Oba bispektra, valčni in Fourierev, podajata enako informacijo o sklopitvi. Razlika je vidna v obliki vrhov, ki so v primeru valčnega bispektra širši. To je pričakovati, saj je frekvenčna ločljivost za visoke frekvence nižja kot pri bispektru na osnovi Fouriereve transformacije. Hkrati je opazna večja časovna ločljivost valčnega bispektra predvsem iz časovnega poteka bifaze, slika 9 (c) in (d).

[2] Dolžina Morletvega osnovnega valčka, $s = 1$ s.
[3] Vrednost Gaussove funkcije na robu Morletovega valčka.

PRIMERJAVA FOURIEREVEGA IN VALČNEGA BISPEKTRA

Vpeljano metodo valčnega bispektra uporabimo na signalih krvnega pretoka, ki smo jih že analizirali z uporabo Fourierevega bispektra na osnovi KČFT. Parametri valčne bispektralne transformacije so nastavljeni na tipske vrednosti, ugotovljene na podlagi testnih signalov.

Valčni bispekter za celotno frekvenčno področje signala krvnega pretoka b_a je prikazan sliki 10 (a). Razvidnih je več vrhov. Področje našega interesa je srčno-respiratorna sklopitev, področje okoli bifrekvence (f_1, f_2), ki je podrobnejše prikazano na sliki 10 (b). Natančna analiza pokaže, da se v bispektru nahajajo vsi vrhovi, našteti v preglednici 1. Izračun bifaz in biamplitud za vse vrhove pa razkrije, da so v časovnem intervalu od 77,1 s do 170,4 s izpolnjeni vsi pogoji za nelinearno kvadratično sklopitev, katere dolžina je T_{qc} = 93,3. Primer vrhov, biamplitud in bifaz za vrhova 1 in 2 prikazuje slika 11.

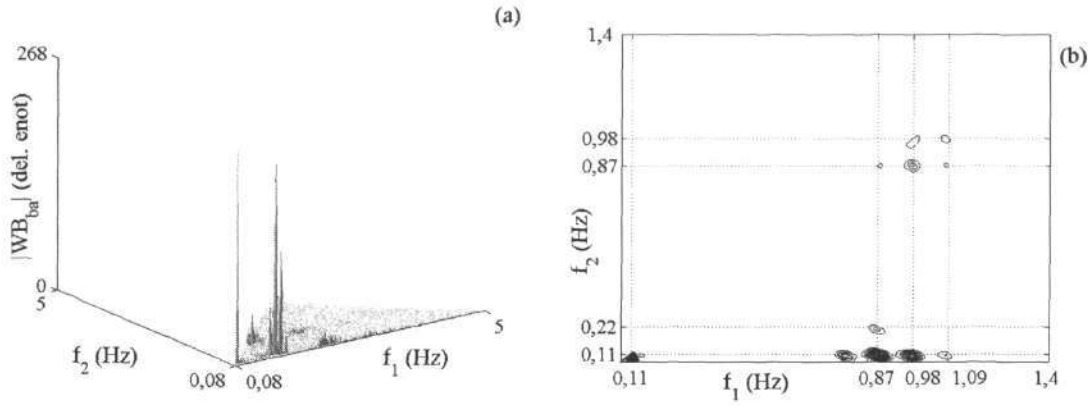

Slika 10: (a) Valčni bispekter $|WB|$ signala b_a, izračunan iz K = 33 segmentov, 87 % prekrivanjem, T_m = 8 s, G_c = 0,001 in z uporabo Morletovega valčka s konstantno dolžino T_{HF} = 80 s za izračun visokih frekvenc. (b) Nivojni prikaz dela bispektra $f_1, f_2 < 1,4$ Hz, ki nas zanima.

Primerjava rezultatov, dobljenih z valčnim bispektrom, s tistimi, dobljenimi s Fourierevim bispektrom, razkrije, da z obema metodama ugotovimo enako pozicijo vrhov v bispektru. Vrhovi, dobjeni z valčnim bispektrom, so širši kot v primeru Fourierevega bispektra. Časovni poteki biamplitud so zelo podobni. Pojavlja se enako število izstopajočih vrhov v enakih časovnih trenutkih. Izračun križno-korelacijskega koeficienta za biamplitudi prvega vrha obeh metod je enak 0,95. Podobno velja za časovni potek bifaz. Opazimo lahko, da so spremembe bifaze veliko bolj izrazite v primeru valjčnega bispektra. Čeprav si po obliki časovni poteki bifaz niso tako podobni, kot velja za biamplitude, pa se pojavljajo platoji s konstantno bifazo v enakih časovnih trenutkih. Z obema metodama ugotovimo

prisotnost kvadratične sklopitve. V primeru valčnega bispektra je za 2,3 s krajša, kar je 2,4 odstotna razlika.

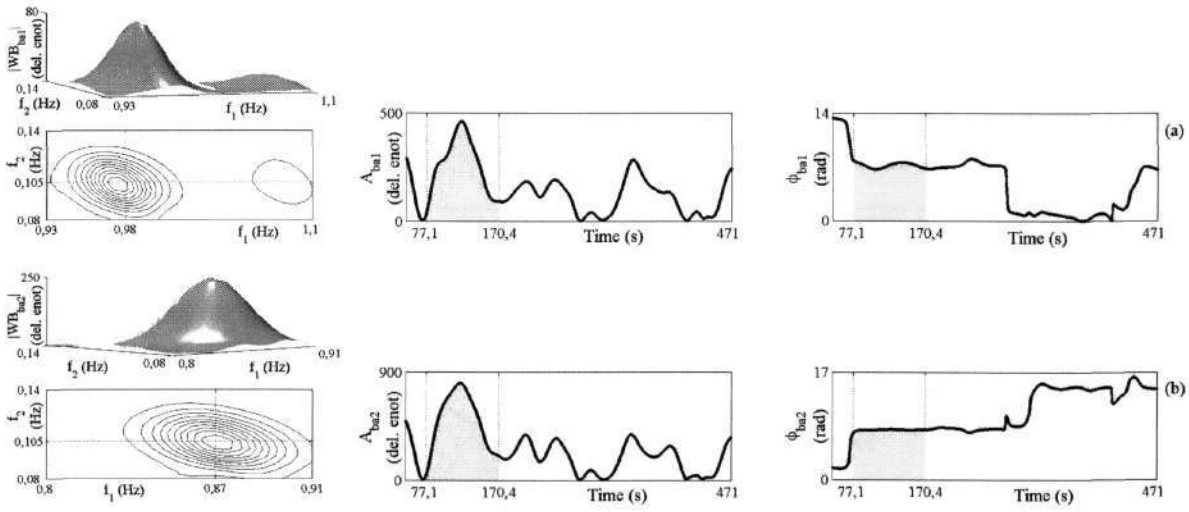

Slika 11: Analiza krvnega pretok signala $b_a(t)$, izračunanega iz K = 33 segmentov, 87 % prekrivanjem, z 0,1 s časovnim korakom, T_m = 8 s, G_e = 0,001 in z uporabo Morletovega valčka s konstantno dolžino T_{HF} = 80 s za izračun visokih frekvenc, za vrhova (a) 1 in (b) 2; levi stolpec, bispekter $|B_{ba}|$ s pripadajočim nivojnim prikazom; sredinski, biamplituda A_{ba}; in desni, bifaza ϕ_{ba}.

Če povzamemo, dobimo z obema metodama zelo podobne rezultate. Iz širine vrhov v bispektru lahko sklepamo, da je frekvenčna ločljivost Fourierevega bispektra višja, medtem ko časovna ločljivost valčnega bispektra višja, saj bolje zazna hitre bifazne spremembe. Valčna metoda ne da opazno boljših rezultatov. To velja za primer analize srčno-respiratorno sklopitve, in sicr pri določenih pogojih, po katerih sklepamo na nelinearno sklopitev. V tem primeru je izbrano okno za izračun Fourierevega bispektra ravno tisto, ki zadovolji potrebni frekvenčni ločljivosti in hkratni časovni ločljivosti. Posledično ne dobimo znatnih razlik med rezultati obeh metod.

Razliko si oglejmo na primeru generičnega testnega signala dveh kvadratično sklopljenih Poincaré oscilatorjev z dodanim Gaussovim šumom, i = 1, 2, kjer sta f_1 = 1,1 Hz in f_2 = 0,24 Hz:

$$\begin{aligned}
\dot{x}_1 &= -x_1 q_1 - \omega_1 y_1 + \eta_2 (x_1 - x_2)^2 + \xi(t), \\
\dot{y}_1 &= -y_1 q_1 + \omega_1 x_1 + \eta_2 (y_1 - y_2)^2, \\
\dot{x}_2 &= -x_2 q_2 - \omega_2 y_2, \\
\dot{y}_2 &= -y_2 q_2 + \omega_2 x_2, \\
q_i &= \alpha_i (\sqrt{x_i^2 + y_i^2} - a_i).
\end{aligned} \tag{25}$$

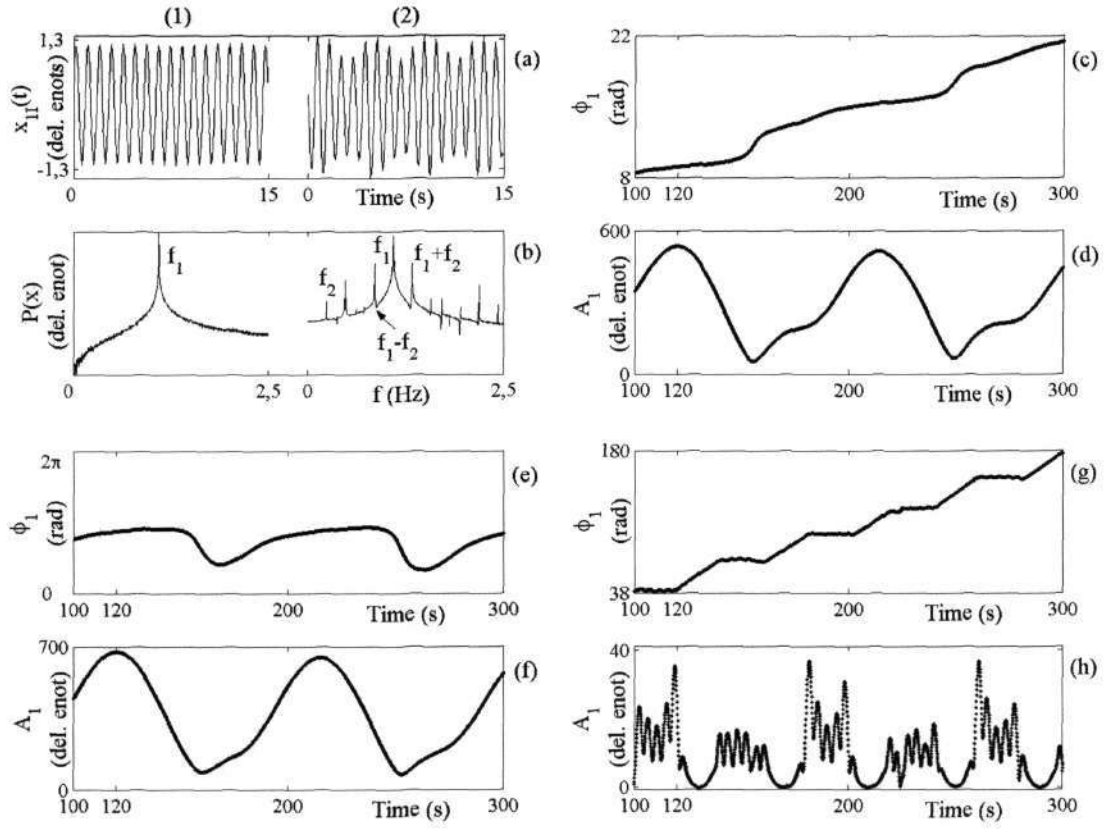

Slika 12: Rezultati, dobljeni s Fourierevim (c)-(f) in valčnim (g)-(h) bispektrom za primer prekinjajoče se kvadratične sklopitve dveh Poincaré oscilatorjev z dodanim Gaussovim šumom. (a) Testni signal x_{11}, spremenljivka x_1 prvega oscilatorja s karakteristično frekvenco f_1 = 1,1 Hz. Karakteristična frekvenca drugega oscilatorja je f_2 = 0,24 Hz. Oscilatorja sta sklopljena enosmerno kvadratično z dvema različnima jakostima sklopitve: η_2 = 0,0 (1); in 0,2 (2). Sklopitev (2) je prisotna vsakih 20 s in traja 20 s. Signal je dolg 1200 s in vzorčen z vzorčno frekvenco f_s = 10 Hz. Za vsak primer je prikazan signal za prvih 15 s. (b) Močnostni spekter. (c) Bifaza ϕ in (d) biamplituda A za bifrekvenco (1,1 Hz, 0,24 Hz) izračunani s 100 s dolgim oknom za oceno diskretne Fourierevе transformiranke. (e) Bifaza ϕ in (f) biamplituda A za bifrekvenco (1,1 Hz, 0,24 Hz) izračunani s 130 s dolgim oknom za oceno diskretne Fourierevе transformiranke. V obeh primerih z 0,1 s časovnim korakom, K = 33 segmenti, s 66 % prekrivanjem in z uporabo okna Blackman. (g) Bifaza ϕ in (h) biamplituda A za bifrekvenco (1,1 Hz, 0,24 Hz), izračunani z valčnim bispektrom s K = 33 segmenti, z 0,1 s časovnim korakom, 66 % prekrivanjem, G_e = 0,01, T_m = 8 s in z uporabo Morletovega valčka s konstantno dolžino T_{HF} = 20 s za izračun visokih frekvenc.

Tako dobljeni generični signal $x_{11}(t)$ je prikazan na sliki 12 (a) s pripadajočim močnostnim spektrom, slika 12 (b), za dve jakosti sklopitev: $\eta_2 = 0$; in $\eta_2 = 0{,}2$, ki se izmenjujeta vsakih 20 s. Dodatni vrhovi, poleg karakterističnih za kvadratično sklopitev, so posledica analize celotnega signala naenkrat. Zaradi diskretnih sprememb sklopitve pride do bogate harmonske vsebine signala. Opazujemo le vrh pri bifrekvenci (1,1 Hz, 0,24 Hz). V prvem primeru uporabimo 100 s dolgo okno za izračun Fourierevega bispektra. Iz poteka bifaze, slika 12 (e), bi lahko napačno sklenili, da ni fazne sklopitve, saj le-ta ni konstantna, temveč narašča s časom. V drugem primeru uporabimo 130 s dolgo okno za izračun

Fourierevega bispektra. Iz poteka biamplitude in bifaze, slika 12 (e) in (f), bi lahko sklenili, da sta oscilatorja ves čas sklopljena, saj je biamplituda nad kritično vrednostjo, bifaza pa brez faznih preskokov, t.j. znotraj π rad intervala.

Šele z uporabo valčnega bispektra razkrijemo pravo naravo sklopitve, slika 12 (g) in (h). Biamplituda kaže prisotnost sklopitve na vsakih 20 s, prav v teh intervalih pa je tudi bifaza konstantna, sicer pa monotono narašča.

Glavna razlika med valčnim in Fourierevim bispektrom je prav časovna in frekvenčna ločljivost. Po Heisenbergovem principu nedoločenosti [43] sta hkratni natančni določitvi frekvence in časa vzajemno si izključujoči

$$\Delta t \, \Delta f \geq 1/(4\pi), \tag{26}$$

kjer je Δt časovni interval in Δf frekvenčni pas. Enačaj velja le v primeru, ko je okno Gaussovo. Medtem ko sta frekvenčna in časovna ločljivost pri KČFT določeni z izbranim oknom (njegovo dolžino) in se ne spreminjata, se pri valčnem bispektru frekvenčna in časovna ločljivost spreminjata s skalo. Razmerje med frekvenco in frekvenčno ločljivostjo je konstantno. Visoke frekvence se spreminjajo hitreje in nizke počasneje, valčni bispekter *WB* ima visoko frekvenčno ločljivost nizkih frekvenc in visoko časovno ločljivost visokih frekvenc, zato je zmožen zaznati kratkotrajne fazne sklopitve. Prav z uporabo Morletovega valčka dosežemo optimalno razmerje med frekvenčno in fazno ločljivostjo. Fourierev bispekter s povprečjem izloči večino časovno povezane informacije. Vendar pa moramo biti pazljivi pri uporabi VT, saj je lahko pri visokih frekvencah časovna ločljivost previsoka, frekvenčna pa prenizka. Tako bodo bispektralne ocene občutljive na šum, po drugi strani pa to pelje k slabi/nepravilni določitvi karakterističnih frekvenc.

Pri Fourierevem bispektru je frekvenčni korak določen s širino okna, pri valčnem bispektru pa je poljuben, saj je valčna transformacija zvezna, kar je velika prednost. To ima za posledico prevzorčenje, ki pa se nas, če ne iščemo inverzne transformacije, ne dotika. Če izberemo $f_0 = 1$, je interpretacija valčnega bispektra enaka kot v primeru Fourierevega. Prav tako je enostavna normalizacija na energijo (moč). Prednosti sta še manjša statistična napaka in računska zahtevnost.

Med VT in KČFT obstaja še tako imenovana modificirana kratkočasovna Fouriereva transformacija ali selektivna diskretna Fouriereva transformacija (SDFT), ki sta jo prvič predstavili Keselbrenerjeva in Akselrodova [47]. Podobno kot KČFT je časovno odvisna Fouriereva transformacija. Časovno-frekvenčno občutljivost dosežemo z uporabo okna specifične dolžine okoli analizirane podatkovne točke za izračun vsake spektralne komponente posebej. Za vsako frekvenčno komponento izvedemo

diskretno Fourierevo transformacijo. Dolžina okna je obratno sorazmerna frekvenci izračuna, podobno kot krčenje in raztegovanje osnovnega valčka pri VT, kar pomeni, da so nizke frekvence ocenjene z dobro frekvenčno ločljivostjo in visoke z dobro časovno ločljivostjo.

Zaradi uporabe pravokotnih oken pri izračunu diskretne Fouriereve transformiranke pride do pojava razlivanja. Da ga omilimo, uporabimo okna za glajenje, kot so na primer Hammingovo, Hanningovo ali Blackmanovo [47].

Obe, SDFT in VT, sta primerni za generalizacijo bispektralne analize, saj omogočata izbiro med dobro frekvenčno in časovno ločljivostjo. Medtem ko uporaba Morletovega valčka omogoča optimalno časovno-frekvenčno ločljivost, pa se ji lahko s SDFT s primerno izbiro parametrov le približamo. Še vedno pa ima VT prednost, da je zvezna, medtem ko SDFT ni.

OSTALE MOŽNOSTI UPORABE VALČNE BISPEKTRALNE METODE

Za proučevanje kardiovaskularnega sistema nismo nujno vezani samo na kardiovaskularne signale. Informacija o sklopitvah nevrogenega kardiovaskularnega podsistema je vsebovana tudi v možganskih valovih. Če ugotovimo, da nastopi sinhronizacija med posameznimi centri v možganih, lahko sklepamo, da so ti centri med seboj sklopljeni. V večini primerov je sinhronizacija povezana z obnašanjem specifičnih struktur, frekvenc in stanja obnašanja. Na splošno nizkofrekvenčne oscilacije izvirajo iz večjih struktur kot visokofrekvenčne. Pod določenimi pogoji, kot je primer splošne anestezije, lahko opazimo pri merjenju signala elektroencefalograma (EEG) sinhronizacijo kot organizirane, razločljive vzorce. Ti vzorci so odvisni od povzročitelja anestezije in globine anestezije [107]. Delta možganski valovi so najpočasnejši izmed možganskih valovanj (0-4 periode na sekundo). Povezani so z globokim spanjem brez sanj, s stanjem transa, povečanjem imunskih funkcij, hipnozo in je zato pričakovati, da se pojavijo med anestezijo. Prostorska homogenost v EEG signalu med anestezijo se pogosto ugotavlja na osnovi spektralnih metod [21, 86, 122].

Merjenje kvadratične fazne sklopitve med komponentami EEG signala je prvi uvedel G. Dumermuth z uporabo bispektralne analize leta 1969 [51]. Številne EEG študije, ki so uporabljale matematična orodja spektrov višjih redov, so bile od tedaj objavljene [12, 27, 53, 65]. Za merjenje globine anestezije in stopnje sprostitve [84, 88, 98] se pogosto uporablja tako imenovani bispektralni indeks (BIS) [89]. Ta kompleksni parameter je sestavljen iz komponent pridobljenih na osnovi različnih analiz in samo ena je povezana z bispektrom. Na splošno stacionarnosti v signalih EEG ne moremo

pričakovati, zato se za analizo uporabljajo predvsem časovnofrekvenčne porazdelitve, TV, časovno spremenljive avtoregresijske metode na osnovi gibajočih se povprečjih (ARMA) in druge, ki ponujajo zadostno časovno in frekvenčno ločljivost. Razvita je bila tudi časovno spremenljiva bispektralna metoda [5, 69, 98]. Medtem ko se ti pristopi osredotočajo na časovnofrekvenčni prostor (spektri drugega reda) ali na obliko v frekvenčno-frekvenčnem prostoru (spektri tretjega reda), pa je naš namen izločiti časovno sklopitveno informacijo iz frekvenčno-frekvenčne domene bispektra, to je biamplitudo in bifazo.

Nedavno je bila opravljena analiza EEG signalov podgan med splošno anestezijo z izračunom sinhronizacijskih indeksov [63, 64]. Analiza je pokazala, da imajo ti signali več časovno spremenljivih frekvenčnih komponent. Najbolj dominantne so v delta frekvenčnem področju (0-4 Hz). Podoben vzorec je bil opažen pri vseh izmerjenih podganah. Na začetku je dominantna ena, počasi spreminjajoča se frekvenčna komponenta okoli centralne frekvence 2 Hz. Okoli nje so višje frekvenčne komponente, ki na začetku niso razločljive. Ko se začnejo podgane spontano premikati in spontano dihati, dominantna frekvenčna komponenta v EEG signalu izgine. Sinhronizacijski indeksi so bili izračunani za primer (a) valovi delta iz EEG in EKG, (b) valovi delta iz EEG in dihanje in (c) EKG in dihanje. Samo za zadnji primer je bila sinhronizacija očitna. V vseh primerih se je pojavljal splošni vzorec, na začetku sinhronizacija 2:1 ali 3:1, ki kasneje preide v 4:1 ali 5:1 in se kasneje vrne nazaj v 3:1 ali 2:1 sinhronizacijo. Na koncu signalov ni sinhronizacije, kar povezujemo s prehodom v manj globoko anestezijo. Izračunane so bile tudi smeri in jakosti sklopitev oscilatorjev. Medtem ko lahko vidimo, da na začetku respiratorni oscilator vodi oscilacije, ki izhajajo iz delta valovanja iz EEG, pa ne moremo ničesar zaključiti o smeri sklopitve in jakosti med srčnim oscilatorjem in valovi delta iz EEG signala.

Globina anestezije je povezana s sinhronizacijo med srčnim in respiratornim oscilatorjem [63, 64]. Globino anestezije lahko dobimo iz signala EEG, ta pa je povezana z bispektrom. V tem poglavju analiziramo signal EEG podgane rat20, že obravnavane v poglavju „Razmerje med bispektri in sinhronizacijo", z metodo valčnih bispektrov za ponazoritev zmožnosti metode. Želimo ugotoviti, ali lahko z izračunom valčnega bispektra, biamplitude in bifaze izvlečemo enako informacijo iz univariatnega signala EEG, kot jo da bivariatna sinhronizacija EKG in dihalnega signala.

Signal EEG smo najprej obdelali, tako da smo odstranili zelo nizke in zelo visoke frekvence z uporabo oken z drsečim povprečjem; dolžine 200 s za trend in 0,04 s za visoke frekvence in ga hkrati prevzorčili na 50 Hz. Signal smo dalje normalizirali med nič in ena in mu odstranili srednjo vrednost. Signal EEG podgane rat20 in njegov močnostni spekter sta prikazana na sliki 13 (a-b).

Za jasnejšo interpretacijo smo ~63 min dolg EEG signal podgane rat20 razdelili na štiri odseke a, b, c in d, glede na dobljeni sinhrogram med srčnim in respiratornim oscilatorjem za podgano rat20, slika 13 (c). Vsak odsek je določen tako, da se v tem času v sinhrogramu pojavi samo en sinhronizacijski pojav, to je sinhronizacija ali brez sinhronizacije.

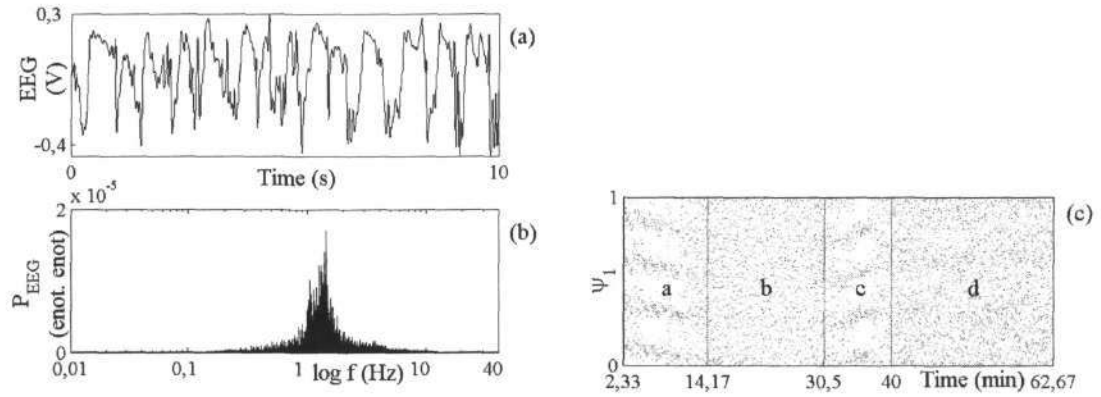

Slika 13: (a) 10 s detrendiranega, prevzorčenega, normaliziranega in osrediščenega EEG(t) signala in njegov močnostni spekter (b) za podgano rat20 med splošno anestezijo, ~63 min dolg in prevzorčen na f_s = 50 Hz (c) Srčno-respiratorni sinhrogram za podgano rat20, razdeljen na 4 odseke a-d.

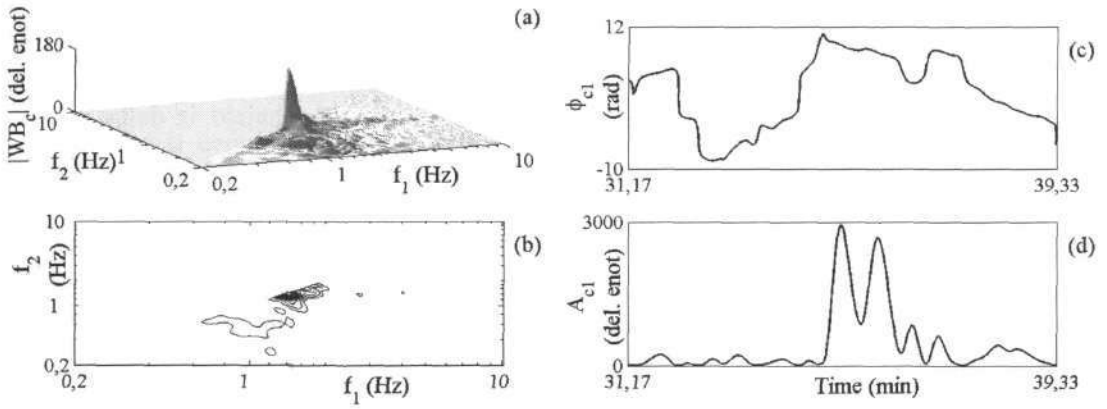

Slika 14: Primer rezultatov za podgano rat20 med splošno anestezijo. (a) Valčni bispekter $|WB_c|$ EEG signala podgane za odsek c izračunan iz K = 33 segmentov, 81 % prekrivanjem, G_e = 0.001, T_m = 8 s, z uporabo Morletovega valčka s konstantno dolžino T_{HF} = 20 s za izračun visokih frekvenc in (b) njegov nivojski prikaz. (c) Bifaza ϕ in (d) biamplituda A za bifrekvenco (1,4 Hz, 1,4 Hz), izračunana iz K = 33 segmentov, z 81 % prekrivanjem, G_e = 0.001, T_m = 8 s, 0,1 s časovnim korakom in z uporabo Morletovega valčka s konstantno dolžino T_{HF} = 80 s za izračun visokih frekvenc.

Pri izračunu valčnih bispektrov za visoke frekvence smo uporabili okno dolžine 20 s, za oceno bifaz in biamplitud za bifrekvenco, kjer se pojavi najvišji vrh v valčnem bispektru, pa dolžine 80 s. S tem smo zagotovili visokofrekvenčno ločljivost za visoke frekvence, kjer je kompleksen EEG signal

koncentriran, okoli 1 Hz. Frekvenco smo povečevali s korakom 0,02 Hz, da smo ohranili frekvenčno pravilo vsote (19), okno pa premikali vzdolž serije s korakom 0,1 s. Kritična vrednost biamplitude je bila 2. Opazovali smo samo sklopitve med valovi delta iz EEG signala podgane.

V posameznih odsekih zaznamo z valčnim bispektrom fazne sklopitve. Primer bispektra, biamplitude in bifaze za odsek c signala EEG podgane rat20 so prikazani na sliki 14. Če upoštevamo potrebne pogoje za nastop nelinearne sklopitve, vendar samo za vrh samosklopitve, dobimo fazne samosklopitve, zbrane v preglednici 3.

Preglednica 3: Fazne sklopitve ugotovljene v EEG signalu podgane rat20. T_{pc} je časovni interval, za katerega z valčno bispektralno analizo ugotovimo, da je so valovi delta iz EEG signala fazno samosklopljeni pri bifrekvenci (f_1, f_1). Produkt $T_{pc} \times f_1$ pove, koliko period valov delta iz EEG signala je trajala fazna sklopitev. V času trajanja T_{pc} smo izračunali še največjo biamplitudo vrha A_{max} ter največjo spremembo bifaze $\Delta\phi$, njeno povprečno vrednost $\overline{\phi}$ in standardno deviacijo σ_ϕ.

Odsek	t_1 (min)	t_2 (min)	f_1 (Hz)	T_{pc} (s)	$T_{pc} \times f_1$	A_{max} (del. enot)	$\Delta\phi$ (rad)	$\overline{\phi}$ (rad)	σ_ϕ (rad)
a	2,67	3,55	1,1	49	57	753	1,16	3,24	0,23
a	5,87	6,33	1,1	28	33	494	0,24	3,59	0,05
a	7,45	8,17	1,1	43	50	1224	0,81	-8,14	0,29
a	8,22	10,83	1,1	157	183	1894	2,53	-9,62	0,69
a	12,38	13,03	1,1	39	45	535	0,58	-6,05	0,12
b	18,83	19,50	1,3	40	67	922	1,31	-1,77	0,34
b	23,83	24,31	1,3	29	48	3249	1,33	-39,44	0,30
c	35,00	36,17	1,4	70	141	2931	2,43	8,45	0,62
c	36,42	36,75	1,4	20	40	839	0,99	3,64	0,23
c	36,92	37,45	1,4	32	65	617	1,09	7,92	0,34
d	40,67	41,53	1,6	52	130	558	1,02	4,50	0,31

Največ faznih sklopitev se nahaja v odseku a in c. Te sklopitve so najmočnejše in trajajo najdaljši čas T_{pc}. Če združimo vse biamplitude posameznih odsekov, potem izstopata dva vrhova. V času, ko nastopita vrhova je bifaza znotraj π intervala. Čas nastopa in trajanje faznih sklopitev sta prikazana na sliki 15. Ta dva dogodka zaznamo tudi v sinhrogramu srčno-respiratorne sklopitve, slika 13 (c), ko se pojavi in ko izgine sinhronizacija 4:1. V vmesnem času sinhrogram ne pokaže nobene sinhronizacije, z valčnim bispektrom pa zaznamo kratkotrajne fazne sklopitve, ki ne morejo sinhronizirati sklopljenih oscilatorjev, saj se bifaza spreminja uniformno.

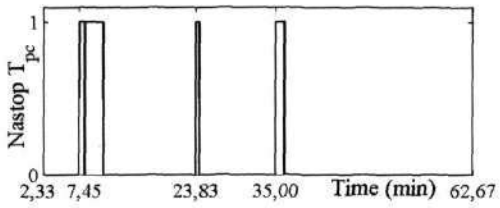

Slika 15: Fazne sklopitve T_{pc}, ki izstopajo po amplitudi biamplitude (1000 del. enot in več) v preglednici 3. Prikazan je čas njihovega nastopa in trajanje. Prvi in zadnji T_{pc} sovpada z nastopom in izginotjem fazne sinhronizacije med srčnim in respiratornim oscilatorjem, slika 13 (c).

Na podoben način kot smo analizirali srčno-respiratorno sklopitev bi lahko analizirali tudi sklopitev med srčnim oscilatorjem in valovi delta iz EEG signala in respiratornim oscilatorjem in valovi delta iz EEG signala, kar pa ni predmet tega dela. Valčni bispekter se je izkazal kot obetavno orodje za analizo EEG signalov med anestezijo.

ZAKLJUČEK

Osnovna motivacija dela je bil razvoj orodja za proučevanje medsebojnega vpliva podsistemov kardiovaskularnega sistema. Z orodjem, ki bi bilo občutljivo na časovno spremenljivo vsebino, želimo povečati možnosti razkrivanja narave in pomena sklopitev. Sklopitve omogočajo izmenjavo informacije med procesi in so tako temelj za pravilno delovanje sistema krvnega obtoka. Frekvenca in amplituda vsake opazovane oscilacije nam pričata o aktivnosti oscilatorja in učinku vseh sklopitev. Sklopitve so torej ključnega pomena za razumevanje kardiovaskularnega in morda tudi celotnega človeškega sistema. Bolezensko stanje vodi v fiziološke spremembe, ki se odražajo v spremembah dinamičnih lastnosti kardiovaskularnega sistema. Poznavanje sklopitev pomeni možnost zaznavanja bolezenskega stanja v njegovem začetnem stadiju, ko je potreben minimalni zdravniški poseg.

Razvito časovno občutljivo bispektralno metodo omogoča določitev narave sklopitev med sklopljenimi oscilatorjimi. Prednosti so: (i) možnost hkratnega opazovanja celotnega frekvenčnega področja; (ii) ugotavljanje sklopitev dveh ali več medsebojno sklopljenih oscilatorjev; (iii) določanje jakosti sklopitve; (iv) določanje narave sklopitve: linearna, nelinearna kvadratična ali parametrična v eni od frekvenc; (v) metoda je primerna za analizo šumnih signalov.

Učinek sklopitev med srčnim in respiratornim oscilatorjem je prej epizodičen kot stalen in nespremenljiv. Frekvenčne in fazne sklopitve se izmenjujejo. Nelinearne sklopitve obstajajo tako med spontanim kot enakomernim dihanjem. Sklopitve med oscilatorji so šibke. Bispektralna in križna bispektralna analiza sta pokazali, da je informacija o sklopitvi med srčnim in respiratornim procesom lastna procesoma in prostorsko invariantna. Oba procesa sta centralnega izvora. Njuno fazno razmerje lahko opazujemo v signalu EKG, signalu krvnega pretoka in signalu krvnega pritiska, izmerjenih na različnih med seboj oddaljenih mestih. Nelinearna narava sklopitev med srčnim in respiratornim je vrojena in postane bolj izrazita, ko je frekvenca dihanja konstantna. Bispektralna analiza je torej sposobna določevati frekvenčne in fazne sklopitve med CV procesi in s tem primerna za razumevanje kardiovaskularnih signalov.

V primerjavi s sinhrogramom je bolj občutljiva na sklopitve in manj občutljiva na šum. Zazna fazne sklopitve, vendar na drugačen način kot jih podaja sinhrogram. Med sklopitveno informacijo, dobljeno s sinhrogramom in z bispektrom, ne moremo določiti enostavne povezave.

Valčna bispektralna metoda signalov krvnega pretoka ne da opazno boljših rezultatov kot Fourierova bispektralna metoda. To velja pri analizi srčno-respiratorno sklopitve pri določenih pogojih, po katerih sklepamo na nelinearno sklopitev.

Za obdelavo signalov sta primernejša valčni in križno valčni bispekter kot bispekter na osnovi Fouriereve transformacije. Omogočata ugotavljanje kratkočasovnih faznih sklopitev, optimalno časovno in frekvenčno ločljivost, enostavno povezavo med skalo in frekvenco, neposredno interpretacijo, normalizacijo na energijo (moč), manjšo statistično napako, poljuben frekvenčni korak in sta računsko manj potratna.

Iz dobljenih rezultatov valčne bispektralne analize signala EEG podgane med anestezijo lahko sklepamo, da so srčni in respiratorni kardiovaskularni oscilator in valovi delta iz EEG signala med anestezijo sklopljeni. Anestezija lahko vpliva na valove delta iz EEG signala tako, da ti vodijo srčni in respiratorni sistem v sinhronizacijo.

Valčni bispekter lahko omogoči povezavo med teoretičnim kardiovaskularnim modelom in eksperimentalnimi meritvami.

IZVIRNI PRISPEVKI K ZNANOSTI

Pomembnejši izvirni prispevki k znanosti:

1. Ugotavljanje sklopljenih nelinearnih oscilatorjev z uporabo časovno občutljivih bispektralnih cenilk za biamplitudo in bifazo.

Vpeljali smo časovno občutljivi bispektralni cenilki - biamplitudo (6) in bifazo (5) - za razkrivanje faznih sklopitev v univariatnih podatkih (poglavje 3, strani od 13 do 16). Pokazali smo, da je vpeljana metoda primerna za proučevanje sklopljenih nelinearnih oscilatorjev. Sposobna je meriti jakost fazne sklopitve z bispektralno cenilko - biamplitudo, katere vrednost je proporcionalna vrednosti koeficienta medsebojne sklopitve ϵ (2.6) sklopljenih nelinearnih oscilatorjev (poglavje 2, strani od 7 do 12) in razkriti naravo sklopitve, t.j., ali je sklopitev dodana linearna, kvadratična ali parametrična v eni od frekvenc (poglavje 4, strani od 17 do 28).

2. Potrditev hipoteze o sklopitvi med srčnim in respiratornim oscilatorjem v človeškem kardiovaskularnem sistemu.

Prvi smo uporabili vpeljano časovno bispektralno metodo na signalih krvnega pretoka za proučevanje narave srčno-respiratorne sklopitve. Kljub omejeni možnosti za razkrivanje metode med linearno in nelinearno sklopitvijo v ekstremnih razmerah je metoda uporabna, dokler sklopitve ne postanejo preveč zapletene, upoštevajoč fiziološko poznavanje kardiovaskularnega sistema (poglavje 5, strani od 29 do 56). Sklopitve med srčnim in respiratornim oscilatorjem so epizodične, prej kot stalne in nespremenljive. Frekvenčne in fazne sklopitve se izmenjujejo. Nelinearne sklopitve obstajajo tako med spontanim kot enakomernim dihanjem. Izrazitejše so pri enakomernem dihanju. Sklopitve med oscilatorji so šibke (poglavji 5 in 6, strani od 28 do 37 in od 57 do 76). Informacija o sklopitvi med srčnim in respiratornim procesom je lastna procesoma in prostorsko, znotraj CVS, invariantna. Oba procesa sta centralnega izvora. Njuno fazno razmerje lahko opazujemo v signalu EKG, signalu krvnega pretoka in signalu krvnega pritiska, izmerjenih na različnih med seboj oddaljenih mestih (poglavje 5, strani od 37 do 46).

3. Posplošitev bispektralnih cenilk na transformacijo z valčki

Bispektralni cenilki - biamplitudo (22) in bifazo (21) - smo posplošili na transformacijo z valčki. Metoda je primernejša za ugotavljanje kratkočasovnih sklopitev. Omogoča za nas optimalno časovno in frekvenčno ločljivost. Valčni bispekter lahko omogoči povezavo med

teoretičnim kardiovaskularnim modelom in eksperimentalnimi meritvami (poglavji 7 in 8, strani od 77 do 106).

4. Ugotovitev sklopitve med srčnim in respiratornim sistemom ter delta valovi signala EEG z uporabo posplošenih bispektralnih značilk.

Delta valovi iz EEG signala podgane med splošno anestezijo razkrivajo fiziološko razmerje med srčnim in respiratornim sistemom in delta valovi iz EEG signala. Srčno-respiratorna sinhronizacija je lahko posledica vodenja delta valov iz EEG signala podgane med splošno anestezijo (poglavje 9, strani od 107 do 114).

Nekateri deli disertacije so objavljeni v naslednjih člankih:

1. J. Jamšek, A. Stefanovska, P.V.E. McClintock and I.A. Khovanov, Time-phase bispectral analysis, Phys. Rev. E **68**, 016201 (2003).

2. J. Jamšek, A. Stefanovska and P.V.E. McClintock, Nonlinear cardio-respiratory interactions revealed by time-phase bispectral analysis, Physics in Medicine and Biology **49**, 4407 (2004).

Nekateri deli disertacije so bili predstavljeni na sledečih znanstvenih srečanjih:

1. J. Jamšek and A. Stefanovska, Bispectral analysis of cardiovascular signals, Nonlinear Seminar, Department of nonlinear physics, Lancaster University, United Kingdom (7.2. 2002).

2. J. Jamšek, A. Stefanovska and P.V.E. McClintock, Time-phase bispectral analysis, basic theory and applications, Nonlinear Seminar, Department of nonlinear physics, Lancaster University, United Kingdom (12.5. 2002).

3. J. Jamšek, A. Stefanovska and P.V.E. McClintock, Cardiovascular System, Cardiovascular system, time-phase bispectral analysis, basic theory and application, 2nd Slovenia-Japan Seminar, Center for Applied Mathematics and Theoretical Physics University of Maribor, Slovenia (28.5.-5.6 2003).

4. J. Jamšek and A. Stefanovska, Quadratic cardio-respiratory coupling?, INTAS international Workshop, Department of Physics, University of Pisa, Italy (22-24.4. 2003).

5. J. Jamšek, A. Stefanovska and P.V.E. McClintock, Nonlinear cardio-respiratory interaction, INTAS-ESF international Workshop, Ljubljana, Slovenia (10-13.11. 2003).

ABSTRACT

Bispectral analysis, a technique based on high-order statistics, is extended to encompass time dependence for the case of coupled noisy nonlinear oscillators. It is applicable to univariate, as well as to multivariate, data obtained respectively from one or more of the oscillators. It is demonstrated for a generic model of interacting systems, whose basic units are Poincaré oscillators. Their frequency and phase relationships are explored for different coupling strengths, both with and without Gaussian noise. The distinctions between additive linear, quadratic, and parametric (frequency modulated) interactions in presence of noise are illustrated.

Bispectral analysis has been used to study the nature of the coupling between cardiac and respiratory activity. Univariate blood flow signals recorded simultaneously on both legs and arms were analysed. Coupling between cardiac and respiratory activity was also checked by use of bivariate data and computation of the cross-bispectrum between ECG and respiratory signals and surrogate data of blood flow signals. Measurements were made on six healthy males, aged 25-27 years, during spontaneous breathing and during paced respiration, at frequencies, both lower and higher than that of spontaneous respiration.

It was confirmed that the dynamics of blood flow can be usefully considered in terms of coupled oscillators, and demonstrated that interactions between the cardiac and respiratory processes are weak and time-varying, and that they can be nonlinear. Nonlinear coupling was revealed to exist during both spontaneous and paced respiration. Relation of bispectral analysis to synchronization is outlined in the example of cardiovascular ECG and respiration signals of rats undergoing anaesthesia. Bispectrum proves to be more sensitive to interactions than the synchrogram. It detects the phase synchronization, and nevertheless, yields different information from that which can be resolved from a synchrogram.

Wavelet transform was incorporated into bispectrum and adopted to analyse cardiovascular signals using a Morlet wavelet as a mother wavelet. A time dependant biphase/biamplitude estimate, with higher frequency resolution at low frequencies, and higher time resolution at higher frequencies, was obtained. Its advantages, compared to Fourier based bispectrum, are discussed and demonstrated for a generic model of interacting systems, whose basic units are Poincaré oscillators, in the application of CV blood flow signals, and in the application of EEG signal of rat undergoing anaesthesia. The wavelet bispectrum may provide a link between theoretical CVS models and experimental measurements.

CONTENTS

NOMENCLATURE

a	oscillator's amplitude
a_m	multiplication factor for additional Morlet mother wavelet stretching
A	biamplitude
$b(t)$	blood flow signal
$B(k, l) = Ae^{j\phi}$	discrete bispectrum
$B_a(k, l)$	adapted discrete bispectrum
$B_c(k, l)$	cross-bispectrum
$c^*, c \in C$	complex conjugation
c_n	normalization constant
C	reconstruction constant
d	exponential decay of Gaussian function of Morlet wavelet
D	noise intensity
f	oscillator's characteristic (cyclic) frequency
f_s	sampling frequency
Δf	frequency step
F	forcing amplitude
G_e	Gaussian function of Morlet wavelet edge value
$H_{i,j}$	coupling term
j	unit imaginary
k	discrete frequency (in bins)
$(k, l, k+l)$	triplet
K	number of data segments
l	discrete frequency (in bins)
L	$L \cdot L$ area for bispectrum frequency averaging
L_t	number of samples for time averaging
M	discrete Fourier transform window size
$M_3(k, l)$	third-order moment
n	discrete time
N_p	number of periods entering the windowed signal
N_W	number of samples in the interval T: $\{T_0 - T/2 \leq \tau \leq T_0 + T/2\}$
O	percentage of segments overlapping
$p(t)$	blood pressure signal
$P(k)$	discrete power spectrum

r	limit cycle radius
$r(t)$	respiration signal
$s(t)$	surrogate data
t	continuous time
Δt	time step
T_{HF}	fixed Morlet wave length for high frequencies
T_m	Morlet mother wavelet length
T_{qc}	Time duration of quadratic coupling
$w(n)$	window
$W(s, t)$	wavelets transform
WB	wavelet bispectrum
WB_c	cross-wavelet bispectrum
$\mathbf{x}$	state vector
$x(n)$	discrete signal
$X(k)$	discrete Fourier transform

α	oscillator's limit cycle approaching rate
ε	coupling coefficient
μ	coupling coefficient
η	coupling coefficient
η_m	frequency modulation strength coeficient
ψ	phase difference between interacting oscillators
$\xi(t)$	zero-mean white Gaussian noise
π	constant = 3.141592...
ϕ	biphase
ϕ_0	initial biphase
ω	angular frequency; $\omega = 2\pi f$
Ω	observed frequency of interacting oscillator

Notation convention. For conciseness the notation $B(f_1, f_2)$ is often used in this thesis to denote the discrete bispectrum at the discrete bifrequency (k, l) which corresponds most closely to the normalised bifrequency (f_1, f_2). If the frequencies f_1, f_2 fall exactly on discrete frequency bins, then $(k = Mf_1, l = Mf_2)$. If they fall in between the discrete bins then $(k \approx Mf_1, l \approx Mf_2)$.

Acronyms and abbreviations

BIS	Bispectral Index
CV	CardioVascular
CVS	CardioVascular System
DFT	Discrete Fourier Transform
EEG	ElectroEncephaloGram
ECG	ElectroCardioGram
FT	Fourier Transform
FB	Fourier Bispectrum
HOS	High-Order Statistics
IT	Inner Triangle
RSA	Respiratory Sinus Arrhythmia
SDFT	Selective Discrete Fourier Transform
STFT	Short time Fourier Transform
WB	Wavelet Bispectum
WT	Wavelet Transform

1 INTRODUCTION

Most real systems are nonlinear and complex. In general, they may be regarded as a set of interacting subsystems; given their nonlinearity, the interactions can also be expected to be nonlinear.

Phase relationships between a pair of interacting oscillators can be obtained from bivariate data (i.e., where the coordinate of each oscillator can be measured separately) by use of the methods recently developed for analysis of synchronization, or generalized synchronization, between chaotic and/or noisy systems. Not only can the interactions be detected [79], but their strength and direction can also be determined [72, 93, 94, 103]. The next logical step in studying the interactions among coupled oscillators must be to determine the nature of the couplings; the methods developed for synchronization analysis do not provide us with the means to answer this question.

Studies of higher order spectra, or polyspectra, offer a promising way forward in digital signal processing. The approach is applicable to interacting systems, quite generally, regardless of whether or not they are mutually synchronized. Following the pioneering work of Brillinger and Rosenblatt [11], increasing applications of polyspectra have appeared in a diversity of fields, such as: telecommunications, radar, sonar, speech, biomedical, geophysics, imaging systems, surface gravity waves, acoustics, econometrics, seismology, nondestructive testing, oceanography, plasma physics and seismology. An extensive overview can be found in [120]. The use of bispectrum as a means of investigating the presence of second-order nonlinearity in interacting harmonic oscillators has been of particular interest during the last few years [20, 25, 48, 68, 74, 85].

Systems are usually taken to be stationary. For real systems, however, the mutual interaction among subsystems often results in time-variability of their characteristic frequencies. Frequency and phase couplings can occur temporally, and the strength of coupling between pairs of individual oscillators may change with time. In studying such systems, bispectral analysis for stationary signals, based on time averages, is no longer sufficient. Rather, the time evolution of bispectral estimates is required.

Priestley and Gabr [80] were probably the first to introduce the time-dependent bispectrum for harmonic oscillators. Most of the subsequent work has been related to the time-frequency representation and is based on high-order cumulants [5, 26]. The parametric approach has been used to obtain approximate expressions for the evolutionary bispectrum [87]. Furthermore, Perry and Amin have proposed a recursion method for estimating the time-dependent bispectrum [76]. Dandawaté and

Giannakis have defined estimators for cyclic and time-varying moments, and cumulants of cyclostationary signals [16]. Schack *et al.* [98] have recently introduced a time-varying spectral method for estimating the bispectrum and bicoherence: the estimates are obtained by filtering in the frequency domain and then obtaining a complex time-frequency signal by inverse Fourier transform. Their assumption is, however, that the interacting oscillators are harmonic.

Millingen *et al.* [61, 62] introduced the wavelet bicoherence, and were the first to demonstrate the use of bispectra for studying interactions among nonlinear oscillators. They used the method to detect periodic and chaotic interactions between two coupled van der Pol oscillators, but without concentrating on time-phase relationships in particular.

It has long been known that the heart of a healthy human subject in repose does not beat regularly. The rhythmic variation in the heart rate occurring at the frequency of respiration is known as respiratory sinus arrhythmia (RSA), which can be seen in [3, 18, 23, 34, 117] and references therein; it is not the only arrhythmia [112]. In fact, at least *five* characteristic frequencies can be seen in blood flow signals, at ~1 Hz, 0.3 Hz, 0.1 Hz, 0.04 Hz and 0.01 Hz. The first two components correspond to the cardiac and respiratory oscillators respectively. The component at ~0.1 Hz is often attributed to intrinsic myogenic activity. The other two correspond respectively to neural and endothelial related metabolic activity. The wavelet transforms of such signals have been discussed in detail [6, 7, 111].

The cardiac and respiratory systems can be perceived from the nonlinear dynamics point of view as coupled autonomous oscillators, each with its own characteristic frequency [112, 115, 116]. It is respiratory sinus arrhythmia - the rhythmic fluctuations of electrocardiographic R-R intervals, or the rhythmic modulation of the instantaneous cardiac frequency - that provides the most obvious manifestation of their coupling. Although the interaction between the cardiac and respiratory rhythms has been known to exist since the early works by Hales [29] and Ludwig [56], the underlying physiological mechanisms are not completely understood. In his recent review, Eckberg [23] discusses several possible mechanisms for respiratory gating, of both central and peripheral origin: central, secondary to efferent respiratory motoneurone activity; and peripheral, secondary to afferent neural activity from pulmonary and thoracic stretch receptors. He presents a wide range of evidence favouring the influence of respiration on R-R interval fluctuations (as well as on the fluctuations in systolic blood pressure that are strongly correlated to the R-R fluctuations), rather than the influence of peripheral baroreceptor physiology as an origin of modulation. As the physiological mechanisms of cardio-respiratory coupling are not fully understood, even less is known about the nature of this coupling, e.g., whether it is linear, quadratic, or of an even higher-order.

In addition to the modulation, a mutual adjustment of the cardiac and respiratory rhythms may occur, leading to their synchronization: in a conscious healthy subject at rest, the cardiac and respiratory systems have been shown to synchronize for short periods of time [10, 99-101]. The state of the system is characterized by the interactions and couplings between the oscillatory physiological processes. For instance, in anaesthesia, the cardiac and respiratory systems synchronize for more extended periods of time [114]. It has also been shown that during anaesthesia, RSA is reduced [1, 83].

Not only CV signals are relevant for studying CVS. Neural CV subsystem coupling information is incorporated in the brain waves. Bispectral index (BIS) is a processed electroencephalogram (EEG) parameter that purports to measure the level of hypnosis in anaesthetized patients. The BIS was formulated retrospectively using a large database of EEG recordings and clinical correlative data. It incorporates parameters derived by high-order spectra, and is one of the most widely applied cases of high-order spectra [89] use. The EEG measures electrical activity in the brain, i.e., brainwaves of different frequencies and short-lived evoked potentials that occur when the brain responds to sensory input. Quantification of nonlinear quadratic phase-coupling between EEG signal components has been established since G. Dumermuth's pioneered investigations using bispectral analysis in 1969 [51]. A number of EEG studies have been published using the mathematical tools of high-order spectra analysis EEG [12, 27, 53, 65]. Recently the depth of anaesthesia was found to be related to synchronization states between the cardiac and respiratory oscillators [63, 64].

The interactions can be detected by analysis of the recorded time series, and their strength and direction can also be determined [72, 73, 93, 94, 103]. The next logical step in studying interactions among the coupled oscillators must be to determine the nature of the couplings from the time series.

A long-term aim is therefore to develop a coupled oscillator model that can provide a description of the system, quantify the couplings and relate their values to its different states of health or disease. We may thus aim for improved techniques of early diagnosis, better assessment of the efficacy of treatment for a range of cardiovascular diseases, and perhaps quantification of depth of anaesthesia.

The thesis is organised as follows: Chapters 2 provides a brief overview of the human cardiovascular system, viewed from a point as a dynamical system, and outlines cardio-respiratory interaction; Chapter 3 briefly describes bispectral analysis and introduces our development of a new approach [40] that introduces time dependence to the bispectral analysis of univariate data, while focusing on the time-phase relationships between two (or more) interacting systems. Chapter 4 presents our demonstration/testing of the aforementioned technique on a well-characterized simple model.

Examples of different kinds of interaction among the subsystems, e.g., additive linear or quadratic, or parametric frequency modulation, both with, and without, the consideration of zero-mean white Gaussian noise. Chapter 5 gives application of the new technique to univariate cardiovascular (CV) blood flow signals, which reflect the activities of both the local and central mechanisms of cardiovascular regulation [41]. We summarise how measurements are made, discuss how the resultant data are analysed, and present the results. In 5.8 Discussion, it is shown that the cardiac and respiratory processes can be nonlinearly phase coupled. Chapter 6 establishes the relation between bispectral analysis and synchronization. Chapter 7 introduces the time-frequency variant resolution in the bispectrum, using wavelet transform. Chapter 8 compares bispectrum based on Fourier transform, and bispectrum based on wavelet transform. Chapter 9 displays these new potentials of usage, using the case of an electroencephalogram signal. Chapter 10 provides an overview of the main results of the work, and outlines areas where more work is required. Chapter 11 presents drawn conclusions.

Appendix A details the normalization techniques used for comparison of the different measurements. Appendix B provides an analysis of harmonic generation by a pair of weakly-coupled weakly-nonlinear oscillators.

2 CARDIOVASCULAR SYSTEM

Rhythms are among the most conspicuous properties of living systems. They occur at all levels of biological organization, from unicellular to multicellular organisms, with periods ranging from fractions of a second to years, Tab. 2.1. In humans, the cardiac and respiratory functions and the circadian rhythms of a sleep and wakefulness point to the key role of periodic processes in the maintainance of life. In spite of their close association with physiology, however, periodic phenomena are by no means restricted to living systems. Oscillatory chemical reaction was discovered by Bray in 1921, the reaction of Bray, Belousov and Zhabotinsky reaction in 1959, respectively 1964 and others.

Tab. 2.1: A list of the main biological rhythms, classified according to increasing period.

Rhythm	Period
Neural rhythms	0.01 to 10 s (and more?)
Cardiac rhythms	1 s
Calcium oscillations	1 s to several minutes
Biochemical oscillations	1 minute to 20 minutes
Mitotic cycle	10 minutes to 24 h (or more)
Hormonal rhythms	10 minutes to several hours (also 24 hours)
Circadian rhythms	24 hours
Ovarian cycle	28 days (human)
Annual rhythms	1 year
Epidemiology and ecological oscillations	years

However, oscillatory behaviour does not always possess a simple periodic nature. Thus, both in chemistry and biology, oscillations sometimes present complex patterns of bursting, in which successive trains of high-frequency spikes are separated at regular intervals by phases of quiescence. In the phase space, sustained oscillations correspond to the evolution towards a closed curve called a limit cycle by Poincaré of it's uniqueness and independence from initial conditions (Minorsky, 1962). Time taken to travel along the closed curve represents the period of oscillations. When a single limit cycle exists, the system always evolves towards the same closed curve characterized by a fixed

amplitude and period, for a given set of parameter values, regardless of the initial state of the system. Moreover, sustained oscillations of limit cycle type can be viewed as a temporal dissipative structure (Prigogine, 1968).

2.1 Background

The human cardiovascular or circulatory system is one of the basic systems that plays an essential role in the maintenance of a constant internal body environment [3, 55]. It distributes matter and energy to the cells and removes by-products of their metabolism. The cells extract matter and energy from the blood which is pumped by the heart into the network of vessels. The lungs, where the blood becomes oxygenated, are also part of the cardiovascular network.

The circulatory system can be divided into two parts: the pulmonary circulation, which moves blood trough the lungs for exchange of oxygen and carbon dioxide and systemic circulation, which supplies all other tissues. Both, the pulmonary and systemic circulation have a pump, an arterial system, capillaries and a venous system. Arteries and arterioles function as a distribution system. Capillaries serve to exchange diffusible substances between blood and tissue. Venules and veins serve as collection and storage vessels that return the blood to the heart.

The heart of a relaxed, healthy subject, pumps an amount equivalent to the total amount of blood in the body (i.e., 4-6 litres or 7-8 % of the body weight) in approximately one minute [55]. Thus, in cardiovascular dynamics we consider the dynamics of blood distribution trough the cardiovascular network on a time scale of approximately one minute. It can be characterised by the dynamics of the blood flow and the blood pressure in the system, and the activity of the lungs and the heart pump.

The research has shown [8, 9, 10, 110-112, 117], that cardiovascular blood flow signals posses a deterministic dynamic, meaning, that the cardiovascular system is a result of a final number of subsystems (oscillators), each with its own characteristic frequency. Five subsystems take part in blood flow regulation: cardiac, respiratory, myogenic, neural and endothelial metabolic system. They all regulate blood flow that they have in common.

The function of the heart is manifested as electric potentials spread across the heart muscle, and as a mechanical pump that rhythmically expels the blood into the arterial network approximately once per

second (1 Hz[4]) [55]. However, the period of the heart cycle is not constant but, rather, varies in time. The lungs can be seen as a pressure generator [55]. The frequency of respiration also varies between 0.15 and 0.3 Hz consequently, the flow and the pressure change in an oscillatory fashion with time, and do so on several different time scales. Peripheral blood flow depends from the systems that control the blood vein diameter - the blood flow resistance. The smooth-muscle cells in the vessel walls respond continually to the changes in intravascular pressure, which is known as the myogenic response. This intrinsic rhythmic activity of the vessels, caused by the pacemaker cells in the smooth muscles of their walls, is called myogenic activity. The vessels contractions respond to the changes in the blood flow and blood pressure and are related to the characteristic frequency at approximately 0.1 Hz [50].

Beside the myogenic activity at least two more systems influence the veins resistance. The first one is the neural control, provided by the autonomous nerve innervations of vessel. Having it's origin in some centres in the brainstem that are connected to other parts of the central nervous system, and sensors throughout the whole network of vessels, it provides synchronization of the function of the entire system. It's characteristic frequency is approximately 0.04 Hz [45]. The second one corresponds to metabolic activity. A number of substances, which are required for cellular metabolism or are produced as metabolites, have an effect on the state of contraction of vascular musculature. The rhythmic regulation of vessel resistance to the blood flow, initiated by concentrations of metabolic substances, can be related to characteristic frequency at approximately 0.01 Hz [3, 8, 110].

2.2 Coupled oscillators

Cardiovascular subsystems do interact among them selves even at healthy human in rest, therefore their characteristic frequencies are not constant but, rather, varie in time and their amplitudes are modulated [3, 18, 23, 34, 117]. Each system can be regarded as an autonomous nonlinear oscillator with its own characteristic frequency that can be detected in the power spectrum of the cardiovascular blood flow signal. Phase couplings and synchronization can onset among separate oscillators. It has been shown recently [9, 79, 94, 97, 113, 114] that cardiac and respiratory oscillations are synchronized. Synchronization or adjusting in time onsets when two or more nonlinear oscillators are coupled. It can be seen in form of their frequency or phase interactions. After Huygens the synchronization is frequency adjustment of autonomous harmonic oscillators[5] due to their weak

[4] Characteristic frequencies differ from human to human. Given values are result of estimated characteristic frequencies obtained by frequency analysis of blood flow signals for case of young, healthy male humans.
[5] Oscillators can be chaotic or noisy.

interaction. Phase coupling is thus onset of some phase relations among interacting systems while it doesn't necessary exist any amplitude correlation.

The coupling effect on the interacting oscillator's behaviour depends on coupling strength. While weak couplings result in oscillator's characteristic frequency varying, strong couplings can cause qualitative changes in system behaviour named as phase transitions [13]. If there were no couplings among cardiovascular oscillators sharp peaks would occur in power spectrum and the characteristic frequency ratio would be proportional what is not the case for healthy human in rest where the ratio is at most rational. Appearance of a resonance is a phenomenon, where the system breaks down and the death occurs.

Couplings enable information exchange among processes and are basic for normal cardiovascular system activity. Understanding of physiological nature of these couplings is of essential meaning for the understanding of the whole system. Each detected oscillations frequency and amplitude describes the oscillator's activity and impact of all couplings. It is not possible to measure separate oscillator's activity, therefore various methods are used to analyse phase, frequency and amplitude couplings.

A subsystem of the cardiovascular system may be represented as an oscillator, described by a state vector **x** which satisfies [115, 116]:

$$\frac{d\mathbf{x}}{dt} = f(\mathbf{x}, s), \tag{2.1}$$

where **x** is the nonlinear rate function and s denotes the parameter of the oscillator. A simple limit cycle oscillator, as proposed by Poincaré [128],

$$\frac{dx_1^i}{dt} = \alpha_i x_1^i (a_i - r_i) - 2\pi f_i x_2^i, \tag{2.2}$$

$$\frac{dx_2^i}{dt} = \alpha_i x_2^i (a_i - r_i) + 2\pi f_i x_1^i,$$

where

$$r_i = \sqrt{x_1^{i\,2} + x_2^{i\,2}}, \tag{2.3}$$

can be used to describe a basic unit of the system. It possesses the structural stability and robustness necessitated by physiological understanding and the analysis of measured time series. The state variables x_1^i and x_2^i describe the flow and velocity of the flow contributed by the i-th oscillator.

Five oscillators are assumed to contribute to the blood flow trough the cardiovascular system: cardiac, respiratory, myogenic, neural and endothelial related metabolic activity. Each of them is characterized by a frequency f_i and amplitude a_i. The constant α_i determines the rate at which the state vector approaches the limit cycle. In polar coordinates, with radius r_i and angle ϕ_i the state variables are

$$x_1^i = r_i \cos\phi_i \text{ and } x_2^i = r_i \sin\phi_i. \tag{2.4}$$

The system (2.2) then becomes

$$\begin{aligned} \frac{dr_i}{dt} &= \alpha_i r_i (a_i - r_i), \\ \frac{d\phi_i}{dt} &= 2\pi f_i. \end{aligned} \tag{2.5}$$

The system has two steady-state solutions, where $dr_i/dt = 0$, at $r_i = 0$ and $r_i = a$. The limit cycle oscillations at $r_i = a$ is stable and globally attracting for all initial conditions, except the origin. In the limit as $t \to \infty$ the state of the oscillator on the limit cycle is essentially described by the angle ϕ, the phase. The periodic solution travels around with period $T_i = 1/f_i$, Fig. 2.1.

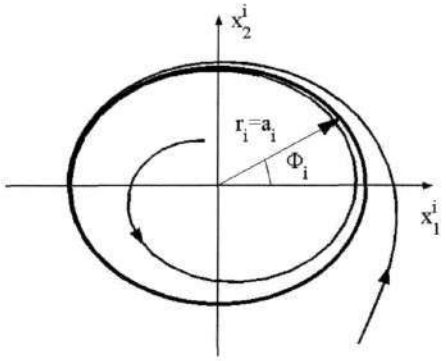

Fig. 2.1: The phase plane solutions of differential equations (2.2) for a basic oscillator. The asymptotically stable limit cycle is $r_i = a_i$ with phase $\phi_i = 2\pi f_i t$, if $\phi_i = 0$ is taken at $t = 0$.

However, the characteristic frequencies of the cardiovascular system vary in time [6, 7, 110, 111]. Therefore, besides the autonomous part, we suppose that there also exists a component resulting from mutual interactions. Accordingly, we add a coupling term to differential equations (2.2) $H_{i,j}(\mathbf{x}_1^j, \mathbf{x}_2^j)$, $j \neq$ i:

$$\frac{dx_1^i}{dt} = \alpha_i x_1^i (\alpha_i - r_i) - 2\pi f_i x_2^i + \varepsilon_i H_{i,j}(\mathbf{x}_1^j, \mathbf{x}_2^j), \tag{2.6}$$

$$\frac{dx_2^i}{dt} = \alpha_i x_2^i(\alpha_i - r_i) + 2\pi f_i x_1^i + \varepsilon_i H_{i,j}(\mathbf{x}_1^j, \mathbf{x}_2^j),$$

where ϵ_i is a coupling coefficient. $H_{i,j}(x_1^j, x_2^j)$ represents all possible influences from the rest of the system on the *i*-th oscillator.

In case of cardio-respiratory interaction, the coupling terms are not symmetrical, i.e., impact of respiration on the heart differs from the impact of the heart on respiration.

If there is no coupling between the oscillators ($\epsilon_i = 0$), each will oscillate at its own frequency and the state vector in the four dimensional phase space approaches the so-called attracting invariant torus. Analogously to the one-dimensional system discussed above, in the limit as $t \to \infty$, the original system of four differential equations can be reduced to a two dimensional system describing the flow on a two dimensional torus. The amplitudes of both oscillators define the torus, while the flow on a torus can be described entirely in terms of the rate of change of phases of the first (ϕ_1) and second (ϕ_2) oscillator. In the uncoupled case,

$$\frac{d(\phi_1 - \phi_2)}{dt} = 2\pi(f_2 - f_1), \tag{2.7}$$

and so the phase difference increases at a constant rate, determinated by the differences between the natural frequencies of both oscillators (f_1 and f_2).

If two oscillators are loosely coupled ($\epsilon_i << 0$), so that each has only small effect on the other, the invariant torus does not vanish, but is only slightly different. There states are close, $|x^1(t) - x^2(t)| \sim 0$, but remain different. Different types of synchronization may be expected, depending on the type of coupling.

Synchronization is defined as phase locking or frequency entrainment [79]. In case of cardiovascular system, with time-varying characteristic frequencies, phase synchronization may onset, while the frequencies may or may not be entrained, we use a weaker condition for phase locking [79]

$$|n\phi_1 - m\phi_2 - \delta| < \text{const}, \tag{2.8}$$

where n and m are integers, ϕ_1, ϕ_2 are the phases of two oscillators and δ is some phase shift. In case of real systems, measured data contain some noise. It can be instrumental, numerical (resulting from

quantization of analogue signals) or physiological (the effect of interactions with the rest of the system on the measured quantity). For weak noise the phase difference $\phi_{n,m} = n\phi_1 - m\phi_2$ would be expected to fluctuate in a random way around a constant value. In case of strong noise, phase slips would occur.

3 METHOD

Bispectral analysis belongs to a group of techniques, based on high-order statistics (HOS) that may be used to analyse non-Gaussian signals, to obtain phase information, to suppress Gaussian noise of unknown spectral form, and to detect and characterize signal nonlinearities [60, 68, 69]. In what follows we extend bispectral analysis to extract useful features from nonstationary data, and we demonstrate the modified technique by application to test signals generated from coupled oscillators.

3.1 Bispectral analysis

The bispectrum involves third-order statistics. Spectral estimation is based on the conventional Fourier type direct approach, through computation of the 3rd-order moments which, in the case of 3rd order statistics, are equivalent to 3rd-order cumulants [60, 66-69].

The classical bispectrum estimate is obtained as an average of estimated 3rd-order moments (cumulants) $\hat{M}_3^i(k,l)$ [69]:

$$\hat{B}(k,l) = \frac{1}{K}\sum_{i=1}^{K} \hat{M}_3^i(k,l), \tag{3.1}$$

where the 3rd-order moment estimate $\hat{M}_3^i(k,l)$ is performed by a triple product of Discrete Fourier Transforms (DFTs) at discrete frequencies k, l and $k+l$ [69]:

$$\hat{M}_3^i(k,l) = X_i(k)X_i(l)X_i^*(k+l), \tag{3.2}$$

with $i = 1,..., K$ segments into which the signal is divided to try to obtain statistical stability of the estimates [67]. Algorithm for bispectrum estimation is described in detail in [39].

The bispectrum $B(k, l)$ is a complex quantity, defined by magnitude A and phase ϕ

$$B(k,l) = |B(k,l)|e^{j\angle B(k,l)} = Ae^{j\phi}. \tag{3.3}$$

Consequently, for each (k, l), its value can be represented as a point in a complex space, $\Re[B(k, l)]$ versus $\Im[B(k, l)]$, thus defining a vector. Its magnitude (length) is known as the biamplitude. The phase, which for the bispectrum is called the biphase, is determined by the angle between the vector and the positive real axis.

As discussed in detail in [39], the bispectrum quantifies the relationships among the underlying oscillatory components of the observed signals. Specifically, bispectral analysis examines the relationships between the oscillations at two basic frequencies, k and l and a harmonic component at the frequency $k + l$. This set of three frequencies is known as a triplet $(k, l, k + l)$. The bispectrum $B(k, l)$, a quantity incorporating both phase and power information, can be calculated for each triplet.

A high bispectrum value at bifrequency (k, l) indicates that there is at least frequency coupling within the triplet of frequencies k, l, and $k \pm l$. Strong coupling implies that the oscillatory components at k and l may have a common generator. Such components may synthesize a new component at the combinatorial frequency, $k \pm l$, if a quadratic non-linearity is present.

3.2 Time-phase bispectral analysis

The classical bispectral method is adequate for studying stationary signals whose frequency content is preserved over time. We now wish to encompass time dependence within the bispectral analysis. In analogy with the Short Time Fourier transform (STFT), we accomplish this by moving a time window $w(n)$ of length M across the signal $x(n)$, calculating the DFT at each window position [81]

$$X(k,n) \cong \frac{1}{M}\sum_{n=0}^{M-1} x(n)w(n-\tau)e^{-j2\pi nk/M}. \tag{3.4}$$

Here, k is the discrete frequency, n the discrete time and τ the time shift. The choice of window length M is a compromise between achieving optimal frequency resolution and optimal detection of the time-variability. The instantaneous biphase is then calculated: from Eqs. (3.2) and (3.3), it is

$$\phi(k,l,n) = \phi_k(n) + \phi_l(n) - \phi_{k+l}(n). \tag{3.5}$$

If the two frequency components k and l are frequency and phase coupled, $\phi_{k+l} = \phi_k + \phi_l$, it holds that the biphase is 0 (2π) radians. For our purposes the phase coupling is less strict because dependent frequency components can be phase-delayed. We consider phase coupling to exist if the biphase is constant (but not necessarily = 0 radians) for at least several periods of the lowest frequency component. Simultaneously, we observe the instantaneous biamplitude from which it is possible to infer the relative strength of the interaction:

$$A(k,l,n) = \left| X_k(n) X_l(n) X^*_{k+l}(n) \right|. \tag{3.6}$$

We thus hope to be able to observe the presence and persistence of coupling among the oscillators.

3.3 Normalization

Just as the discrete power spectrum has a point of symmetry at the folding frequency $f_s/2$, the discrete bispectrum has many symmetries in the k, l plane [77, 78]. For real signals, the bispectrum has 12 symmetry regions. Because of these, it is necessary to calculate the bispectrum only in the non-redundant region, or principal domain, as shown in Fig. 3.1.

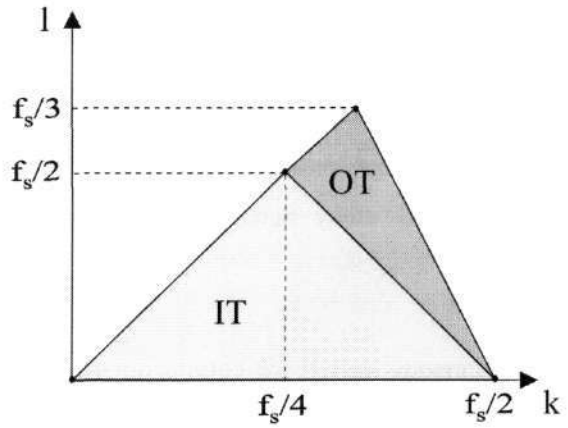

Fig. 3.1: The principal domain of the discrete bispectrum of a band-limited signal can be divided into two triangular regions, the inner triangle (IT) and the outer triangle. k and l are discrete frequencies, f_s is the sampling frequency.

The latter can be divided into two triangular regions in which the discrete bispectrum has different properties: the inner triangle (IT), and the outer one [32, 33, 105]. In the current work it is the IT that

is of primary interest. Thus it is sufficient to calculate the bispectrum over the IT of the principal domain defined in [25, 69]: $0 \leq l \leq k$, $k+l \leq f_s/M/2$.

To be able to compare results a normalization procedure was performed. For each bispectrum and biphase estimate, a bispectrum was first calculated for the whole IT using the same parameters, i.e., number of segments, segment length, percentage of segment overlap, type of tapering window, and size of window for frequency averaging. The normalization value was calculated as the average bispectrum estimate over the IT [40].

Normalization is parameter dependent. The more segments (short windows) for the bispectrum calculation, the higher its average value over the IT becomes. It has local maxima, because the width of the window directly affects the frequency resolution. The better the frequency resolution, the smaller the leakage effect. Higher percentages of overlap result in a lower average value over the IT, whereas the frequency averaging window increases the average value.

The normalized bispectrum also indicates the average level of quadratic nonlinear phase coupling and, in a way, serves as an indicator of how non-Gaussian the signal is [31].

The critical values for the bispectrum and biamplitude estimates were normalized to 1. If the estimated value is higher than the average value of bispectrum in the IT, then it is taken as valid. By critical value is meant a value that exceeds the leakage affect, the noisy background (other than Gaussian), and rounding errors.

4 ANALYSIS OF COUPLINGS

To illustrate the essence of the method, and to test it, we use a generic model of interacting systems whose basic unit is the Poincaré oscillator [128]:

$$\begin{aligned} \dot{x}_i &= -x_i q_i - \omega_i y_i + g_{x_i}, \\ \dot{y}_i &= -y_i q_i + \omega_i x_i + g_{y_i}, \\ q_i &= \alpha_i(\sqrt{x_i^2 + y_i^2} - a_i). \end{aligned} \tag{4.1}$$

Here, x and y are vectors of the oscillator state variables, α_i, a_i and ω_i are constants and $g_y(y)$ and $g_x(x)$ are coupling vectors. The activity of each subsystem is described by the two state variables, x_i and y_i, where $i = 1,..., N$ denotes the subsystem.

The form of the coupling terms can be adjusted to study different kinds of interaction among the subsystems, e.g., additive linear or quadratic, or parametric frequency modulation. Examples will be considered both without, and with, a zero-mean white Gaussian noise to obtain more realistic conditions.

Different cases of interaction are demonstrated for signals generated by the proposed model. In each case we analyse the x_1 variable of the first oscillator, recorded as a continuous time series. For the first 400 s, the inter-oscillator coupling strength was zero. It was then raised to a small constant value. After a further 400 s, it was increased again. The first 15 s and corresponding power spectrum for each coupling strength are shown in the figures for each test signal, in order to demonstrate the changes in spectral content and behaviour caused by the coupling. For bispectral analysis the whole signal is analysed as a single entity, but the transients caused by the changes in coupling strength are removed prior to processing. First the classical bispectrum is estimated. Bifrequencies where peaks provide

evidence of possible frequency interactions are then further studied by calculation of the biphase and biamplitude as functions of time. They were calculated using a window of length 100 s, moved across the signal in 0.3 s steps. For this analysis the proposed normalization in Sec. 3.3 was not used. In all cases bispectral estimates were calculated and then the values were multiplied by a constant 10^9.

4.1 Linear couplings

Let us start with the simplest case of a linear interaction between coupled oscillators. We suppose the model (4.1) to consists of only two oscillators, $i = 1, 2$. The parameters of the model are set to $\alpha_1 = 1$, $a_1 = 0.5$ and α_2, $a_2 = 1$. The coupling term is unidirectional and linear

$$g_{x_1} = \eta_2 x_2, g_{y_1} = \eta_2 y_2. \tag{4.2}$$

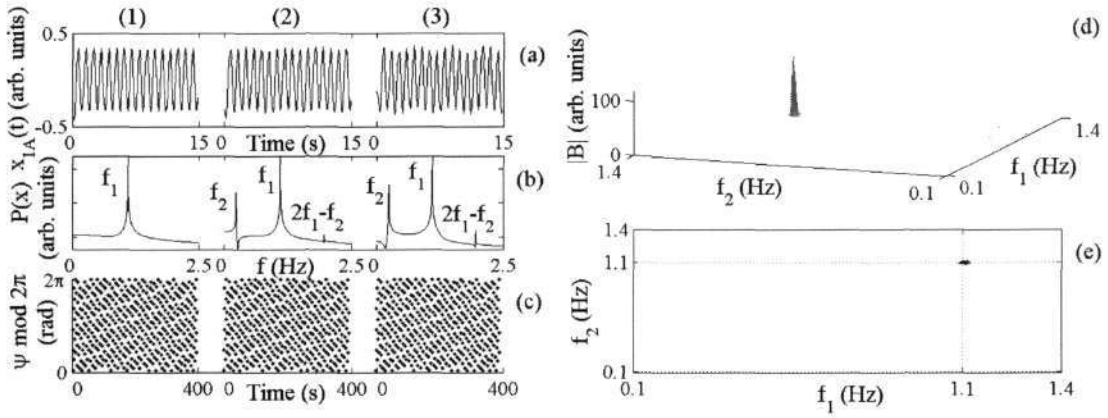

Fig. 4.1: Results in the absence of noise. (a) The test signal $x_{1A}(t)$, variable x_1 of the first oscillator with characteristic frequency $f_1 = 1.1$ Hz. The characteristic frequency of the second oscillator is $f_2 = 0.24$ Hz. The oscillators are unidirectionally and linearly coupled with three different couplings strengths: $\eta_2 = 0.0$ (1); 0.1 (2); and 0.2 (3). Each coupling lasts for 400 s at sampling frequency $f_s = 10$ Hz. Only the first 15 s are shown in each case. (b) Its power spectrum and (c) synchrogram. (d) The bispectrum $|B|$, using $K = 33$ segments, 66 % overlapping and the Blackman window to reduce leakage and (e) its contour view.

The test signal $x_{1A}(t)$ is the variable x_1 of the first oscillator. It is presented in Fig. 4.1 (a) with the corresponding power spectrum for three different coupling strengths: no coupling $\eta_2 = 0$; and weak couplings $\eta_2 = 0.1$, 0.2. The peaks labelled as $f_1 = 1.1$ Hz and $f_2 = 0.24$ Hz are the independent harmonic components of the first and the second oscillator. These frequencies are deliberately chosen to approximately have a non-integer ratio. There is also at least one peak present at the harmonically

related position $f_3 = 2f_1 - f_2$ attributable to interaction between the two oscillators. It arises from the nonlinearity of the first oscillator, but is caused by the forcing of the second oscillator.

The principal domain of the bispectrum for the test signal x_{1A}, Fig. 4.1 (d), shows one peak at the bifrequency (1.1 Hz, 1.1 Hz), the so called self-coupling. No other peaks are present. Bispectral analysis examines the relationships between oscillations at the two basic frequencies, f_1 and f_2 and a modulation component at the frequency $f_1 \pm f_2$ which is absent from the power spectra in Fig. 4.1 (b). Therefore no peak is present at bifrequency (1.1 Hz, 0.24 Hz). Thus the method as it stands is incapable of detecting the presence of linear coupling between the oscillators by analysis of the test signal x_{1A}. Nonetheless, we still suggest the use of bispectral analysis to investigate the presence of non-linearity, but based on an adapted way of calculating the bispectrum.

In general the bispectral method can be used to examine phase and frequency relationships at arbitrary time. It is thus well suited for detecting the presence of quadratic couplings and frequency modulation, since they both give rise to frequency components at the sum and difference of the interacting frequency components.

To be able to detect linear couplings using the bispectral method, as proposed, it is necessary to change the frequency relation. Study of coupled Poincaré oscillators demonstrates the presence of a component at frequency $2k - l$ as a consequence of nonlinearity. This component was detected numerically, and is not necessarily characteristic of all nonlinear oscillators. By modifying the bispectral definition to

$$B_a(k,l) = E\left[X(k)X(l)X^*(2k-l)\right], \tag{4.3}$$

the biphase turns into

$$\phi_a(k,l) = \phi_k + \phi_l - \phi_{2k-l} - \phi_c, \tag{4.4}$$

where index a is introduced and will be used in what follows to indicate that the values are obtained using the adapted method. To obtain 0 radians in the case of phase coupling we have to correct the adapted biphase expression (4.4) by subtracting $\phi_c = 2\phi_1 - \phi_k$. In the presence of a harmonically related frequency component, and phase coupling, the biphase will then be 0 radians.

The adapted bispectrum $|B_a|$ for the signal x_{1A} exhibits several peaks, as shown in Fig. 4.2 (a). It peaks where $f_1 = f_2$; a triple product (f_1, f_2, f_3) of power at frequencies $f_1 = f_2 = f$, and also $f_3 = 2f_1 - f_2 = f$, raises a high peak at the bifrequency (f, f). The self-coupling peak is physically meaningless, and it is

therefore cut from the adapted bispectrum. It can be used for additional checking, since it strongly implies non-linearity [127].

The peak of primary interest is at bifrequency (1.1 Hz, 0.24 Hz). There is also a high peak positioned at bifrequency (0.67 Hz, 0.24 Hz) lying on the line where the third frequency in the triplet is equal to the frequency of the first oscillator and is therefore a consequence of the method. The small peaks present in the adapted bispectrum are the result of leakage effects and numerical rounding error due to the DFT calculation.

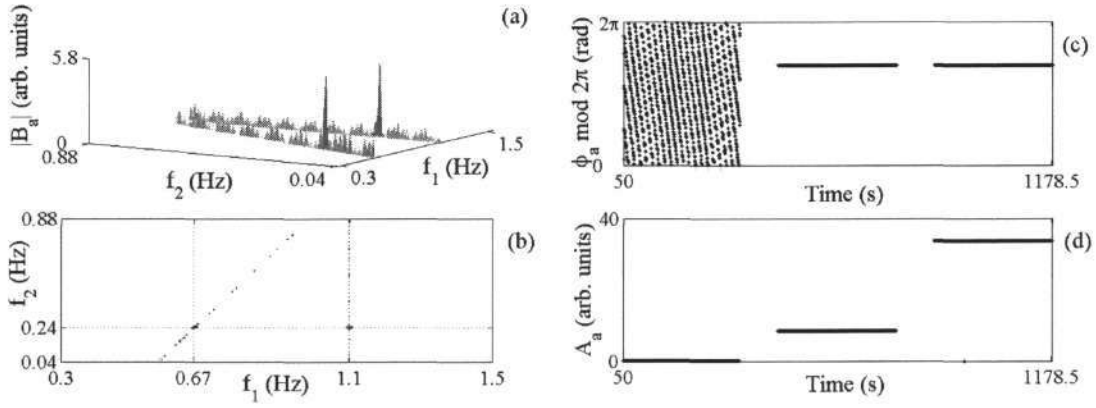

Fig. 4.2: (a) Adapted bispectrum $|B_a|$, calculated from the test signal x_{1A} using K = 34 segments, 80 % overlapping and the Blackman window and (b) its contour view. Regions of the adapted bispectrum above $f_2 >$ 0.88 Hz and below $f_1 < 0.3$ Hz are cut, because the triplets (1.1 Hz, 1.1 Hz, 1.1 Hz) and (0.24 Hz, 0.24 Hz, 0.24 Hz) produce high peaks that are physically meaningless. (c) Adapted biphase ϕ_a and (d) biamplitude A_a for bifrequency (1.1 Hz, 0.24 Hz), using a 0.3 s time step and a 100 s long Blackman window for estimating the DFT.

The peak (1.1 Hz, 0.24 Hz) indicates that oscillations at those pairs of frequencies are at least linearly frequency-coupled. Frequency coupling alone is sufficient for a peak in the bispectrum to occur. Although the situation can in principle arise by coincidence, frequency and phase coupling together strongly imply the existence of nonlinearities. To be able to distinguish between different possible couplings we calculate the adapted biphase Fig. 4.2 (c).

During the first 400 s of test signal x_{1A}, where no coupling is present, the adapted biphase changes continuously between 0 and 2π radians. For the same time of observation it can be seen that the adapted biamplitude is 0, Fig. 4.2 (d). During the second and third 400 s of the signal x_{1A}, a constant adapted biphase can be observed indicating the presence of linear coupling. The value of the adapted biamplitude is higher in the case of stronger coupling. The coupling constant η_2 can be obtained by normalization, and we are thus able to define the relative strengths of different couplings.

When the oscillators are coupled bidirectional the frequency content of each of them changes and components $2f_1$ and $2f_2$ are generated. Both of these characteristic frequencies can be observed in the time series of each oscillator. Two combinatorial components are also present in their spectra, $2f_1 - f_2$ and $f_1 - 2f_2$, assuming that $f_1 > f_2$. In analysing bidirectional coupling the procedure described above can be extended and two combinatorial components should be analysed in the same way.
Making use of the calculated instantaneous phases of both oscillatory components we also construct a synchrogram (Fig 4.1 (c)), as proposed by Schäfer *et al.* (see Ref. [79] and the references therein), and can immediately establish whether or not the coupling also results in synchronization.

The instantaneous phases can also be used to calculate the direction and strength of coupling, using the methods recently introduced by Schreiber, Rosenblum *et al.* and Paluš *et al.* [72, 93, 94, 103].

4.2 Linear couplings in presence of noise

We now test the method for the case where noise is added to the variable x_1 of the first oscillator:

$$\begin{aligned} \dot{x}_1 &= -x_1 q_1 - \omega_1 y_1 + g_{x_1} + \xi(t), \\ \dot{y}_1 &= -y_1 q_1 + \omega_1 x_1 + g_{y_1}, \\ q_1 &= \alpha_1 (\sqrt{x_1^2 + y_1^2} - a_1). \end{aligned} \tag{4.5}$$

Here, $\xi(t)$ is zero-mean white Gaussian noise, $\langle \xi(t) \rangle = 0$, $\langle \xi(t), \xi(0) \rangle = D\delta(t)$, and $D = 0.08$ is the noise intensity. In this way we obtain a test signal $x_{1B}(t)$, Fig. 4.3 (a).

For nonzero coupling strength η_2, the component at frequency position f_3 can still be seen in the power spectrum despite the noise Fig. 4.3 (b). The adapted biphase Fig. 4.3 (f) can clearly distinguish between the presence and absence of coupling. When coupling is weaker, the adapted biamplitude [Fig. 4.3 (g)] is lower and the adapted biphase is less constant.

The bispectrum for the signal x_{1B}, shown in Fig. 4.4 (a), differs from that in the case of zero noise, Fig. 4.1 (d). Noise raises two additional peaks positioned at (1.1 Hz, 0.24 Hz) and (0.86 Hz, 0.24 Hz). The former could be the result of interaction; the latter is due to the method: the sum of the frequencies in this bifrequency pair gives the frequency of the first oscillator. Close inspection of the (1.1 Hz, 0.24 Hz) peak by calculation of the biphase gives Fig. 4.4 (c). When coupling is present the characteristic frequency of the second oscillator appears in the power spectrum Fig. 4.3 (b). Two frequencies of high amplitude result in a small peak even if no harmonics are present at the sum and/or difference

frequencies. The second peak is not of interest to us. It can easily be checked whether a phase coupling exists among the bifrequencies from the time evolution of the biphase.

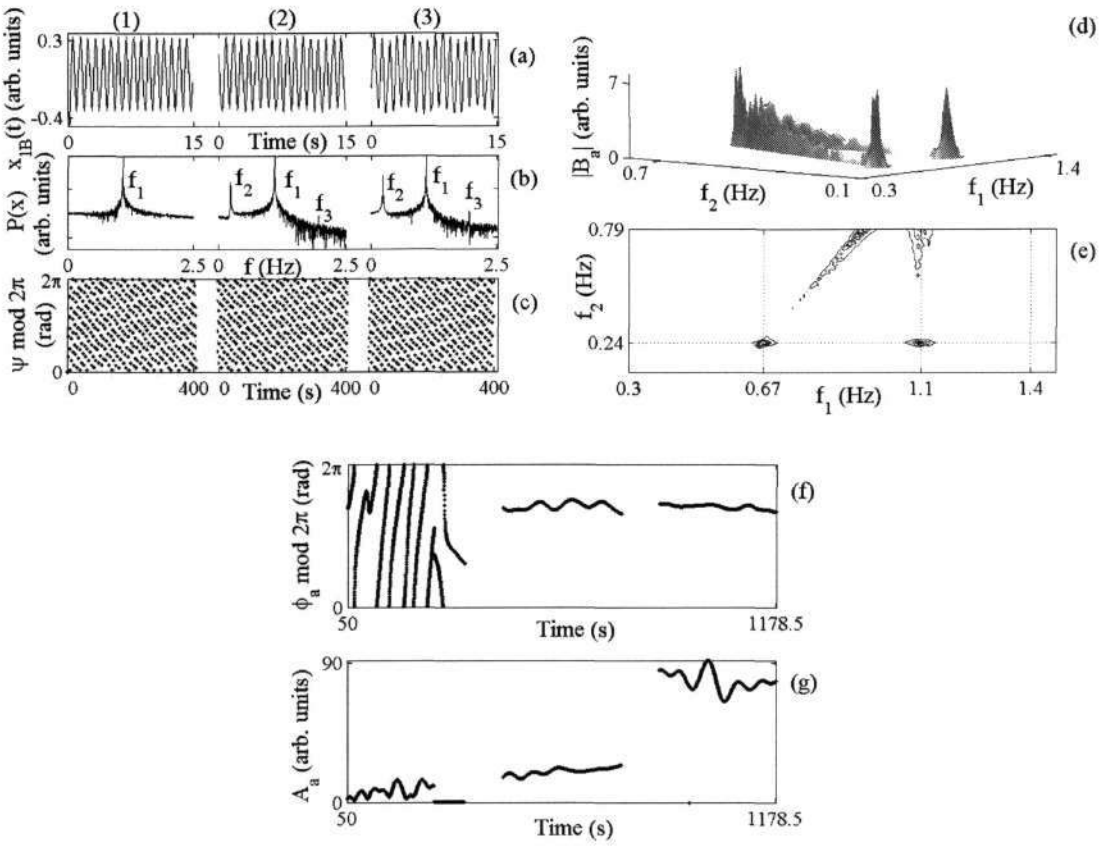

Fig. 4.3: Results in the presence of additive Gaussian noise. (a) Test signal x_{1B}, variable x_1 of the first oscillator with characteristic frequency f_1 = 1.1 Hz. The characteristic frequency of the second oscillator is f_2 = 0.24 Hz. The oscillators are unidirectionally and linearly coupled with three different coupling strengths; η_2 = 0.0 (1); 0.1 (2); and 0.2 (3). Each coupling lasts for 400 s at a sampling frequency f_s = 10 Hz. Only first 15 s are shown in each case. (b) Its power spectrum and (c) synchrogram. (d) Adapted bispectrum $|B_a|$ using K = 33 segments, 66 % overlapping and the Blackman window and (e) its contour view. The parts of the $|B_a|$ above $f_2 > 0.79$ Hz and below $f_1 < 0.3$ Hz are omitted because the triplets (1.1 Hz, 1.1 Hz, 1.1 Hz) and (0.24 Hz, 0.24 Hz, 0.24 Hz) produce a high peak that is physically meaningless. (f) Adapted biphase ϕ_a and (g) adapted biamplitude A_a for bifrequency (1.1 Hz, 0.24 Hz), using 0.3 s time step and 100 s long window for estimating the DFT using the Blackman window.

In general, besides estimating bispectral values, one can also observe the time dependences of the phase and amplitude for each frequency component, and their phase relationships. This applies particularly to frequencies that form a bifrequency giving a high peak in the bispectrum or adapted bispectrum. Synchrograms, Fig. 4.1 (c) and 4.3 (c), are obtained by first calculating the instantaneous phase of each oscillator, and then their phase difference [79]. The phase difference in this case is

between two fixed frequencies. We do not calculate their instantaneous frequencies, although it is possible to follow the frequency variation by calculating the phase difference at neighbouring bifrequencies around the observed one and showing them simultaneously on the same plot. Examples of the phase difference $\Psi = \phi_1 - \phi_2$ between the phases of the first ϕ_1 and the second ϕ_2 interacting oscillators are shown in Fig. 4.4 (e) and (f). Bispectral relation to synchronization is discussed in detail in Chapter 6.

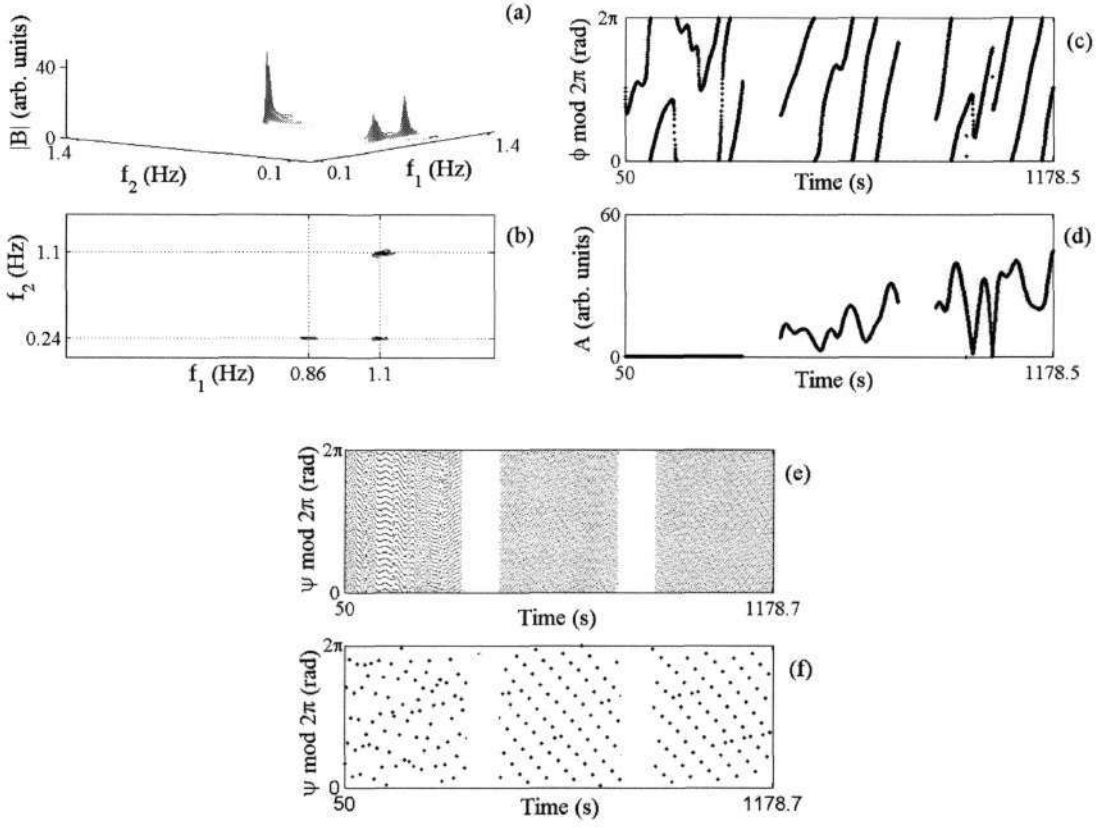

Fig. 4.4: Bispectrum $|B|$, calculated from the signal x_{1B} presented in Fig. 4 (a), using $K = 33$ segments, 66 % overlapping and Blackman window to reduce leakage and (b) its contour view. (c) Biphase ϕ and (d) biamplitude A for bifrequency (1.1 Hz, 0.24 Hz), using a 0.3 s time step and a 100 s long window for estimating the DFTs using a Blackman window. (e) Phase difference Ψ between ϕ_1 of the characteristic frequency component f_1 of the first oscillator and ϕ_2 of the characteristic frequency component f_2 of the second oscillator, for time step $1/f_s$ and (f) at each period of lowest frequency $1/f_2$ in the bifrequency pair (1.1 Hz, 0.24 Hz), using interpolation and 100 s long window for estimating DFTs using Blackman window.

4.3 Quadratic couplings

We now assume that two Poincaré oscillators can interact with each other nonlinearly. A quadratic nonlinear interaction generates higher harmonic components in addition to the characteristic frequencies [69]. In order to study an example where the first f_1 = 1.1 Hz and second f_2 = 0.24 Hz oscillators are quadratically coupled, we change the coupling terms in the model (3.1) to quadratic ones

$$g_{x_1} = \eta_2 (x_1 - x_2)^2, g_{y_1} = \eta_2 (y_1 - y_2)^2. \tag{4.6}$$

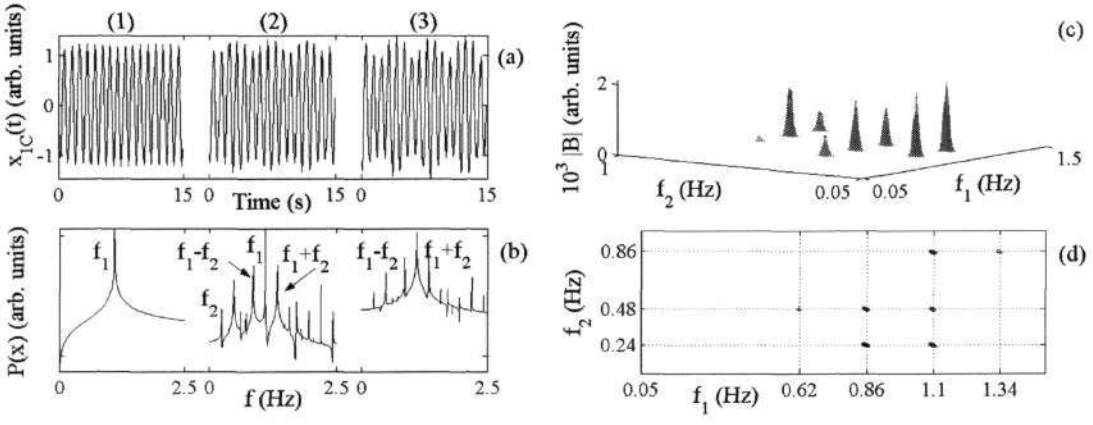

Fig. 4.5: Results for quadratic coupling in the absence of noise. (a) The test signal x_{1C}, variable x_1 of the first oscillator with characteristic frequency f_1 = 1.1 Hz. The characteristic frequency of the second oscillator is f_2 = 0.24 Hz. Oscillators are unidirectionally and quadratically coupled with three different couplings strengths: η_2 = 0.0 (1); 0.05 (2); and 0.1 (3). Each coupling lasts for 400 s at sampling frequency f_s = 10 Hz. Only the first 15 s are shown in each case. (b) Its power spectrum. (c) The bispectrum $|B|$ using K = 33 segments, 66 % overlapping and the Blackman window to reduce leakage and (d) its contour view. The part of the bispectrum above f_2 > 1,0 Hz is cut, because triplet (1.1 Hz, 1.1 Hz, 1.1 Hz) produces a high peak that is not physically significant.

Clearly, the test signal x_{1C} presented in Fig. 4.5 (a) for three different coupling strengths (no coupling η_2 = 0 (1); and weak couplings η_2 = 0.05 (2), η_2 = 0.1 (3)) has a richer harmonic structure. In addition to the characteristic frequencies, it contains components with frequencies $2f_1$, $2f_2$, $f_1 + f_2$ and $f_1 - f_2$ Fig. 4.5 (b). Eq. (4.6) also indicates that, as well as having a particular harmonic structure, the components of the signal x_{1C} also have related phases, $2\phi_1$, $2\phi_2$, $\phi_1 + \phi_2$ and $\phi_1 - \phi_2$.

We expect several peaks (three and not four, because the triplet $(f_1, f_2, f_1 + f_2)$ has the same peak in the bispectrum as the triplet $(f_1, f_2, f_1 - f_2)$) to arise in the bispectrum. The peak of principal interest is at bifrequency (1.1 Hz, 0.24 Hz). As before, the self-coupling peaks are at (1.1 Hz, 1.1 Hz) and (0.24 Hz, 0.24 Hz) are of no interest, so they are cut from the bispectrum. Additional peaks appear at the

bifrequencies (0.86 Hz, 0.24 Hz), (0.62 Hz, 0.48 Hz), (0.86 Hz, 0.48 Hz), (1.1 Hz, 0.48 Hz), (1.1 Hz, 0.86 Hz) and (1.34 Hz, 0.86 Hz). The triplet of harmonically related frequency components (f_1, f_2, f_3) would peak in the bispectrum when the power for all these frequencies differs from zero. The components 0.48 Hz, 0.86 Hz, 1.34 Hz and 2.2 Hz resulting from quadratic couplings form such triplets which peak in the bispectrum: (0.86 Hz, 0.24 Hz, 1.1 Hz), (0.86 Hz, 0.48 Hz, 1.34 Hz) and (1.34 Hz, 0.86 Hz, 2.2 Hz). Besides these, there are also other peaks e.g., that at the bifrequency (0.62 Hz, 0.48 Hz) arising from the triplet (0.62 Hz, 0.48 Hz, 1.1 Hz); the sum/difference combination of such frequencies always give the characteristic frequency, or one that results from quadratic coupling. The existence of such peaks has no other meaning than as a strong indicator of second-order nonlinearity. Consequently, the biphase for all peaks due to possible nonlinear mechanisms in the bispectrum must have the same value, and same behaviour, as shown e.g., in Figs. 4.6 (a) and 4.6 (c). The biphase is constant in the presence of quadratic coupling. From the biamplitude, the coupling constant can be determined by normalization.

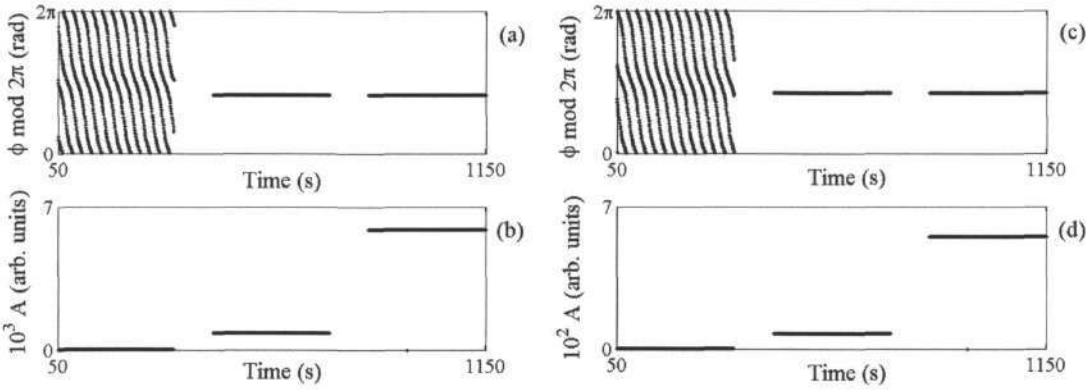

Fig. 4.6: (a) The biphase ϕ and (b) biamplitude A for the test signal x_{1C} for bifrequency (1.1 Hz, 0.24 Hz), using 0.3 s time step and 100 s long window for estimating DFT using Blackman window. (c) Biphase and (d) biamplitude for the bifrequency (0.86 Hz, 0.24 Hz), with a 0.3 s time step and a 100 s long window for estimating DFT using the Blackman window.

In the power spectrum there is a component at frequency $2f_1 - f_2$, even although linear coupling is absent. It arises from nonlinearity in the Poincaré oscillator. The adapted bispectrum for the signal x_{1C} shows a peak at bifrequency (1.1 Hz, 0.24 Hz), but the adapted biphase varies continuously: we may therefore exclude the possibility of linear coupling being present.

4.4 Quadratic couplings in the presence of noise

As in the case of linear coupling (Sec. 4.2.) we add a noise term to the quadratic coupling g_{x1} and obtain the test signal x_{1D}, presented in Fig. 4.7 (a).

Using the bispectral and adapted bispectral methods, we find that we obtain results very similar to those in the absence of noise. The method is evidently noise robust. The results for non-zero coupling are quite different from those where coupling is absent, Fig. 4.7 (e).

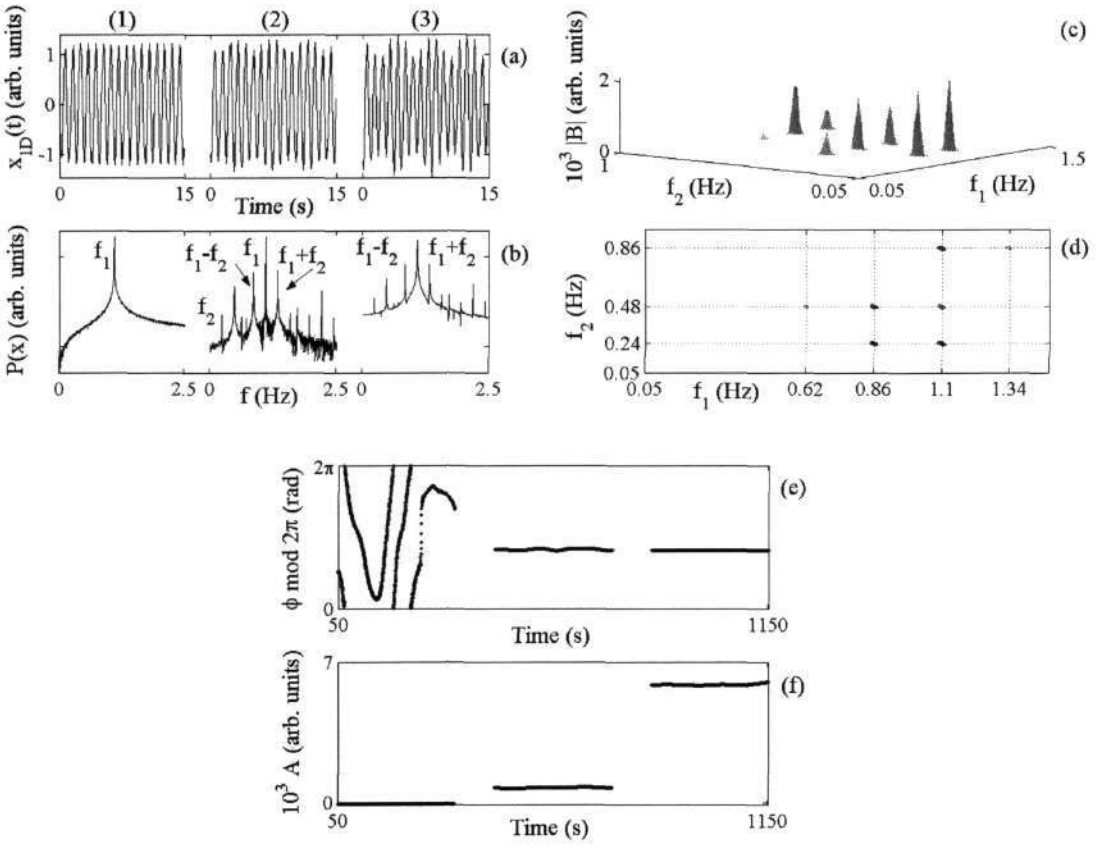

Fig. 4.7: Results for quadratic couplings in the presence of additive Gaussian noise. (a) The test signal x_{1D}, variable x_1 of the first oscillator with characteristic frequency f_1 = 1.1 Hz. The characteristic frequency of the second oscillator is f_2 = 0.24 Hz. The oscillators are unidirectionally and quadratically coupled with three different coupling strengths: η_2 = 0.0 (1); 0.05 (2); and 0.1 (3). Each coupling lasts for 400 s at a sampling frequency f_s = 10 Hz. Only the first 15 s are shown in each case. (b) Its power spectrum. (c) The bispectrum $|B|$ calculated with K = 33 segments, 66 % overlapping and using the Blackman window to reduce leakage and (d) its contour view. The part of the bispectrum above f_2 > 1.0 Hz is cut, because the triplet (1.1 Hz, 1.1 Hz, 1.1 Hz) produce a high peak that is physically meaningless. (e) The biphase ϕ and (f) biamplitude A for bifrequency (1.1 Hz, 0.24 Hz), with a 0.3 s time step and a 100 s long window for estimating DFTs using the Blackman window.

4.5 Frequency modulation in the presence of noise

We are also interested of being able to detect parametric frequency modulation and to distinguish it from quadratic coupling. Parametric modulation produces frequency components at the sum and difference of the characteristic frequency and the modulation frequency, i.e., the same two frequency components that can also result from quadratic coupling. Let us now consider an example where the first oscillator f_1 = 1.1 Hz is frequency modulated by the second one f_2 = 0.24 Hz. For this purpose the equations of the first oscillator become

$$\begin{aligned} \dot{x}_1 &= -x_1 q_1 - y_1(\omega_1 + \eta_m x_2) + \xi(t), \\ \dot{y}_1 &= -y_1 q_1 + x_1(\omega_1 + \eta_m y_2), \\ q_1 &= \alpha_1(\sqrt{x_1^2 + y_1^2} - a_1). \end{aligned} \tag{4.7}$$

The model parameters $\alpha_{1,2}$, $a_{1,2}$ and the noise intensity D are chosen to be the same as in the previous examples.

We thus obtain a test signal x_{1E}. It is the time evolution of the variable x_1 of the first oscillator, presented in Fig. 4.8 (a) with the corresponding power spectrum 4.8 (b) for three different parametric frequency modulation strengths: no modulation $\eta_m = 0$ (1); and modulation $\eta_m = 0.1$ (2), $\eta_m = 0.2$ (3). The bispectrum of the test signal x_{1E}, Fig. 4.8 (c), exhibits several high peaks. The highest are at bifrequencies (1.1 Hz, 0.86 Hz), (0.86 Hz, 0.24 Hz) and (1.1 Hz, 0.24 Hz), in addition to the (1.1 Hz, 1.1 Hz) peak. They also appear in the case of quadratic coupling. In general, however, the other peaks that appear for quadratic coupling are absent. The reason is that although the component of the second oscillator f_2 (one component of the triplet) is not present in the power spectrum, its value is not exactly zero.

Observing the biphase, no epochs of constant biphase can be observed, although for strong frequency modulation the biphase is less variable. In the power spectrum, Fig. 4.8 (b), no component rises above the noise level at frequency f_2, of the bifrequency pair, where the bispectrum peaks. This is an indication that there is parametric coupling between the oscillators as there is a high value of biamplitude. The biphase changes runs between 0 and 2π, and is modulated in the absence of noise. There are also no rapid 2π phase slips of the kind that are normal if no modulation is present. In the absence of couplings and modulation, but with noise present, there would be no such peaks in the power spectrum and bispectrum.

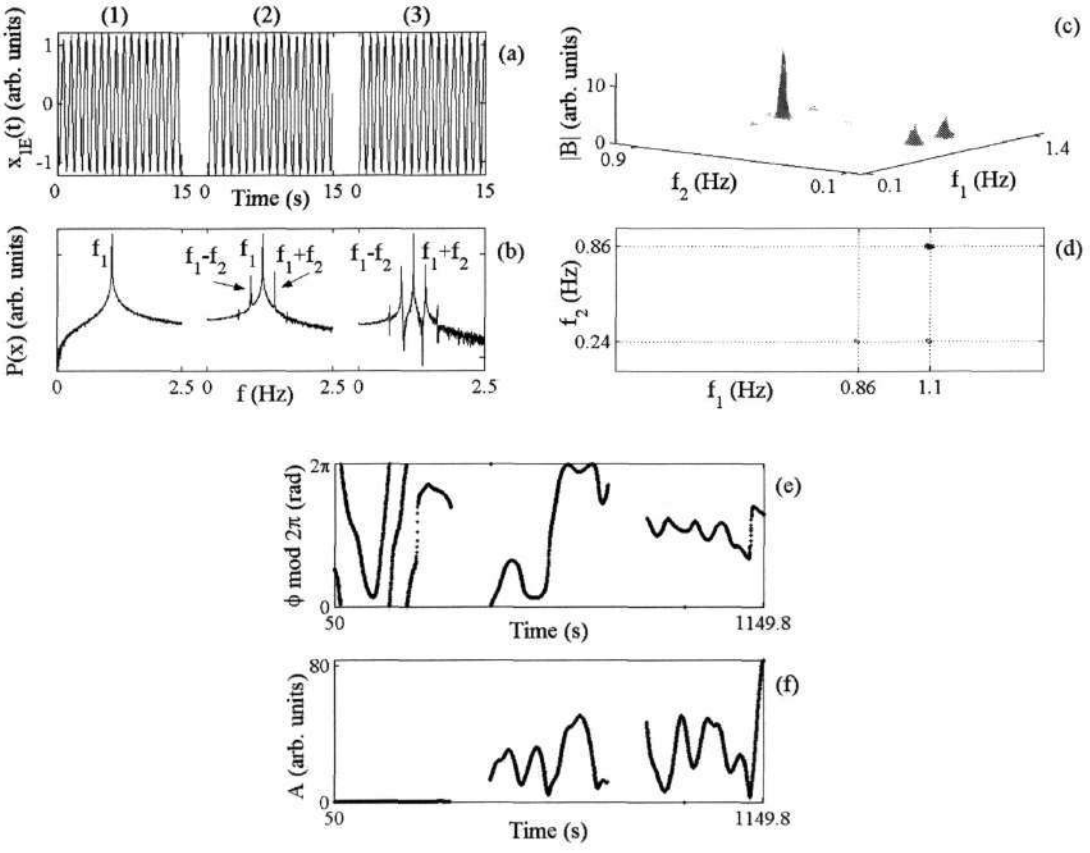

Fig. 4.8: Results for parametric frequency modulation in the presence of additive Gaussian noise. (a) The test signal x_{1E}, of variable x_1 of the first oscillator with characteristic frequency f_1 = 1.1 Hz frequency modulated by the second oscillator f_2 = 0.24 Hz with three different frequency modulation strengths; η_m = 0.0 (1), 0.1 (2) and 0.2 (3). Each frequency modulation lasts for 400 s, at sampling frequency f_s = 10 Hz. Only the first 15 s are shown in each case. (b) Its power spectrum. (c) The bispectrum $|B|$ calculated with K = 33 segments, 66 % overlapping and using the Blackman window to reduce leakage and (d) its contour view. The part of the bispectrum above f_2 > 1.0 Hz is cut, because the triplet (1.1 Hz, 1.1 Hz, 2.2 Hz) produces a high peak that is physically meaningless. (e) The biphase ϕ and (f) biamplitude A for bifrequency (1.1 Hz, 0.24 Hz), with a 0.3 s time step and a 100 s long window for estimating the DFTs using the Blackman window.

5 CARDIO-RESPIRATORY INTERACTIONS

5.1 Data acquisition

The interaction between two harmonic components can in practice contribute to the power at their sum and/or difference frequencies. We assume that the cardiac and respiratory oscillators are weakly coupled and can interact with each other nonlinearly. The coupling is assumed to be weak in part because of the transient/episodic character of cardio-respiratory synchronization in healthy subjects; the assumption of weak nonlinearity is on account of several factors including the lack of combinatorial components near the cardiac frequency. We return to these questions and discuss them in more detail at the end of Sec. 5.8.2. A quadratic interaction will give rise to higher harmonic components with frequencies $2f_1$, $2f_2$, $f_1 + f_2$ and $f_1 - f_2$, in addition to the characteristic frequencies [68, 69]. As well as having a particular harmonic structure, the components also have phases that are related, $2\phi_1$, $2\phi_2$, $\phi_1 + \phi_2$ and $\phi_1 - \phi_2$.

As discussed in detail in [39], the bispectrum quantifies the relationships among the underlying oscillatory components of the observed signals. Specifically, bispectral analysis examines the

relationships between the oscillations at two basic frequencies, f_1 and f_2 and a modulation component at the frequency $f_1 \pm f_2$. This set of three frequencies is known as a triplet $(f_1, f_2, f_1 \pm f_2)$.

A high bispectrum value at bifrequency (f_1, f_2) indicates that there is at least frequency coupling within the triplet of frequencies f_1, f_2, and $f_1 \pm f_2$. Strong coupling implies that the oscillatory components at f_1 and f_2 may have a common generator, or that the cardiovascular circuit they drive may, through with some non-linear interaction, synthesize a new, dependent component at the modulation frequency, $f_1 \pm f_2$.

Nonlinear transformation causes the appearance of self-coupling peaks in the bispectrum [69, 127]. In periodic signals, peaks at the self-frequency without self-phase couplings are common. Again, the simultaneous appearance of both couplings is a very strong indicator of the presence of nonlinearity.

5.2 Measurements

The data acquisition techniques have already been described [112] but, in summary, were as follows. A four-channel laser Doppler blood flow monitor (floLAB, Moor Instruments Ltd., UK) was used for simultaneous recordings of blood flow at the four different sites: both arms (left and right caput ulnae) and both legs (left and right medial maleollus). Skin over bony prominences was chosen in order to standardize the measurement sites for the four extremities. A standard calibration (flux standard) of all the probes was made in order to be able to compare signals, and the blood flow was expressed in arbitrary units (arb. units). The electrical activity of the heart or electrocardiogram (ECG), respiration and blood pressure were also simultaneously recorded. The respiratory effort was measured using the TSD101B Respiratory Effort Transducer (Biopac Systems, Inc., USA). It consists of a piezoresistive sensor equipped with a silicon rubber strain assembly that measures the change in thoracic or abdominal circumference. The electrical conductivity of the sensor is proportional to the increase of abdominal circumference. The blood pressure was also measured with a piezoelectric transducer, and the ECG was recorded using a standard technique with two electrodes placed on the shoulders and one below the heart.

Six males aged 25-27 years with no history of cardiopulmonary disease participated in the study. Each of them lay in repose on a bed for 15 minutes before the start of data recording. One set of measurements was taken in the normal relaxed state, with spontaneous breathing, and a further two/three measurement under differently paced breathing. The duration of the measurements was 20 minutes for spontaneous breathing, and 12 minutes for paced breathing. Blood flow signals were

digitized with 16-bit resolution and sampled at 40 Hz, whereas the ECG, respiration and pressure signals were sampled at 400 Hz. The paced respiration frequency was held constant during the measurement of a given time series and the rhythm was paced by metronome. Altogether 22 recordings were made, as summarized in Tab. 5.1.

Tab. 5.1: Data for six subjects measured during spontaneous and paced respiration. $\overline{V_T}$ is average tidal volume, $\sigma_{\overline{V_T}}$ is its standard deviation, f_1 is average heart frequency and f_2 is average respiratory frequency during spontaneous f_{2s} and paced f_{2p} respiration. The tidal volume is obtained as a value between minimum voltage recorded during expiration and a succeeding maximum voltage recorded during inspiration. The voltages were not calibrated to express volumes in litres; rather, values were normalized to the average tidal volume obtained for each subject during spontaneous respiration. Data marked with * are presented in Tab. 5.3.

Person	Breathing	Age (yr)	f_1 (Hz)	f_2 (Hz)	$\overline{V_T} / \overline{V}_{T_S}$	$\sigma_{\overline{V_T}} / \overline{V}_{T_S}$	Note
1	f_{2s}	27	1.10	0.13	1.00	0.27	
	$f_{2p} < f_{2s}$		1.08	0.11	1.31	0.17	
	$f_{2p} > f_{2s}$		1.00	0.23	1.08	0.18	*
	$f_{2p} > f_{2s}$		0.97	0.34	2.56	0.68	*
2	f_{2s}	27	1.16	0.14	1.00	0.13	*
	$f_{2p} < f_{2s}$		1.06	0.09	1.33	0.22	
	$f_{2p} < f_{2s}$		1.05	0.10	0.83	0.11	*
	$f_{2p} < f_{2s}$		0.98	0.11	0.67	0.10	*
3	f_{2s}	25	1.03	0.16	1.00	0.20	
	$f_{2p} < f_{2s}$		1.08	0.13	1.40	0.11	*
	$f_{2p} > f_{2s}$		1.10	0.26	0.95	0.23	*
4	f_{2s}	25	0.99	0.16	1.00	0.20	
	$f_{2p} < f_{2s}$		1.01	0.10	1.82	0.28	*
	$f_{2p} < f_{2s}$		0.99	0.11	1.88	0.12	*
	$f_{2p} > f_{2s}$		1.03	0.20	1.08	0.26	
5	f_{2s}	26	1.20	0.15	1.00	0.49	
	$f_{2p} < f_{2s}$		1.20	0.10	4.31	0.90	*
	$f_{2p} < f_{2s}$		1.20	0.11	1.84	0.70	
	$f_{2p} > f_{2s}$		1.14	0.21	0.44	0.12	
6	f_{2s}	25	0.95	0.27	1.00	0.22	
	$f_{2p} > f_{2s}$		0.89	0.35	0.15	0.07	
	$f_{2p} < f_{2s}$		0.92	0.24	0.55	0.11	

5.3 Data analysis

The blood flow signals were first pre-processed. Both very low and very high frequencies were removed by use of moving average windows: drift with a 200 s long window; and high frequencies with a 0,2 s window while, and at the same time, the signal was resampled to 10 Hz. By using the moving average before resampling, we avoid problems of aliasing [81]. In addition, each signal was normalized to lie between zero and one, and its mean value was then subtracted. The characteristic cardiac f_1 and respiratory f_2 frequencies, and their components at harmonically related positions were identified: for each signal, the power spectrum was computed to identify f_1 and f_2, and to detect those components possibly caused by nonlinear interactions, $2f_1$, $2f_2$, and $f_1 \pm f_2$. Then the bispectrum estimates were calculated. For each time series the signal was divided into several segments and to ensure stationarity the average value within each window was also subtracted. The chosen window length affected both frequency resolution and the statistical stability of the estimates. Because of the finite length of the time series, optimal choice of the number of segments requires a measure of compromise: the more segments the better the estimates, but increasing the number of segments also reduces the length of individual segments which, in turn, reduces the frequency resolution. To obtain reliable estimates 30 or more segments are necessary [39]. The compromise can be optimised by an appropriate overlapping of the segments (see below).

Tab. 5.2: Peaks at bifrequencies in the bispectrum, arising as the result of a nonlinear interaction between the two oscillators f_1 and f_2.

Peak	Bifrequency
1	(f_1, f_2)
2	(f_1-f_2, f_2)
3	$(f_1-f_2, 2f_2)$
4	$(f_1, 2f_2)$
5	(f_1, f_1-f_2)
6	(f_1+f_2, f_1-f_2)
7	(f_2, f_2)
8	(f_1, f_1)

In the case of quadratic coupling, for which we wish to test, several peaks occur in the bispectrum. Besides the peaks at the bifrequencies (f_1, f_2), the cardiac self-coupling (f_1, f_1) and respiration self-coupling (f_2, f_2), others occur as a consequence of the interactions. Those of primary interest were at bifrequency (f_1, f_2), representing the coupling between the two oscillators at f_1 and f_2, and five others.

To investigate the cardio-respiratory coupling eight peaks were analysed for each signal, as shown in Tab. 5.2. To be able to compare results, a normalization procedure was performed.

The maximum biphase and biamplitude were calculated for each peak. The frequency resolution was set to be 1/10 of the lowest respiration frequency or better. The slowest-paced breathing, f_2, was approximately 0.1 Hz, so that a window of 100 s or longer was necessary for estimation of the bispectrum, biphase and biamplitude. Short plateaus in the estimated biphase occur frequently. To exclude coincidence interactions we focused on those that lasted for at least about 10 periods of the lower coupling frequency f_2. The length of the window also determines the time resolution. In the case of the slowest-paced breathing, where f_2 was 0.1 Hz we were seeking approximately 10 times $(1/f_2)$ = 100 s long epochs of constant biphase. Therefore a window length of 100 s or less was necessary to meet the criterion for time resolution. Due to the Heisenberg uncertainty principle [43], the scope for choice of window length is limited, and compromise is needed between time and frequency resolution. The window was moved along the time series with a minimum time step of $1/f_s = 0.1$ s, where f_s is the sampling frequency. The critical value for the biamplitude estimate to be considered valid was set in all cases to 2, i.e., twice the average value of the bispectrum within its so-called inner triangle (IT).

To be able to conclude that quadratic coupling exists, we require several condition to be fulfilled: (i) A constant biphase during at least 10 periods of the lower interacting component; (ii) Biphases for all six (eight) peaks must be present at the same time as the biphase plateau; (iii) No phase slips must occur during the coupling, and the biphase variations must stay within π rad interval (the biphase being expected to be more or less constant, depending on the coupling strength and noise intensity: phase slips are frequent when the interaction is extremely weak; they are mostly due to noise, but sometimes caused by modulation; strong modulation is expected to result in a biphase with fewer phase slips); (iv) The biamplitude must be above the specified critical value, i.e., be more than twice the average bispectrum value within the IT.

5.4 Results

Examples of detrended, resampled, blood flow signals are presented in the left-hand column of Fig. 5.1. These signals correspond to the case of paced respiration slower than the natural frequency. Their calculated frequency content is presented in the right hand column. The peak at ~0.98 Hz belongs to cardiac activity, f_1; that at ~0.11 Hz to respiratory activity, f_2, which was also obtained directly as a check by use of a piezo sensor. Although the characteristic frequencies differ from person to person, they all lie within defined frequency bounds. Stefanovska proposed in [112] that the respiration

frequency interval should be defined as 0.14-0.6 Hz with a median frequency 0.3 Hz. The spontaneous respiratory frequency for person 2 was 0.14 Hz, i.e., it fell at the lower limit of this interval. The slowest *paced* respiration frequency was set to 0.09 Hz.

Assuming nonlinear cardio-respiratory coupling the cardiac side peaks are positioned at their sum $f_1 + f_2 = \sim 1.09$ Hz, and difference $f_1 - f_2 = \sim 0.87$ Hz. Cardiac $2f_1$ and respiratory $2f_2$ second harmonics are also present. It can be seen that their precise values vary in time, which is what makes the analysis difficult. The widths of the peaks indicate their time-variable frequency content, which makes a time-frequency domain presentation more convenient [9, 43]. The effect is, of course, associated with the interactions between cardiovascular oscillators.

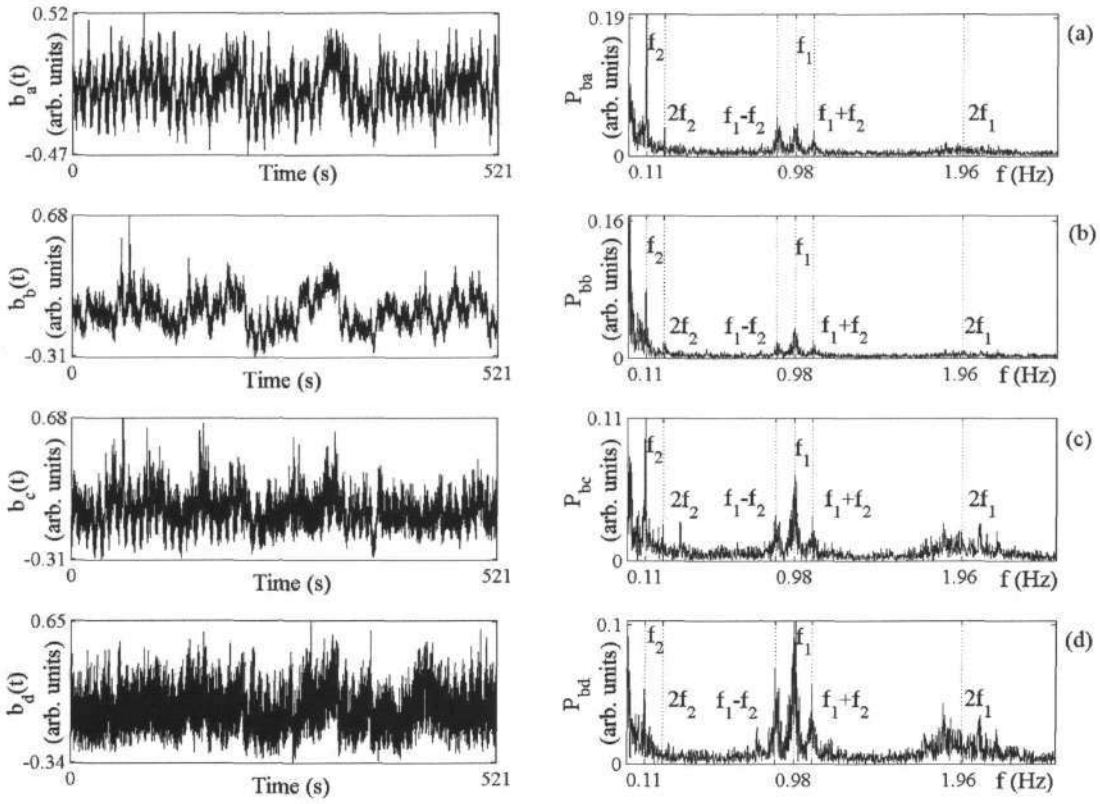

Fig. 5.1: Blood flow signals $b(t)$ measured simultaneously at four different sites. Each of them was detrended, resampled, normalized, and brought to zero mean by subtraction of its average value. The records are each 521 s long, resampled to a sampling frequency of f_s = 10 Hz. (a) Signal from the right wrist $b_a(t)$ and its power spectrum; (b) left wrist $b_b(t)$ and its power spectrum; (c) right ankle $b_c(t)$ and its power spectrum; (d) left ankle $b_d(t)$ and its power spectrum.

A typical bispectrum for the whole frequency domain for signal b_a is presented in Fig. 5.2 (a). A very high peak located at bifrequency (0.11 Hz, 0.11 Hz), belonging to the respiratory self-coupling can be seen in the bispectrum, Fig. 5.2 (b). At least four other peaks are clearly evident: at (0.98 Hz, 0.11 Hz)

attributable to cardio-respiratory coupling; at (0.87 Hz, 0.11 Hz) which we assume to be coupling between the respiratory component f_2 and the difference f_1 - f_2, that could be due to a nonlinear coupling mechanism; and two peaks attributable to interaction with lower cardiovascular characteristic components. The latter interactions (with the intrinsic myogenic and neural oscillators) are not of interest in the present context. Also, other lower frequency peaks can be seen in the bispectrum. Their positions can be seen in the bispectrum contour view shown in Fig. 5.2 (c).

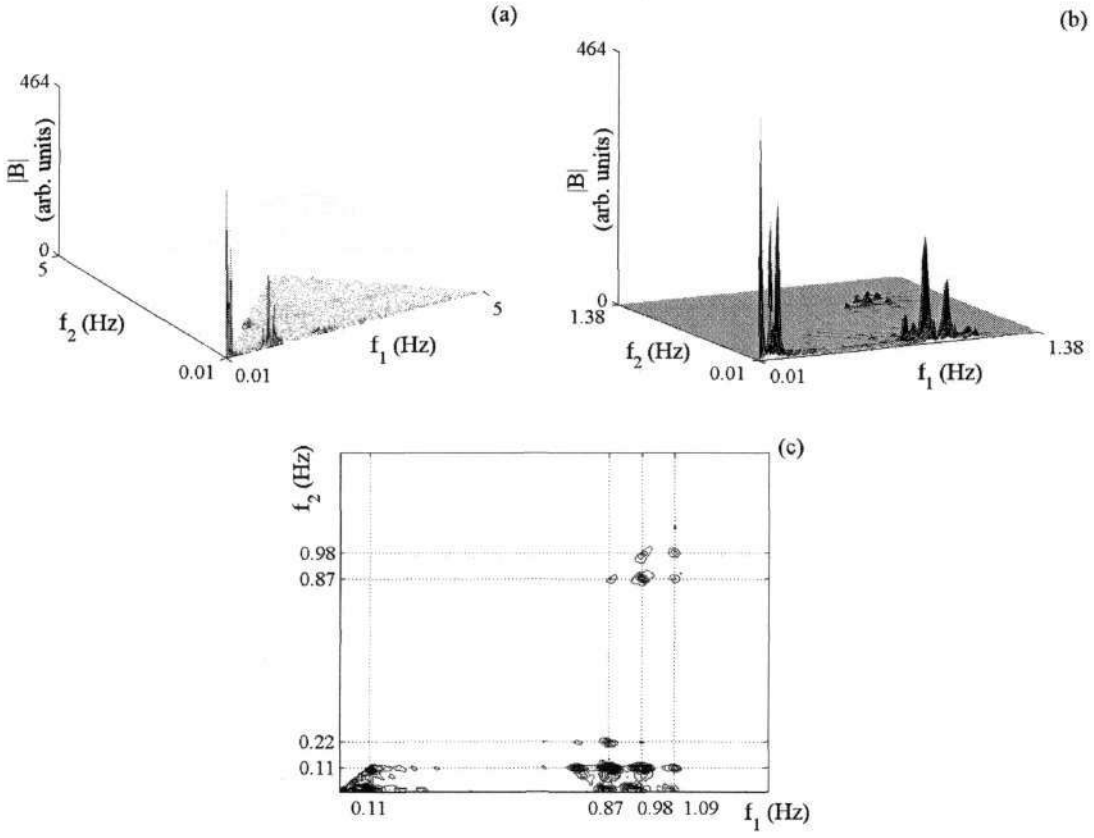

Fig. 5.2: (a) The bispectrum $|B|$ for a signal b_a, calculated with $K = 33$ segments, 87 % overlapping and using the Blackman window to reduce leakage. (b) Part of the bispectrum $f_1, f_2 < 1.4$ Hz that is of our interest and (c) its contour view.

The bispectrum is sensitive to time-variations of the frequency components, yielding in the bispectrum a characteristic diagonal elongation of peaks. The cardiac frequency f_1 spans 0.93-1.02 Hz. Although the respiratory frequency f_2 extends from 0.09 Hz to 0.12 Hz, this large range is actually the result of a single deep breath: the respiratory frequency (being paced) is constant for most of the time, leading to a high bispectrum. The cardio-respiratory bifrequency coupling consequently has a wide frequency range resulting mainly from variation of the cardiac frequency (in Fig. 5.2 it is elongated along the f_1 axes).

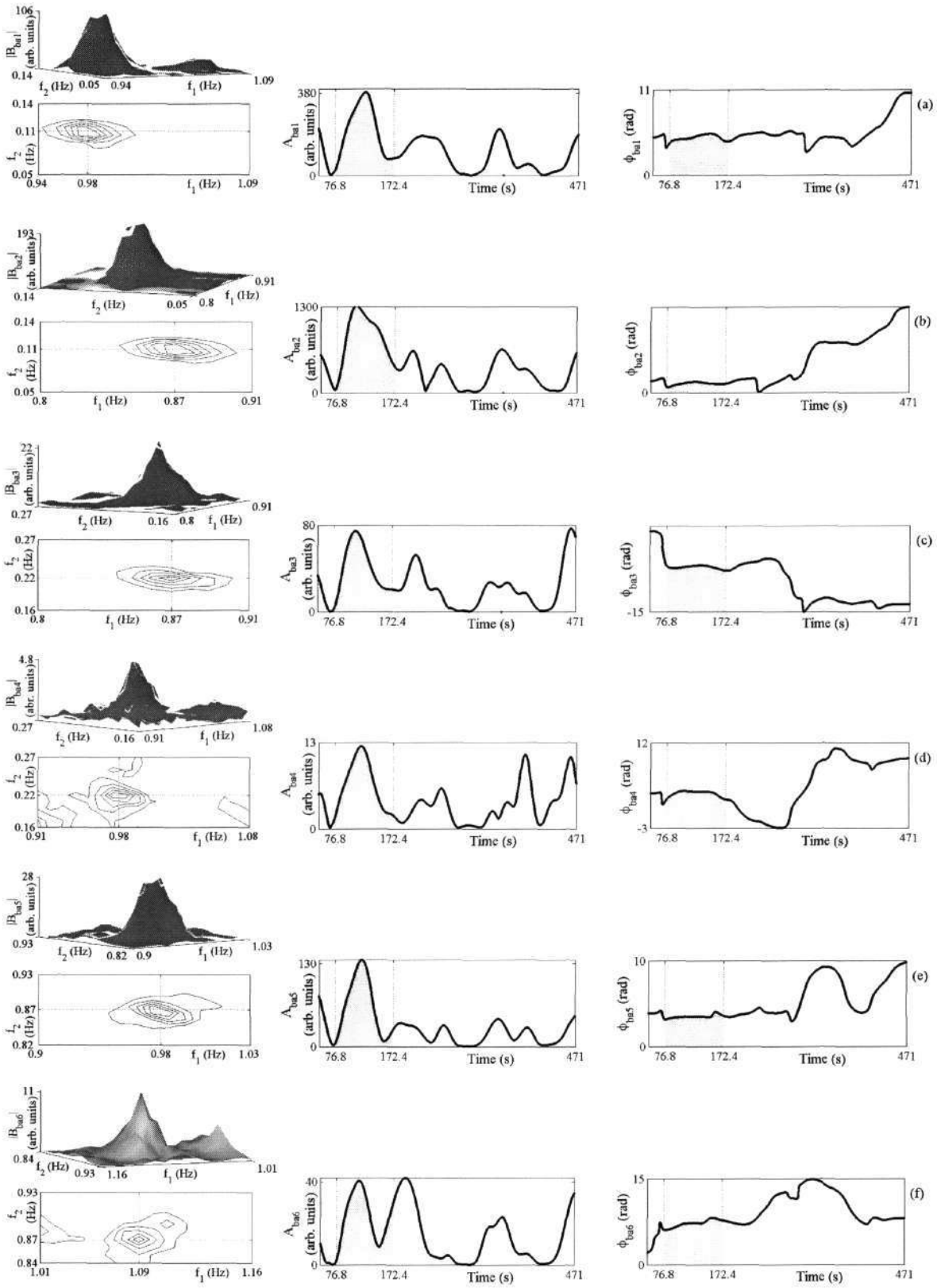

Fig. 5.3: Blood flow analyses for signal $b_a(t)$, calculated with $K = 33$ segments, 87 % overlapping, using a 0.1 s time step and a 100 s long window for estimating the DFT, with a Blackman window to reduce leakage, for peaks (a) 1, (b) 2, (c) 3, (d) 4, (e) 5 and (f) 6; left column, the bispectrum $|B_{ba}|$ with its corresponding contour plots; middle, the biamplitude A_{ba}; and right, the biphase ϕ_{ba}.

The peaks corresponding to cardiac activity are lower, mainly due to time frequency variations. In the presence of quadratic nonlinear coupling, peaks should be present at all six of the bifrequencies summarized in Tab. 5.2. Significant values of the bispectrum (i.e., exceeding twice the average bispectrum within the IT) were obtained near all these bifrequencies (see the left-hand column of Fig. 5.3), showing that the peaks are indeed present.

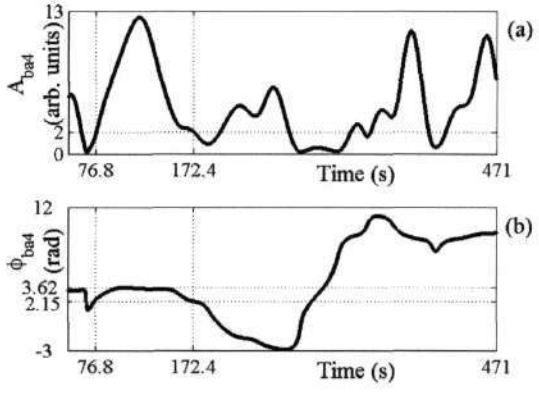

Fig. 5.4: (a) Determination of quadratic nonlinear coupling interval T_{qc} and (b) maximum biphase variation $\Delta\phi$ for signal b_a for peak 4.

Once the peaks at the defined bifrequencies had been confirmed, the time biphase and biamplitude were calculated at the bifrequency peaks. The time interval T_{qc} during which quadratic coupling persisted was determined; if all 6 peaks fulfilled our conditions, then the T_{qc} interval was calculated for all peaks and the boundaries were defined such that the biamplitude for all the peaks in T_{qc} interval would be above the condition Fig. 5.4 (a). For each T_{qc} interval, the maximum variation of the biphase $\Delta\phi$, was determined as shown on Fig. 5.4 (b).

It can be seen that the biamplitude during the time interval from 76.8 s to 172.4 s meets our criterion of being more than twice as large as the average bispectrum in the IT: see middle column of Fig. 5.3 (a) to (f). The biphase in this time interval, 95.6 s long (shaded area), remains constant within a 1.47 rad interval, i.e., there are no phase slips. The biphases at bifrequencies 1, 2, 3 and 5 are very constant; those at 4 and 6 are less so, but they still remain within the π rad interval.

5.5 Surrogates

In many areas of signal processing, an important problem exists in determining whether an observed time series is deterministic, contains a deterministic component, or is purely stochastic. The surrogate

data method provides a rigorous way to determine if an observed time series has a statistically significant deterministic component [102, 106].

The question of whether or not the cardiovascular system possesses a deterministic dynamic was already subject to many research activities by a variety of analyses [6, 8, 109, 110, 112]. These provided notable evidences that the system that regulates blood flow is deterministic.

In this work we use the surrogate data method to validate bispectral analysis to determine whether the obtained biphases from the cardiovascular blood flow signals are a result of the deterministic dynamic of blood flow, or as a result of its stochastic component.

For this purpose, we use the phase randomization method of generating the surrogates [44, 102, 106, 123, 124]. The discrete Fourier transform is computed from the original data, which consists of amplitude and phase at each frequency, and then shuffled to destroy all correlations. The surrogate is the inverse discrete Fourier transform of the shuffled data. Besides phase shuffling, one can also perform phase randomization or data shuffling. Each amplitude is replaced by the amplitude of the same frequency as in the original data. After the inverse Fourier transform, the amplitude of the surrogate data is adjusted by applying a nonlinear transform to give the surrogate data the same distribution as in the original data.

In this way we obtain surrogate data which have similar spectral properties as that of the original data. The surrogate data sequence has the same mean, the same variance, the same autocorrelation function, and therefore, the same power spectrum as the original sequence, but the phase relations are destroyed. The generated surrogate data are output of a linear Gaussian process.

We posit a null hypothesis:

H_0: Quadratic nonlinear coupling is present.

We determine the null hypothesis on surrogate data $s_{ba}(t)$ generated from blood flow signal $b_a(t)$. The obtained surrogate signal $s_{ba}(t)$, Fig. 5.5 (a), has almost the same power spectrum. Fig. 5.5 (b), as it is the power spectrum P_{ba} of the original signal $b_a(t)$, Fig 5.1 (a). As expected, we also obtained a similar bispectrum for the whole frequency domain, Fig. 5.5 (c). The peaks are lower, and less evident, compared to bispectrum of $b_a(t)$, Fig. 5.2. (b).

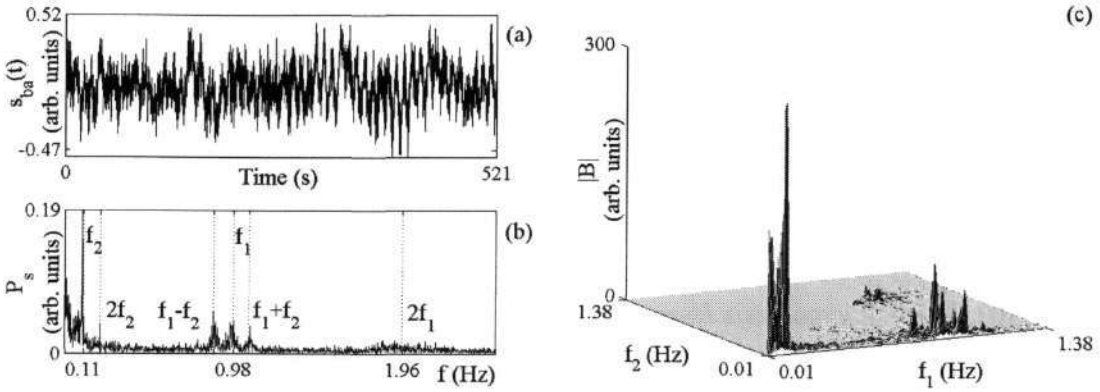

Fig. 5.5: (a) Surrogate of blood flow signal from the right wrist $s_{ba}(t)$, its power spectrum (b), and (c) its bispectrum $|B|$, calculated with K = 33 segments, 87 % overlapping and using the Blackman window to reduce leakage.

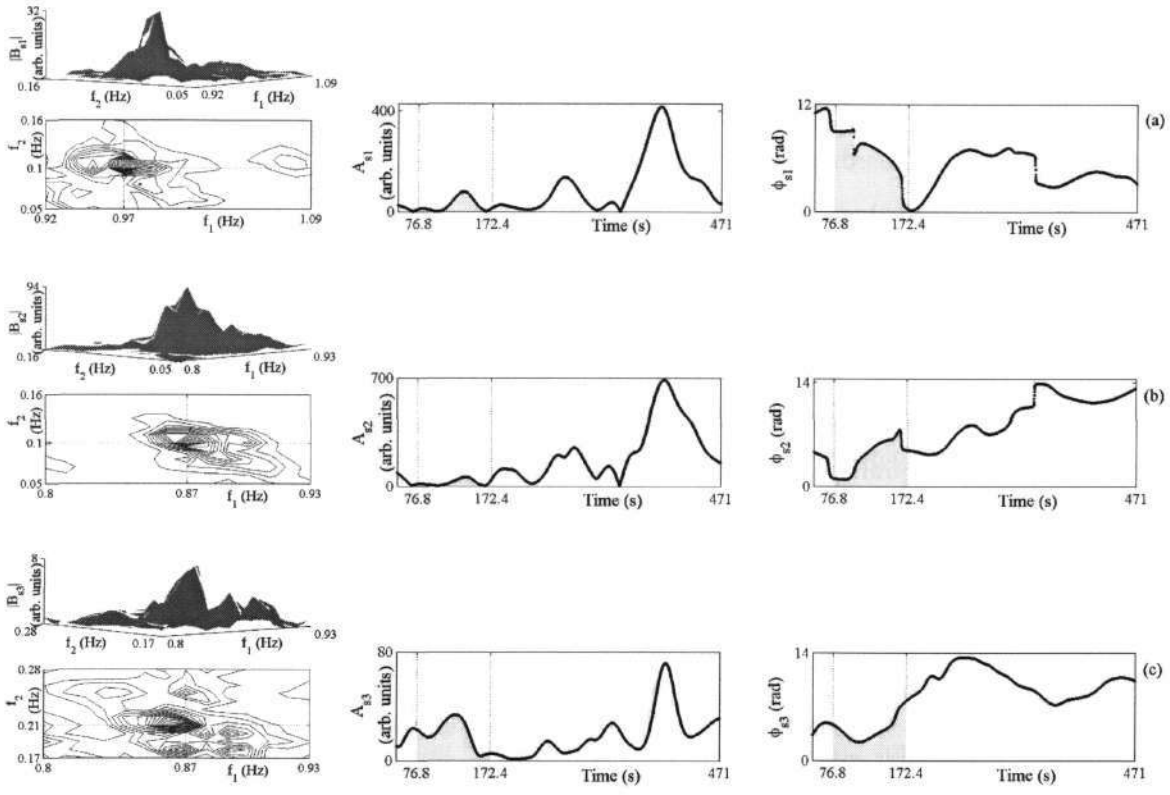

Fig. 5.6: Blood flow analyses for surrogate signal $s_{ba}(t)$, calculated with K = 33 segments, 87 % overlapping, using a 0.1 s time step, a 100 s long window for estimating the DFT, and using a Blackman window to reduce leakage, for peaks (a) 1, (b) 2 and (c) 3; left column, the bispectrum $|B_s|$ with its corresponding contour plots; middle, the biamplitude A_s; and right, the biphase ϕ_s.

By calculating the biphases for all of the six bifrequencies summarized in Tab. 5.2, we conclude that the necessary conditions for quadratic nonlinear coupling are not fulfilled. Fig 5.6 shows peaks,

biamplitudes and biphases for the first three bifrequencies of bispectum B_s. It can be seen that all the biphases, ϕ_{s1}, ϕ_{s2} and ϕ_{s3} tend to always drift. They do not show any plateaus of constant biphase, as is expected, since the phase information is *randomized* in the surrogate signal. Moreover, the biamplitude condition is also not fulfilled.

We performed the hypothesis on bispectral analysis for seven different realizations of surrogate signal for signal $b_a(t)$. The null hypothesis H_0 was not consistent with the data and was rejected in all seven cases. We can conclude that the phase information possessed in cardiovascular blood flow signal is deterministic.

5.6 Global couplings

The heart's pumping action is manifested in every single vessel, and it is also present in the microcirculation through the capillary bed. Peripheral blood flow is controlled by both extrinsic (central) and intrinsic (local) mechanisms, and so it must reflect the activities of both the local and central mechanisms of cardiovascular regulation [6, 7, 9, 108, 110]. The origin of respiratory frequencies in peripheral blood flow was discussed by Hoffman et al [35].

Blood flow signals reflect central and local mechanisms of regulation in the cardiovascular system. Those derived from widely separated sites can be remarkably similar. Although they reflect the flow in the capillary bed, each of them contains the same information on the spatially invariant periodic activities seen in the centrally generated cardiac and respiratory signals. The power of each oscillatory component in the peripheral blood flow varies with the vessels' diameters and the network density, i.e., the local resistance to the flow. Measurement sites of similar network density were chosen [9, 112], viz on bony prominences of the wrist and ankle joints, thus avoiding any large vessels.

Our measured signals, i.e., channels a to d, come from widely differing sites. Nonetheless, in agreement with the earlier work, the respiratory and cardiac characteristic frequency components preserve the same values and, moreover, their phase relationships contain the same information. The left-hand column of Fig. 5.7 shows the bispectrum for peak 1 for signals b_b, b_c and b_d measured on channels c-d. The maximum amplitude of the peak is positioned at the same bifrequency (0.98 Hz, 0.11 Hz) as already seen for peak 1 of the signal b_a measured on channel a, Fig. 5.7, midddle column. The left-hand column of Fig. 5.8 shows the bispectrum for peak 6 for signals b_b, b_c and b_d measured on channels c-d. As excepted the maximum amplitude of the peak is positioned at the same bifrequency (0.98 Hz, 0.11 Hz) as already seen for peak 6 of the signal b_a measured on channel a, Fig. 5.8, midddle

column. The correlation of the biamplitude and biphase for signals b_a and b_b-b_d for all peaks 1-6 is very high. For peak 6, for signal b_a and b_d, is it is 0.85 for both, the correlation of the biamplitude and biphase, as can also be seen from their time evolution presented in the right-hand and middle column of Fig. 5.8.

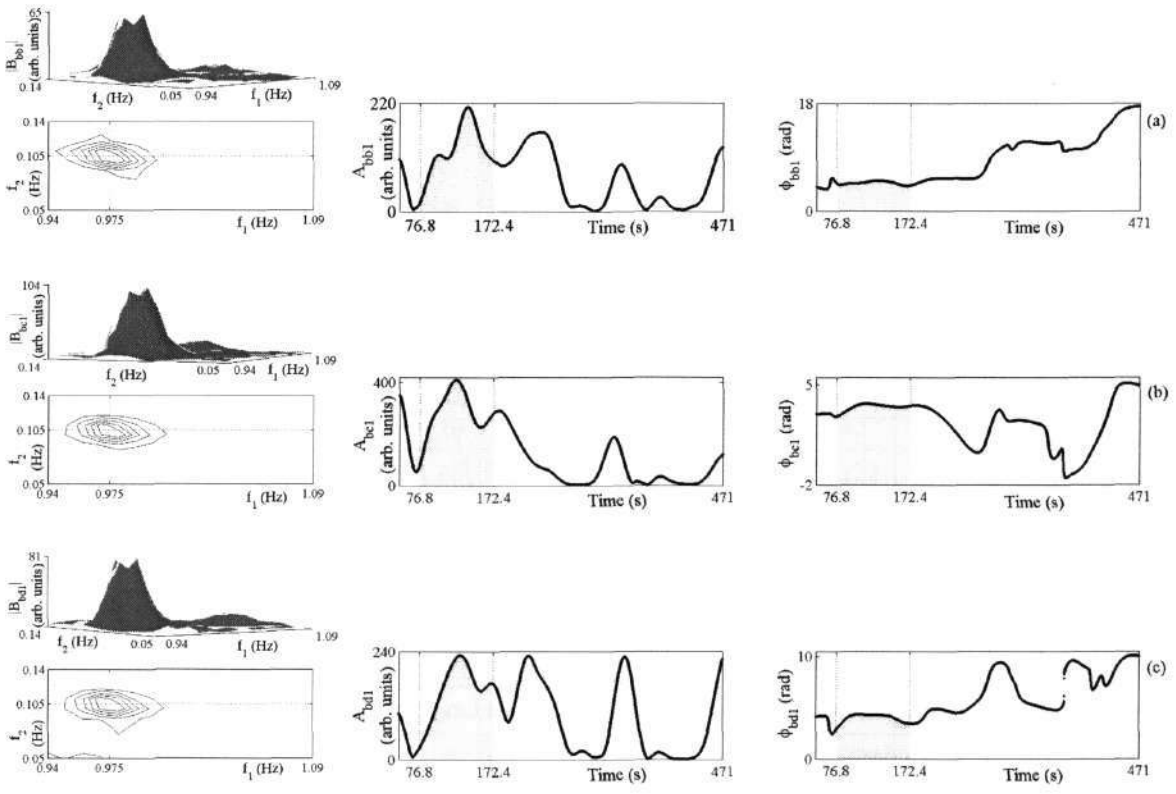

Fig. 5.7: Left: the bispectrum |B| calculated with $K = 33$ segments, 87 % overlapping, and using the Blackman window to reduce leakage for the test signal (a) b_b, (b) b_c and (c) b_d for peak 1 with its contour view. Middle: the biamplitude A, and right the biphase ϕ; a 0.1 s time step and 100 s long window were used for computation of the DFT using a Blackman window.

The biamplitude meets our amplitude criterion within the same time interval from 76.8 s to 172.4 s, and the biphase is also constant during this interval. We obtain the same coupling information at all four measuring sites for all the peaks (1-8). The results obtained from time-bispectral analyses of the measured signals are summarized in Tab. 5.3. Inspecting the data in Tabs. 5.1 and 5.3 we see no obvious correlation between the average tidal volume and the onset of nonlinear cardio-respiratory interaction.

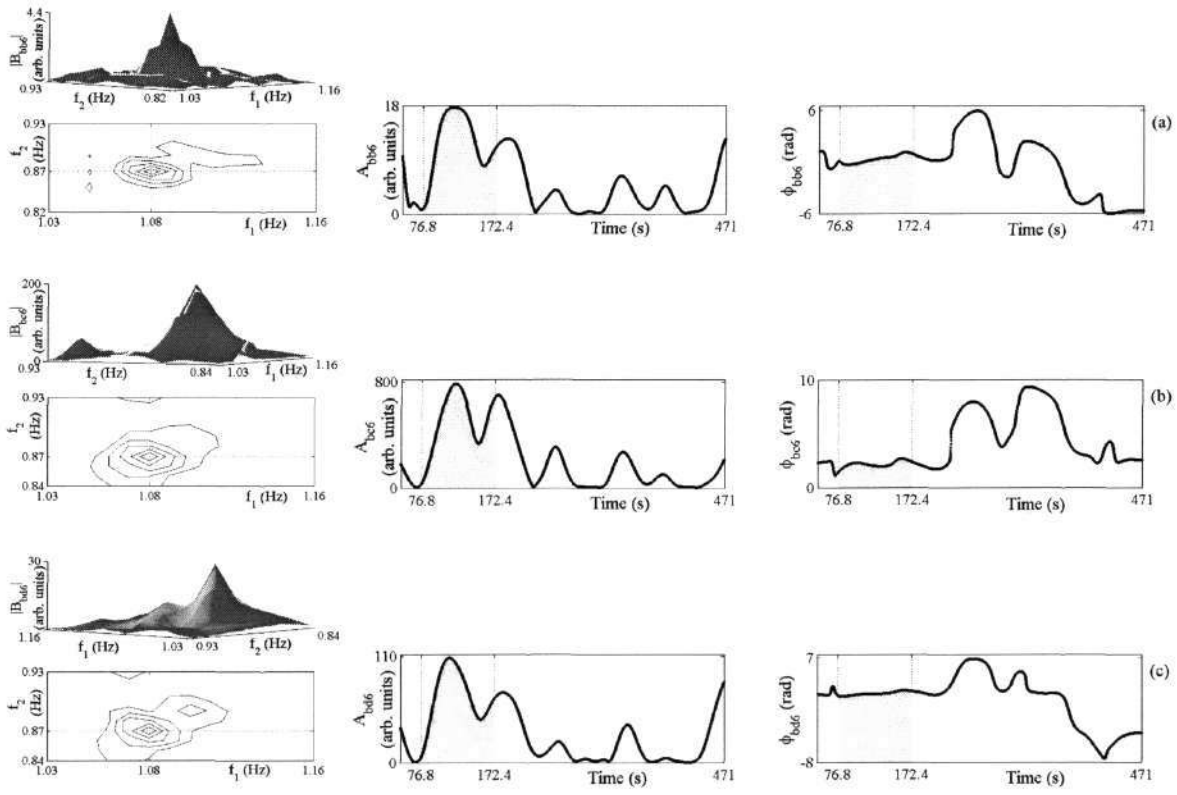

Fig. 5.8: Left: the bispectrum |B| calculated with K = 33 segments, 87 % overlapping and using the Blackman window to reduce leakage for the test signal (a) b_b, (b) b_c and (c) b_d for peak 6 with its contour view. Middle: the biamplitude A, and right the biphase ϕ; a 0.1 s time step and 100 s long window were used for computation of the DFT using a Blackman window.

Tab. 5.3: Quadratic nonlinear couplings detected in blood flow signals marked by * in Tab. 5.1. For each measurement, four blood flow signals were measured simultaneously at different sites, channels a-d. T_{qc} is the time interval during which the bispectral analysis showed that the heart oscillator f_{hr} and the respiratory oscillator f_{res} might be nonlinear coupled. The product of $T_{qc} \cdot f_{res}$ tells us over how many respiratory periods the interaction persisted. During T_{qc} the maximum biamplitude is calculated for the peak 1 that is of our primary interest. In addition, the maximum variation of the biphase $\Delta\phi$, its average value $\bar{\phi}$, and its standard deviation σ_ϕ were calculated during T_{qc}.

Person	Breathing	Channel	f_{hr} (Hz)	f_{res} (Hz)	T_{qc} (s)	$T_{qc}:f_{res}$	A_{1max} (arb. units)	$\Delta\phi$ (rad)	$\bar{\phi}$ (rad)	σ_ϕ (rad)
1	paced	a	1.08	0.11	105.7	11.6	190	1.11	8.92	0.20
1	paced	d	1.00	0.23	56.8	13.1	62	0.92	10.93	0.29
1	paced	b	0.97	0.34	18.9	6.4	50	0.84	0.47	0.28
2	spontaneous	a	1.16	0.14	82.0	11.5	352	1.87	32.68	0.47
2	paced	c	1.05	0.10	89.5	9.0	122	1.48	4.05	0.34
2	paced	a	0.98	0.11	95.6	10.5	383	1.47	3.22	0.42
3	paced	d	1.08	0.13	56.5	7.3	334	1.29	2.21	0.48
3	paced	c	1.10	0.26	52.4	13.6	52	0.46	4.96	0.10
4	paced	d	1.01	0.10	105.6	10.6	407	2.47	0.58	0.18
4	paced	d	0.99	0.11	95.6	10.5	219	2.19	-6.51	0.76
5	paced	d	1.20	0.10	57.5	5.8	1009	2.05	5.88	0.67

5.7 Cross-bispectrum

The bispectrum as defined in [40] can be seen as a special case of the cross-bispectrum when the three signals are the same. In addition to the blood flow signals, the ECG $e(t)$, respiration $r(t)$ and blood pressure $p(t)$ were also simultaneously recorded. This gave us the possibility of globally checking the coupling between cardiac and respiratory activity using bivariate data. Let us define the cross-bispectrum as [69]

$$B_{XYY}(k,l) = X(k)Y(l)Y^*(k+l), \tag{5.1}$$

where X and Y are discrete Fourier transforms of two different signals $x(t)$ and $y(t)$ at discrete frequencies k, l and $k + l$. We calculated the cross-bispectrum B_{cebb} (where c stands for cross, e for signal $e(t)$ and b for signal $b(t)$), for the case where $x(t)$ is the ECG signal $e(t)$ and $y(t)$ is the blood flow signal $b_a(t)$. The ECG signal tells us primarily about the cardiac electrical activity. The phase of

the first, cardiac component f_1, in the triplet (f_1, f_2, f_1+f_2) is thus directly extracted from the ECG signal. The respiratory component f_2 and the component at the harmonically related position $f_1 + f_2$ are extracted from the blood flow signal.

We also define the cross-bispectrum as

$$B_{XYX}(k,l) = X(k)Y(l)X^*(k+l), \tag{5.2}$$

and calculate it for 2 different cases: (i) B_{cbrb}, where $x(t)$ is the blood flow signal $b_a(t)$ and $y(t)$ is the respiration signal $r(t)$. The signal $r(t)$ most directly describes the activity of the respiratory oscillator. Therefore the phase of the second component in the triplet $(f_1, f_2, f_1 + f_2)$ is directly extracted from the respiratory signal. (ii) B_{cprp}, where $x(t)$ is the blood pressure signal $p(t)$ and $y(t)$ is the respiration signal $r(t)$. By calculating the latter cross-bispectrum we are interested in establishing whether the information about coupling between the heart and the respiratory oscillators is signal-independent, i.e., whether it is also present in other CV signals.

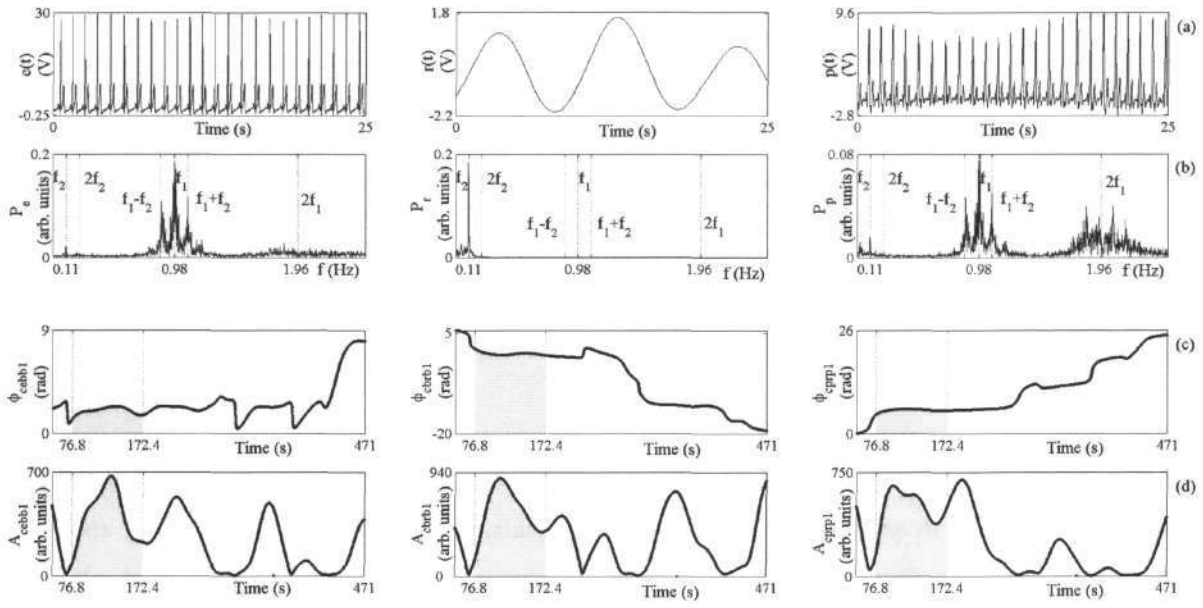

Fig. 5.9: Results for the cross-bispectrum. Row (a) shows the first 25 s of the signals: left ECG signal $e(t)$, middle respiration signal $r(t)$, and right differentiated blood pressure signal $p(t)$; whereas row (b) shows their power spectra. The sampling frequency was f_s = 400 Hz. In the lower rows (c) the biphase ϕ and (d) the biamplitude A are shown; a 0.1 s time step and 100 s long window were used for computation of the DFT using a Blackman window. The biphase and the biamplitude were calculated using the cross-bispectrum (left) B_{ebb}, (middle) B_{brb} and (right) B_{prp}.

We proceeded as discussed above in Sec. 5.3. for each of the three different cross-bispectrum cases. The time evolution of the signals $e(t)$, $r(t)$ and $p(t)$ and their power spectra are presented in Fig. 5.9 (a) and (b). For the cross-bispectrum B_{cebb} all the peaks from 1 to 8 are present at the same bifrequencies as in the case of auto-bispectrum of the blood flow signal. Since the power spectrum of the respiratory signal P_r exhibits only components of the respiratory oscillator we cannot expect peaks 5, 6 and 8 to appear in the cross-bispectrum B_{cbrb} and B_{cprp}. All the rest of the peaks are present at the same bifrequencies as in case of the auto-bispectrum. The biamplitude meets our amplitude criterion within the same time interval from 76.8 s to 172.4 s, for all peaks; moreover the biphase is constant during this time interval. Examples of the biamplitude and biphase time evolution for peak 1 for the three different cross-bispectrum are presented in Fig. 5.9 (c) and (d).

Cross-bispectrum were also calculated with surrogate data, where the phases of the frequency components of the signals $e(t)$, $r(t)$ and $p(t)$ were randomized. No phase couplings were detected in this case. The coupling information among cardiac and respiratory process seems to be signal independent.

5.8 Discussion

The signals were measured on six persons, whereas in the first column of Tab. 5.3 data are only provided for five; the sixth person also showed evidence of nonlinear couplings, but over time, these intervals were too short to fulfil our required conditions. Four blood flow signals, simultaneously measured in different places (channels a, b, c, and d), were available for each recording. We usually first analysed the one with the most distinctive characteristic frequencies in its power spectrum and, if our criteria were fulfilled, checked the other three signals as well. The time interval, T_{qc}, during which quadratic coupling persisted, was determined; if all 6 peaks fulfilled our conditions, then the T_{qc} interval was calculated for all peaks, and the boundaries were defined such that the biamplitude for all the peaks in T_{qc} interval would be above the condition.

Also shown in Tab. 5.3 are three cases where the couplings T_{qc} lasted less than $10 \cdot 1/f_2$, where $1/f_2$ is the longest respiratory period, since they could be detected very distinctly and clearly. Column A_{1max} is the maximum biamplitude for peak 1 during the T_{qc} interval. The strength of the coupling is, in general, not correlated with its duration. For each T_{qc} interval, the maximum variation $\Delta\phi$ of the biphase, its average value, and its standard deviation, were calculated.

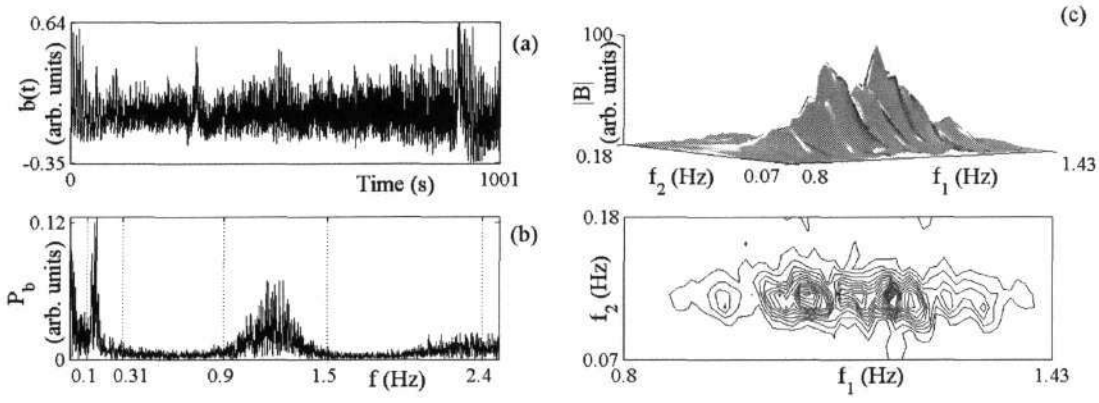

Fig. 5.10: (a) Example of blood flow signal during spontaneous breathing for person 5, channel a and (b) its power spectrum. (c) Bispectrum |B| and its contour view calculated with $K = 33$ segments, 87 % overlapping, and using the Blackman window to reduce leakage.

There was only a single case of spontaneous breathing for which the coupling lasted long enough (82 s without phase slips) to fulfil the criteria. During the spontaneous respiration phase slips are relatively frequent, and epochs with constant biphase are short.

Fig. 5.10 shows an example of data for spontaneous breathing (a) and its power spectrum (b). Signals of this kind are, in general, very difficult to analyse due to their large time-variable frequency content, which results in broadened and coalescing peaks, as seen in Fig. 5.10 (c). Peaks 1-6 cannot easily be resolved due to time-frequency resolution restrictions.

5.8.1 Definition of the phase

As already mentioned above in Sec. 2.2, the cardiac and respiratory systems can be perceived as coupled autonomous oscillators [6, 7, 9, 13, 59, 75, 99-101, 110, 111, 115]. Using a bispectrum based on Fourier transform, which is a decomposition of the signal in terms of complex exponential (sinusoidal) components, each component can be represented as a point in a complex space, $\Re[X(k)]$ versus $\Im[X(k)]$, thus defining a vector, where X is DFT and k is a discrete frequency. Its magnitude represents a power, whereas the phase is determined by the angle between the vector and the positive real axis. The phase of an oscillator is defined as the phase of the sinusoidal component that lies closest to the characteristic frequency of the oscillator, with a corresponding spectral peak. Thus our phase definition differs from that in Kuramoto phase reduction, [54]. In this way it is possible to study the phase relations and resolve the nature of the couplings.

5.8.2 Nonlinear coupling, or linear coupling of strongly nonlinear oscillators?

Our study is based on the assumptions that the cardiac and respiration processes can be described as weakly nonlinear oscillators and that the interaction between them is also weak [116]. It is pertinent to investigate what happens when these assumptions are not fulfilled. We have addressed the question in two different ways based on analytic approximation and digital simulation, respectively.

The analysis in Appendix B considers harmonic generation by a pair of coupled, weakly nonlinear, oscillators. It confirms that, for weak coupling, the appearance of additional harmonics at $2\omega_2$, $2\omega_1$, $2\omega_1 \pm 2\omega_2$, $\omega_1 \pm \omega_2$, $3\omega_1 \pm \omega_2$ can confidently be associated with the presence of quadratic coupling. For a sufficiently nonlinear oscillator and sufficiently strong coupling, these and other combinatorial harmonics can in principle be generated, as a second-order effect, even for linear coupling. As will be illustrated below, however, the appearance of these combinatorial harmonics does not in itself fulfil the necessary conditions to support a conclusion that there is nonlinear coupling when tested by bispectral analysis: the high biamplitude and constant biphase may be absent. In any case, the bispectral approach cannot be expected to yield reliable information about the nature of the coupling when the nonlinearities are extremely strong.

We have therefore complemented the analysis of Appendix B with a digital simulation, exploring the range of extreme conditions where the bispectral approach is expected to fail. We have chosen to simulate a generic model (5.3) of the van der Pol relaxation oscillator, with an additional nonlinear term, linearly driven by another relaxation van der Pol oscillator via an additive coupling [125]

$$\begin{aligned} \dot{x}_1 &= y_1, \\ \dot{y}_1 &= \varepsilon_1(1-x_1)^2 y_1 - \omega_1^2 x_1 + \eta_1 x_1^2 + \mu_1(x_1 - x_2) + \xi(t), \\ \dot{x}_2 &= y_2, \\ \dot{y}_2 &= \varepsilon_2(1-x_2)^2 y_2 - \omega_2^2 x_2. \end{aligned} \tag{5.3}$$

The activity of the oscillators is described by the two state variables x_i and y_i, where ε_i and $\omega_i = 2\pi f_i$ are constants, and $i = 1, 2$ denote respectively the driven or the driving oscillator. η_1 is a constant that sets the strength of the additional nonlinear term in the driven oscillator, and μ_1 is the strength of the coupling. Here, $\xi(t)$ is zero-mean white Gaussian noise, $\langle \xi(t) \rangle = 0$, $\langle \xi(t), \xi(0) \rangle = D\delta(t)$ and $D = 0.8$ is the noise intensity. Following the pioneering work of van der Pol and van der Mark [125], the parameters are set to $\varepsilon_1 = 70$, and $\varepsilon_2 = 3$.

A detailed parameter space analysis has been completed, showing that a situation indeed exists for which the bispectral technique fails to distinguish between the two situations when: (i) two oscillators are *strongly* nonlinear, but linearly coupled; or (ii) when they are nonlinear and nonlinearly coupled. As an illustration, bispectral analysis was performed for two coupled van der Pol oscillators, with and without added Gaussian noise, for different sets of parameters. In the first case the strength of the additional nonlinearity was changed, while μ_1 was kept constant: (a) μ_1 = const. = 1; η_1 was 0, 0.5, 1, 2, 5, 10, 12 and 15, and from 20 to 90 was varied with step 10 and 93 was also included. (b) μ_1 = const. = 25; η_1 was varied from 1 to 10 with step 1, values 12, 15, 18 and 25 were also considered, and again values from 20 to 60 with step 10. In the second case the strength of the coupling was changed while η_1 was kept constant: (a) η_1 = const. = 1; μ_1 was varied from 0.1 to 1 with step 0.1, from 1 to 10 with step 1, then values 2.5, 3.5, 11, 15, 20, 25, 30, 35, 120 and 200 were considered, and again values from 40 to 100 with step 10. (b) η_1 = const. = 5; μ_1 = 25. (c) η_1 = const. = 15: μ_1 was varied from 1 to 10 with step 1, values 12, 15, 17, 20, 24 and 25 were considered, and again from 30 to 60 with step 10.

The test signal $x_{1F}(t)$ is the variable x_1 of the driven oscillator, recorded as a continuous time series. For the first 400 s, the strength of the additional nonlinear term, i.e., η_1 = 15 was very strong and the coupling, i.e., μ_1 = 1 was relatively strong; μ_1 was then substantially increased to 25, whereas the strength of the additional nonlinear term was decreased to 1. After a further 400 s, the strength of the additional nonlinear term was increased back to 15. The first 5 s and corresponding power spectrum for each coupling strength are shown in Fig. 5.11 (a) and (b). The peak 1.1 Hz in the absence of coupling, labelled as f_1, represents the driven cardiac oscillator; and f_2 = 0.24 Hz represents the driving respiratory oscillator. These frequencies are deliberately chosen such that their ratio is not an integer.

The power spectra, Fig. 5.11 (b), for all the three different cases of the strengths of the linear coupling and additional nonlinear term exhibit rich frequency content. As the coupling gets stronger, and/or the strength of the additional nonlinear term increases, the frequency content of the signal x_{1F} becomes richer. The power spectra clearly exhibit components at the harmonically related positions $f_1 + f_2$ and $f_1 - f_2$.

The principal domain of the bispectrum for the test signal x_{1F}, Fig. 5.11 (c) and (d), shows a peak at the bifrequency (0.96 Hz, 0.24 Hz) that is of our primary interest. A window length of 100 s was chosen to calculate the instantaneous biphase and biamplitude, Fig. 5.11 (e) and (f), and was moved across the signal in 0.1 s steps. The whole signal is analysed as a single entity, but transients caused by the changes in coupling and/or in the strength of the additional nonlinear term are removed prior to processing.

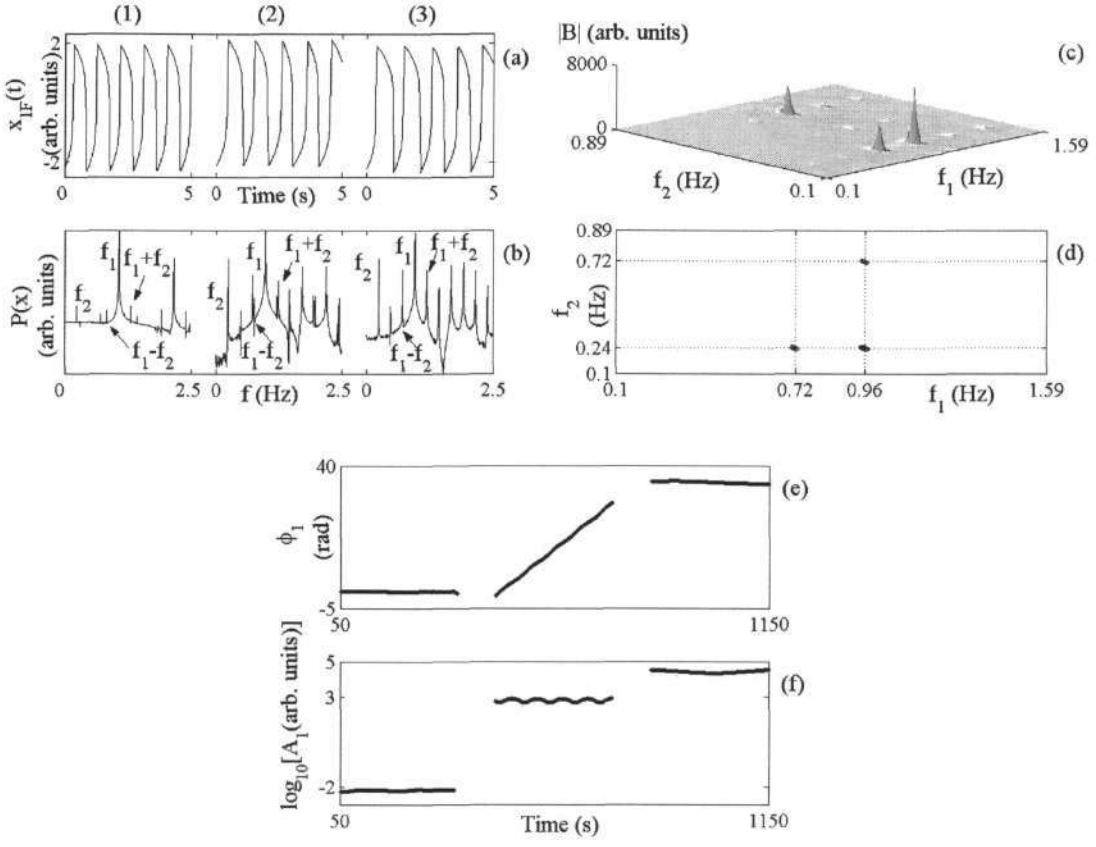

Fig. 5.11: Digital simulation illustrating a situation where the bispectral method fails. The simulation models two unidirectionally, *very* strongly coupled, relaxation van der Pol oscillators with additional *very* strong nonlinear terms, in the presence of additive Gaussian noise. (a) The test signal x_{1F} of variable x_1 of the forced van der Pol oscillator with characteristic frequency f_1 = 1.1 Hz periodically forced at frequency f_2 = 0.24 Hz for three different coupling strengths $\mu_1 = 1$ (1), 25 (2), and 25 (3), with strengths of the additional nonlinear term $\eta_1 = 15$ (1), 1 (2), and 15 (3). Each coupling lasts for 400 s, at sampling frequency f_s = 50 Hz. Only the first 5 s are shown in each case. (b) The power spectrum of x_{1F}. (c) Its bispectrum $|B|$ calculated with K = 34 segments, 67 % overlapping and using the Blackman window to reduce leakage and (d) its contour view. (e) The biphase ϕ and (f) the biamplitude A for bifrequency (0.96 Hz, 0.24 Hz), with a 0.1 s time step and a 100 s long window for estimating the DFTs using the Blackman window, for cases (1), (2) and (3). Note that only for (3) are both conditions (i.e., high enough biamplitude, and constant biphase) for the (incorrect) inference of nonlinear coupling satisfied.

During the period of relatively weak coupling $\mu_1 = 1$ and strong nonlinearities, no peak is present in the bispectrum as can be seen from the biamplitude, Fig. 5.11 (f), which remains far below unity (0.012). Moreover, at value $\eta_1 = 0.7$ the frequency component at modulation position $f_1 + f_2$ appears in the power spectrum for the first time. The modulation components $f_1 \pm f_2$ become large and almost equal in size in the power spectrum, but not until $\eta_1 = 15$. However, even then, not all the necessary

peaks (also peak at bifrequency (f_1, $2f_2$)) in the bispectrum are present and the method correctly resolves the absence of nonlinear coupling, even though the biphase is constant, Fig. 5.11 (e).

By grossly exaggerating the strength of the coupling, with $\mu_1 = 25$, the frequency components that might also arise from nonlinear coupling become large. This results in an substantial increases of the biamplitude at bifrequency (f_1, f_2) in the bispectrum; the biphase is then non-constant, however, and increases continuously. Again the required conditions for the identification of nonlinear coupling are not fulfilled.

In the most extreme example shown, with very strong coupling and very strong additional nonlinearity, i.e., with $\eta_1 = 15$, $\mu_1 = 25$, we are unable to distinguish between strong nonlinearity of the oscillators and strong nonlinear coupling. In a signal coming from a "black box", the observed frequency components could mistakenly be attributed to nonlinear coupling: the bispectrum, Fig. 5.11 (c), contains all the necessary peaks (only three of them are visible, the rest of them being much smaller, although fulfilling the necessary amplitude condition). There are other frequency components that could result from nonlinear coupling, and the biphase remains constant. In this case the method clearly fails.

There are, however, compelling arguments suggesting that the cardiac and respiratory subsystems should be in fact treated as weakly nonlinear oscillators that are weakly coupled. (i) In healthy subjects, breathing spontaneously, only *occasional* and *brief* episodes of synchronization are seen [10, 99-101], indicative of relatively weak coupling. (ii) Sinus arrhythmia is small at spontaneous breathing frequencies and only slightly larger at very low breathing frequencies [23], again supporting a weak-coupling description. (iii) The couplings can sometimes decrease almost to vanishing point, e.g., in coma [112]. Without couplings, the dynamics becomes drastically simplified - with complete absence of synchronization or modulation. The fact that virtually no variability is seen in any of the natural frequencies, despite small amplitude variations attributable to internal noise, suggests that the oscillators themselves are at most weakly nonlinear. (iv) If there were strong oscillator nonlinearity, and strong (but linear) coupling, we would observe many combinatorial components around the cardiac frequency, which is not the case (see Fig. 5.1 (a) - (d)). The excessively strong-coupling regime explored in the above simulations would appear, therefore, to be largely irrelevant to the cardio-respiratory interaction that we study in this work: our bispectral technique [40] should be applicable as we have assumed.

5.8.3 Relationship to synchronization

The fact that inter-oscillator interaction can give rise to synchronization, as well as to modulation, has excited much attention in studies of the phase relationships between the cardiac and the respiratory oscillators [10, 24, 42, 46, 52, 71, 92, 95, 97, 100, 101, 113, 114, 118]. Indeed, it was the possibility of synchronization that motivated us to develop new techniques to investigate further the interactions between the systems: the direction, strength and, in particular, the nature of the couplings. They can be obtained from bivariate data (respiration and ECG signal) by use of the methods recently developed for analysis of synchronization, or generalized synchronization, between chaotic and/or noisy systems (see [79] and references therein). We now consider whether or not synchronization is onsets under conditions where we have clear evidence of interaction.

Fig. 5.12 (d) shows a cardio-respiratory synchrogram based on the stroboscopic technique [79] for person 2 during paced respiration, supplementing bispectral results for signal b_a. It is constructed by plotting the normalized relative phase of a heartbeat within m respiratory cycles [79]

$$\psi_m(t_k) = \frac{1}{2\pi}\left(\phi_2(t_k) \bmod 2\pi m\right), \tag{5.4}$$

where t_k is the time of k-th heart beat and ϕ_2 is the instantaneous phase of respiration. In perfect n:m phase locking, $\Psi_m(t_k)$ attains exactly the same n different values within each m adjacent respiratory cycles and the synchrogram consists of n horizontal strips. The instantaneous phase of the cardiac activity was obtained by characteristic or marker events - the R peaks in the ECG signal. A 2π increase of phase is attributed to the interval between subsequent R peaks. The instantaneous phase of respiration was obtained in a similar way, using zero-crossing as the marker event.

For $m = 1$ we cannot see any horizontal structure that would resolve n:1 phase locking during 77-172 s. By differentiating the instantaneous phases we obtain the instantaneous (a) cardiac and (b) respiratory frequencies and (c) their ratio as shown in Fig. 5.12. In the histogram of frequency ratio (not shown) two peaks appear, one at $f_2/f_1 = 9$ and the other at $f_2/f_1 = 10$, as can also be seen from the Fig. 5.12 (c). The synchrogram presented in Fig. 5.12 (e) shows the case where $m = 9$. The vertical inclined lines suggest that the frequency ratio is almost constant, whereas phase drift is present most of the time. No synchronization is evident in either synchrogram. It looks as though the cardiac oscillation has a tendency to synchronize with the respiratory one, but cannot tune due to the slow-paced respiration frequency. In other words, it appears that, for most of the time, the cardiac frequency

is just modulated by the respiratory rhythm, i.e., what is commonly referred to as respiratory sinus arrhythmia.

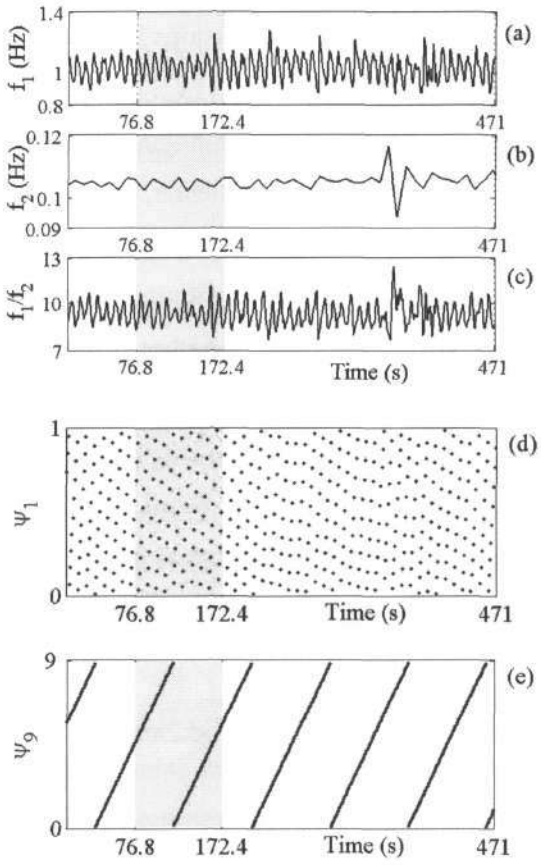

Fig. 5.12: (a) Instantaneous cardiac frequency f_1, (b) instantaneous respiratory frequency f_2 and (c) their frequency ratio for person 2 during paced respiration, supplementing bispectral results for blood flow signal b_a. (d) Synchrogram based on stroboscopic technique calculated for $m = 1$ and (e) $m = 9$.

Using the synchrogram technique we thus detect the existence of frequency modulation but no synchronization for the case of paced, low frequency, respiration. We conclude, therefore, that bispectral analysis yields different information from that which can be resolved from a synchrogram. The relation to synchronization in more general way is going to be discussed in detail in the subsequent chapter.

5.8.4 Synchronization, modulation and type of coupling

Just as frequency modulation does not necessarily coexist with synchronization between the cardiac and respiratory systems, there is not a one-to-one correspondence between quadratic coupling and modulation. As seen in Fig. 5.12 (a), the cardiac frequency is continuously modulated by the

respiratory frequency throughout the recording, whereas quadratic coupling is reliably detected only in the interval between 77 s and 172 s. Using bispectral analysis we can obtain additional information about the possible presence of modulation. Inspection of the time evolution of the amplitudes and phases for all the frequencies that constitute the triplets for bifrequencies summarized in Tab. 5.3 has shown that the observed nonlinear coupling does not correspond directly to frequency modulation.

It remains an open question whether the observed interchange and coexistence between modulation, synchronization and other manifestations of coupling arise through complexity of the cardio-respiratory interaction itself, or through indirect interactions involving the other oscillatory processes (see [110] and the references therein) known to exist in the cardiovascular system.

5.8.5 Unidirectional or bidirectional coupling

We have studied the combinatorial frequencies, that arise from the influence of the respiratory on the cardiac system. This naturally begs the question of whether the coupling is unidirectional or bidirectional. Using the same method, one could equally well analyse the combinatorial frequencies responsible for the influence of cardiac on the respiratory system. In fact, using newly developed algorithms for analysis of the direction of coupling [72, 93, 94, 103] has already shown [73, 117], that the two systems are *bidirectionally* coupled.

5.8.5.1 Forced oscillator

The effect of respiratory system is, however, dominant (i.e., is the driving system) at all respiratory frequencies, whether paced or spontaneous [73, 117]. The interaction between the cardiac and respiratory oscillators can be seen as unidirectional: the respiratory system drives the cardiac one. A particular case is the case of the paced respiration. Although, during paced respiration, the respiration frequency is kept constant, the situation differs from that of a forced oscillator (with the cardiac oscillator being driven, and the respiration oscillator being the drive). Paced respiration experiments can in fact be perceived as a state of the system of two coupled oscillators, where, although the frequency of one of them (respiration) is forced and kept constant, the interaction between the two oscillators remains spontaneous.

To illustrate how this happens, we use a generic model (5.5) of an almost periodic, Poincaré oscillator periodically, driven by a weak external force

$$\begin{aligned}\dot{x} &= -xq - \omega_1 y + F\sin(\omega_2 t + \phi_0) + \xi(t),\\ \dot{y} &= -yq + \omega_1 x,\\ q &= \alpha(\sqrt{x^2 + y^2} - a).\end{aligned} \tag{5.5}$$

The activity of the oscillator is described by the two state variables x and y, α, a and ω_1 are constants and F is the forcing amplitude with frequency ω_2 and initial force phase ϕ_0. Here, $\xi(t)$ is zero-mean white Gaussian noise, $\langle\xi(t)\rangle = 0$, $\langle\xi(t), \xi(0)\rangle = D\delta(t)$, and $D = 0.1$ is the noise intensity. The parameters of the model are set to $\alpha = 1$, and $a = 0.5$.

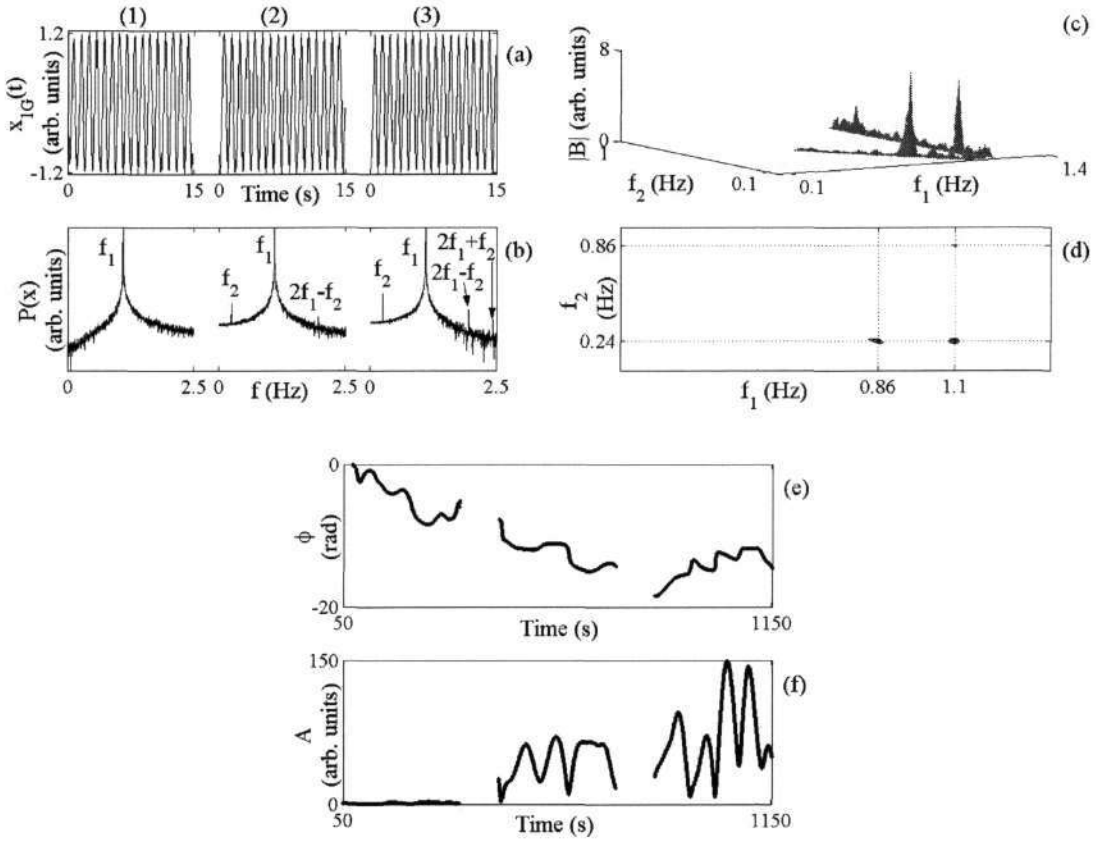

Fig. 5.13: Results for a forced Poincaré oscillator in the presence of additive Gaussian noise. (a) The test signal x_{1G}, of variable x of the forced oscillator with characteristic frequency f_1 = 1.1 Hz periodically forced at frequency f_2 = 0.24 Hz with three different forcing amplitudes; F = 0.0 (1), 0.1 (2) and 0.2 (3). Each forcing lasts for 400 s, at sampling frequency f_s = 10 Hz. Only the first 15 s are shown in each case. (b) Its power spectrum. (c) The bispectrum $|B|$ calculated with K = 33 segments, 66 % overlapping and using the Blackman window to reduce leakage and (d) its contour view. The part of the bispectrum above f_2 > 1.0 Hz is cut, because the triplet (1.1 Hz, 1.1 Hz, 2.2 Hz) produces a high peak that is physically meaningless. (e) The biphase ϕ and (f) biamplitude A for bifrequency (1.1 Hz, 0.24 Hz), with a 0.3 s time step and a 100 s long window for estimating the DFTs using the Blackman window.

The test signal $x_{1G}(t)$ is the variable x of the driven oscillator, recorded as a continuous time series. For the first 400 s, there was no forcing, i.e., the amplitude was set to zero. It was then raised to a small constant value 0.1. After a further 400 s, it was increased again to 0.2. The first 15 s and corresponding power spectrum for each forcing strength are shown in Fig. 5.13 (a) and (b) in order to demonstrate the changes in spectral content and behaviour caused by the forcing. The peak labelled as f_1 = 1.1 Hz represents the driven cardiac oscillator and the f_2 = 0.24 Hz represents the driving respiratory oscillator. These frequencies are deliberately chosen to have an irrational ratio.

For nonzero forcing strength F, there is at least one peak present at the harmonically related position $2f_1 - f_2$ attributable to forcing of the cardiac oscillator. It arises from the nonlinearity of the first oscillator, but is caused by the forcing. Clearly, the power spectrum does not exhibit any components at the harmonically related positions $f_1 + f_2$ and $f_1 - f_2$ that are present in case of real cardiovascular blood flow signals.

The principal domain of the bispectrum for the test signal x_{1G}, Fig. 5.13 (c) and (d), shows a peak at the bifrequency (1.1 Hz, 0.24 Hz) that is of our primary interest. A window length of 100 s was chosen to calculate the instantaneous biphase and biamplitude, Fig. 5.13 (e) and (f), and was moved every 0.3 s across the signal. The whole signal is analysed as a single entity, but transients, caused by the changes in forcing strength are removed prior to processing.

Longer epochs of constant biphase cannot be observed: it changes continuously and many phase slips are present.

Note, that the cardio-respiratory interaction is more complex than just a driven oscillator, since this cannot produce the observed frequency components, and nor is the biphase constant during the forcing. Although the respiration frequency is kept constant, the situation differs from that of a forced oscillator (with the cardiac oscillator being driven, and the respiration oscillator being the drive). In a sense, the respiratory oscillator is a driven one, with which the cardiac oscillator interacts. Beside the mechanical interaction there is also the interaction via the central nervous system. Bispectral analysis shows different information, which can be resolved from the synchrogram. In the power spectra of the cardiovascular signals higher harmonic components are present, as well as components at the modulation frequency. The higher harmonic components could be, due to nonlinear coupling, nonlinearity of the oscillators, or blood propagation through the veins. The latter possibility must be excluded, however, since the modulation components in question are also present in the ECG signal. In the present work we are concerned not with the origin of these components, but mainly with their phase relationships.

6 BISPECTRAL RELATION TO SYNCHRONIZATION

The question of bispectral analysis related to synchronization was already opened and discussed in Sec. 5.8.3 and 5.8.4. At that time, it was not possible to give well-founded conclusions. In the following chapter, we further investigate the question in more detail. We use signals obtained from rats undergoing anaesthesia. The signals have already been analysed using a synchronization technique [63, 64]. Two signals which were chosen for analysis, using the bispectrum as their synchrograms, express very clear episodes of synchronization. Since there is not a unique way of defining the synchronization, we will start with a brief synchronization definitions overview.

6.1 Synchronization definition

Synchronization is a basic phenomenon in physics, discovered at the beginning of the modern age of science by Huygens [37]. In the classical sense, synchronization means the adjustment of frequencies of periodic oscillations due to weak interactions [2, 4, 30]. The most fundamental definitions of synchronization are frequency and phase synchronization. These definitions have been generalized to encompass synchronization phenomenon from coupled (two or more) periodic, noisy to chaotic oscillators [79]. Throughout this work, we use synchronization as an abbreviation for phase synchronization.

Frequency synchronization. Generally, the interaction between two systems is nonsymmetrical: either one oscillator is more powerful than the other, or they influence each other to different extents, or both. If the action in one direction is essentially stronger than in the other one, then we have a particular case of external forcing. In this case, the frequency of the driven system is pulled towards the frequency of the drive. The main point in a bidirectional interaction is that the frequencies of both oscillators change. Let us denote the frequencies of the autonomous systems as f_1 and f_2, and let $f_1 < f_2$; the observed frequencies of interacting oscillators are denoted as $\Omega_{1,2}$. If the coupling is sufficiently strong, frequency locking or entrainment appears as the mutual adjustment of frequencies, so that $\Omega_1 = \Omega_2 = \Omega$, where typically $f_1 < \Omega < f_2$. Whether or not synchronization takes place, depends on coupling strength and frequency detuning, or mismatch. The identity of the frequencies that hold within a finite detuning range is the hallmark of synchronization, and is called frequency locking (also mode locking). The entire family of curves, $\Omega - f_2$ vs f_2 (f_2 is the drive), for different values of the forcing amplitude, ε, determine the region in (f, ε) plane that corresponds to the synchronized state of the oscillator, called synchronization region or Arnold tongue [79].

Phase synchronization. The onset of a certain relationship between the phases of two synchronized self-sustained oscillators is often called phase locking. Frequency locking implies a certain relation between the phases that depend, not only on the frequency detuning and coupling strength, but also on the way in which the systems are interacting. Let us consider two nearly identical, symmetrically coupled oscillators. If the interaction is weak, then we can assume that only the phases are influenced, and that they shift the points along the limit cycles, but not the amplitudes. Phase-attractive interaction leads to in-phase synchronization, whereas the phase-repulsive one results in anti-phase synchronization.

Mutual synchronization. It is a special case of phase synchronization when two oscillators equally affect each other. This case covers the classical experiment of Huygens [37]. Mutual phase synchronization of chaotic oscillators is also possible. In this case, synchronization notation is specified more precisely, because it is not obvious how to characterize the rhythm of a chaotic oscillator. Chaotic oscillatory process can be characterized by mean frequency [79]

$$\langle f \rangle = \frac{N\tau}{\tau}, \tag{6.1}$$

where τ is a large time interval and N_τ number of cycles within interval τ. If the coupling is large enough, than the mean frequencies of the two oscillators become equal. This does not imply that the

signals must also coincide. Weak coupling does not affect the chaotic nature of both oscillators; the amplitudes remain irregular and uncorrelated, whereas the frequencies are adjusted.

High-order synchronization. Generally, when the incommensurate frequencies of an uncoupled system obey relation $nf_1 \approx mf_2$, synchronization of order n:m arises for sufficiently strong couplings. The frequencies of interacting systems become locked, $nf_1 \approx mf_2$, and the phases ϕ_1 and ϕ_2 are also related. The condition of phase locking can be formulated as [79]

$$\phi_{n,m} = n\phi_1 - m\phi_2 = const., \tag{6.2}$$

where n and m are integers. For periodic oscillators, the condition of phase locking is equivalent to the notation of the frequency locking [79]:

$$nf_1 - mf_2 = \text{const.} \tag{6.3}$$

This phase locking condition (6.2) can be used only for quasi-periodic oscillators. For more general forms of nonlinear oscillators, i.e., relaxation oscillators, a weaker condition of phase locking is used,

$$\left|n\phi_1 - m\phi_2 - \delta\right| < const., \tag{6.4}$$

where δ is some phase shift. A phase shift between the oscillators depends on the initial detuning of the interacting systems and the type and parameters of coupling.

Lag synchronization. Lag synchronization is defined as a coincidence of states of two systems shifted in time, $\mathbf{x}_2(t + \tau) = \mathbf{x}_1(t)$ [91]. It is an appearance of shift between times of characteristic points of the first (T_1) and the second (T_2) oscillator, formulated as [91]

$$nT_1 - mT_2 = const. \tag{6.5}$$

Global synchronization. In large ensembles of oscillators, where each element interacts with all others, it is also denoted as all-to-all coupling. A phase-transition-like phenomenon, characterized by the appearance, or disappearance, of collective oscillations in the oscillator communities is known as Kuramoto self-synchronization transition [54].

Complete synchronization. Contrary to phase synchronization, it can be observed in any chaotic system, not necessarily autonomous systems. This phenomenon is not close to the classical synchronization of periodic oscillations, due to the lack of rhythm adjustment. Complete synchronization is the suppression of differences in coupled identical systems. This effect cannot be described as entrainment or locking, as it is closer to onset of symmetry. Regime, where each of the systems demonstrate that chaos and their states are identical at each moment in time, is called complete synchronization[6].

Generalized synchronization. This is the synchronization of nonidentical systems. Clearly, the states cannot coincide exactly, but they can be rather close to each other. In particular, it may be that for a large enough coupling, there is a functional relation $\mathbf{x}_2 = \mathbf{F}(\mathbf{x}_1)$ between the states of the two systems. This means that knowing the functions **F,** one can uniquely determine the state of the second system, if the first is known. The regime is called generalized synchronization [96]. Complete synchronization is a particular case of generalized synchronization when the functions **F** are simply identity functions. Typically, generalized synchronization is observed for unidirectional coupling when the first (driving) system forces the second (driven) system, but there is no back-action, known as a master-slave coupling.

Synchronization and noise. In general, synchronization can be destroyed in the presence of noise. Measured data sets contain some noise. It can be instrumental, thermal, physiological, or numerical, i.e., resulting from quantization of analogue signals. By physiological, we mean the effect of interactions on the measured quantity with the rest of the system. It manifests as a complex modulation of the natural frequency of the subsystem under observation. However, if the noise is small, the frequencies are nearly locked. Phase difference would be expected to fluctuate around a constant value. In this case, the condition (6.3) is fulfilled on an average, $n\langle f_1\rangle = m\langle f_1\rangle$. Large noise can cause phase slips, i.e., the phase performs random-walk-like motion. Strictly speaking, the synchronization region shrinks to a point where the largest phase-locking intervals survive as regions of nearly constant mean frequency.

If we consider synchronization in the presence of noise, synchronization of chaotic systems, or synchronization of oscillators with modulated natural frequencies, phase and frequency locking, may no longer be equivalent [101]. One can distinguish between several forms of synchronization frequency and phase locking, phase locking without frequency locking and frequency locking without phase locking [79]. The question of whether it is synchronous or not cannot be answered in a unique

[6] Sometimes the terms *identical*, *full* and *chaotic* are also used.

way, but only treated in a statistical sense. Phase synchronization can be understood as the appearance of a peak in the distribution of the cyclic relative phase [79]

$$\Psi_{n,m} = \phi_{n,m} \bmod 2\pi, \tag{6.6}$$

and interpreted as the existence of a preferred stable value of the phase difference $\phi_{n,m}$ between the two oscillators.

In the case of the cardiovascular system, with time-varying characteristic frequencies, phase synchronization may onset, while the frequencies may or may not be entrained. The notation (6.4) is used for phase synchronization.

6.2 Measurements

Electrical activity of the heart (ECG), respiration, EEG and temperature were recorded from rats undergoing anaesthesia. 21 rats all weighted 250 g, most of them males, were measured. The first 11 rats were of testing nature used for calibration of the measuring devices and determination of the signal quality. They were not used for the subsequent data analysis. The measurements started 4-7 minutes after the anaesthetic (Rompun- ksilizinhydrochlorid, Ketalar-ketaminhydrochlorid) infusion and ended once the rats started to move spontaneous (pinch test). The duration of the measurements was ~70 min. All signals were digitized with 16-bit resolution and sampled at 1000 Hz using National Instruments measuring device. Temperature was set to 24 ± 1 °C. Rats were lying on abdomen during the measurement in Faraday's cage. The data acquisition techniques are described in [63] but, in summary, were as follows. The respiratory effort was measured using the TSD101B Respiratory Effort Transducer (Biopac Systems, Inc., USA). It consists of a piezoresistive sensor mounted on an inelastic band. To detect the respiratory movements, the band was wrapped around rat abdomen. The electrical conductivity of the sensor was proportional to the increase of abdominal circumference. The electrical activity of the rat's heart was obtained using three electrodes. The reference electrode was mounted on the rat's tail whereas the remaining two electrodes were put on the front legs of the rat. EEG, the electrical activity of the rat's brain was measured using one differential signal and one reference electrode. The electrodes were realised with medicine needles that were thrusted into the rat's head. And finally the temperature was measured using NTK (negative temperature coefficient) resistors in differential binding.

6.3 Data analysis

We proceeded as already discussed above in Sec. 5.6. for the calculation of cross-bispectrum B_{cere}, where c stands for cross, e for signal $e(t)$ and r for signal $r(t)$. The ECG and respiration signals were first pre-processed. Both very low and very high frequencies were removed by use of moving average windows: drift with a 200 s long window; and high frequencies with a 0.04 s window while, and at the same time, the signal was resampled to 50 Hz. By using the moving average before resampling, we avoid problems of aliasing [81]. In case of cross-bispectrum calculation the signals have been further normalized between zero and one, and their mean value subtracted.

The maximum biphase and biamplitude were calculated for each peak. The frequency resolution was set to be 1/20 of the lowest respiration frequency or better. The slowest-paced breathing, f_2, was approximately 1 Hz, so that a window of 20 s or longer was necessary for estimation of the cross-bispectrum, biphase and biamplitude. Short plateaus in the estimated biphase occur frequently. To exclude coincidence interactions we focused on those that lasted for at least about 10 periods of the lower coupling frequency f_2. The length of the window also determines the time resolution. In the case of the slowest-paced breathing, where f_2 was 1 Hz we were seeking approximately 10 times $(1/f_2) = 10$ s long epochs of constant biphase. Therefore a window length of 10 s or less was necessary to meet the criterion for time resolution. Due to the Heisenberg uncertainty principle [43], the scope for choice of window length is limited, and compromise is needed between time and frequency resolution. 20 s long window was chosen. The window was moved along the time series with a time step of 0.1 s. The critical value for the biamplitude estimate to be considered valid was set in all cases to 2, i.e., twice the average value of the bispectrum within its so-called inner triangle (IT), as discussed in Sec. 3.3.

By calculating the cross-bispectrum we are interested in establishing relation to the information about coupling between the heart and the respiratory oscillators and one obtained from the synchrogram.

6.4 Results

We show results of cross-bispectrum obtained from rat16 and rat20 rats signals undergoing anaesthesia where a clear episodes indicating synchronization were detected.

6.4.1 Rat16

Examples of detrended, resampled and their mean value subtracted ECG $e(t)$ and respiration $r(t)$ signals for rat16 undergoing anaesthesia are presented on Fig. 6.1 (a) and (c).

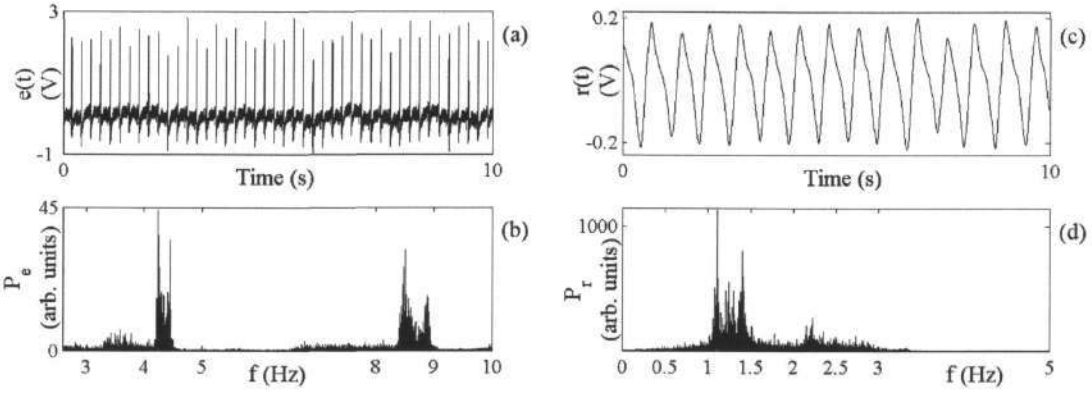

Fig. 6.1: 10 s of detrended, resamlpled and removed zero mean (a) ECG $e(t)$ and (c) respiration $r(t)$ signal for the case of rat16 undergoing anaesthesia, ~72 minutes long at sampling frequency f_s = 50 Hz and power spectrums (b) and (d).

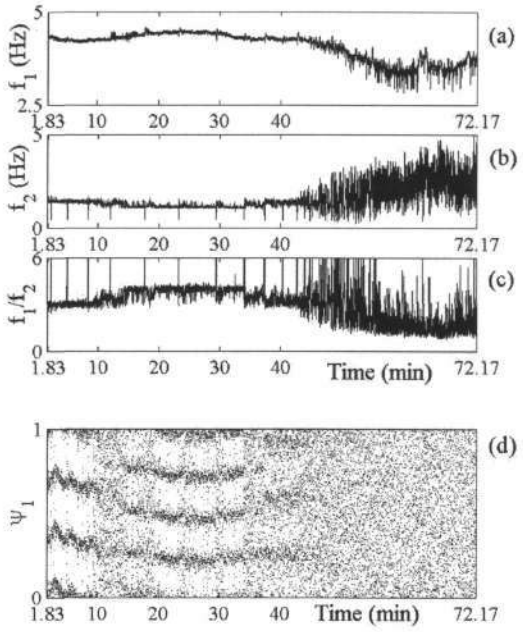

Fig. 6.2: (a) Instantaneous cardiac, (b) respiration frequency and (c) their frequency ratio for a rat16 undergoing anaesthesia. (d) Cardio-respiratory synchrogram for the rat16.

The peak in the power spectrum, Fig. 6.1 (b), at frequency of ~4.4 Hz belongs to cardiac activity, f_1; the ones at ~1-1.5 Hz belong to the respiratory activity, f_2, Fig. 6.1 (d). It can be seen that their precise

values vary in time, which is what makes the analysis difficult. The widths of the peaks indicate their time-variable frequency content.

The instantaneous phase of the cardiac activity was obtained by characteristic or marker events - the R peaks in the ECG signal. A 2π increase of phase is attributed to the interval between subsequent R peaks. The instantaneous phase of respiration was obtained in a similar way, using expiration moment as the marker event. By differentiating the instantaneous phases we obtain the instantaneous (a) cardiac and (b) respiratory frequencies and (c) their ratio as shown in Fig. 6.2.

Fig. 6.2 (d) shows a cardio-respiratory synchrogram based on the stroboscopic technique [79] for rat16 undergoing anaesthesia. A 3:1 phase locking can be seen lasting from 1.83 until approximately 9.1 min. Ψ_1 attains same 3 different values within each 1 adjacent respiratory cycle resulting in 3 horizontal strips in synchrogram during this time. Just before time equals 20 minutes horizontal structures appear again resolving a 4:1 phase locking during breathing indicating synchronization and then disappear before time equals approximately 33.6 min. It cannot be clearly seen that 3 strips occur after that indicating weak 3:1 synchronization till approximately 44.6 min.

In the histogram of frequency ratio, Fig. 6.3, two high peaks appear, one at $f_2/f_1 = 3$ and the other at $f_2/f_1 = 4$ as one would expect from the content of the synchrogram.

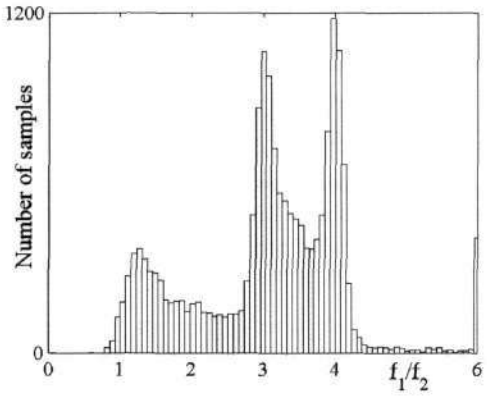

Fig. 6.3: Histogram of cardiac f_1 and respiratory f_2 frequency ratio for the rat16.

Cross-bispectrum for rat16 is presented in Fig. 6.4. High peaks are indicating frequency and/or phase interactions between cardiac and respiratory activity. From the contour view of the cross-bispectrum it can be clearly seen that at bifrequency of our primary interest two peaks occur. The first one is located at (4.25 Hz, 1.1 Hz), and the second one at (4.45 Hz, 1.4 Hz) resolving that there was a frequency shift

in cardiac and respiratory activity. For both peaks we are looking for further three peaks, according to their frequency relations, Tab. 5.2. All of them are present.

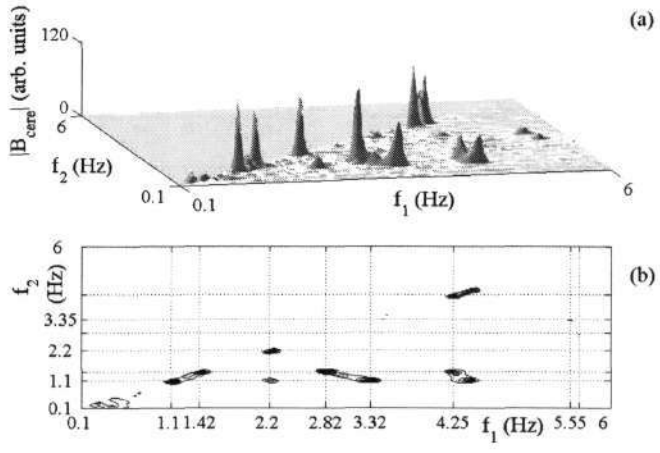

Fig. 6.4: Results for a rat16 undergoing anaesthesia. (a) The cross-bispectrum $|B_{cere}|$ calculated with K = 211 segments, 0 % overlapping and using the Blackman window to reduce leakage and (b) its contour view.

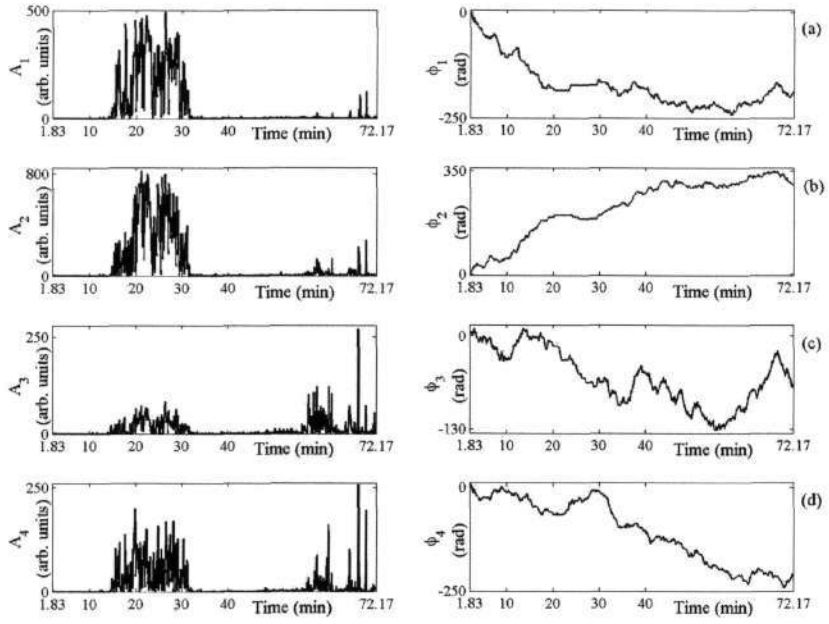

Fig. 6.5: The biphase ϕ and biamplitude A for bifrequencies: (a) peak 1 (4.25 Hz, 1.4 Hz), (b) peak 2 (2.85 Hz, 1.4 Hz), (c) peak 3 (2.85 Hz, 2.8 Hz) and (d) peak 4 (4.25 Hz, 2.8 Hz) with a 0.1 s time step and a 20 s long window for estimating the DFTs using the Blackman window.

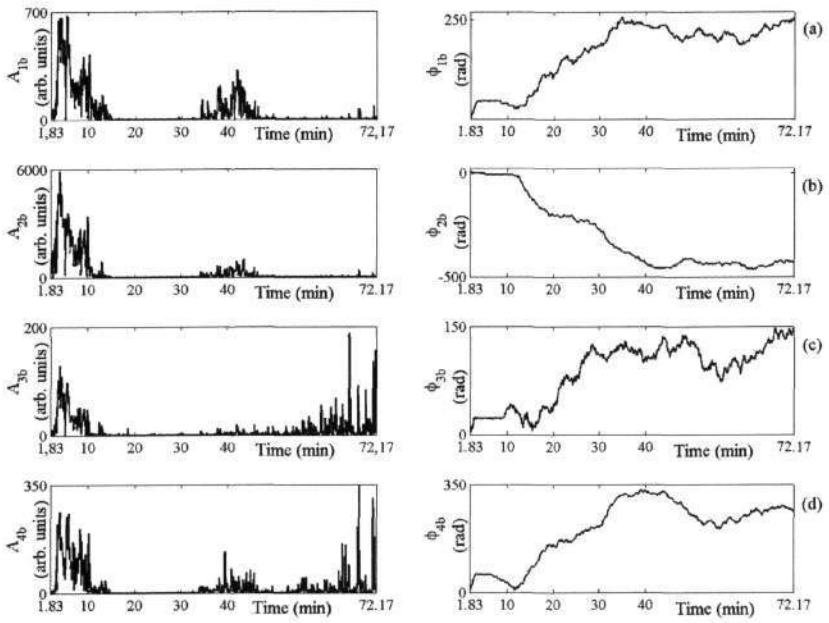

Fig. 6.6: The biphase ϕ and biamplitude A for bifrequencies: (a) peak 1 (4.45 Hz, 1.1 Hz), (b) Peak 2 (3.35 Hz, 1.1 Hz), (c) Peak 3 (3.35 Hz, 2.2 Hz) and (d) Peak 4 (4.4 Hz, 2.2 Hz) with a 0.1 s time step and a 20 s long window for estimating the DFTs using the Blackman window.

6.4.2 Rat20

Examples of detrended, resampled and their mean value subtracted ECG $e(t)$ and respiration $r(t)$ signals for rat20 undergoing anaesthesia are presented on Fig. 6.7 (a) and (c).

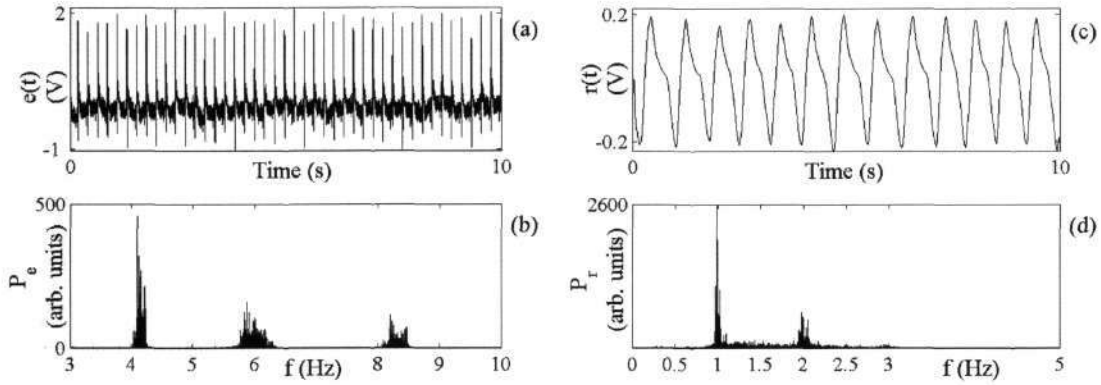

Fig. 6.7: 10 s of detrended, resampled, normalized and removed zero mean (a) ECG $e(t)$ and (c) respiration $r(t)$ signal for the case of rat20 undergoing anaesthesia, ~72 minutes long at sampling frequency f_s = 50 Hz and their power spectrums (b) and (d).

The peak in the power spectrum, Fig. 6.7 (b), at frequency of ~4.3 Hz belongs to cardiac activity, f_1; the one at ~1 Hz belongs to the respiratory activity, f_2, Fig. 6.7 (d). Beside second harmonic of the f_2 a peak can be seen ~6 Hz. This peak occurs when the rat starts wakening from anaesthesia, the inclined transition in the instantaneous cardiac frequency at approximately 40 min, Fig. 6.8 (a). Instantaneous respiratory frequency and ratio of cardiac and respiratory frequencies are shown in Fig. 6.8. (b) and (c).

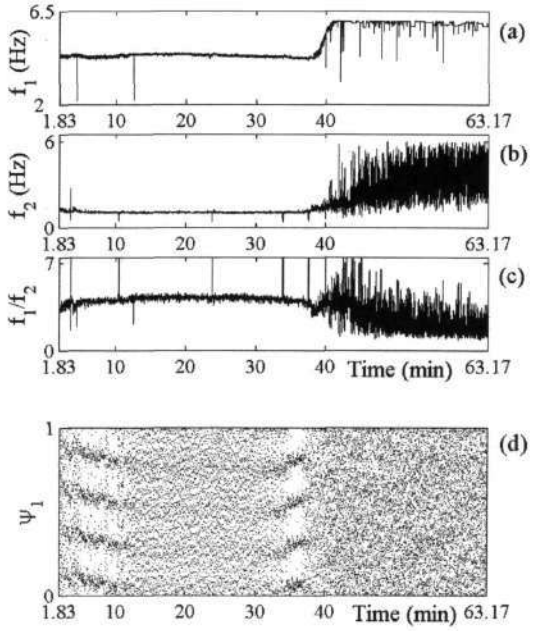

Fig. 6.8: (a) Instantaneous cardiac, (b) respiration frequency and (c) their frequency ratio for a rat20 undergoing anaesthesia. (d) Cardio-respiratory synchrogram for the rat20.

Fig. 6.8 (d) shows a cardio-respiratory synchrogram for rat20 undergoing anaesthesia. A 4:1 phase locking can be seen starting at approximately 4.4 minutes until approximately 10.7 minutes and from approximately 33.7 minutes until approximately 37.9 minutes, both resulting in 4 horizontal strips in synchrogram during that time.

In the histogram of frequency ratio, Fig. 6.9, one high peak appears at $f_2/f_1 = 4.2$ as one would expect from the content of the synchrogram. The peak at frequency ratio 1.6 is due to rat20's onset of spontaneous breathing from approximately 38 to 42 minutes, Fig. 6.8 (b), and is thus irrelevant.

Cross-bispectrum for rat20 is presented in Fig. 6.10. High peaks appear, indicating at least frequency interactions between cardiac and respiratory activity. From the contour view of the cross-bispectrum it can be clearly seen that at bifrequency (4.3 Hz, 1.05 Hz), that is of our primary interest a peak appears. Close inspection of the cross-bispectrum resolves all three other, according to their frequency relations, Tab. 5.2, necessary peaks. They are all present.

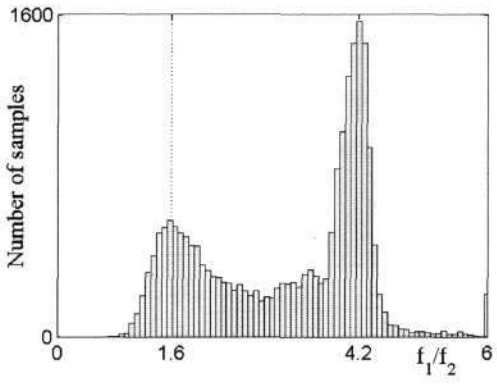

Fig. 6.9: Histogram of cardiac f_1 and respiratory f_2 frequency ratio for the rat20.

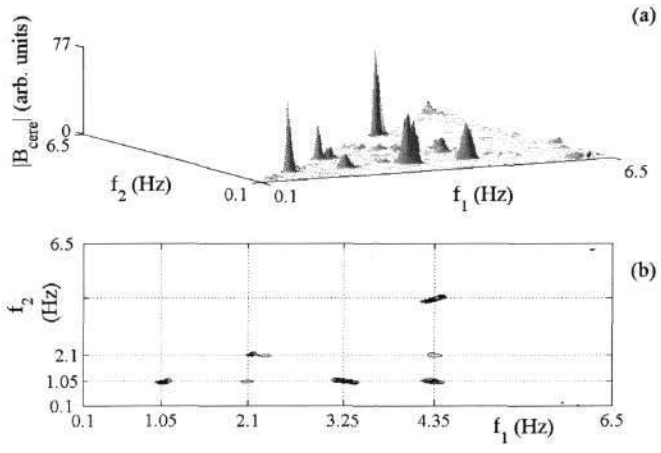

Fig. 6.10: Results for a rat20 undergoing anaesthesia. (a) The cross-bispectrum $|B_{cere}|$ calculated with K = 185 segments, 0 % overlapping and using the Blackman window to reduce leakage and (b) its contour view.

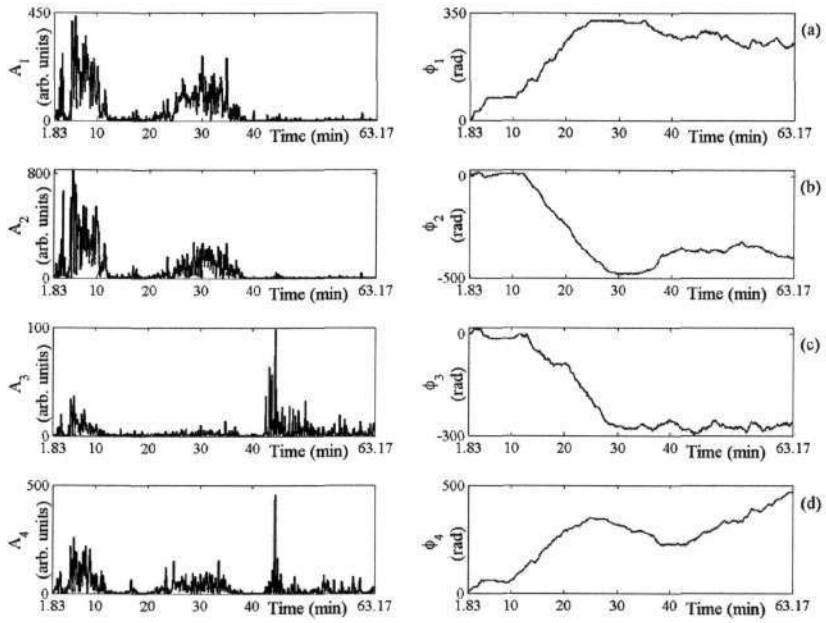

Fig. 6.11: The biphase ϕ and biamplitude A for bifrequencies: (a) peak 1 (4.3 Hz, 1.05 Hz), (b) peak 2 (3.25 Hz, 1.05 Hz), (c) peak 3 (3.25 Hz, 2.1 Hz) and (d) peak 4 (4.3 Hz, 2.1 Hz) with a 0.1 s time step and a 20 s long window for estimating the DFTs using the Blackman window.

6.5 Discussion

Rat16. Both cross-bispectrum and synchrogram analysis produced very similar results. The cardio-respiratory synchronization appears in synchrogram in the beginning of the signal, at 1.83 minutes, in the ratio 3:1, and lasting until approximately 9.1 minutes. This interaction can be seen in the cross-bispectrum as presence of the peaks. Close inspection, i.e., calculating the biamplitude and biphase for the peak of our primary interest at bifrequency (4.45 Hz, 1.1 Hz), indicates high amplitude and a constant biphase during this time, Fig. 6.6 (a). This indicates a phase coupling between the cardiac and respiratory oscillators. Moreover, inspecting peaks 2-4 at frequency positions related according to Tab. 5.2, we obtain the same results. Biamplitudes are high and biphases are constant during this time, Fig. 6.6 (b) - (d). Taking into account the conditions for nonlinear quadratic interaction, we obtain two distinct time intervals, T_{qc1} and T_{qc2}, where they are all fulfilled, Tab. 6.1. The first, T_{qc1}, starts at 4.20 minutes and lasts for 47 seconds, or 66 breathing cycles. The second, T_{qc2}, starts at 5.25 minutes and lasts for 66 seconds, or 92 breathing cycles.

Analysing further, according to the synchrogram after the 3:1 synchronization stops, we obtain a 4:1 synchronization starting at approximately 20 minutes, and persisting until approximately 33 minutes. In cross-bispectrum, a peak at bifrequency (4.25 Hz, 1.4 Hz) appears. Other peaks also appear that are frequency related according to Tab. 5.2. From the biamplitude's time dependences, Fig. 6.5 left

column, we obtain high biamplitudes at all inspected bifrequencies, A_1 - A_4, during this time. Biphases also tend to be constant during this time, Fig. 6.5 right column. Biphases A_1 and A_2 are constant, whereas biphases A_3 and A_4 have many phase slips. There is only one longer time interval when conditions for nonlinear quadratic interaction are fulfilled. It starts at 20.33 minutes and lasts for 14 seconds, or 15 breathing cycles.

In the synchrogram, it cannot be clearly seen that three strips occur after 4:1 synchronization at approximately 38 minutes, indicating weak 3:1 synchronization until approximately 44.6 minutes. This weak interaction can also be detected with the cross-bispectrum. There is a biamplitude rise above 0 during this time, Fig. 6.6 left column, and biphase ϕ_{b1} tends to be constant, Fig. 6.6 (a). Peak 3 is absent, and we cannot detect any nonlinear interaction during this time.

Rat20. Cross-bispectrum and synchrogram analysis results differ. The cardio-respiratory synchronization appears in synchrogram at the beginning of the signal at approximately 4.4 minutes, in the ratio 4:1, and lasts until approximately 10.7 minutes. This interaction can be also seen in the cross-bispectrum, indicating the presence of peaks. Calculating the biamplitude and biphase for the peak of our primary interest at bifrequency (4.3 Hz, 1.05 Hz), indicates high amplitude and a constant biphase during this time, Fig. 6.11 (a). This indicates a phase coupling between the cardiac and respiratory oscillators. Further inspection of peaks 2-4 at frequency positions related according to Tab. 5.2, provided the same results. Biamplitudes are high and biphases are constant during this time, Fig. 6.11 (b) - (d). Taking into account when the conditions for nonlinear quadratic interaction are fulfilled, we obtain an interval starting at 7.33 minutes, that lasts for 76 seconds, or 80 breathing cycles, Tab. 6.1.

Second synchronization section, from approximately 33.7 to 37.9 minutes in the synchrogram, when the 4:1 synchronization reappears. In this case, the information obtained from the cross-bispectrum differs from the synchrogram. From biamplitude A_1 time dependence, a high amplitude can be seen during the interval at 25-35 minutes. During this time, biphase ϕ_1 is constant, but only until 33 minutes when 4:1 synchronization is detected in the synchrogram. At this point, biphase ϕ_1 is no longer constant, and biamplitude A_1 begins to decrease until it reaches 0, at which point, the synchronization stops. Peak 3 is not present during this time.

The data of Rat20 was specifically chosen, as there is constant frequency ratio from approximately 15 minutes to 30 minutes, Fig. 6.8 (c), but no synchronization can be seen in the synchrogram, Fig. 6.8 (d). Bispectrum resolves more information about the coupling. From the Fig. 6.11 (a), (b) and (d) there is high biamplitude during this time whereas (c) is low. The biphase for peak 1 is constant from 25

minutes onwards. This strongly suggests that modulation takes place. In the following chapter this will be discussed in detail.

Tab. 6.1: Quadratic nonlinear couplings detected in rat16 and rat20 signals. T_{qc} is the time interval during which the bispectral analysis showed that the heart oscillator, f_{hr}, and the respiratory oscillator, f_{res}, might be nonlinear coupled. The product of $T_{qc} \times f_{res}$ provides us with the amount of respiratory periods over which the interaction persisted. During T_{qc}, the maximum biamplitude is calculated for peak 1, which is of primary interest to us. In addition, the maximum variation of biphase $\Delta\phi$, its average value $\bar{\phi}$, and its standard deviation σ_ϕ, were calculated during T_{qc}.

Rat	t_1 (min)	t_2 (min)	f_{hr} (Hz)	f_{res} (Hz)	T_{qc} (s)	$T_{qc} \times f_{res}$	A_{1max} (arb. units)	$\Delta\phi$ (rad)	$\bar{\phi}$ (rad)	σ_ϕ (rad)
16	4.20	4.98	4.25	1.4	47	66	608	0.57	-1.81	0.14
16	5.25	6.35	4.25	1.4	66	92	679	1.05	58.25	0.29
16	20.23	20.47	4.45	1.1	14	15	304	0.71	-14.33	0.21
20	7.33	8.60	4.30	1.05	76	80	353	1.25	-13.82	0.27

It is not possible to discern from synchrogram whether the horizontal strips are due to synchronization or modulation. Moreover, both phenomena can overlap. Nevertheless, if the modulation is very strong, then the horizontal strips are not equidistant, and the modulation can be detected.

6.5.1 Synchronization and modulation

Synchronization analysis, based on the mutual prediction approach [93, 94] and on information-theoretic functional [70, 73] for rat16 and rat20, showed that during the synchronization episodes, the respiratory system is dominant (i.e., is the driving system) and drives the cardiac system [63]. In Sec. 5.8.5.1, we have demonstrated the case of a forced oscillator illustrating the unidirectional interaction between the cardiac and respiratory oscillators, where the respiration frequency is kept constant. In this example, cardiac and respiratory oscillators are not synchronized. In Sec. 4.5, we showed a numerical example of frequency modulation. Again, there was no synchronization of the interacting oscillators.

Besides the modulation, when two oscillators are interacting, whether unidirectionally or bidirectionally, synchronization can also onset. These phenomena are distinct, although they can overlap. There can be modulation without synchronization, synchronization without modulation, or a combination of both effects. To illustrate how efficient bispectral analysis is in the latter two

examples, we use a generic model (6.7) of an almost periodic, Poincaré oscillator, periodically driven by a weak external force, as in case of the model (5.5) with additional frequency modulation

$$\begin{aligned} \dot{x} &= -xq - (\omega_1 + \eta_m \sin(\omega_2 t + \phi_0))y + F\sin(\omega_2 t + \phi_0) + \xi(t), \\ \dot{y} &= -yq + (\omega_1 + \eta_m \sin(\omega_2 t + \phi_0))x, \\ q &= \alpha(\sqrt{x^2 + y^2} - a). \end{aligned} \tag{6.7}$$

The activity of the oscillator is described by the two state variables, x and y. α, a and ω_1 are constants. F is the forcing amplitude with frequency ω_2 and initial force phase ϕ_0, and η_m is the strength of modulation by the forcing oscillator. Here, $\xi(t)$ is zero-mean white Gaussian noise, $\langle \xi(t) \rangle = 0$, $\langle \xi(t), \xi(0) \rangle = D\delta(t)$, and $D = 0.2$ is the noise intensity. The parameters of the model are set to $\alpha = 1$, and $a = 0.5$.

The test signal $x_{1H}(t)$ is the variable x of the driven oscillator, recorded as a continuous time series. For the first 400 s, there was no forcing, i.e., the amplitude was set to zero. It was then raised to a small constant value 0.1, without frequency modulation. After a further 400 s, the forcing was increased to 0.2 and the modulation strength was set to 0.2 (moderate). The corresponding power spectrum for the first 15 s and for each forcing strength are shown in Fig. 6.12 (a) and (b), in order to demonstrate the changes in spectral content and behaviour caused by the forcing. The peak labelled as $f_1 = 1$ Hz represents the driven cardiac oscillator, and the peak labelled $f_2 = 0.2$ Hz represents the driving respiratory oscillator. These frequencies are deliberately chosen to have an integer ratio 5:1.

In case of n:1 locking, the effect of the forcing can be twofold. It causes modulation on the period of the oscillator that occurs with the period of the forcing, and the force adjusts the average period of oscillations, i.e., synchronization. Synchrogram for the test signal x_{1H}, Fig. 6.13, exhibits 5:1 synchronization for the whole signal duration. In the first 400 s, there is no interaction, forcing or modulation on the oscillator. The frequencies and the force of the oscillator are constant and in integer ratio, which is the reason for the synchronization appearing in the synchrogram. In general, one should be cautious when interpreting synchrogram, as it can be misleading. For this case, the bispectrum will be completely flat, without the appearance of any peaks, as can be seen from Fig. 6.12 (f).

From 400 s to 800 s, weak forcing is present. External force tries to change the amplitude as well as the phase of the oscillation. The amplitude is stable, whereas the phase is neutral (it is neither stable nor unstable). Weak force influences the oscillator phase that results in synchronization. A similar case without synchronization was already discussed in Sec. 5.8.5.1 Adapted bispectrum resolves that linear interaction takes place. If biphase is constant for the bifrequency (f_1, f_2), then we can conclude that

they are phase coupled. This results in synchrogram in horizontal strips - synchronization. If the frequency ratio was rational, then horizontal strips would not appear in the synchrogram. Thus, the bispectrum yields the correct information about the coupling.

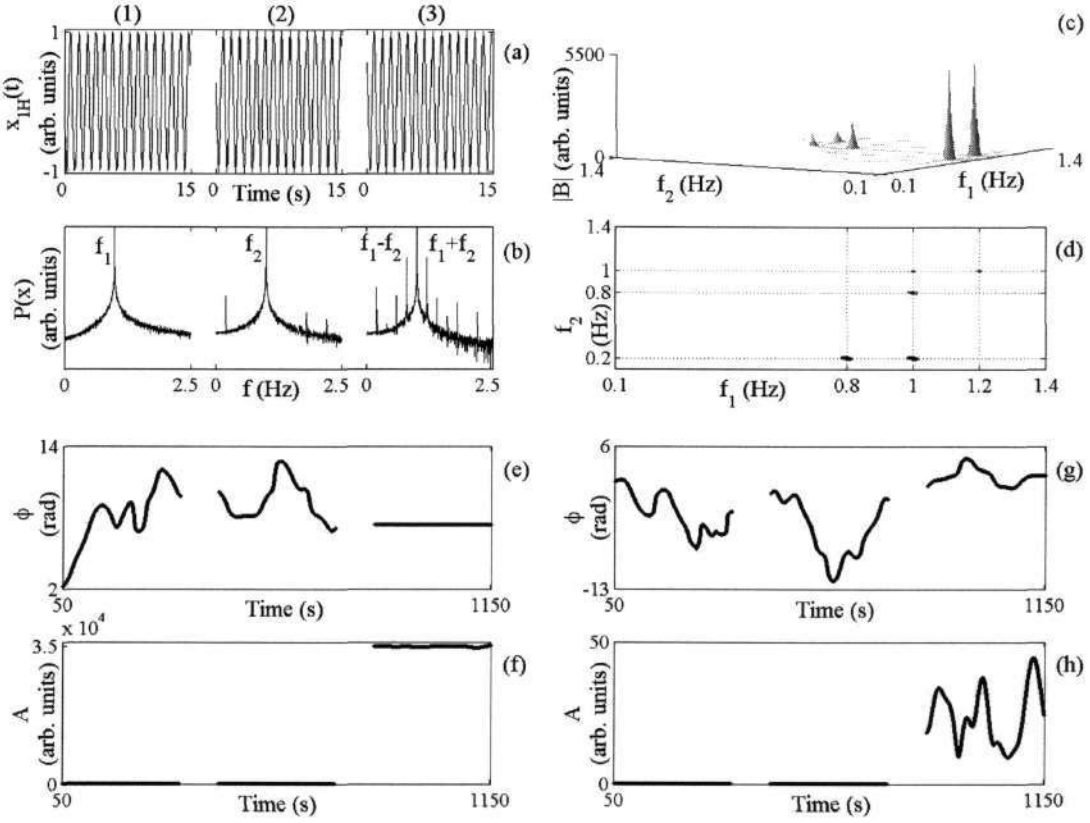

Fig. 6.12: Results for a forced and frequency modulated Poincaré oscillator in the presence of additive Gaussian noise. (a) The test signal x_{1H}, of variable x of the forced oscillator, with characteristic frequency f_1 = 1 Hz periodically forced at frequency f_2 = 0.2 Hz, with three different forcing amplitudes; F= 0.0 (1), 0.1 (2) and 0.2 (3) and three different modulations ; η_m = 0.0 (1), 0.0 (2) and 0.2 (3). Each forcing lasts for 400 s, at sampling frequency f_s = 10 Hz. Only the first 15 s are shown in each case. (b) Its power spectrum. (c) The bispectrum $|B|$ calculated with K = 33 segments, 66 % overlapping and using the Blackman window to reduce leakage, and (d) its contour view. (e) The biphase ϕ, (f) biamplitude A for bifrequency (1,0 Hz, 0,2 Hz) peak 1, (g) biphase ϕ, and (h) biamplitude A for bifrequency (1.2 Hz, 0.8 Hz) peak 6, with a 0.1 s time step, and a 100 s long window, for estimating the DFTs using the Blackman window.

In the last 400 s of the test signal x_{1H}, moderate forcing and moderate modulation take place. The synchronization is preserved, as can be seen from the synchrogram, Fig. 6.13. Combination of forcing and modulation could be misleading in detecting nonlinear interaction using the bispectrum as all the frequency components, except for the appearance of $2f_1$ (the $2f_1$ - f_2 is present) in the power spectrum, Fig. 6.12 (b) (3). It is not as evident as in the case presented in chapter 4.7, where only the modulation

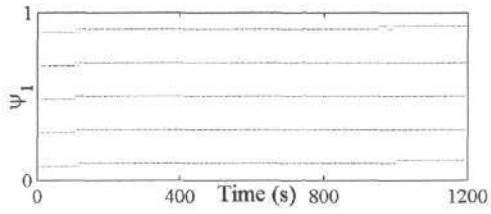

Fig. 6.13: Synchrogram for test signal x_{1H}.

takes place, but one can determine it by calculating all the necessary peaks for the nonlinear coupling. Biamplitude for the peak of primary interest is very high and the biphase is constant, Fig. 6.12 (e) and (f), whereas for peak 6, it is not, Fig. 6.12 (g). Also significant for the modulation, is the appearance of very high peaks (1 and 2), compared to the others (3-6). From the constant biphase for peak 1, we can conclude that the interacting oscillators are in phase and synchronized. If the phase would not be that constant, then it would be difficult to say that they are synchronized, as it was seen in the case of rat20, where only modulation was detected, since the biphase of peak 2, Fig. 6.11 (b), is not similarly time dependant at that time, as is the case for peak 1.

6.6 Conclusions

For the case of synchronization, we can conclude as follows:

- **Strong synchronization.** Synchrogram and bispectrum (cross-bispectrum) provide us with the same results. We only inspect the peak at bifrequency of our primary interest. When there is a strong synchronization between two interacting oscillators, then clear horizontal strips appear in synchrogram indicating synchronization. In bispectrum, the synchronization is indicated with a high biamplitude value and constant biphase at bifrequency of our primary interest (f_1, f_2).

- **Weak synchronization.** Horizontal strips in synchrogram can hardly be detected or they cannot be detected. Bispectrum results in moderate biamplitude and less constant biphase, with more phase slips at bifrequency of our primary interest (f_1, f_2).

- **No synchronization.** The synchrogram contains no horizontal strips. Bispectrum results in zero biamplitude at bifrequency of our primary interest (f_1, f_2). Although there is no coupling, synchronization can onset in synchrogram, due to constant frequency ratio.

As synchronization can take place simultaneously with frequency modulation/forcing/nonlinear coupling, we can further conclude:

- **Synchronization and nonlinear coupling.** Nonlinear coupling can appear while synchronization takes place, whereas while there is nonlinear coupling, synchronization does not necessarily onset. There is no obvious link between the two phenomena. Analysis of rats undergoing anaesthesia shows that nonlinear coupling occurs during synchronization, while analysis of CV blood flow signals of humans in resting shows nonlinear coupling when synchronization is not present.

- **Frequency modulation**. Frequency modulation can be detected using bispectrum. The peak of primary interest (f_1, f_2), and the second peak at bifrequency (f_1 - f_2, f_2), are high in comparison to other peaks (that may not be present at all) that appear in the case of nonlinear interaction. Their biphase is constant if the frequency modulation is strong.

- **Frequency modulation and forcing**. Instantaneous presence of both phenomena can be misleading in detecting the nonlinear coupling. It is necessary to check all the peaks, 1-6. Biphase for peaks 4 and 6 is not constant. It is recommended to analyse the peak of primary interest (f_1, f_2) for adopted bispectrum. Biphase should be constant. In this way, it is possible to resolve this kind of interaction between two oscillators. Nevertheless, one should be careful in interpreting the bispectrum results when strong frequency modulation and strong forcing in the presence of strongly noisy data take place. Observing the phases of each frequency component in the triplet can be helpful.

- **Frequency modulation and nonlinear coupling**. When strong frequency modulation and nonlinear coupling take place simultaneously, it is not possible to detect modulation. When the frequency modulation is weak, this can be seen as undulated biphase at peak of primary interest (f_1, f_2). It is difficult to be sure, as it could also be the case of a weak nonlinear coupling.

We conclude, therefore, that bispectral analysis is more sensitive to interactions and is more noise robust than the synchrogram. It detects the phase synchronization, and nevertheless, yields different information from that which can be resolved from a synchrogram. Frequency modulation interaction can be detected, whereas it is not always possible to resolve it if it simultaneously occurs with other types of interactions.

7 HIGH-ORDER SPECTRA BASED ON WAVELET TRANSFORM

The Fourier transform is based on presumptions (a) of the periodicity of the signal and (b) of infinitely long signal series [57, 58]. Because neither assumption is strictly true for the measured signals, the determination of separate frequencies in a system that possesses strong couplings is very demanding. The difficulty is even greater in the low frequency range, which is of our particular interest, where the characteristic frequencies are close to each other, and are therefore even harder to separate. The uncertainty principle of the Fourier transform limits its ability to separate harmonic components in the frequency domain of the bispectrum [20, 43]. This might cause problems for detection of quadratic phase couplings in the case of frequency pairs that are close together. To ensure good resolution of low frequencies, we need longer sections for calculation of the discrete Fourier transform. This immediately decreases the number of sections possible and weakens the bispectrum estimation. However, we cannot use longer signals, because they lead to nonstationarity, and the variance consequently becomes even larger [69].

7.1 Wavelet Transform

Wavelet analysis can be seen as a generalization of the Fourier analysis [43] by adding time resolution - in a more fundamental way than is permitted by the Short-Time Fourier Transform (STFT) [81]. Wavelet analysis has been applied with considerable success to cardiovascular data [6, 8]. The generalization of bispectrum to wavelet analysis may be expected to be able to detect temporal variation in phase coupling or short-lived couplings, and cope with broadened and coalescing peaks

that cannot be resolved due to time-frequency resolution restrictions by the bispectrum based on STFT.

Morlet first introduced wavelet analysis [28]. Within this transform, the window length is adjusted to the frequency currently being analysed. It is a scale independent method. Window function is called a mother wavelet or basic wavelet $\psi(u)$. It can be any function $\psi(u)$ that satisfies the wavelet admissibility condition [43]

$$c_{\psi} = \int_{-\infty}^{+\infty} |\hat{\psi}(u)|^2 |u|^{-1} du < \infty. \tag{7.1}$$

This function introduces a scale s (its width) into the analyses. Commitment to any particular scale is avoided by using all possible scaling of $\psi(u)$. The mother wavelet is also translated along the signal to achieve time localization. Thus, a family of generally non-orthogonal basis function is obtained [43]

$$\Psi_{s,t} = |s|^{-p} \psi\left(\frac{u-t}{s}\right). \tag{7.2}$$

The parameter p is the normalization choice and is an arbitrary non-negative number. In literature, values of p of 0, ½ and 1 are encountered [17]. The prevailing choice is p = ½. Factor $|s|^{-1/2}$ is used to ensure energy preservation. In this case, the L^2 norm of the wavelet, and thus its energy, is unaffected by the scaling operator s. The continuous wavelet transform of a signal $g(t)$ is defined as [43]:

$$W_g(s,t) = \int_{-\infty}^{+\infty} \Psi^*\left(\frac{\tau - t}{s}\right) g(\tau) d\tau . \tag{7.3}$$

The wavelet transform $W_g(s, t)$ is a mapping of the function $g(t)$ onto the time scale plane. Not every function can be used as the mother wavelet. Only those that enable us to reconstruct the original function $g(t)$ from its wavelet transform $W_g(s, t)$ are admissible. The inverse continuous wavelet transform is defined as [43]:

$$g(t) = \frac{1}{C} \int_{\Re^2} \int |s|^{2p-3} \Psi\left(\frac{\tau - t}{s}\right) W_g(s,\tau)\, ds\, d\tau , \tag{7.4}$$

where the constant C is determined by the shape of the mother wavelet [43]

$$C = \int_{-\infty}^{+\infty} \frac{1}{|f|} |\hat{\psi}(f)|^2 \, df, \tag{7.5}$$

where $\hat{\psi}(f)$ is the Fourier transform of $\psi(u)$. It can be seen from Eq. (7.4) that reconstruction is only possible if $0 < C < \infty$. If $\psi \in \Re$, then $\hat{\psi}(f)$ is continuous, so that C can only be finite if $\hat{\psi}(0) = 0$, i.e., [43]

$$\int_{-\infty}^{+\infty} \psi(u) du = 0. \tag{7.6}$$

Total energy of the signal $g(t)$ can be calculated as [43]

$$\|g\|^2 = C^{-1} \int_{\Re^2} \int |s|^{2p-3} |W_g(s,t)|^2 \, ds \, dt. \tag{7.7}$$

The function

$$\rho = C^{-1} |s|^{2p-3} |W_g(s,t)|^2, \tag{7.8}$$

can be interpreted as the energy density of the signal in the time scale plane, also called a scalogram. Applying Parseval identity $\langle e, a \rangle = \langle \hat{e}, \hat{a} \rangle$ into Eq. (7.4) we obtain

$$W_g(s,t) = \left\langle \Psi_{s,t}, g \right\rangle = \left\langle \hat{\Psi}_{s,t}, \hat{g} \right\rangle. \tag{7.9}$$

Fourier transform of $\Psi_{s,t}$ is

$$\Psi_{s,t} = |s|^{-p} s e^{-j2\pi ft} \hat{\Psi}(sf), \tag{7.10}$$

so that Eq. (7.3) can be written as [43]

$$W_g(s,t) = |s|^{1-p} \int_{-\infty}^{+\infty} e^{-j2\pi ft} \hat{\psi}(sf) \hat{g}(f) df. \tag{7.11}$$

The wavelet transform provides a multiplying constant and phase shift $e^{-j2\pi ft}$ information about $\hat{g}$ inside the window that is determined by instantaneous scale and shape of the mother wavelet.

7.1.1 Discretization

In numerical applications, scale s and time t are restricted to discrete values only. The natural discretization of the scaling parameter is $s_m = \sigma^m$, where $m \in Z$, and the step is a positive number $\sigma \neq 0, 1$. Within the scale σ^m, the signal is sampled only at times $t_n = n\sigma^m$, which means that the sampling rate is automatically adjusted to the scale [43].

For different values of m and n, we obtain the discrete wavelet family

$$\Psi_{m,n}(u) = \sigma^{-m/2}\psi(\sigma^{-m}u - n\tau), \tag{7.12}$$

where we have set the value of parameter p to ½. The discrete wavelet transform, defined by this family, is simply a sampled version of $W_g(s, t)$. By choosing σ near 1, we can get a representation close to the continuous transform.

7.1.2 Wavelet transform adopted to CV signals

The coupling between wavelets makes sense when a frequency can be assigned to wavelet. We restrict our attention to wavelets which have Fourier transforms that exhibit a single dominant peak, and define the location of that peak as the corresponding frequency. In literature [43], several suitable wavelets are mentioned. Issuing from former energy density studies of measured cardiovascular signals, the wavelet transform with Morlet mother wavelet was chosen to be the most suitable one [6, 8].

Morlet proposed the use of Gaussian function modulated by a sin wave. Its Fourier transform is a shifted Gaussian, adjusted slightly so that the admissibility condition $\hat{\psi}(0) = 0$ is fulfilled [43]

$$\hat{\psi}(f) = \sqrt{2\pi}\frac{1}{\sqrt[4]{\pi}}\left[e^{-4\pi^2(f-f_0)^2/2} - e^{-4\pi^2 f^2/2}e^{-4\pi^2 f_0^2/2}\right]. \tag{7.13}$$

In the time domain, simplified expression is [43]

$$\psi(u) = \pi^{-1/4}\left(e^{-j2\pi f_0 u} - e^{-4\pi^2 f_0^2/2}\right)e^{-\frac{u^2}{2}}. \tag{7.14}$$

The choice of f_0 is a compromise between localization in time and in frequency. For smaller f_0, the shape of the wavelet favours localization of singular time events, whilst for larger f_0, more periods of the sin wave in the window improve the frequency localization. For $f_0 > 0.8$, the value of the second term in (7.14) is so small that it can be ignored in practice, and a simplified expression for the Morlet wavelet in the time domain is [43]

$$\psi(u) = \pi^{-1/4} e^{-j2\pi f_0 u} e^{-\frac{u^2}{2}}. \tag{7.15}$$

The corresponding wavelet family consists of Gaussians, centred at a time t with standard deviation s. In the frequency domain, we have Gaussians with a central frequency $f = f_0/s$ and a standard deviation of $1/2\sqrt{2}\pi s$. Therefore, the wavelet transform at a given scale s can also be interpreted as band-pass filtering, giving an estimation of the contribution of the frequencies in this band. The relation between the scale and the central frequency for the Morlet wavelet is [43]

$$f = \frac{f_0}{s}. \tag{7.16}$$

The frequency resolution changes with frequency; at low frequencies (large scales), the resolution is better than at the high frequencies (small scales). Accordingly, the time resolution is better for high frequency than it is for low frequency components. In order for peaks to be detected at f_1 and f_2 ($f_1 > f_2$), they must be separated by at least one half of the standard deviation of the peak at the higher frequency, namely $f_1 - f_2 \geq f_1/4\pi f_0$. The choice of f_0 determines the current frequency resolution. By choosing $f_0 = 1$, a simple relation between scale and frequency was obtained $f = 1/s$.

To obtain the energy density in the time-scale plane, an approximation of the continuous wavelet transform was calculated using the Morlet mother wavelet discretized with $\sigma = 1.05$ and $\tau = 1$ s. However, to make the three-dimensional plots of the transform clearer, time was not discretized as $t_n = n\sigma^m\tau$, but $t_n = n\tau$ was used instead. In this way, the transform is over sampled in time for large scales.

Slow events are examined with a long window, whilst a shorter window is used for faster events, Fig. 7.1. The Morlet wavelet [28], a Gaussian window, i.e., a Gaussian function modulated by a sin wave, is used. Thus, for our purpose, the best time-frequency localization within the limits of the uncertainty principle can be achieved. For details see [43]. For the Morlet mother wavelet, the value C, Eq. (7.5), equals $C = 1.0132$ [8].

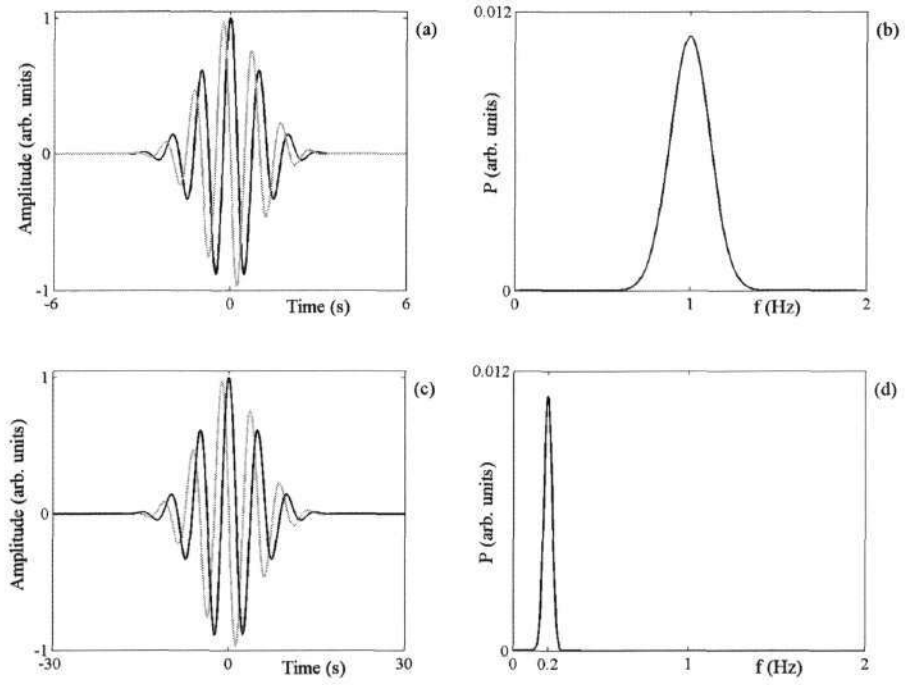

Fig. 7.1: (a) Real (black line) and imaginary (grey line) part of the Morlet mother wavelet for scale $s = 1$ and (c) for scale, $s = 5$, (b) and (d) its Fourier transforms. In both cases, $f_0 = 1$.

7.2 Wavelet bispectrum definition

The definitions are completely analogous to the definitions used in Fourier analysis [67]. The Wavelet Bispectrum (WB) is given by

$$WB(s_1, s_2) = \int_T W_g(s_1, \tau) W_g(s_2, \tau) W_g^*(s, \tau) d\tau, \tag{7.17}$$

where

$$\frac{1}{s_1} + \frac{1}{s_2} = \frac{1}{s}. \tag{7.18}$$

The WB measures the amount of phase coupling in the interval T that occurs between wavelet components of scale lengths s_1 and s_2 and s of signal $g(t)$, such that the frequency sum-rule is satisfied (7.18). It is a complex quantity, defined by magnitude A and phase ϕ

$$WB(s_1, s_2) = \left|WB(s_1, s_2)\right| e^{j\angle WB(s_1, s_2)} = A e^{j\phi}. \tag{7.19}$$

Consequently, for each (s_1, s_2), its value can be represented as a point in a complex space, $\Re[WB(s_1, s_2)]$ versus $\Im[WB(s_1, s_2)]$, thus defining a vector. We define its magnitude (length) as biamplitude, and the phase, which is determined by the angle between the vector and the positive real axis, as biphase.

The instantaneous biphase is then calculated: from Eqs. (7.17) and (7.19), it is

$$\phi(s_1, s_2, t) = \phi_{s_1}(t) + \phi_{s_2}(t) - \phi_s(t). \tag{7.20}$$

If two scale components s_1 and s_2 are scale and phase coupled, $\phi_s = \phi_{s1} + \phi_{s2}$, it holds that the biphase is 0 (2π) radians. For our purposes, the phase coupling is less strict because dependent scale components can be phase-delayed. We consider phase coupling to exist if the biphase is constant (but not necessarily = 0 radians) for at least several periods of the highest scale component.

Simultaneously, we observe the instantaneous biamplitude from which it is possible to infer the relative strength of the interaction

$$A(s_1, s_2, t) = |WB(s_1, s_2, t)|. \tag{7.21}$$

According to the Fourier definition (5.1), a wavelet cross-bispectrum can be defined as:

$$WB_{cfgg}(s_1, s_2) = \int_T W_f(s_1, \tau) W_g(s_2, \tau) W_g^*(s, \tau) d\tau. \tag{7.22}$$

The wavelet cross-bispectrum measures the amount of phase coupling in the interval T that occurs between wavelet components of scale lengths s_2 and s of signal $g(t)$, and wavelet component s_1 of $f(t)$, such that the frequency sum-rule is satisfied (7.18).

For ease of interpretation, the WB is plotted in the (f_1, f_2)-plane, rather than in the (s_1, s_2)-plane. It has the same symmetries in frequency domain as in the case of Fourier based Bispectrum (FB). The non-redundant region is the principal domain of the wavelet bispectrum. Similarly, the principal domain can be divided into two triangular regions in which the wavelet bispectrum has different properties: the inner triangle (IT), and the outer one. The IT is of our interest.

7.2.1 Wavelet bispectrum transform adopted to CV signals

Relation between frequency (scale) and the width of the window that is used for calculation of the wavelet transform, is hyperbolic. Logarithmic-logarithmic scale is natural for its presentation, whereas, to be able to comply with the (7.18) frequency (scale) sum-rule, we need to achieve better frequency (scale) resolution for high frequencies (low scales) (according to the CV frequency bands proposed in [112]), as can be achieved using the Morlet wavelet when f_0 is chosen to be 1 for the reason of the interpretation of the wavelet bispectrum. Otherwise, nearby peaks at high frequencies cannot be resolved.

We introduce a parameter d into the Morlet wavelet that determines the exponential decay of the Gaussian

$$\psi(u) = a_m \cdot c_n \cdot e^{-j2\pi f_0 u} e^{-\frac{u^2}{2d}}. \tag{7.23}$$

This also decays the Morlet wavelet, and thus permits suitable combination of time and frequency (scale) resolution to be selected. The time resolution is $\Delta t = sd$, given by the decay of the exponential part of the wavelet. As d increases ($d > 1$), frequency (scale) resolution improves, whereas time resolution deteriorates. We do not impose the condition that the wavelets must be orthogonal, as we wish to choose the frequencies in the analysis procedure freely, and not restricted to $s \in \{2^n\}$. This implies a certain redundancy in the wavelet transform coefficients, which must be taken into account upon interpreting the results.

The parameter d is calculated so that the Gauss function decays to 0.001 for each scale (d is between 2.5 and 2.6). A high value of d causes a non-zero value of Morlet window at its edges that results in side lobes in wavelet bispectrum. If d would be infinite, than Morlet window would become a unit window, and wavelet transform would become Selective Discrete Fourier Transform (SDFT) [47]. Parameters a_m and c_n are discussed in the following text.

Frequency resolution for high frequencies is yet insufficient. It is necessary to increase the length of the Morlet wavelet for high frequencies. This can be obtained in different ways. Fig. 7.2 shows the hyperbolicous decay of the Morlet wavelet length with the increasing frequency (solid line). The wavelet length can be multiplied by a factor a_m, that is for the one with the lowest frequency of interest, and then increases with the increasing frequency

$$a_m = 2^{\frac{f-f_{\min}}{f_{\max}-f_{\min}}\cdot 1,8}, \tag{7.24}$$

where $f = 1/s$ is the frequency of observation, and $f_{\min}$ and $f_{\max}$ define the frequency range of interest. In this way, we obtain a dotted line on Fig. 7.2. As the wavelet length is prolonged for high frequencies, the frequency resolution increases, whereas the time resolution deteriorates. Other ways to obtain the necessary frequency resolution is by using a fixed wavelet length for all high frequencies - Fig. 7.2, dash-dot line. We propose to use a 20-80 s long wavelet in the case of analysing the human cardiovascular blood flow signal of a normal, healthy subject at rest.

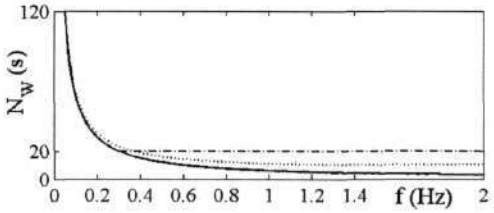

Fig. 7.2: Length of the Morlet wavelet N_W depended from frequency (scale). Morlet wavelet (solid line), adapted Morlet wavelet (dotted line), and fixed wavelet length for high frequencies (dash-dot line).

WB estimation using the proposed Morlet wavelet as a mother wavelet encounters a normalization problem. For each scale, a window of different length is used. In the case of a signal composed of different frequency components, but equal Fourier powers, this would result in different wavelet spectral energies for separate frequencies. Two couplings among different frequencies with the same Fourier powers and the same nature of coupling, would result in different coupling strength in wavelet bispectrum. In (7.2), a factor $|s|^{-1/2}$ is used to ensure energy preservation. We choose to use a factor $1/N_W$ instead, where N_W is the Morlet window length. Constant c_n, Eq. (7.23), equals to $3.9487 \cdot \pi^{-1/4}$. In this way, we can compare results obtained by FB and WB, since both preserve energy.

Normalization of the WB is applied in the same way as on the FB, discussed in Sec. 3.3. The normalized *WB* indicates the average level of quadratic nonlinear phase coupling and, in a way, serves as an indicator of how non-Gaussian the signal is [31]. The critical values for the *WB* and biamplitude estimates were normalized to 1. If the estimated value is higher than the average value of *WB* in the IT, then it is taken as valid. By critical value, it is meant that a value exceeds the noisy background (other than Gaussian), rounding, and estimation errors.

7.3 Wavelet bispectrum example of test signal

Results of WB are illustrated on a numerically generated test signal of two Poincaré oscillators quadratically coupled in the presence of additive Gaussian noise - Eq. (4.6), Sec. 4.4, test signal x_{1D}, presented in Fig. 4.7 (a). Test signal x_{1D} was already analysed using Fourier based bispectrum in Sec. 4.4.

Results obtained using WB, depend on the choice of parameters set for WB calculation. In the first step, the WB is calculated for the whole bifrequencies domain. Similarly, as in the case of FB, one has to set the parameters: K - number of segments into which the signal x_{1D} is divided to try to obtain statistical stability of the estimates; O - percentage of segments overlapping; and L - $L \cdot L$ area for bispectrum frequency averaging. These parameters have already been discussed in detail in [39]. In case of FB, one chooses tapering window (Hamming, Hanning, Blackman or other), whereas WB uses the Morlet mother wavelet. Parameters that can further be chosen are:

- T_m - Morlet mother wavelet length. By choosing $f_0 = 1$, a simple relation between scale and frequency is obtained: $f = 1/s$. Mother wavelet for $f = 1$Hz is then stretched and compressed. The prevailing choice of the T_m is from 8 s (i.e., ± 4 s) to 12 s [6, 7].

- d - exponential decay of Gaussian function of Morlet wavelet. Rather than setting the parameter d, we set Gaussian function of Morlet wavelet edge value to G_e, so that it decays to some small value. The prevailing choice is from 0.01 to 0.0001 (see Sec. 7.2.1 for details).

- Δf - frequency (scale) step. It can be chosen arbitrarily, whereas, to be able to comply with the (7.18) frequency (scale) sum-rule, the prevailing choice is to be at least 1/10 of the slowest frequency in the bifrequency pair of our interest.

- a_m - multiplication factor for additional Morlet wavelet stretching (see Sec. 7.2.1 for details). One can set basis, and the constant in the power. Morlet wavelet length is multiplied by a factor a_m. The factor equals the one of lowest frequency of interest and then increases with the increasing frequency. Either one chooses to use factor a_m whose prevailing choice for basis is 2, and the constant in the power is 1.8, or one chooses to fix the Morlet mother wave length for high frequencies T_{HF}. The prevailing choice of the fixed window length for higher frequencies is from 20 s to 80 s. One should start with a 40 s long window. If the peaks at the bifrequencies of our interest are distinct than shorter fixed window can be used, otherwise longer fixed window must be used.

Once *WB* is obtained, and longer lasting (bispectral averaging over *K* segments eliminates short lasting couplings) phase and/or frequency coupling are detected, biphase and biamplitude time evolution are estimated for bifrequencies of our interest (see Tab. 5.2 for details). Parameters *K*, *O* and *L* do not influence the estimation. Additional parameters can be chosen:

- Δt - time step. Minimum time step is defined with sampling frequency f_s and equals $\Delta t_{min}=1/f_s$. It should be set to such a value that epochs of constant biphase of approximately 10 times the slowest period $(1/f_2)$ of the bifrequency pair (f_1, f_2) can be detected, i.e., at least 1/10 of the epoch length.

- L_t - number of samples for time averaging. In the case of signals with non-Gaussian noise, one can reduce the noise by averaging in the time domain over L_t samples, before and after the time of observation.

WB for the test signal x_{1D} is presented in Fig. 7.3 (a). Parameters are set according to prevailing choice for CV signal analysis as described above (T_m = 8 s, G_e = 0.001, Δf = 0.01 Hz, T_{HF} = 40 s and Δt = 0.1 s). Averaging is neither used in frequency, nor in time domain (L = 0, L_t = 0). Peaks appear at bifrequencies (1.1 Hz, 0.24 Hz), (0.86 Hz, 0.24 Hz), (0.62 Hz, 0.48 Hz), (0.86 Hz, 0.48 Hz), (1.1 Hz, 0.48 Hz), (1.1 Hz, 0.86 Hz) and (1.34 Hz, 0.86 Hz).

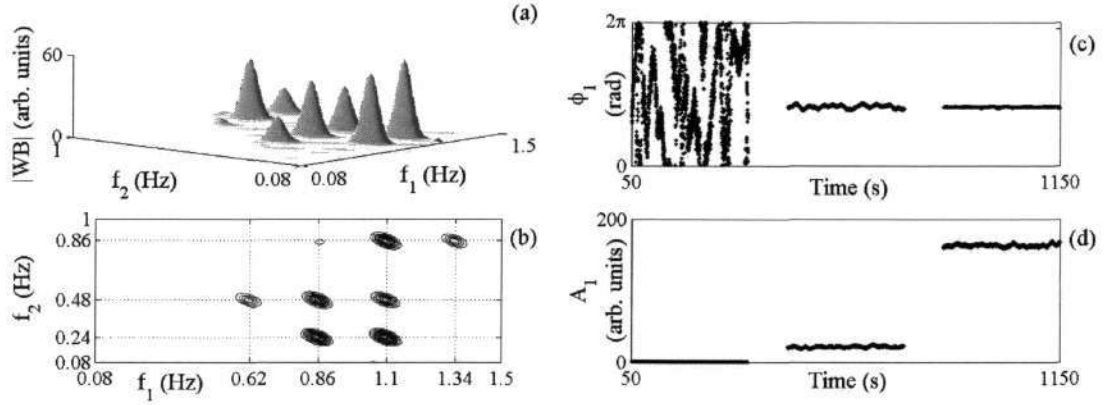

Fig. 7.3: Results for quadratic couplings in the presence of additive Gaussian noise, test signal x_{1D}, obtained with the wavelet bispectrum for comparison with the Fourier bispectrum, Sec. 4.4. (a) The wavelet bispectrum $|WB|$ calculated with K = 33 segments, 66 % overlapping, T_m = 8 s, G_e = 0.001 and using fixed Morlet wavelet length of T_{HF} = 40 s for high frequencies calculation and (b) its contour view. The part of the wavelet bispectrum above $f_2 > 1.0$ Hz is removed, because the triplet (1.1 Hz, 1.1 Hz, 1.1 Hz) produces a high peak that is physically meaningless. (c) The biphase ϕ and (d) biamplitude A for bifrequency (1.1 Hz, 0.24 Hz), with a 0.1 s time step.

As before, the self-coupling peaks at (1.1 Hz, 1.1 Hz) and (0.24 Hz, 0.24 Hz) are of no interest, so they are removed from the wavelet bispectrum. We obtain the same information as with the FB, Fig. 4.7 (c). The most obvious difference is in the shape of the peaks. They are much wider than in the case of FB. This is expected, since frequency resolution for high frequencies is lower than in the case of FB.

Fig. 7.3 (c) shows biphase and (d) biamplitude for the peak of our principal interest at bifrequency (1.1 Hz, 0.24 Hz). We obtain the same information as with FB, Fig. 4.7 (e) and (f). The biphase is constant in the presence of quadratic coupling. Coupling strength can be determined from the biamplitude by normalization. The WB possesses the FB concerning the noise robustness. The results for non-zero coupling are quite different from those where coupling is absent, Fig. 7.3 (d). From the biphase time dependence, it can be seen that the WB is better at detecting biphase changes, since its time resolution is higher than in the case of FB.

7.4 Discussion

In the case of bispectral analysis of cardiovascular interaction, the time-dependent biphase/biamplitude estimate was estimated with an STFT, using a window of constant length. The optimal window length depends, however, on the frequency being studied. The effective length of the window used for each frequency can be varied by applying the wavelet transform. If natural frequencies of the oscillators lie within a relatively narrow frequency interval, then STFT is sufficient for good time and phase/frequency localization. With broader frequency content, however, the wavelet transform, or selective discrete Fourier transform, needs to be applied.

The wavelet and cross-wavelet bispectrum was defined analogous to the definitions used in Fourier based bispectrum and cross-bispectrum. By doing this time-dependant biphase/biamplitude estimate with higher frequency resolution at low frequencies, higher time resolution at higher frequencies was obtained. The wavelet bispectral analysis was adopted for analysing cardiovascular signals. For a mother wavelet modulated Gauss function, the Morlet mother wavelet was used.

The wavelet bispectral analysis was illustrated on a test signal. Since the time resolution of wavelet bispectrum is higher, and the frequency resolution is poorer at high frequencies compared to FB, it is necessary to ensure sufficient frequency resolution before interpretation of the results. Poor frequency resolution would result in poor/incorrect localization of characteristic frequencies. Too high of a time resolution could result in extremely high sensitiveness to noise and statistical error, that would result in phase slips and incorrect oscillator coupling determination. It was necessary to raise frequency resolution for high frequencies, as well as to preserve the scale (frequency) sum condition necessary

for bispectrum estimation. Wavelet bispectrum results are parameter set dependant. Parameter impact on wavelet bispectrum estimation and detailed comparison with Fourier based bispectrum are discussed in the subsequent chapter.

8 FOURIER AND WAVELET BISPECTRUM COMPARISON

In the following section, wavelet bispectrum is compared in detail with Fourier based bispectrum. First, wavelet bispectrum is applied to CV blood flow signals that were already used for studying cardio-respiratory interactions using the Fourier based bispectrum method in Sec. 5. Its benefits and weakness over the Fourier based bispectrum method are then compared in detail and discussed.

8.1 Wavelet bispectrum of CV blood flow signals

For the comparison of WB and FB, we illustrate results obtained for the blood flow signal $b_a(t)$, showed on Fig. 5.1 (a), left column in Sec. 5, used for cardio-respiratory interactions analysis. Data analysis was preformed in the same manner as in Sec. 5, whereas instead of using FB, WB was used. Parameters for WB evaluation were set according to the prevailing choice recommended in section 7.3.

8.1.1 Results

WB for the whole frequency domain for signal $b_a(t)$ is presented in Fig. 8.1 (a). A very high peak located at bifrequency (0.11 Hz, 0.11 Hz), belonging to the respiratory self-coupling, can be seen in the $|WB_{ba}|$, Fig. 8.1 (b). At least three other peaks are clearly evident: at (0.98 Hz, 0.11 Hz) attributable to cardio-respiratory coupling; at (0.87 Hz, 0.11 Hz), which we presume to be coupling between the

respiratory component f_2 and the difference f_1 - f_2; and peak attributable to interaction with lower cardiovascular characteristic components. Their positions can be seen in the $|WB_{ba}|$ contour view shown in Fig. 8.1 (c).

Close inspection of $|WB_{ba}|$, Fig. 8.1 (b), resolves that all the necessary peaks, according to Tab. 5.2, arise as a possible result of a nonlinear interaction between the two oscillators f_1 and f_2 are present. Characteristic frequency at ~0.98 Hz belongs to cardiac activity, f_1; that at ~0.11 Hz to respiratory activity, f_2. Peaks 1 to 6 are presented in Fig. 8.2, left column. Time evolution for biamplitude and biphase for all the peaks are shown in Fig. 8.2, mid and right columns.

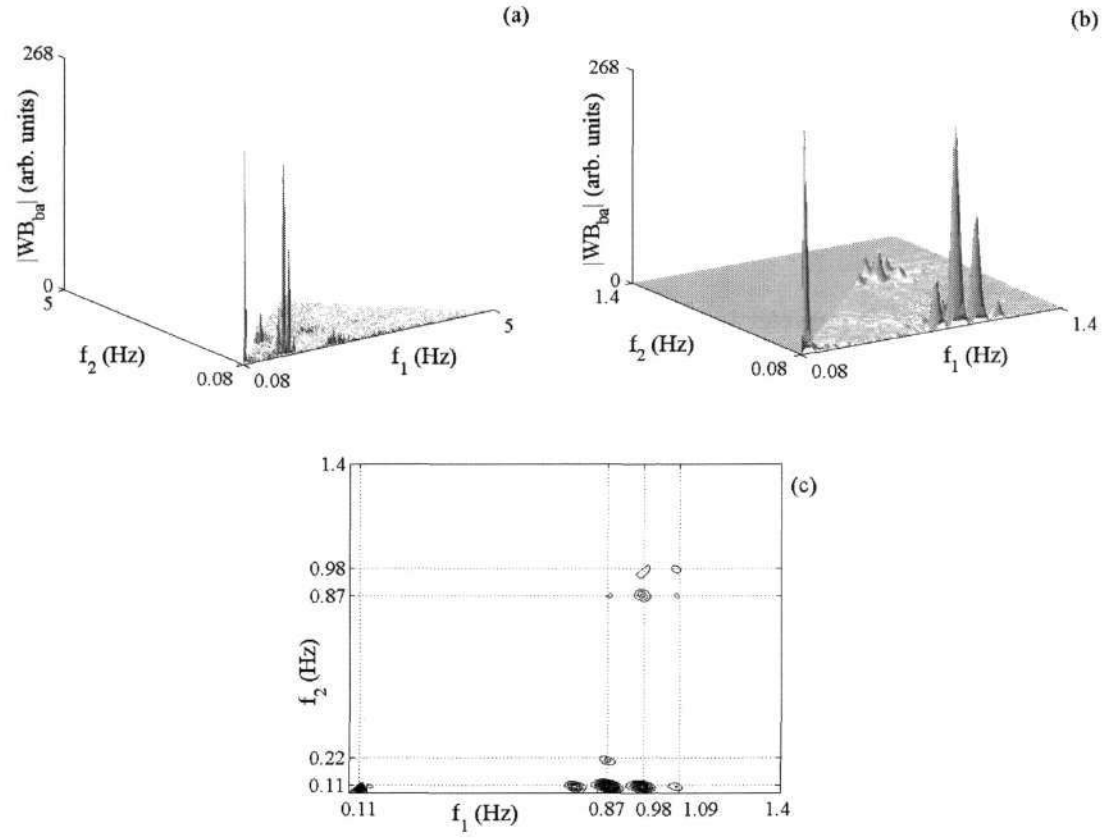

Fig. 8.1: (a) The wavelet bispectrum $|WB_{ba}|$ for signal $b_a(t)$, calculated with $K = 33$ segments, 87 % overlapping, $T_m = 8$ s, $G_e = 0.001$, and using a $T_{HF} = 80$ s long fixed Morlet wavelet for estimating high frequencies. (b) Part of the wavelet bispectrum $f_1, f_2 < 1.4$ Hz that is of our interest, and (c) its contour view.

The time interval T_{qc}, during which quadratic coupling persisted, was determined. If all 6 peaks fulfilled our conditions (see Sec. 5.3 for details), then the T_{qc} interval was calculated for all peaks, and the boundaries were defined such that the biamplitude for all the peaks in T_{qc} interval would be above the condition. It can be seen that the biamplitude during the time interval from 77.1 s to 170.4 s meets our criterion of being more than twice as large as the average wavelet bispectrum in the IT domain;

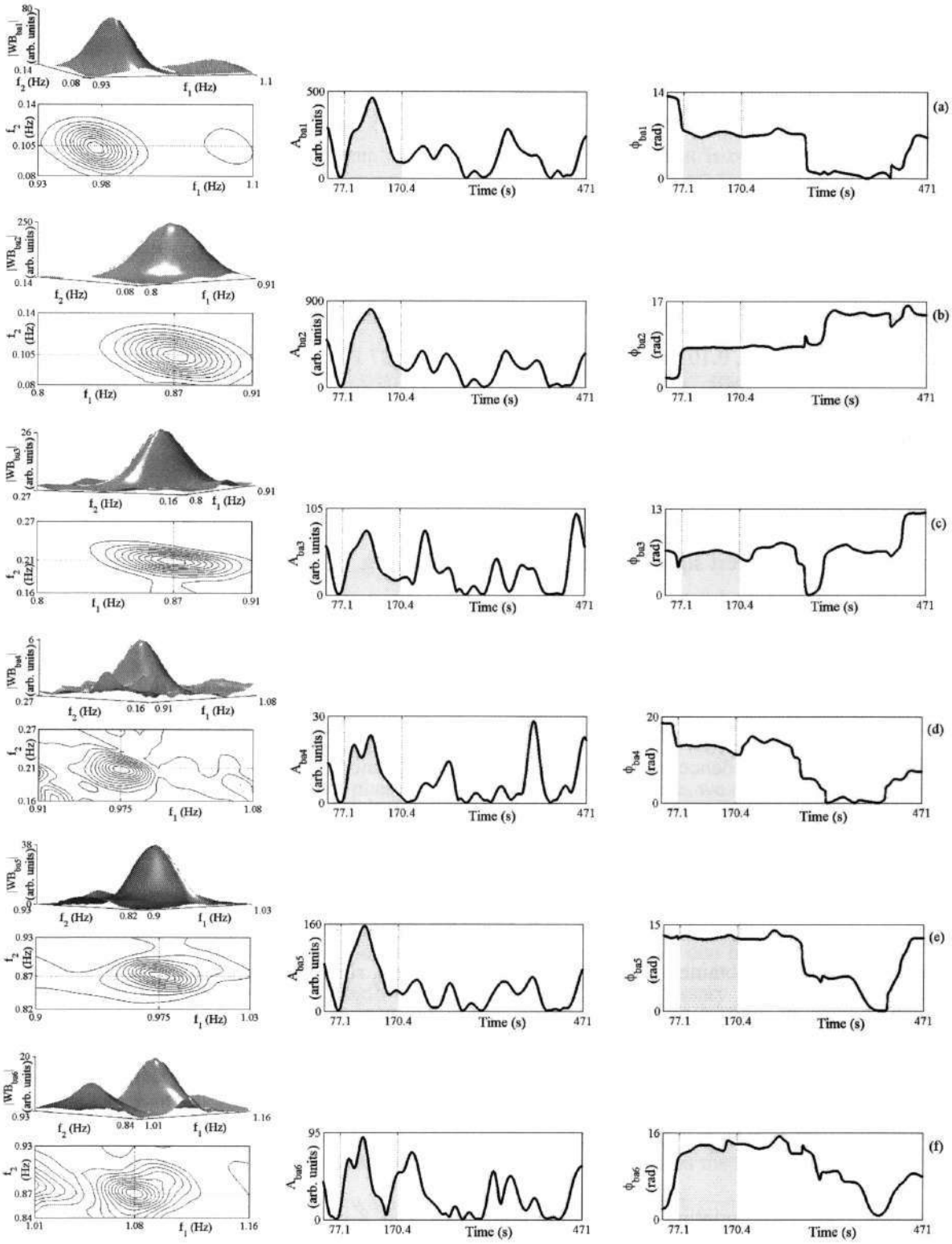

Fig. 8.2: Wavelet bispectrum results for blood flow signal $b_a(t)$, calculated with K = 33 segments, 87 % overlapping, using a 0.1 s time step, T_m = 8 s, G_e = 0.001, and T_{HF} = 80 s long fixed Morlet wavelet for estimating high frequencies for peaks (a) 1, (b) 2, (c) 3, (d) 4, (e) 5 and (f) 6; left column, the wavelet bispectrum $|WB_{ba}|$ with its corresponding contour plots; middle, the biamplitude A_{ba}; and right, the biphase ϕ_{ba}.

see middle column of Fig. 8.2 (a) to (f). The biphase in this time interval, 93.3 s long (shaded area), remains constant within a 3.02 rad interval, i.e., there are no phase slips. The biphases at bifrequencies 1, 2, 3 and 5 are very constant; those at 4 and 6 are less so, but they still remain within the π rad interval.

8.1.2 Fourier and wavelet bispectrum results comparison

Results obtained using WB are most similar to the ones obtained with Fourier based bispectrum. All peaks, 1 to 6; (0.98 Hz, 0.105 Hz), (0.87 Hz, 0.105 Hz), (0.87 Hz, 0.21 Hz), (0.98 Hz, 0.21 Hz), (0.98 Hz, 0.87 Hz), (1.08 Hz, 0.87 Hz), are detected at the same bifrequencies. Characteristic respiratory activity, f_2, is detected at 0.105 Hz, since we used a smaller frequency step for wavelet bispectrum estimation (Δf = 0.005 Hz), than in the case of Fourier based bispectrum (Δf = 0.01 Hz).

Similar to the case of test signal x_{1D}, the peaks are wider, Fig. 8.2 (a) to (e), left column, than in the case of FB obtained results shown in Fig. 5.3 (a) to (e), left column.

Biamplitude time evolution for peak 1, Fig. 8.2 (a), mid column, exhibits three distinguishable peaks. Their time appearance coincides with the peaks obtained with FB, Fig. 5.3 (a), mid column. Moreover, biamplitude time dependence according to it's shape, i.e., number of detectable peaks, their amplitude ratio, and time of occurrence, is highly similar for all the peaks, 1-6. The cross-correlation coefficient for biamplitude, for peak 1, for Fourier and wavelet bispectrum, equals 0.95.

Biphases time evolution obtained with WB, Fig. 8.2 (a) to (f), right column, resemble the time evolution of biphases obtained with FB, Fig. 5.3 8.2 (a) to (f), right column. One can notice that small, sudden changes of biphase obtained using FB, are much more pronounced when WB is used. These changes usually result as sudden biphase slips. Compare biphases at approximately 70 s in Fig. 5.3 (a) and Fig. 8.2 (a), both left column. Although the biphases are not as similar in shape as the biamplitudes are, epochs of constant biphase do coincide for both cases of estimation.

Nonlinear - quadratic coupling is detected in both cases, Tab. 8.1. The one detected with FB lasts from 76.8 s to 172.4 s, shaded area in Fig. 5.3 (a) to (e), mid and right columns, and the one detected with WB lasts from 77.1 s to 170.4 s, shaded area in Fig. 8.2 (a) to (e), mid and right columns. The time interval of quadratic coupling T_{qc} is 2.3 s shorter when estimated with WB. This is less than a 2.4 % difference, Tab. 8.1.

Tab. 8.1: Quadratic nonlinear couplings detected in blood flow signal $b_a(t)$, channel a, for person 1 during paced breathing, detected with both bispectral methods based on Fourier and wavelet transform. T_{qc} is the time interval during which the bispectral (wavelet) analysis showed that the heart oscillator f_{hr} and the respiratory oscillator f_{res} are nonlinear coupled. The product of $T_{qc} \cdot f_{res}$ indicates the span of respiratory periods in which the interaction persisted. During T_{qc}, the maximum biamplitude is calculated for peak 1, that is of our primary interest. In addition, the maximum variation of the biphase $\Delta\phi$, its average value $\bar{\phi}$, and its standard deviation σ_ϕ, were calculated during T_{qc}.

Method	f_{hr} (Hz)	f_{res} (Hz)	T_{qc} (s)	$T_{qc} \times f_{res}$	A_{1max} (arb. units)	$\Delta\phi$ (rad)	$\bar{\phi}$ (rad)	σ_ϕ (rad)
WB	0.98	0.105	93.3	9.8	461	1.09	-1.34	0.32
FB	0.98	1.11	95.6	10.5	383	1.47	3.22	0.42

8.1.3 Results interpretation

Remarkably similar results were obtained with Fourier and wavelet bispectrum. It can be concluded from the width of the peaks, that FB has a higher frequency resolution. Detection of fast, sudden biphase jumps is a result of higher time resolution when using WB. Nevertheless, there were no remarkable differences in quadratical phase coupling detection, therefore, we cannot yet conclude that one method has evident advantages over another. This is correct when analysing cardio-respiratory coupling, where necessary frequency resolution is approximately 1/10 of the lowest interacting component - the respiratory one, f_1 - and where the length of constant biphase episodes that we wish to detect, is approximately 10 times the lowest interacting component. On one hand, it is to ensure that the frequency resolution window length of at least $1/(f_1/10)$ is necessary for Fourier bispectrum estimation, and on the other hand, it is to satisfy that the maximum time resolution window of $10 \cdot (1/f_1)$ is necessary. In this particular case, it is rather an exception, $1/(f_1/10) = 10 \cdot (1/f_1)$, where both resolution conditions are satisfied if a window of $1/(f_1/10)$ length is used. Moreover, this window length is an optimal choice between time and frequency resolution. This is the reason why there are no remarkable differences among the two different Fourier and wavelet transform based bispectral methods.

Choosing the proper window length and the tapering window are the most crucial parameters when applying FB. The parameter choice has already been discussed in detail [39]. WB, adopted for analysis of CV signals, allows one to choose among a set of parameters (T_m, d or G_e, T_{HF} or a - see Sec. 7.3 for details). Proper choice might be crucial when treating the results. Fig. 8.3 illustrates an example of

WB results for blood flow signal $b_a(t)$, for peak 5, for a modified parameter set. In the first example, Fig. 8.3 (a), frequency resolution is emphasized by increasing Morlet mother wavelet length (T_m = 10 s) and setting a longer window for high frequencies estimation (T_{HF} = 50 s). Comparing this to results obtained with the prevailing choice of the parameter set, Fig. 8.2 (e), the difference is obvious. The peak in the wavelet bispectrum is much narrower, Fig 8.3 (a), left column, whereas time evolution for biamplitude, Fig. 8.3 (a), mid column, and biphase, Fig 8.3 (a), right column, are both smoothened out as a result of lower time resolution. In the second example, Fig 8.3 (b), the time resolution is emphasized by compressing Morlet mother wavelet length (T_m = 8 s) and setting a shorter window for high frequencies estimation (T_{HF} = 24 s). The peak in the wavelet bispectrum is much wider, Fig 8.3 (b), left column, whereas biamplitude, Fig. 8.3 (b), mid column and biphase, Fig 8.3 (b), right column, are more sensitive to changes. In the first example, Fig. 8.3.(a), mid column, biamplitude has only one predominant peak, whereas in the second example, Fig. 8.3 (b), right column, biphase has a longer epoch of constant biphase. In the latter case, one could detect a much longer lasting episode of nonlinear cardio-respiratory interaction.

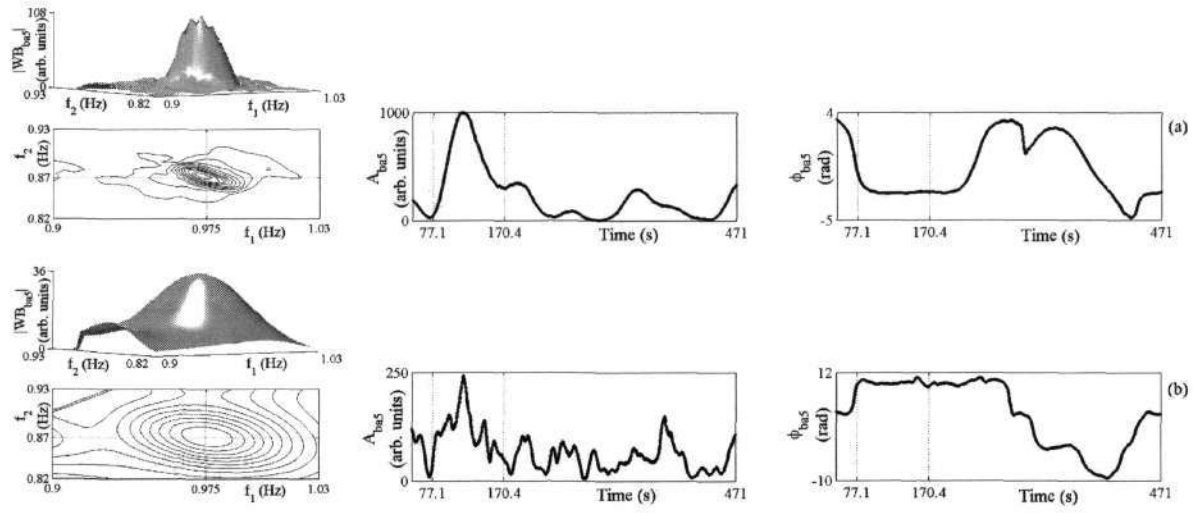

Fig. 8.3: Wavelet bispectrum results for blood flow signal $b_a(t)$, for peak 5, for a modified parameter set. Left column, the wavelet bispectrum $|WB_{ba}|$ with its corresponding contour plots; middle column, the biamplitude A_{ba5}; and right column, the biphase ϕ_{ba5}. (a) Calculated with Morlet mother wavelet (f = 1 Hz) length (a) T_m = 20 s and T_{HF} = 50 s long fixed wavelet for estimating high frequencies, and (b) T_m = 16 s and T_{HF} = 24 s long fixed Morlet wavelet for estimating high frequencies. In both cases, a 0.1 s time step, K = 33 segments and G_e = 0.1 was used.

The question is, which parameter set gives us more realistic results? Let us study two Poincaré oscillators, where the first f_1 = 1.1 Hz and the second f_2 = 0.24 Hz oscillators are quadratically coupled:

$$
\begin{aligned}
\dot{x}_1 &= -x_1 q_1 - \omega_1 y_1 + \eta_2 (x_1 - x_2)^2 + \xi(t), \\
\dot{y}_1 &= -y_1 q_1 + \omega_1 x_1 + \eta_2 (y_1 - y_2)^2, \\
\dot{x}_2 &= -x_2 q_2 - \omega_2 y_2, \\
\dot{y}_2 &= -y_2 q_2 + \omega_2 x_2, \\
q_i &= \alpha_i (\sqrt{x_i^2 + y_i^2} - a_i).
\end{aligned}
\tag{8.1}
$$

Here, $\xi(t)$ is zero-mean white Gaussian noise, $\langle \xi(t) \rangle = 0$, $\langle \xi(t), \xi(0) \rangle = D\delta(t)$, and $D = 0.08$ is the noise intensity. The parameters of the model are set to $\alpha_1 = 1$, $a_1 = 0.5$ and α_2, $a_2 = 1$. In this way, we obtain a test signal $x_{11}(t)$, presented in Fig. 8.4 (a), with the corresponding power spectrum for two different coupling strengths, which are interchanging every 20 s: no coupling $\eta_2 = 0$; and weak coupling $\eta_2 = 0.2$, Fig. 8.4 (b), (1) and (2).

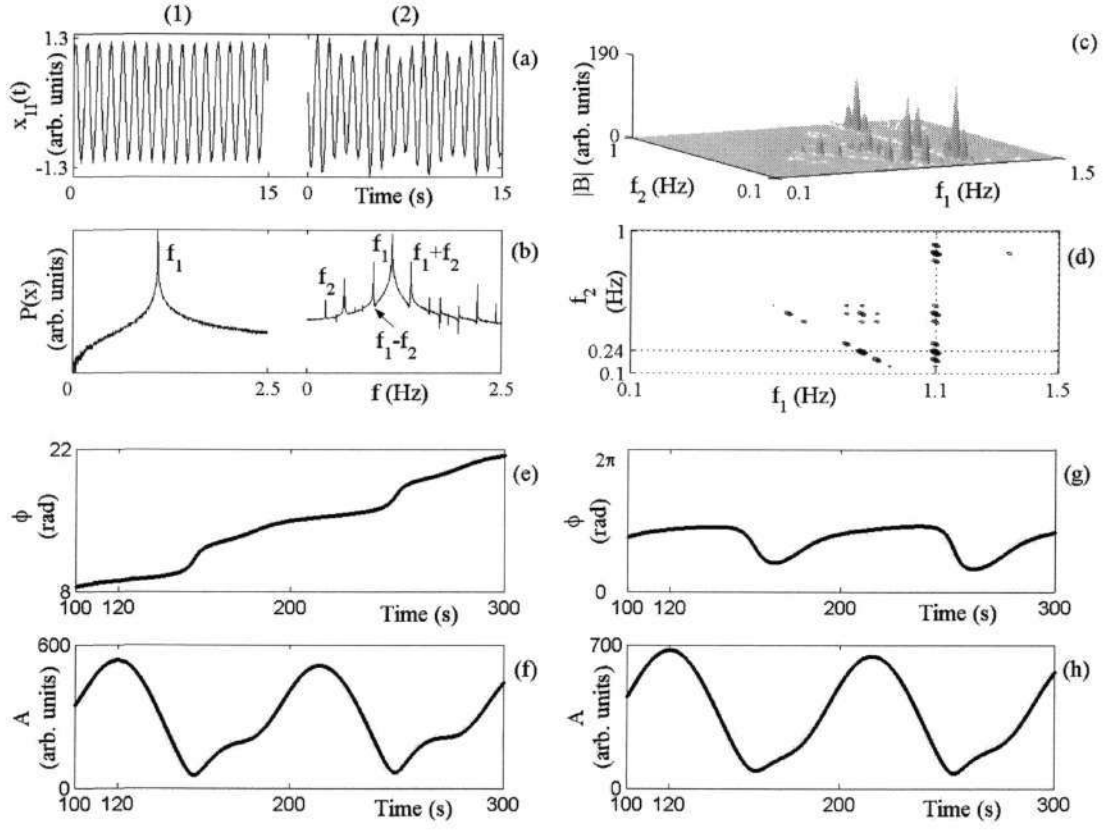

Fig. 8.4: Results for time intermittent quadratic couplings in the presence of additive Gaussian noise analysed using Fourier bispectrum. (a) The test signal x_{11}, variable x_1 of the first oscillator with characteristic frequency f_1 = 1.1 Hz. The characteristic frequency of the second oscillator is f_2 = 0.24 Hz. The oscillators are unidirectionally and quadratically coupled with two different coupling strengths: $\eta_2 = 0.0$ (1); and 0.2 (2). The coupling (2) is present every 20 s and lasts for 20 s. The signal is 1200 s long and sampled with sampling frequency f_s = 10 Hz. Only the first 15 s are shown in each case. (b) Its power spectrum. (c) The bispectrum $|B|$ calculated with K = 33 segments, 66 % overlapping and using the Blackman window to reduce leakage and (d) its contour view. The part of the bispectrum above $f_2 > 1.0$ Hz is cut, because the triplet (1.1 Hz, 1.1 Hz, 1.1 Hz)

produces a high peak that is physically meaningless. (e) The biphase ϕ and (f) biamplitude A for bifrequency (1.1 Hz, 0.24 Hz), calculated with a 100 s long window for estimating DFTs and (g) biphase ϕ and (h) biamplitude A, calculated with a 130 s long window for estimating DFTs. In both cases, a 0.3 s time step and the Blackman window was used.

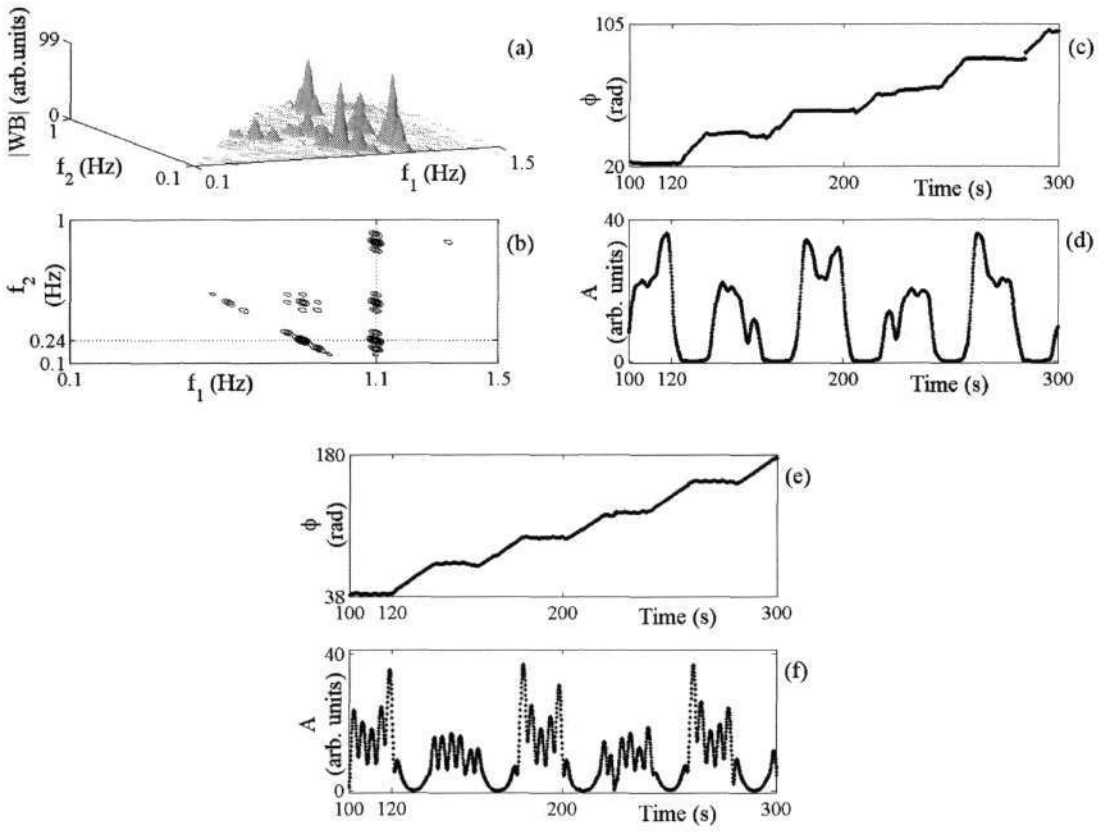

Fig. 8.5: Results for time intermittent quadratic couplings in the presence of additive Gaussian noise analysed using wavelet bispectrum. (a) The wavelet bispectrum $|WB|$ calculated with K = 33 segments and 66 % overlapping. The part of the bispectrum above $f_2 > 1.0$ Hz is removed, because the triplet (1.1 Hz, 1.1 Hz, 1.1 Hz) produces a high peak that is physically meaningless. (c) The biphase ϕ and (d) biamplitude A for bifrequency (1.1 Hz, 0.24 Hz), calculated with a $G_e = 0.01$ and (e) biphase ϕ and (f) biamplitude A, calculated with a $G_e = 0.0001$. In both cases, a 0.1 s time step, $T_m = 8$ s and $T_{HF} = 20$ s long fixed Morlet wavelet for estimating high frequencies was used.

Fig. 8.5 (a) shows wavelet bispectrum, and Fig. 8.5 (b) shows its contour view, obtained for signal x_{II}. It gives the same information about the peak's relative amplitude and bifrequency position. Wavelet bispectrum parameter set, ($T_{HF} = 100$ s, $T_m = 8$ s and $G_e = 0.01$), was deliberately chosen in such a way that time resolution for high frequencies was increased. Results of biamplitude and biphase estimates are presented in Fig. 8.5 (c) and (d). Biamplitude clearly exhibits episodes when coupling is present and when it is not, i.e., every 20 s. From biphase time evolution, episodes of constant biphase can be seen. Episodes of constant biphase, i.e., without phase slips, last longer than the coupling between the

oscillators, i.e., more than 20 s. By taking into account the biamplitude condition for quadratical coupling occurrence, (Sec. 5.3), it is possible to determine the correct quadratic coupling time persistence. Increasing time resolution of wavelet bispectrum even higher, (T_{HF} = 100 s, T_m = 8 s and G_e = 0.0001), we obtain an even more realistic result. Whereas biamplitude, Fig. 8.5 (f), is estimated to be poorer due to lower frequency resolution, but still preserving true information about the time of quadratic coupling occurrence. The biphase, Fig. 8.5 (e), correctly exhibits 20 s of constant biphase episodes, and then 20 s of constantly growing biphase episodes.

8.2 Fourier and wavelet bispectrum advantages and weakness

Time and frequency resolution. To observe a given frequency, the signal must be observed over at least one period of this frequency what excludes the time localization. Due to the Heisenberg uncertainty principle [43] sharp localization in time and frequency are mutually exclusive

$$\Delta t\, \Delta f \geq 1/(4\pi), \tag{8.2}$$

where Δt is time interval and Δf frequency band. The equality holds if and only if the window is Gaussian. They are defined as [43]

$$\Delta t \equiv \frac{1}{\|w\|} \int_{-\infty}^{+\infty} |w(t)|^2 (t - t^*)^2 \, dt, \tag{8.3}$$

$$\Delta f \equiv \frac{1}{\|w\|} \int_{-\infty}^{+\infty} |w(f)|^2 (f - f^*)^2 \, df,$$

where w is in general some window function and $\|w\|^2$ is its norm. For STFT the representation of function $g(u)$ in time-frequency plain $G(t, f)$ has not sharp time and frequency parameters, but represents an interval around centre time t^* or frequency f^*. Time-frequency window is

$$[t + t^* - \Delta t/2, t + t^* + \Delta t/2] \cdot [f + f^* - \Delta f/2, f + f^* + \Delta f/2]. \tag{8.4}$$

For wavelet transform the representation of $W_g(s, t)$ in time-frequency plain is

$$[t + st_0^* - s\Delta t_0/2, t + st_0^* + s\Delta t_0/2] \cdot [f_0^*/s - \Delta f_0/2s, f_0^*/s + \Delta f_0/2s], \tag{8.5}$$

where t_0^* and f_0^* are mother wavelet centres of gravity in time and frequency plain and corresponding deviations of Δt_0 and Δf_0. Note that the centre of the time window depends only on parameter t, whereas the centre of the frequency window depends only on parameter s. On the contrary to the STFT the wavelet transform's frequency resolution changes with frequency (low frequencies have better frequency resolution) and so does the time resolution (high frequencies have better time resolution). The ratio between centre frequency $f^*(s) = f_0^*/s$ and bandwidth $\Delta f(s) = \Delta f_0/s$ is equal to $f_0^*/\Delta f_0$ and is scaling independent.

In general WB detects intermittent phase couplings whereas FB averages out most of the time relevant information. Triplet (f_1, f_2, f_3) results in a high peak in bispectrum if the coupling condition $f_3 = f_1 + f_2$, is satisfied. Nevertheless, the coupling condition needs to be satisfied only within the frequency resolution. This condition is less strict in wavelet bispectral analysis. For example if there is a mismatch in coupling frequency Δf such that $f_3 = f_1 + f_2 + \Delta f$, and Δf is larger than the frequency resolution of the Fourier bispectrum but smaller than the wavelet bispectrum frequency resolution corresponding to a high bispectrum value for the triplet (f_1, f_2, f_3), than the wavelet bispectrum will peak whereas the Fourier bispectrum will not. Increasing the frequency resolution of wavelet bispectrum by increasing the length of the Morlet wavelet for high frequencies results in gradually approximate results as obtained with the Fourier bispectrum.

On the other hand if there is a short lasting coupling present in the signal the Fourier bispectrum cannot detect the coupling due to large time window used, whereas the wavelet bispectrum will detect the coupling if assuming the coupling has a certain minimum duration. Wavelet bispectrum allows intermittent couplings to be detected.

Applying Fourier bispectrum to real data we have to ensure the necessary frequency resolution to be able to distinguish separate frequency components and at the same time achieving sufficiently time resolution to be able to detect the onset of the couplings among CVS oscillators. The scope for choice of window length is limited due to the Heisenberg uncertainty principle [43], and compromise is needed between time and frequency resolution.

Wavelet bispectrum based on Morlet mother wavelet in contrast to the Fourier bispectrum enables us to gain the optimum time and frequency resolution at the same time what is an advantage compared to the Fourier bispectrum.

Since the time resolution of the wavelet bispectrum is higher and the frequency resolution is poorer at high frequencies compared to Fourier bispectrum it is necessary to ensure sufficient frequency

resolution before interpretation of the results. Poor frequency resolution would result in poor/incorrect localization of characteristic frequencies. To high time resolution could result in to high sensitiveness to noise and statistical error, what would result in phase slips and incorrect oscillators coupling onset determination. Setting the time and frequency resolution so that episodes of approximately 10 periods of the lower coupling frequency are detectable and its characteristic frequency can be estimated to at least one tenth or less should be considered.

Frequency step. Once the window length is chosen the frequency resolution is set and fixed for the Fourier based bispectrum. This is not the case when using wavelet transform. Since the wavelet transform is continuous we can choose the frequency step arbitrary. In this way, the transform can be over sampled in time for large scales but we are not concerned for the inverse transform.

Energy preservation. CV signals are power signals [81]. The Fourier bispectrum is based on the DFT which gives the signals energy (power). In case of wavelet bispectrum the normalization is necessary to obtain the signals energy (power).

Statistical error. Integrating over finite time series in order to calculate the wavelet bispectrum causes noise contribution to it's estimation. It is called statistical noise level since it is the value of wavelet bispectrum that would be attained by a white noise input signal, and is caused by finite statistics (i.e., using a limited number of values in the integrating or averaging process). Beside the noise contribution there is also error estimate, which is the product of uncertainties in the determination of the individual wavelet bispectrum coefficients [43, 61, 62, 69].

To calculate the wavelet bispectrum Eq. (7.17) the wavelet coefficients are determinated for each $N_W = T f_s$ samples in the interval T: $\{T_0 - T/2 \leq \tau \leq T_0 + T/2\}$ and averaged Eq. (7.3). Let us assume that all the estimates of the wavelet bispectrum are independent, than the averaged wavelet bispectrum suffers a statistical error of $1/\sqrt{N_W}$ due to summation over N_W values. Similarly in case of Fourier bispectrum the summation is carried out over N/M ensembles, where M is the number of points in each statistically independent ensemble for which M-points Fourier transform is calculated. The statistical error in the Fourier bispectrum decays as $\sqrt{M/N}$, and a factor of M more points are needed to obtain the same statistical error as with the wavelet bispectrum. From this point of view, the wavelet bispectrum represents a significant improvement in the time resolution of the bispectrum.

However, the wavelet coefficients are not all statistically independent, since the chosen wavelet family is not orthogonal. Each coefficient is calculated by evaluating Eq. (7.3) integrating over the range $-\infty < t < +\infty$. Due to the periodicity s of the wavelets of scale s (Fig. 7.1), two statistically independent

estimates of the wavelet coefficients are separated by a time $s/2$, or a number of points $M(s) = sf_s/2$, where f_s is the sampling frequency. Thus the summation done in the evaluation of the wavelet bispectrum is not really carried out over N_W points, but only over $N_W / \max(M(s))$, where the maximum is taken over the values of s that come into account for the evaluation of a specific value of the wavelet bispectrum. An estimate for the statistical noise level in $WB(f_1, f_2)$ is

$$\varepsilon(WB(f_1, f_2) \approx \left[\frac{f_s/2}{\min(f_1 f_2, f_1 + f_2)} \frac{1}{N_W} \right]^{1/2}. \tag{8.6}$$

The statistical error in the determination of $WB(f_1, f_2)$ can be deduced from Eq. (7.17). Each factor in this equation that is obtained by integrating over T suffers an error of $1/\sqrt{N_W}$, so that the error is estimated by

$$\frac{\Delta(WB(f_1, f_2))}{WB(f_1, f_2)} \approx \frac{2}{\sqrt{N_W}}. \tag{8.7}$$

Eqs. (8.6) and (8.7) imply that wavelet bispectral analysis is able to detect coherent signals in extremely noisy data, provided the coherency remains constant during sufficiently long times, since the noise contribution falls off rapidly with increasing N.

Bispectrum interpretation. By choosing $f_0 = 1$ a simple relation between scale and frequency can be obtained $f = 1/s$. In this case the interpretation of the wavelet bispectrum is the same as for the FB otherwise it is not straightforward.

Computation. Default wavelet bispectrum window length drops hyperbolically, whereas Fourier bispectrum used fixed window length. Wavelet bispectrum is therefore computational less demanding and much faster. Also relatively short data sequences are sufficient to perform an analysis, in contrast to the Fourier bispectrum that needs long time series to obtain both sufficient frequency resolution and statistics.

8.3 Other possible methods for bispectrum estimation

A hybrid between Fourier and wavelet transform is Selective Disctrete Fourier Transform (SDFT) which can also be used to perform the bispectrum calculation. It is a modified STFT first introduced by Keselbrener and Akselrod [47]. Like STFT it is time dependent FT. The time-frequency sensitivity

is obtained by windowing with a window of specific length around the analysed data point for estimating each spectral component. Low frequencies are expected to vary slowly on the other hand high frequencies are expected to show fast or sudden changes. For each frequency of interest, a DFT calculation is preformed, while the time window around the considered data point is selected inversely proportional to the frequency of interest. This is similar to wavelet transform's stretching and compressing of the mother wavelet. Therefore narrow windows are used for estimating high frequencies and wide ones for low frequencies, what implies estimating low frequencies with good frequency resolution and high frequencies with good time resolution.

For each time of interest spectral components are calculated using different length of window. The window duration is chosen so that $T = N_p/f$. Parameter N_p, $N_p \in Z$, is the number of entire periods entering the windowed signal. A high value of N_p will lead to poor time resolution (wide window), while on the contrary, a small value could lead to a less reliable estimation of the spectral components in case of noisy signals. The value is determined experimentally to gain best results, usually between the range of 3 and 7 [38].

Leakage may appear in the spectrum, if the signal entering the rectangular window is not periodic, or at least if the amplitude of the end points is not equal. In order to remove such leakage, the data is usually convolved with some kind of smoothing window, such as Hamming, Hanning or Blackman windows. Their role is to taper the windowed data in order to make the two end points amplitudes smoothly equal. Besides the leakage removal, this tapering windows also improve the time resolution of the time-dependent spectral analysis.

SDFT and WT provide similar results. Both transforms are using a specific window length to estimate each spectral component. SDFT uses convolution with Blackman, Hanning, Hamming, or other taper window whereas WT uses different mother wavelets such as Morlet or other. Both methods enable a choice between a good time and a good frequency resolution. We can change frequency and time resolution by changing parameters, but we cannot gain both of them simultaneously, according to the Heisenberg uncertainty principle. The WT obtained by Morlet wavelet enables an optimal time-frequency resolution, while using SDFT it can be approached by an appropriate choice of parameters. They can both be normalised to energy. The main difference between the transforms is that the WT is continuous whereas the SDFT is not.

8.4 Discussion

Wavelet bispectrum was applied to CV blood flow signals. Parameters were set to the prevailing choice, Sec. 7.3. The WB method is suitable for studying cardio-respiratory interaction from the CV blood flow signals. Results obtained with WB analysis are the same as the ones obtained with the Fourier based bispectrum method. There are no obvious advantages of WB over FB when detecting cardio-respiratory interaction that fulfils the conditions defined in Sec. 5.3.

Our motivation was to develop a method that will be able to provide insight into the nature of the CV subsystem couplings. Dynamics of CV blood flow can be considered in terms of coupled oscillators. There are at least five subsystems that take part in blood flow regulation: cardiac, respiratory, myogenic, neural and metabolic system [8, 9, 10, 110-112, 117]. Analysing interaction among cardiac and respiratory system is thus the first step taken. The effect of respiration on heart rate has been the most intensively studied.

The question, what do the revealed nonlinear cardio-respiratory couplings mean, and how they arise, are yet to be resolved. One possibility is that they result from nonlinearity of the carotid baroreceptor-cardiac reflex [22]; another is that they are attributable to the active involvement of the peripheral vessels during cardiac and respiratory wave propagation in the network, or they are due to modulation of the cardiac filling pressure during respiratory movements [126].

In order to be able to analyse all other CVS interactions like cardio-myogenic, cardio- neural, cardio-metabolic, respiratory-myogenic, respiratory-neural, respiratory-metabolic, myogenic-neural, we need to use the wavelet bispectral method. Namely an important feature of CV signals is that they are nonlinear, time-varying, and subject to fluctuation [3, 18, 23, 34, 117]. In low frequency range, which is of our particular interest, the characteristic frequencies are close to each other, and are therefore even harder to separate. The uncertainty principle of the FT, limits its ability to separate harmonic components in the frequency domain of the bispectrum [20, 69]. This might cause problems for detection of the quadratic phase couplings in the case of frequency pairs that are close together. To ensure good resolution of low frequencies, we need longer sections for calculation of the discrete Fourier transform. This immediately decreases the number of sections possible and weakens the bispectrum estimation. However, we cannot use longer signals, because they lead to nonstationarity, and the variance consequently becomes even larger [69]. Moreover, determining short-lasting couplings, shorter than 10 times the lower period in a bifrequency pair, makes the Fourier based bispectrum incapable of coping with the necessary time-frequency resolution, as was also clearly demonstrated using a model of coupled oscillators (8.1).

Tab. 8.2: Summary of Fourier bispectrum (FB), using STFT and wavelet bispectrum (WB), time and frequency discretized using adapted Morlet mother wavelet comparison for CV signals analysis. * -denotation in the table means that no method is in advantage.

Property\Method	Fourier bispectrum	Wavelet bispectrum	In advantage
Type	Discrete	Continuous	WB
Basis function	Orthogonal	Nonorthogonal	FB
Interpretation	Straightforward	Straightforward	*
Window	Rectangle	Adapted Morlet	WB
Frequency step	$1/M/f_s$	Arbitrary	WB
Time resolution	Constant	Variable	WB
Frequency resolution	Constant	Variable	FB
Time and freq. resolution	$\Delta t\,\Delta f > 1/(4\pi)$	$\Delta t\,\Delta f \geq 1/(4\pi)$	WB
Bispectrum computation[7]	100 %	19 % (2.6 %)	WB
Energy preservation	Direct	Normalization necessary	FB
Statistical error	$\sqrt{M/N}$	$\approx 2/\sqrt{W_N}$	WB

Aside from WB being able to trace fast changes of high frequency components, and being able to locate slow frequency components at the same time, there are many other advantages of wavelet bispectrum (adopted for CV signals) over the Fourier bispectrum. An overview is shown in table 8.2. Since WB is continuous, and FB is not, it allows an arbitrary frequency step to be chosen, and thus a better frequency component location. It allows intermittent phase couplings to be detected, whereas Fourier bispectrum averages out most of the time relevant information. The Heisenberg uncertainty principle, [43], limits simultaneous time and frequency resolution. Using the wavelet bispectrum, the optimum time and frequency resolution can be achieved; there is a simple relation between scale and frequency; and it has smaller statistical error; and is computationally less demanding.

The only drawback of WB, compared to FB, is that it has to be normalized to obtain signal energy, and it is not orthogonal. Normalization can be preformed, whereas we are not concerned with the inverse wavelet transform.

A hybrid between Fourier and wavelet transform, the selective discrete Fourier transform, can also be used to perform the bispectrum calculation. It is a modified STFT, that was first introduced by

[7] Bispectrum for signal $x_{1D}(t)$ (see Sec. 4.4) was computed for the whole IT of the principal domain, Fig. 3.1. Fourier bispectrum $|B|$ was computed with $K = 34$ segments, 67 % overlapping and using the Blackman window to reduce leakage. Wavelet bispectrum $|WB|$ was computed with $K = 34$ segments, 67 % overlapping, $T_m = 8$ s, $G_e = 0.001$ and using fixed Morlet wavelet length of $T_{HF} = 40$ s for high frequencies calculation. 100 % is the number of computations preformed for FB. 81 % less computations are necessary for WB estimation. If we use hyperbolically decreasing Morlet wavelet length then computation of WB is approximately 40 times faster than computation of FB (only 2.6 % of FB computations are necessary).

Keselbrener and Akselrod [47], but the wavelet transform is more adequate, since it is continuous, whereas the SDFT is not.

9 OTHER POSSIBLE APPLICATIONS OF WAVELET BISPECTRUM METHOD

CV signals are not the only ones relevant for studying CVS. Neural CV subsystem coupling information is incorporated in the brain waves. Synchronization among separate brain centres indicates an interaction between them. In most cases, it is associated with oscillatory behaviour in specific structures, frequencies and behaviour states. Electroencephalogram (EEG) measures electrical activity in the brain, i.e., brainwaves of different frequencies, and short-lived evoked potentials that occur when the brain responds to sensory input. Generally, low frequency oscillations originate from larger structures than do high-frequency oscillations. In certain conditions, such as general anaesthesia, synchronization can be seen in EEG measurements as organized, distinguishable patterns. These patterns depend on the anaesthetic agent and the level of anaesthesia [107]. Delta waves are the slowest oscillating waves (0-4 cycles per second). They are associated with a deep dreamless sleep, trance state, lucid dreaming, increased immune functions and hypnosis, and are thus expected to occur during anaesthesia.

In some cases, synchronization can be observed over large distances in the consistent time lags between signals, using cross-correlation techniques. However, the cross-correlation techniques might encounter problems when compared to signals that are not stationary, or to oscillations that are weakly related. In the concept of phase synchronization of chaotic oscillators [90], the solution is approached with the consideration of two time series, originating from two coupled oscillators. The amount of coupling can be quantified from the phase difference of the signals. Spatial heterogeneity in EEG during anaesthesia is often studied by means of amplitude and spectral estimate-based methods [21, 86, 122].

The quantification of quadratic phase-coupling between EEG signal components has been established since G. Dumermuth's pioneered investigations using bispectral analysis in 1969 [51]. A number of

EEG studies have been published using the mathematical tools of high-order spectra analysis EEG [12, 27, 53, 65]. Additionally, the so-called bispectral index (BIS) [89] is a frequently used parameter for the quantification of anaesthesia and sedation depth [84, 88, 98]. The BIS is a statistically based, empirically derived complex parameter that is composed of a combination of time domain, frequency domain and high-order spectral sub parameters.

By means of bispectral analysis, non-linear interactions of EEG signal brainwaves can be quantified. The stationarity of the signal is one important prerequisite for consistent bispectrum estimation. Generally, the mathematical property of stationarity cannot be obtained from real EEG signals. Therefore, methods for spectral analysis of non-stationary signals have been introduced. Time-frequency distributions, wavelet transform, and time-variant autoregressive moving average (ARMA) modelling are the most prominent classes of such approaches with sufficient time and frequency resolution. By means of time-frequency analysis, only transient linear relations of, and between, signal components can be captured. Transient nonlinear interactions are undetectable. Therefore, approaches for time-variant bispectral analysis have been developed [5, 69, 98]. While these approaches concentrate on time-frequency domain (second-order spectra) or on shape in (third-order spectra) frequency-frequency domain, we extract time information related to coupling from the frequency-frequency domain of bispectrum, i.e., the biamplitude and the biphase.

Recently, the synchronization index technique was applied to signals of rats undergoing anaesthesia [63, 64]. EEG signals contain several time-varying frequency components. The most dominant ones are in the delta frequency range. Similar signal pattern was observed for all rats analysed while undergoing anaesthesia. At the beginning, there is one dominant, slightly-varying, frequency component around the central frequency of 2 Hz. In its surrounding, there are higher frequency components that are not distinctly at the beginning. The predominant frequency component in the EEG signal vanishes when rats started to move and breath spontaneous. Synchronization indexes have been calculated for the case of delta waves of EEG and ECG, delta waves of EEG and respiratory, and ECG and respiratory signals. Synchronization was distinctive only in the latter case. There is one general pattern that occurs in all cases: 2:1 or 3:1 synchronization at the beginning, which eventually transits to 4:1 or 5:1, and then later returns back to 3:1 or 2:1. At the end of the signal there is no synchronization what is in connection with rat transition from deeper to less deep anaesthesia (wakening). Furthermore, direction and strength of the coupling was studied. While there can be seen that in the first part the respiratory oscillator drives the oscillations contributed to delta waves of EEG signal, there cannot be made any conclusions about cardiac and delta waves of EEG signal direction and strength of the interaction.

The depth of anaesthesia is related to synchronization states between cardiac and respiratory oscillator [63, 64]. Anaesthesia deepness can be extracted from the EEG signal therefore relation between the cardio-respiratory synchronization and the bispectrum of EEG signal is expected. In this chapter we apply the wavelet bispectrum to EEG signal. For the demonstration of its applicability we use the EEG signal from the rat20 as already analysed in Chapter 6. By estimating the biamplitude and the biphase we wish to test whether the wavelet bispectrum can extract the same information from the univariate EEG signal as can be obtained from synchrogram of bivariate ECG and respiration signals.

9.1 Measurements

Measurements have already been discussed in the Sec. 6.1. In this analysis we use only the EEG signal measured on rat20 undergoing the anaesthesia.

9.2 Data analysis

The EEG signal was first pre-processed. Both very low and very high frequencies were removed by use of moving average windows: drift with a 200 s long window; and high frequencies with a 0.04 s window while, and at the same time, the signal was resampled to 50 Hz. By using the moving average before resampling, we avoid problems of aliasing. The signal has been further normalized between zero and one and its mean value was subtracted.

For clearer interpretation of the results we divided ~63 minutes long EEG signal of rat20 to four parts a, b, c and d, each of them containing only one phenomenon, i.e., synchronization or no synchronization. First we calculated the wavelet bispectrum for each separate EEG part for the whole frequency domain. We used fixed, 20 s long, wavelet for calculation of high frequencies as discussed in Sec. 7.2.1. Than we estimated the biphase and the biamplitude for the highest peak appearing in the wavelet bispectrum. For this calculation 80 s long fix wavelet was used to increase frequency resolution for high frequencies since the signal EEG is highly complex and the signal power is concentrated at approximately 1 Hz. Frequency step was equidistant and set to 0.02 Hz to preserve the Eq. (7.18) condition. Morlet window was moved along the time series with a time step of 0.1 s. The critical value for the biamplitude estimate to be considered valid was set in all cases to 2, i.e., twice the average value of the WB within its so-called inner triangle (IT).

9.3 Results

Example of detrended, resampled and it's mean value subtracted EEG signal for rat20 undergoing anaesthesia is presented on Fig. 9.1 (a) and its power spectrum (b). As it can be seen from the power spectrum that it's power is concentrated in range 0.5-5 Hz with maximum between 1 Hz and 2 Hz.

The synchrogram between the rat20 ECG and respiration signal is presented in Fig. 9.1 (c). Four distinctive parts can be seen; a and c where synchronization 4:1 takes place and b and d where no synchronization is evident. The EEG signal was divided according to marked parts and analysed separately for the sake of clarity. Figure 9.2 (a) - (d) shows WB for each part separately with its contour view. In all the WB-s there is a dominant peak. In the part a it is located around bifrequency (1.1 Hz, 1.1 Hz), in part b around bifrequency (1.3 Hz, 1.3 Hz), in part c around bifrequency (1.4 Hz, 1.4 Hz) and in the last part around bifrequency (1.6 Hz, 1.6 Hz). For each part biamplitude and biphase were calculated for the dominant, the highest peak appearing in the obtained WT. A longer fixed Morlet wavelet was used, T_{HF} = 80 s, for estimating high frequencies as in the case of $|WB_{a\text{-}d}|$ calculation, where fixed Morlet wavelet of 20 s was used for estimating high frequencies. The reason is that $|WB_{a\text{-}d}|$ exhibit reach bispectral contents, therefore higher frequency resolution is necessary. In all the cases the highest peak appears at the so-called self-coupling bifrequencies. We observe self-phase couplings of delta waves of EEG signal.

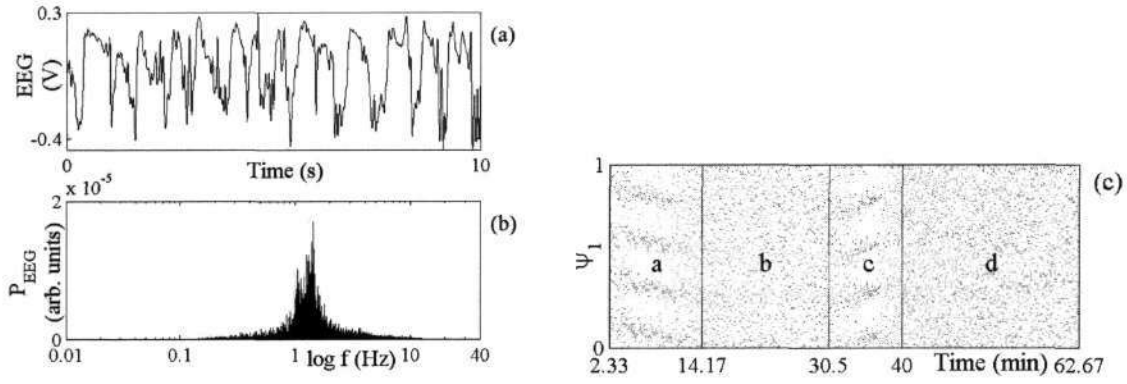

Fig. 9.1: (a) 10 s of detrended, and removed zero mean signal EEG(t) and its power spectrum (b) for the case of rat20 undergoing anaesthesia, ~63 minutes long at sampling frequency f_s = 50 Hz. (c) Cardio-respiratory synchrogram for rat20 divided into four parts a-d.

Biamplitude A_{a1}, Fig. 9.3 left (a), shows some coupling activity over the whole time with two higher peaks from approximately 7 minutes until approximately 10 minutes. During this time the biphase ϕ_{a1}, Fig. 9.3 right (a), tends to be within π interval. We detect phase coupling T_{pc}. During part b the

biamplitude A_{b1}, Fig. 9.3 left (b), shows three short lasting peaks while the biphase ϕ_{b1}, Fig. 9.3 right (b), tends to decrease all the time of observation. In part 3 the biamplitude A_{c1}, Fig. 9.3 left (c), shows a very distinct and high peak lasting from 35 minutes to 36.17 minutes, when the synchronization is the strongest. In this time the biphase ϕ_{c1}, Fig. 9.3 right (c), changes for 2.43 rad what is within the π interval and can be treated as phase coupling. The last part d shows no coupling, biamplitude A_{d1}, Fig. 9.3 left (d), except at the very beginning where the biphase ϕ_{d1}, Fig. 9.3 right (d), is also constant whereas otherwise is not.

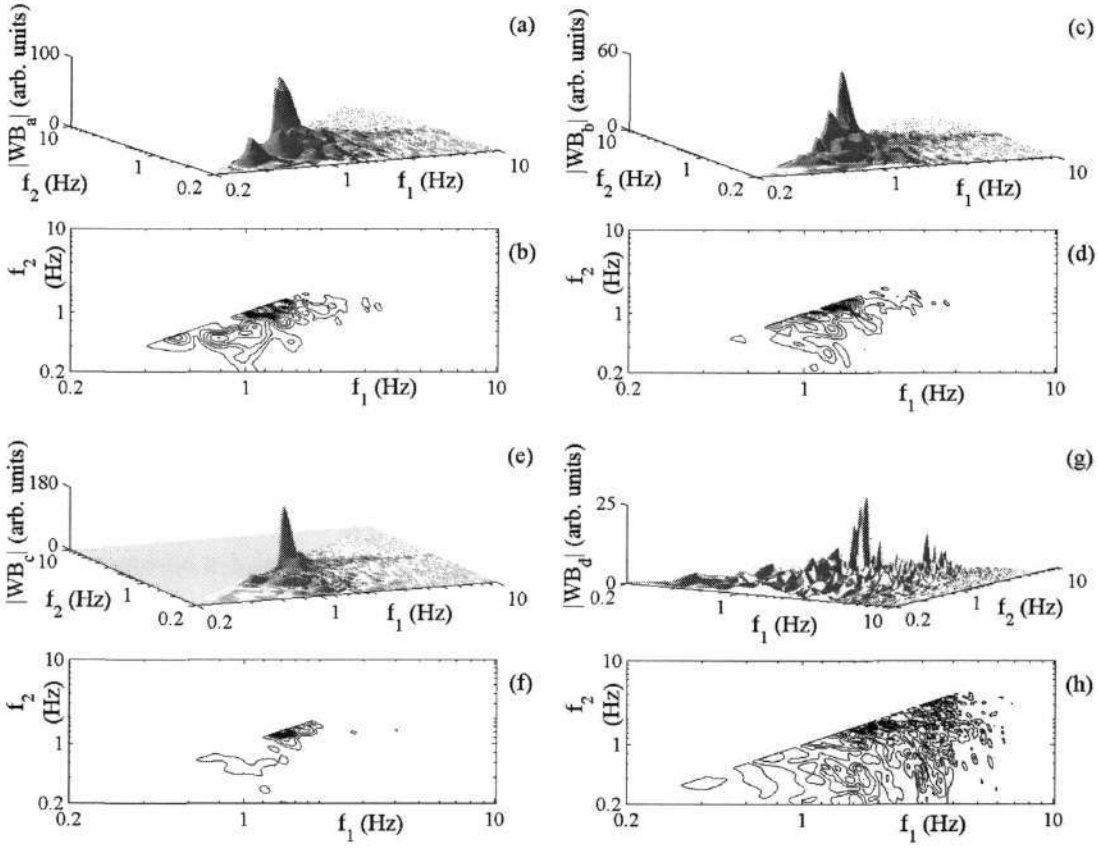

Fig. 9.2: Results for the rat20 undergoing anaesthesia. (a) The wavelet bispectrum $|WB_a|$ for part a calculated with 74 % overlapping and (b) its contour view, (c) $|WB_b|$ for part b calculated with 65 % overlapping and (d) its contour view, (e) $|WB_c|$ for part c calculated with 81 % overlapping and (f) its contour view and (g) $|WB_d|$ for part d calculated with 49 % overlapping and (h) its contour view. In all cases of WB K was set to 33 segments, whereas $G_e = 0.001$, $T_m = 8$ s and $T_{HF} = 20$ s long fixed Morlet wavelet for estimating high frequencies was used.

By applying the necessary conditions for the nonlinear quadratic coupling to be present to analysis of rat20's EEG signal, we consider the conditions only for the peak of observation - the self-coupling peak, Sec. 5.3. All detected phase couplings are summarized in Tab. 9.1.

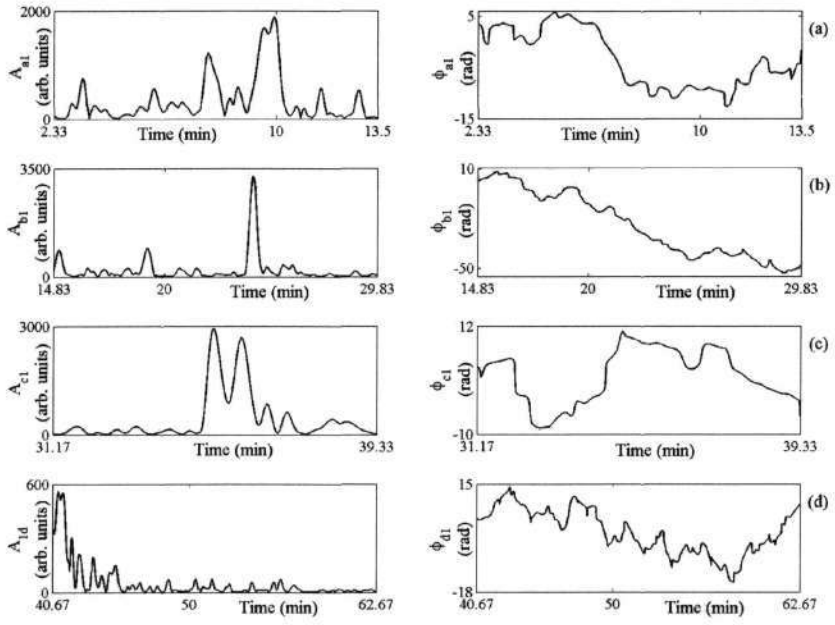

Fig. 9.3: Left column the biphase ϕ and right column the biamplitude A for bifrequencies: (a) part a (1.1 Hz, 1.1 Hz) calculated with 74 % overlapping, (b) part b (1.3 Hz, 1.3 Hz) calculated with 65 % overlapping, (c) part c (1.4 Hz, 1.4 Hz) calculated with 81 % overlapping and (d) part d (1.6 Hz, 1.6 Hz) calculated with 49 % overlapping. In all cases a 0.1 s time step, K = 33 segments, G_e = 0.001, T_m = 8 s and T_{HF} = 80 s long fixed Morlet wavelet for estimating high frequencies was used.

Tab. 9.1: Phase couplings detected in rat20 EEG signal. T_{pc} is the time interval during which the wavelet bispectral analysis showed that the delta waves of EEG signal are self-phase coupled at bifrequency (f_1, f_1). The product of $T_{pc} \cdot f_1$ tells us over how many delta waves of EEG signal periods the phase coupling persisted. During T_{pc} the maximum biamplitude A_{max} is calculated for the peak. In addition, the maximum variation of the biphase $\Delta\phi$, its average value $\overline{\phi}$, and its standard deviation σ_ϕ were calculated during T_{pc}.

Part	t_1 (min)	t_2 (min)	f_1 (Hz)	T_{pc} (s)	T_{pc}:f_1	A_{max} (arb. units)	$\Delta\phi$ (rad)	$\overline{\phi}$ (rad)	σ_ϕ (rad)
a	2.67	3.55	1.1	49	57	753	1.16	3.24	0.23
a	5.87	6.33	1.1	28	33	494	0.24	3.59	0.05
a	7.45	8.17	1.1	43	50	1224	0.81	-8.14	0.29
a	8.22	10.83	1.1	157	183	1894	2.53	-9.62	0.69
a	12.38	13.03	1.1	39	45	535	0.58	-6.05	0.12
b	18.83	19.50	1.3	40	67	922	1.31	-1.77	0.34
b	23.83	24.31	1.3	29	48	3249	1.33	-39.44	0.30
c	35.00	36.17	1.4	70	141	2931	2.43	8.45	0.62
c	36.42	36.75	1.4	20	40	839	0.99	3.64	0.23
c	36.92	37.45	1.4	32	65	617	1.09	7.92	0.34
d	40.67	41.53	1.6	52	130	558	1.02	4.50	0.31

9.4 Discussion

From Tab. 9.1, it can be seen that phase couplings onset mostly in part a and part c. These couplings are the strongest and have the longest lasting time, T_{pc}. If we put all biamplitudes from A_{a1} to A_{d1} together as one time evolution of biamplitude, and do this similarly with biphases from ϕ_{a1} to ϕ_{d1}, then two (or three) peaks stand out by their biamplitude. At the times where the peaks appear, the biphase tends to be constant (within the π interval). The time of onset and phase coupling duration is shown in Fig. 9.4. These two events can also be detected, as shown in the synchrogram Fig. 9.1 (c), when the synchronization 4:1 onsets and when it disappears. In the time between these events, the synchrogram does not show synchronization to be present, whereas from the *WB*, there are visible, short-time phase-coupling events that cannot synchronize the interacting oscillations as the biphase decays uniformly.

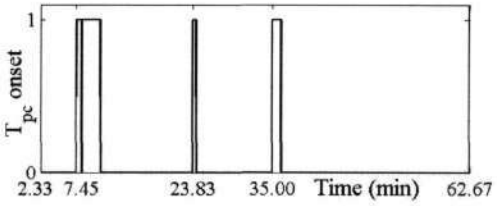

Fig. 9.4: In Tab. 9.1, phase couplings, T_{pc}, that stand out by their biamplitude (1000 and more). Their onset times and duration are shown. The first and the last T_{pc} coincide with the onset and disappearance of the phase synchronization between the cardiac and respiratory oscillators, Fig 6.8 (d).

We can conclude that cardiac and respiratory CV systems and delta waves of EEG signal are coupled during the anaesthesia. The question arises whether the delta waves of EEG signal drive the cardiac and respiratory systems in synchronization when rat20 is undergoing anaesthesia, or slow respiration synchronizes with the cardiac system that further influences the delta waves of EEG signal. There is one applausive hypothesis of anaesthesia reducing the RSA [83, 84]. Anaesthesia may stimulate inhibitory glycine and GABAergic synapses in the NTS-NA axis, whose projections then inhibit higher brain centres, such as the limbic system. It also modulates the level of endogenous hypothalamic peptides, responsible for the natural control of brain metabolism that are known to affect vagal control of cardiac rhythm [82], and which would be affected if anaesthesia artificially reduces brain metabolism [1]. That is, anaesthesia may affect the delta waves of EEG signal in such a manner that they drive the cardiac and respiratory system to synchronization.

Similarly, as we analysed the cardio-respiratory interaction, we could also analyse cardio-delta waves of EEG signal and respiratory-delta waves of EEG signal interaction to study their interaction and the nature of couplings, whereas this is not the intent of this work. Wavelet bispectrum proved to be a

promising tool to analyse EEG signals during anaesthesia. It can detect the phase synchronization onset and its disappearance.

10 SUMMARY

The bispectrum is the first high-order spectrum after ordinary spectral analysis, and is useful for the investigation of non-linear interactions of the lowest-order (i.e., quadratic interactions). Powerful noise reduction is an integral part of the standard technique, as non-coherent contributions are averaged out, and weak coherent signals can be detected in very noisy data [68, 69]. The bispectral method has been extended to encompass time dependence, and has demonstrated the potential of the extended technique to determine the type of couplings among interacting nonlinear oscillators [40]. Time-phase couplings can be observed by calculating the bispectrum and adapted bispectrum, and obtaining the time-dependent biphase and biamplitude. The method has the advantage that it allows an arbitrary number of interacting oscillatory processes to be studied.

Recently introduced methods for synchronization analysis among chaotic and noisy oscillations (see [79] and references therein) have stimulated applications to a variety of different systems. Methods for quantifying the strength and identifying the direction of couplings, based on nonlinear dynamic or information theory approaches, have recently been proposed [72, 93, 94, 103]. In this work, the question of the type of coupling that may result in synchronization was addressed, and a method was proposed for its analysis. It is applicable to both univariate data (a single signal from the coupled system) and multivariate data (a separate signal from each oscillator).

Millingen *et al.* [61, 62] have analysed multivariate data using a combined wavelet and bispectral method, and have discussed its application in the field of chaos analysis. Here we have concentrated on univariate data and illustrated the potential of the time-phase bispectral method for the detection of higher-order couplings in the presence of noise. The possibility of using univariate data is of particular importance when dealing with real signals, as in practice, we often cannot observe and measure the separate subsystems directly, but only their combination, which is intrinsically difficult. Most of the methods proposed so far for synchronization analysis and detection of the direction of couplings are based on bivariate or multivariate data [72, 79, 93, 94, 103]. In conjunction with frequency or time-frequency filtering [113, 121] or mode decomposition [36] to obtain two or more "separate" signals, these methods can be used for univariate data as well. Synchronization can also be detected in univariate data through an analysis of angles and radii [42] in return time maps [119].

The time-phase bispectral method proposed in this work is not only applicable to the synchronization analysis of univariate data, but also, at the same time, allows one to determine the nature of the couplings among the interacting nonlinear oscillators. Its benefits include: (i) the possibility of

observing the whole frequency domain simultaneously; (ii) detecting that two or more subsystems are interacting with each other; (iii) quantification of the strength of the interaction; and (iv) determination of whether the coupling is additive linear or quadratic, or parametric in one of the frequencies. We have shown the method to be suitable for the analysis of noisy signals.

Although it was shown that the technique works effectively on a well-characterized simple model, there are some difficulties to be faced and overcome in applying it to real problems, e.g., to data from the cardiovascular system. Understanding the content of the bispectrum, and identification of the peaks of interest, are not always straightforward. To appreciate which peaks are the ones to focus on, one has to be aware of the basic properties of the system and its fundamental frequencies. Distinguishing a quadratic interaction from parametric frequency modulation may be easy when the coupling/modulation is relatively strong, but becomes more difficult in the case of relatively weak coupling/modulation. In the latter case, observing each phase in the triplet separately can be helpful. Also, it is not always an easy task to distinguish between quadratic interaction and parametric frequency modulation in cases when both of them occur simultaneously. Furthermore, where the possible basic frequencies are relatively close, it will be hard to detect them separately. This could cause particular problems in the detection of quadratic phase couplings where frequency pairs are close together. Although it is possible in principle to study an arbitrary number of interacting oscillators, it is advisable in practice to study them in pairs: knowledge of the basic frequency of each is necessary.

The blood flow signal contains a great deal of information and is exceptionally challenging in relation to processing. It possesses components whose amplitudes and frequencies vary in time. Moreover, the interactions among its characteristic oscillations also vary in time, and their nature (frequency, phase, linear and/or quadratic couplings) also changes, giving rise to the observed complexity of cardiovascular dynamics.

Bispectral analysis has provided insight into the nature of the couplings. Results in this work support the inference that the dynamics of blood flow can usefully be considered in terms of coupled oscillators. Application to the cardio-respiratory interaction has shown for the first time that nonlinear coupling is present [41]. Although evidence for couplings beyond second-order has not been sought, higher-order coupling may also exist.

In this work, it was shown that the effect of the coupling between the cardiac and respiratory oscillations is episodic, rather than fixed and permanent. Moreover, an interchange between frequency and phase couplings is also present, as demonstrated by the evolution of their time-biphase.

Nonlinear coupling was revealed, and shown to exist during spontaneous, as well as during paced, respiration. Episodes with nonlinear coupling were detected in 11 out of the 22 recordings, and lasted between 19 s, in the case of high respiratory frequency (f_{2p} = 0.34 Hz), and 106 s, in the case of low paced frequency of respiration (f_{2P} = 0.11 Hz). The episodic nature of the cardio-respiratory interaction in a healthy human during spontaneous and paced respiration had already been demonstrated using quite different techniques of analysis [10, 46, 95, 97, 101, 104]. It allows us to infer that the inter-oscillator coupling is probably relatively weak. There are, however, compelling arguments suggesting that the cardiac and respiratory subsystems should be, in fact, treated as weakly nonlinear oscillators that are weakly coupled. (i) In healthy subjects, breathing spontaneously, only *occasional* and *brief* episodes of synchronization are seen [10, 99-101], indicative of relatively weak coupling. (ii) Sinus arrhythmia is small at spontaneous breathing frequencies and only slightly larger at very low breathing frequencies [23], again supporting a weak-coupling description. (iii) The couplings can sometimes decrease almost to a vanishing point, e.g., in coma [112]. Without couplings, the dynamics become drastically simplified - with complete absence of synchronization or modulation. The fact that virtually no variability is seen in any of the natural frequencies, despite small amplitude variations attributable to internal noise, suggests that the oscillators themselves are, at most, weakly nonlinear. (iv) If there were strong oscillator nonlinearity, and strong (but linear) coupling, we would observe many combinatorial components around the cardiac frequency, which is not the case.

Using bispectral and cross-bispectral analysis, it was also shown that the coupling information among cardiac and respiratory processes is inherit from the processes and spatially invariant. Both processes are of central origin, and their phase relationships can be observed in ECG, blood flow and blood pressure signals derived from widely separated sites. It would appear that the information is incorporated within the wave motion of the blood propagating through the vessels.

It is of interest to compare results of this experiment with that of [19]. They had also studied physiological time series while respiration was being paced at a constant rate; in addition, they also guided the ventilatory amplitude (tidal volume) so as to produce a sinusoidal modulation envelope with a period of 60 s. It resulted in oscillations of the same period in several physiological quantities, including the R-R intervals, blood pressure, and the cardiac stroke volume and output. In this study, the ventilatory amplitude was left to the subject's spontaneous choice. The slow amplitude modulation of [19] was selected to mimic the pattern of Cheyne-Stokes respiration, which is often associated with heart failure. The question addressed in this work was to examine whether or not the relationship between cardiac and respiratory oscillations can be nonlinear, without any amplitude modulation. It is difficult to decide whether the nonlinear interactions, shown to occur episodically in the present study, would or would not have occurred if the amplitude of respiratory oscillations had also been controlled,

as in the study by [19]. It was shown, however, that quadratic coupling exists even when both the frequency and the amplitude of respiration are spontaneous. We may therefore conclude that the nonlinear nature of the interaction between the cardiac and respiratory oscillations is inherent, and that it becomes more pronounced when the frequency of respiration is kept constant.

The question of what the nonlinear couplings mean, and how they arise, are yet to be resolved. One possibility is that they result from nonlinearity of the carotid baroreceptor-cardiac reflex [22]; another is that they are attributable to the active involvement of the peripheral vessels during cardiac and respiratory wave propagation in the network. A full understanding of these couplings is essential to gain insight into the physiology and pathophysiology of cardiovascular dynamics, as well as for the construction of mathematical models that offer novel possibilities for obtaining clinically relevant physiological information. It can be concluded that bispectral analysis provides a promising tool for the determination of frequency and phase couplings in the processing and understanding of cardiovascular signals.

One of the coupling phenomena that can onset among interacting oscillators is phase synchronization. The most natural way to study the phase relations among interacting oscillators is by using synchronization techniques. As bispectral analyses provides information about frequency and phase coupling, and moreover, the nature of the coupling oscillators, we draw its relation to the synchronization. In the case of strong phase synchronization, the synchrogram and bispectrum provide the same results. The phase synchronization is indicated with a high biamplitude value and constant biphase at bifrequency of our primary interest (f_1, f_2). Weak phase synchronization usually does not result in obvious horizontal strips in synchrogram, whereas bispectrum results in moderate biamplitude and less constant biphase, with more phase slips at the bifrequency of our primary interest. No phase synchronization results in zero biamplitude at the bifrequency of our primary interest. Bispectral analysis is more sensitive to interactions than the synchrogram. It detects the phase synchronization, and nevertheless, yields different information from that which can be resolved from a synchrogram.

Synchronization can take place simultaneously with other type of interaction, such as frequency modulation, forcing and/or nonlinear coupling. Nonlinear coupling can appear while phase synchronization occurs, whereas synchronization does not necessarily appear while there is nonlinear coupling. There is no obvious link between the two phenomena. Analysis of rats undergoing anaesthesia shows that nonlinear coupling occurs during synchronization while analysis of CV blood flow signals of humans in resting shows nonlinear coupling while no synchronization is present.

Frequency modulation alone can be detected using bispectrum. Peak of primary interest (f_1, f_2) and the second peak at bifrequency (f_1-f_2, f_2) are high in comparison to other peaks (which may not be present at all) that appear in the case of nonlinear interaction, and their biphase is constant (strong frequency modulation). Instantaneous presence of frequency modulation and forcing can be misleading in detecting the nonlinear coupling. Thus, it is necessary to check all the 1-6 peaks, and analyse the peak of primary interest (f_1, f_2) for modified bispectrum, and observe the phases of each frequency component in the triplet. When strong frequency modulation and nonlinear coupling are occur simultaneously, detection of the frequency modulation is not possible.

In the case of bispectral analysis of cardiovascular interaction, the time-dependent biphase/biamplitude estimate was estimated with a short time Fourier transform, using a window of constant length. The optimal window length depends, however, on the frequency being studied. The effective length of the window used for each frequency can be varied by applying the wavelet transform, or the selective discrete Fourier transform. For demonstration purposes above, the natural frequencies of the oscillators were chosen to lie within a relatively narrow frequency interval. An STFT was therefore sufficient for good time and phase/frequency localization. With broader frequency content, however, the wavelet transform or selective discrete Fourier transform needs to be applied.

Wavelet transform to higher-order spectra was presented in this work. The wavelet and cross-wavelet bispectrum was defined analogous to the definitions used in Fourier based bispectrum and cross-bispectrum. By doing this time-dependant biphase/biamplitude estimate with higher frequency resolution at low frequencies, higher time resolution at higher frequencies was obtained. The wavelet bispectral analysis was adopted to analyse cardiovascular signals. For a mother wavelet modulated Gauss function, the Morlet mother wavelet was used.

Wavelet bispectral analysis was illustrated using a test signal. Since the time resolution of wavelet bispectrum is higher, and the frequency resolution is poorer at high frequencies compared to Fourier based bispectrum, it is necessary to ensure sufficient frequency resolution before interpretation of the results. Poor frequency resolution would result in poor/incorrect localization of characteristic frequencies. Too high of a time resolution could result in extremely high sensitiveness to noise and statistical error, which would result in phase slips and incorrect oscillator coupling determination. It was necessary to raise frequency resolution for high frequencies, and also to preserve the scale (frequency) sum condition necessary for bispectrum estimation. Wavelet bispectrum results are parameter set dependant.

Wavelet bispectrum was applied to CV blood flow signals. Parameters were set to the prevailing choice. The wavelet bispectral method is suitable for studying cardio-respiratory interaction from the

CV blood flow signals. Parameter impact on wavelet bispectrum estimation and detailed comparison with Fourier bispectrum was preformed. Results obtained with WB analysis resemble the ones obtained with Fourier bispectrum method. There are no obvious advantages of WB over FB when detecting cardio-respiratory interaction that fulfils the defined necessary conditions for quadratical coupling occurrence.

Our motivation was to develop a method that will be able to provide insight into the nature of the CV subsystems couplings. Analysing interaction among cardiac and respiratory systems is thus the first step taken. In order to be able to analyse all other CVS interactions, such as cardio-myogenic, cardio-neural, cardio-metabolic, respiratory-myogenic, respiratory-neural, respiratory-metabolic, myogenic-neural, and others, we need to use the wavelet bispectral method. Namely, an important feature of CV signals is that they are nonlinear, time-varying and subject to fluctuation [3, 18, 23, 34, 117]. In the low frequency range, which is of our particular interest, the characteristic frequencies are close to each other, and are therefore even harder to separate. The uncertainty principle of the Fourier transform limits its ability to separate harmonic components in the frequency domain of the bispectrum [20, 69]. This might cause problems for detection of the quadratic phase couplings in the case of frequency pairs that are close together. To ensure good resolution of low frequencies, we need longer sections for calculation of the discrete Fourier transform. This immediately decreases the number of sections possible and weakens the bispectrum estimation. However, we cannot use longer signals, because they lead to nonstationarity, and the variance consequently becomes even larger [69]. Moreover, determining short-lasting couplings, shorter than 10 times the lower period in a bifrequency pair, makes the Fourier based bispectrum incapable of coping with the necessary time-frequency resolution, as was also clearly demonstrated using a model of nonlinearly coupled Poincaré oscillators.

Aside from WB being able to trace fast changes of high frequency components, and being able to locate slow frequency components at the same time, there are many other advantages of wavelet bispectrum (adopted for CV signals) over the Fourier bispectrum. Since WB is continuous, and the FB is not, it allows an arbitrary frequency step to be chosen, and thus a better frequency component location. It allows intermittent phase couplings to be detected, whereas Fourier bispectrum averages out most of the time relevant information. The Heisenberg uncertainty principle, [43], limits simultaneous time and frequency resolution. Using the wavelet bispectrum, the optimum time and frequency resolution can be achieved: there is a simple relation between scale and frequency; it has smaller statistical error; and is computationally less demanding.

The only drawback of WB compared to FB, is that it has to be normalized to obtain signal energy, and it is not orthogonal. Normalization can be preformed, whereas we are not concerned with the inverse wavelet transform.

A hybrid between Fourier and wavelet transform, the Selective Discrete Fourier Transform (SDFT), can also be used to perform the bispectrum calculation. It is a modified STFT, that was first introduced by Keselbrener and Akselrod [47], but the wavelet transform is more adequate, since it is continuous, whereas the SDFT is not.

Not only CV signals are relevant for studying CVS. Neural CV subsystem coupling information is incorporated in the brain waves. Synchronization among separate brain centres indicates an interaction between them. In certain conditions, such as general anaesthesia, synchronization can be seen in EEG signals [107] as the onset of delta brainwaves (0-4 cycles per second). Generally, EEG signals do not satisfy the stationarity condition, which is generally necessary for high-order spectra estimation. Therefore, methods for spectral analysis of non-stationary signals have been introduced. Time-frequency distributions, wavelet transforms and time-variant autoregressive moving average (ARMA) modelling are the most prominent classes of such approaches with a sufficient time and frequency resolution [12, 27, 51, 53, 65]. Spatial heterogeneity in EEG during anaesthesia is often studied by means of amplitude and spectral estimate-based methods [21, 86, 122]. These approaches concentrate on time-frequency space (second-order spectra) or on shape in (third-order spectra) frequency-frequency space. Using the introduced time dependant wavelet bispectrum, one can extract time information related to coupling from the frequency-frequency space of bispectrum, i.e., the biamplitude and the biphase.

Recently, the synchronization index technique was applied to signals of rats undergoing anaesthesia [63, 64]. EEG is a highly complex signal, which contains several time-varying frequency components. The signal power is concentrated at delta brainwave range, at approximately 1 Hz - 2 Hz. The predominant frequency component in the EEG signal vanishes when rats started to move and breath spontaneous. Synchronization indexes have been calculated for the case of delta waves of EEG and ECG, delta waves of EEG and respiratory, and ECG and respiratory signals. Synchronization was distinctive only in the latter case. The depth of anaesthesia is related to synchronization states between the cardiac and respiratory oscillators. We applied the wavelet bispectrum to the EEG signal of rat20 undergoing anaesthesia, in order to demonstrate its applicability. The analysis showed that the cardio-respiratory synchronization can be detected in the EEG signal. It can be distinctively seen from the evolution of the biamplitude and the biphase, when the synchronization 4:1 onsets and when it disappears. We can conclude that cardiac and respiratory CV systems and delta waves of EEG signal are coupled during the anaesthesia. The physiological question arises whether cardio-respiratory synchronization might be a consequence of, or result in, delta waves of EEG signal when rats are undergoing anaesthesia. One possible hypothesis explains that anaesthesia reduces RSA [83, 84].

Anaesthesia may stimulate inhibitory glycine and GABAergic synapses in the NTS-NA axis, whose projections then inhibit higher brain centres such as the limbic system. It also modulates the level of endogenous hypothalamic peptides responsible for the natural control of brain metabolism that are known to affect vagal control of cardiac rhythm [82], and which would be affected if anaesthesia artificially reduces brain metabolism [1]. That is, anaesthesia may affect the delta waves of EEG signal in such a manner that they drive the cardiac and respiratory systems to synchronization.

Similarly, as we analysed the cardio-respiratory interaction, we could also analyse cardio-delta waves of EEG signal and respiratory-delta waves of EEG signal interaction to study their interaction and the nature of couplings, whereas this is not the intent of this work. Wavelet bispectrum proved to be a promising tool to analyse EEG signals during anaesthesia. It can detect the delta waves of EEG signal phase coupling states.

A long-term aim is therefore to develop a coupled oscillator model that can provide a description of the system, quantify the couplings and relate their values to its different states of health or disease. The wavelet bispectrum may provide a link between theoretical CVS models and experimental measurements.

Higher order spectral methods can be used to study arbitrary interactions among coupled oscillators: of quadratic, cubic, or even higher order. In this work we have concentrated on the lowest interaction, using the third-order spectrum or bispectrum. It has been suggested to proceed to the calculation of even higher-order spectra than the third-order bispectrum. For higher orders, the volume of the calculations rises substantially, and the method becomes increasingly demanding, numerically. However, the difficulty is not mathematical, since the generalization of the bispectrum to higher order is straightforward, but practical. The representation and interpretation of such high-order spectra become increasingly difficult which is the limiting factor. We aspect new, powerful computer visualization tools to open up this direction of development in the coming future.

11 CONCLUSIONS

The time-phase bispectral method allows us to determine the nature of the couplings among the interacting nonlinear oscillators. Its benefits include: (i) the possibility of observing the whole frequency domain simultaneously; (ii) detecting that two or more subsystems are interacting with each other; (iii) quantification of the strength of the interaction; (iv) determination of whether the coupling is additive linear or quadratic, or parametric in one of the frequencies; and (v) the method is suitable for the analysis of noisy signals.

The effect of the coupling between the cardiac and respiratory oscillations is episodic, rather than fixed and permanent. Frequency and phase couplings interchange. Nonlinear coupling exists during spontaneous as well as during paced respiration. The inter-oscillator coupling is relatively weak.

Bispectral and cross-bispectral analysis showed that the coupling information among cardiac and respiratory processes is inherit from the processes, and is spatially invariant. Both processes are of central origin, and their phase relationships can be observed in ECG, blood flow and blood pressure signals derived from widely separated sites.

The nonlinear nature of the interaction between the cardiac and respiratory oscillations is inherent, and it becomes more pronounced when the frequency of respiration is kept constant.

Bispectral analysis is capable of determination of frequency and phase couplings in the processing and understanding of cardiovascular signals.

Bispectral analysis is more sensitive to interactions and is more noise robust than the synchrogram. It detects the phase synchronization, and nevertheless, yields different information from that which can be resolved from a synchrogram. A simple relation between the synchrogram and the bispectrum revealed information cannot be drawn.

Results of CV blood flow signals analysed using wavelet bispectral method gave the same results as in the case of using the Fourier based bispectrum method. There are no obvious advantages of wavelet bispectral method over the Fourier bispectral method, when detecting cardio-respiratory interaction that fulfils the conditions defined for quadratical coupling onset.

It is recommended that the wavelet and cross-wavelet bispectrum are applied to cardiovascular signals, rather than to the Fourier based bispectrum. They allow intermittent phase couplings to be detected, optimum time and frequency resolution, simple relation between scale and frequency, direct interpretation, normalization to signal energy, smaller statistical error, arbitrary frequency step and are computationally less demanding.

We can conclude that cardiac and respiratory CV systems and delta waves of EEG signal are coupled during the anaesthesia. Anaesthesia may stimulate inhibitory glycine and GABAergic synapses in the NTS-NA axis, whose projections then inhibit higher brain centres, such as the limbic system. It also modulates the level of endogenous hypothalamic peptides, responsible for the natural control of brain metabolism that are known to affect vagal control of cardiac rhythm, and which would be affected if anaesthesia artificially reduces brain metabolism. Anaesthesia may affect the delta waves of EEG signal in such a manner that it drives the cardiac and respiratory system to synchronization.

A long-term aim is therefore to develop a coupled oscillator model that can provide a description of the system, quantify the couplings and relate their values to its different states of health or disease. The wavelet bispectrum may provide a link between theoretical CVS models and experimental measurements.

REFERENCES

[1] M.T. Alkire, C.D.J. Pomfrett, Toward a monitor of depth: Bispectral index (BIS) and respiratory sinus arrhythmia (RSA) both monitor cerebral metabolic reduction during isoflurane anaesthesia, Anaesthesiology **87**, A421 (1997).

[2] A. Andronov, A. Vitt and S. Khaykin, *Theory of oscillations* (Pergamon Press, Oxford, 1966).

[3] R.M. Berne, M.N. Levy (Eds.), *Physiology* (Mosby, St. Louis, Missouri, 1998).

[4] I. Blekhman, *Synchronization of dynamical systems* (Nauka, Moscow, 1971).

[5] B. Boashash, P.J. O'Shera, Polynomial Wigner-Ville distributions and their relationship to time-varying higher order spectra, IEEE Trans. Signal Processing **42**, 216 (1994).

[6] M. Bračič and A. Stefanovska, Wavelet-based analysis of human blood-flow dynamics, Bull. Math. Biol. **60**, 919 (1998).

[7] M. Bračič and A. Stefanovska, Wavelet analysis in studying the dynamics of blood circulation, Nonlinear Phenom. Complex Syst. **2**, 68 (1999).

[8] M. Bračič Lotrič, *Couplings among Subsystems that regulate Blood Flow,* Ph.D. Thesis, University of Ljubljana, 1999.

[9] M. Bračič, P.V.E. McClintock and A. Stefanovska, Stohastic and Chaotic Dynamics in the Lakes (Melville, New York: American Institute of Physics, 2000).

[10] M. Bračič Lotrič and A. Stefanovska, Synchronization and modulation in human cardiorespiratory system, Physica A **283**, 451 (2000).

[11] D.R. Brillinger and M. Rosenblatt, *Spectral Analysis of Time Series* (New York, Willey, 1967).

[12] T.H. Bullock, J.Z. Achimowicz, R.B. Duckrow, S.S. Spencer, V.J. Iragui-Madoz, Bicoherence of intracranial EEG activity, Electroenceph. Clin. Neurophysiology **103**, 661 (1997).

[13] A.C. Burton and R.M. Taylor, A study of the adjustment of peripheral vascular tone to the requirements of the regulation of body temperature, Am. J. Physiol. **129**, 565 (1940).

[14] V. Chandran, *Two-dimensional Bispectral Analysis and Leakage effects on the Statistics of the Bispectrum*, Ph.D. Thesis, Washington State University, 1990.

[15] V. Chandran and S.L. Elgar, Mean and variance of estimates of the bispectrum of a harmonic random process - an analysis including leakage effects, IEEE Transactions on Signal Processing **39**, 2640 (1991).

[16] A.V. Dandawaté and G.B. Giannakis, Asymptotic theory of mixed time averages and kth-order cyclic-moment and cumulant statistics, IEEE Transaction on Information Theory **41**, 216 (1995).

[17] I. Daubechies, *Ten Lectures on Wavelets*, (Philadelphia, SIAM, 1992).

[18] C.T.M. Davies and J.M.M. Neilson, Sinus arrhythmia in man at rest, J. Appl. Physiol. **22**, 947 (1967).

[19] L.C. Davies, D.P. Francis, A. Crisafulli, A. Concu, A.J.S. Coats and M. Piepoli, Oscillations in stroke volume and cardiac output arising from oscillatory ventilation in humans, Exp. Physiol. **85**, 857 (2000).

[20] V. DeBrunner, M. Ozaydin, and T. Przebinda, Resolution in time-frequency, IEEE Transactions on Signal Processing **47**, 783 (1999).

[21] J.C. Drummond, C.A. Brann, D.E. Perkins, D.E. Wolfe, A comparison of median frequency, spectral edge frequency, a frequency band power ratio, total power, and dominance shift in the determination of depth of anesthesia, Acta. Anaesthesiology Scand. **35**, 693 (1991).

[22] D.L. Eckberg, Nonlinearities of the human carotid baroreceptor-cardiac reflex, Circ. Res. **47**, 208 (1980).

[23] D.L. Eckberg, The human respiratory gate, J. Physiol. **548**, 339 (2003).

[24] P. Engel, G. Hildebrandt, and H.-G. Scholz, Die Messung der Phasenkopplung zwischen Herzschlag und Atmung beim Menschen mit einem neuen Koinzi-denzmeßgerat, Pflügers Arch. **298**, 258 (1968).

[25] J.W.A. Fackrell, *Bispectral Analysis of Speech Signals,* Ph.D. Thesis, University of Edinburgh, 1996.

[26] J.R. Fonollosa, C.L. Nikias, Wigner higher order moment spectra: Definition, properties, computation and application to transient signal analysis, IEEE Trans. Signal Processing **41,** 245 (1993).

[27] R.J. Gajraj, M. Doi, H. Mantzaridis, G.N.C. Kenny, Analysis of the EEG bispectrum, auditory evoked potentials and the EEG power spectrum during repeated transitions from consciousness to unconsciousness, Br. J. Anaesthesy **80,** 46 (1998).

[28] A. Grossmann and J. Morlet, Decomposition of Hardy functions into square integrable wavelets of constant shape, SIAM J. Math. Anal. **15,** 723 (1984).

[29] S. Hales, J. Physiol, *Statistical Essays II, Haemastatisticks* (London, Innings Manby, 1773).

[30] C. Hayashi, *Nonlinear oscillations in physical systems* (McGraw-Hill, New York, 1964).

[31] M.J. Hinch, Testing for Gaussianity and linearity of a stationary time series, J. Time Ser. Anal. **3**, 169 (1982).

[32] M.J. Hinch, Detecting a transient signal by bispectral analysis, IEEE Transactions on Acoustics. Speech. and Signal Processing **38**, 1277 (1990).

[33] M.J. Hinch, On the principal domain of the discrete bispectrum of a stationary signal, IEEE Transactions on Signal Processing 43, 2130 (1995).

[34] J.A. Hirsch and B. Bishop, Respiratory sinus arrhythmia in humans: How breathing pattern modulates heart rate, Am. J. Physiol. **241**, H620 (1981).

[35] U. Hoffman, A. Yanar, U.K. Franzeck, J.M. Edvards, A. Bollinger, The frequency histogram: A new method for the evaluation of laser Doppler flux motion, Microvascular Res. **40**, 293 (1990).

[36] N.E. Huang, Z. Shen, S.R. Long, M.C. Wu, H.H. Shih, Q. Zheng, N. Yen, C.C. Tung, and H.H. Liu, The empirical mode decomposition method and the Hilbert spectrum for non-stationary time series analysis, Proc. R. Soc. Lond. A **454**, 903 (1998).

[37] C.H. Hugenii (Huygens), *Horologium Oscillatorium* (Apud F. Muguet, Parisiis, France, 1673).

[38] J. Jamšek, A. Stefanovska, Selektivna diskretna Fourierova analiza, Zbornik sedme Elektrotehniške in računalniške konference ERK '98 **B**, 339 (1998).

[39] J. Jamšek, *Bispectral Analysis of Cardiovascular Signals*, M.Sc. Thesis, University of Ljubljana, 2000.

[40] J. Jamšek, A. Stefanovska, P.V.E. McClintock and I.A. Khovanov, Time-phase bispectral analysis, Phys. Rev. E **68**, 016201 (2003).

[41] J. Jamšek, A. Stefanovska and P.V.E. McClintock, nonlinear cardio-respiratory interactions revealed by time-phase bispectral analysis, Physics in Medicine and Biology **49**, 4407 (2004).

[42] N.B. Janson, A.G. Balanov, V.S. Anishchenko and P.V.E. McClintock, Phase relationship between two or more interacting processes from one-dimensional time series. I. Basic theory, Phys. Rev. E **65**, 036211 (2002).

[43] G. Kaiser, *A Friendly Guide to Wavelets* (Boston, Birkhäuser, 1994).

[44] D. Kaplan and L. Glass, *Understanding Nonlinear Dynamics* (New York, Springer, 1995).

[45] J. Kastrup, J. Bhlow and N.A. Lassen, Vasomotion in human skin before and after local heating recorded with laser Doppler flowmetry. A method for introduction of vasomotion, Int. J. Microcirc. **8**, 205 (1989).

[46] T. Kenner, H. Passenhofer and G. Schwaberger, Method for the analysis of the entraiment between heart rate and ventilation rate, Pflügers Archiv. **363**, 263 (1976).

[47] L. Keselbrener, S. Akselrod, Selective Discrete Fourier Transform Algorithm for Time-Frequency Analysis, IEEE Transactions on Biomedical Engineering **43**, 789 (1996).

[48] Y.C. Kim, J.M. Beall, E.J. Powers, and R.W. Miksad, Bispectrum and nonlinear wave coupling, *Phys. Fluids* **32**, 258 (1980).

[49] Y.C. Kin and E.J. Powers, Digital bispectral analysis and its applications to nonlinear wave interactions, IEEE Transactions on Plasma Science **PS-7**, 120 (1979).

[50] R.I. Kittney, O. Rompelhan, Analysis of the interaction of the human blood pressure and thermal system, In: J. Perkins (Ed.), Biomedical Computing, Pitman Medical, London, 49 (1977).

[51] B. Kleiner, P.J. Huber, G. Dummermuth, Analysis of the interrelations between frequency bands of the EEG by means of the bispectrum, Electroenceph clin. Neurophysiology **27**, 693 (1969).

[52] H. Koepchen, *Rhythms in Physiological Systems* (Springer-Verlag, Berlin, 1991).

[53] M. Koskinen, T. Seppänen, J. Tuukkanen, A. Yli-Hankala, V. Jäntti, Propofol anesthesia induces phase synchronization changes in EEG, Clinical Neurophysiology **112**, 386 (2001).

[54] Y. Kuramoto, *Chemical Oscillations, Waves, and Turbulence* (Berlin, Springer, 1984).

[55] J.R. Levick, *An Introduction to Cardiovascular Physiology* (London, Arnold, 2000).

[56] C. Ludwig, Beitrage zur Kenntnis des Einflusses des Respirationbewegungen of den Blutumlaf im Aortensystem, Arch. Anat. Physiol. Wiss. Med. **13**, 242 (1847).

[57] V.K. Madiseti and D.B. Williams, *The Digital Signal Processing Handbook* (Florida, CRC Press, 1998).

[58] R. Malek-Madani, *Advanced Engineering Mathematics*, (Reading, Addison Wesley Longman, 1998).

[59] A. Malliani, M. Pagani, F. Lombardi and S. Cerutti, Cardiovascular neural regulation explored in the frequency domain, Circulation **84**, 482 (1991).

[60] J.M. Mendel, Tutorial on higher-order statistics (spectra) in signal processing and system theory: Theoretical results and some applications, Proceedings of the IEEE **79**, 278 (1991).

[61] B.Ph. van Milligen, C. Hidalgo, and E. Sánchez, Nonlinear phenomena and intermittency in plasma turbulence, Physical Rev. Lett. **74**, 395 (1995).

[62] B.Ph. van Milligen, E. Sánchez, T. Estrada et al., Wavelet bicoherence: a new turbulence analysis tool, Phys. Plasmas **2**, 3017 (1995).

[63] B. Musizza, Vzorčne povezave med biološkimi sistemi: Pristop k ugotavljanju globine anestezije, B.Sc. Thesis, University of Ljubljana, 2000.

[64] B. Musizza, F. Bajrović, P.V.E McClintock, M. Paluš, J. Petrovčič, and A. Stefanovska, Cardio-respiratory and neural interactions in anaesthesia, Nature, submited.

[65] J. Muthuswamy, D.L. Sherman, N.V. Thakor, Higher-order spectral analysis of burst patterns in EEG, IEEE Trans. Biomed. Eng. **46**, 92 (1999).

[66] A.K. Nadi, Robust estimation of third-order cumulants in applications of higher-order statistics, IEE Proceedings-F **140**, 380 (1993).

[67] A.K. Nadi, *Higher-order statistics in signal processing* (Cambridge, Cambridge University Press, 1998).

[68] C.L. Nikias and J.M. Mendel, Signal processing with higher-order spectra, IEEE Signal Processing Magazine **7**, 10 (1993).

[69] C.L. Nikias and A.P. Petropulu, *Higher-order spectra analysis:A nonlinear signal processing framework* (Englewood Cliffs, Prentice-Hall, 1993).

[70] M. Paluš, Kolmorogov entropy from time series using information-theoretic functionals, Neural Network World **7**, 269 (1997).

[71] M. Paluš and D. Hoyer, Surrogate data in detecting nonlinearity and phase synchronization, IEEE Engineering in Medicine and Biology **17**, 40 (1998).

[72] M. Paluš, V. Komárek, Z. Hrnčiř and K. Štěbrová, Synchronization as adjustment of information rates: detection from bivariate time series, Phys. Rev. E **63**, 046211 (2001).

[73] M. Paluš and A. Stefanovska, Direction of coupling from phases of interacting oscillators: an information-theoretic approach, Phys. Rev. E **67**, 055201 (R) (2003).

[74] H. Parthasarathy, S. Prasad and S.D. Joshi, An ESPRIT-Like method for quadratic phase coupling estimation, IEEE Transactions on Signal Processing **43**, 2346 (1995).

[75] J. Penaz, Mayer Waves: History and methodology, Automedica **2**, 135 (1978).

[76] R.J. Perry and M.G. Amin, On computing and implementing the running bispectra, IEEE Transaction on Signal Processing **43**, 1017 (1995).

[77] L.A. Pflug, G.E. Ioup, and J.W. Ioup, Sampling requirements and aliasing for higher-order correlations, J. Acoust. Soc. Am. **94**, 2159 (1993).

[78] L.A. Pflug, G.E. Ioup, and J.W. Ioup, Sampling requirements for nth-order correlations, J. Acoust. Soc. Am. **95**, 2762 (1994).

[79] A.S. Pikovsky, M.G. Rosenblum, and J. Kurths, Synchronization; *A universal concept in nonlinear sciences* (Cambridge, Cambridge University Press, 2001).

[80] M.B. Priestley and M.M. Gabr, *Multivariate Analysis: Future Directions* (North Holland, 1993).

[81] J.G. Proakis and D.G. Manolakis, *Digital Signal Processing* (New Jersey, Prentice-Hall, 1996).

[82] V.M. Pokrovsky, O.E. Osadchiy, Regulatory peptides as modulators of vagal influence on cardiac rhythm, Can. J. Physiol. Pharmacol. **73**, 1235 (1995).

[83] C.J.D. Pomfrett, J.R. Sneyd, M. Beech, T.E.J. Healy, Variation in respiratory sinus arrhythmia may reflect levels of anaesthesia, British Journal of Anaesthesia **67**, 6216 (1991).

[84] C.J.D. Pomfrett, Heart rate variability, BIS and the depth of anaesthesia, British Journal of Anaesthesia **82**, 659 (1999).

[85] M.R. Raghuveer, Time-domain approaches to quadratic phase coupling estimation, IEEE Transactions on Automatic Control **35**, 48 (1990).

[86] I.J. Rampil, A primer for EEG signal processing in anesthesia, Anesthesiology **89**, 815 (1998).

[87] T.S. Rao and K.C. Indukumar, Spectral and wavelet methods for the analysis of nonlinear and nonstationar time series, J. Franklin Inst. **33**, 425 (1996).

[88] M. Renna, R. Venturi, Bispectral index and anaesthesia in the eldery, Minerva Anaesthesiology **66**, 398 (2000).

[89] C. Rosow, P.J. Manberg, Bispectral Index Monitoring, Anesthesiol Clin North America **19**, 947 (2001).

[90] M.G. Rosenblum, A.S. Pikovsky, J. Kurths, Phase synchronization of chaotic oscillators, Phys. Rev. Letters **76**, 1804 (1996).

[91] M.G. Rosenblum, A.S. Pikovsky, J. Kurths, From phase to lag synchronization in coupled chaotic oscillators, Phys. Rev. Letters **78**, 4193 (1997).

[92] M.G. Rosenblum, A.S. Pikovsky, C. Schäfer, P. Tass, and J. Kurths, Handbook of Biological Physics (Elsevier, 2000).

[93] M.G. Rosenblum, and A.S. Pikovsky, Detecting direction of coupling in interacting oscillators, Phys. Rev. E. **64**, 045202 (2001).

[94] M.G. Rosenblum, L. Cimponeriu, A. Bezerianos, A. Patzak, and R. Mrowka, Identification of coupling direction: Application to cardirespiratory interaction, Phys. Rev. E **65**, 041909 (2002).

[95] F. Rsachke, *Temporal Disorder in Human Oscillatory Systems* (Springer-Verlag, Berlin, 1987).

[96] N.F. Rulkov, M.M. Sushchik, L.S. Tsimring, and H.D.I. Abarbanel, Generalized synchronization of chaos in directionally coupled chaotic systems, Phys. Rev. E. **51**, 980 (1995).

[97] S. Rzeczinski, N.B. Janson, A.G. Balanov and P.V.E McClintock, Regions of cardiorespiratory synchronization in humans under paced respiration, Phys. Rev. E **66**, 051909 (2002).

[98] B. Schack, H. Witte, M. Helbig, Ch. Schelenz, M. Specht, Time-variant non linear phase coupling analysis of EEG burst patterns in sedated patiens during electroencephalic burst suppression period, Clinical neurophysiology **112**, 1388 (2001).

[99] C. Schäfer, *Analysis of synchronization in complex systems: Application to physiological data,* Ph.D. Thesis, University of Potsdam, 1998.

[100] C. Schäfer, M.G. Rosenblum, J. Kurths, H.H. Abel, Heartbeat synchronized with ventilation, Nature **293**, 239 (1998).

[101] C. Schäfer, M. G. Rosenblum, H.H. Abel and J. Kurths, Synchronization in the human cardiorespiratory system, Phys. Rev. E **60**, 857 (1999).

[102] T. Schreiber and A. Schmitz, Improved surrogate data for nonlinearity tests, Phys. Rev. Lett. **77**, 635 (1996).

[103] T. Schreiber, Phys. Measuring information transfer, Rev. Lett. **85**, 461 (2000).

[104] H. Seidel and H. Herzel, Analysing Entrainment of Heartbeat and Respiration with Surrogates, IEEE Eng. Med. Biol. Mag. **17**, 54 (1998).

[105] I. Sharfer and H. Messer, The bispectrum of sampled data: Part I-detection of the sampling jitter, IEEE Transactions on Signal Processing **41**, 296 (1993).

[106] M. Small and K. C.A. Tse, Detecting determinism in time series: The method of surrogate data, IEEE Trans. on Circuits and Sys. **50**, 663 (2003).

[107] T.B. Solan, Anaesthetic effect on electrophysiologic recordings, J. Clin. Neurophysiology **15**, 217 (1998).

[108] T. Söderström, A. Stefanovska, M. Veber and H. Svenson, Involvement of sympathetic nerve activity in skin blood flow oscillations in humans, Am. J. Physiol. **284**, H1638 (2003).

[109] A. Stefanovska and P. Krošelj, Correlation integral and frequency anlysis of cardiovascular functions, Open Sys. & Infomation Dyn. **4**, 457 (1997).

[110] A. Stefanovska and M. Bračič, Physics of the human cardiovascular systems, Contemporary Phys. **40**, 31 (1999).

[111] A. Stefanovska, M. Bračič and H.D. Kvernmo, Wavelet analysis of oscillations in the peripheral blood circulation measured by laser Doppler technique, IEEE Trans. Biol. Med. Eng. **46**, 1230 (1999).

[112] A. Stefanovska and M. Bračič, Reconstructing cardiovascular dynamics, Control Eng. Pract. **7**, 161 (1999).

[113] A. Stefanovska and M. Hožič, Spatial synchronization in the human cardiovascular system, Prog. of Theor. Phys. Suppl. **139**, 270 (2000).

[114] A. Stefanovska, H. Haken, P.V.E. McClintock, M. Hožič, F. Bajrović and S. Ribarič, Reversible transitions between synchronization states of the cardiorespiratory system, Phys. Rev. Lett. **85**, 4831 (2000).

[115] A. Stefanovska, M. Bračič Lotrič, S. Strle and H. Haken, The cardiovascular system as coupled scillators?, Physiol. Meas. **22**, 535 (2001).

[116] A. Stefanovska, D.G. Luchinsky and P.V.E. McClintock, Modelling couplings among the oscillators of the cardiovascular system, Physiol. Meas. **22**, 551 (2001).

[117] A. Stefanovska, Cardiorespiratory interactions, Nonlinear Phenom. Complex Syst. **5**, 462 (2002).

[118] K. Stutte and G. Hildebrandt, Untersuchungen über die Koordination von Herzschlag und Atmung, Pflügers Arch. **289**, R47 (1966).

[119] K. Suder, F.R. Drepper, M. Schiek and H.H. Abel, One-dimensional, nonlinear determinism characterizes heart rate pattern during paced respiration, Am. J. Physiol. **275**, H1092 (1998).

[120] A. Swami, G.B. Giannakis and G. Zhou, Bibliography on high-order statistics, Signal Processing **60**, 65 (1997).

[121] P. Tass, M.G. Rosenblum, J. Weule, J. Kurths, A. Pikovsky, J. Volkmann, A. Schnitzler, H.-J. Freund, Detection of n:m phase locking from noisy data: Application to magnetoencephalography, Phys. Rev. Lett. **81**, 3291 (1998).

[122] J. H. Thinker, F.W, Sharbrough, J.D. Michenfelder, Anterior shift of the dominant EEG rhythm during anesthesia in the Java monkey, Anesthesiology **46**, 252 (1977).

[123] J. Theiler, S. Eubank, A. Longtin, B. Galdrikian, J.D. Farmer, Testing for nonlinearity in time series: The method of surrogate data. Physica D **58**, 77 (1992).

[124] J. Theiler, D. Prichard, Using `Surrogate Surrogate Data' to calibrate the actual rate of false positives in tests for nonlinearity in time series, Fields Inst. Comm. **11**, 99 (1997).

[125] B. van der Pol and J. van der Mark, The heartbeat considered as a relaxation oscillation, and an electrical model of the heart, Phil. Mag. **7**, 763 (1928).

[126] M.B. Visscher, A. Rupp, and F.H. Scott, Respiratory wave in arterial blood pressure, Am. J. Physiol. **70**, 586 (1924).

[127] G. Zhou, and G.B. Giannakis, Retrieval of self-coupled harmonics, IEEE Transactions on Signal Processing **43**, 1173 (1995).

[128] V.S. Zykov, G. Bordiougov, H. Brandtstädter, I. Gerdes, and H. Engel, Periodic forcing and feedback control of nonlinear lumped oscillators and meandering spiral waves, Phys. Rev. E **68**, 016214 (2003).

INDEX

CONTRIBUTIONS TO SCIENCE

Original contributions to science:

1. The study of interacting nonlinear oscillators, using time-phase bispectral estimators of biamplitude and biphase.

We have introduced, for the first time, time-phase bispectral estimators of biamplitude (3.6) and biphase (3.5) for unveiling phase coupling information from univariate data (Chapter 3, pages 13 to 16). We have shown that the introduced method is suitable for studying interacting nonlinear oscillators, and that it is capable of quantifying the strength of the interaction by bispectral estimate – biamplitude, whose value is proportional to the coupling coefficient value ε (2.6) of coupled nonlinear oscillators (Chapter 2, pages 7 to 12), and revealing the nature of the coupling, i.e., whether the coupling is additive linear or quadratic, or parametric in one of the frequencies (Chapter 4, pages 17 to 28).

2. Cardio-respiratory coupling in human cardiovascular system hypothesis confirmation.

We have applied, for the first time, the time-phase bispectral method to cardiovascular blood flow signals, in order to study the nature of cardio-respiratory interactions. Despite the limitations of the method used to resolve between linear and nonlinear couplings in extreme conditions, the method is applicable before the couplings become too complex, considering the physiological knowledge of the system (Chapter 5, pages 29 to 56). Couplings between cardiac and respiratory oscillations are episodic, rather than fixed and permanent. Frequency and phase couplings interchange. Nonlinear coupling exists during spontaneous, as well as during paced, respiration. It becomes more pronounced when the frequency of respiration is kept constant. The inter-oscillator coupling is relatively weak (Chapter 5 and 6, pages 29 to 37 and 57 to 76). The coupling information among cardiac and respiratory processes is inherent from the processes and is spatially invariant. Both processes are of central origin, and their phase relationships can be observed in ECG, blood flow, and blood pressure signals derived from widely separated sites (Chapter 5, pages 37 to 46).

3. Bispectum estimates generalization to wavelets.

We have generalized bispectum estimates - biphase (7.20) and biamplitude (7.21) - to wavelets. The method is suitable for intermittent phase coupling detection, while providing optimum time

and frequency resolution. It may provide a link between theoretical CVS models and experimental measurements (Chapter 7 and 8, pages 77 to 106).

4. Coupling between cardiac and respiratory systems, and delta waves of EEG signals determination using generalized bispectral estimates.

Delta waves of EEG signals of rats undergoing anaesthesia, reveal a physiological relation between cardiac and respiratory systems and delta waves of EEG signals. The cardio-respiratory synchronization might be a consequence of delta waves of EEG signals of rats undergoing anaesthesia (Chapter 9, pages 107 to 114).

Portions of this thesis were published in the following papers:

1. J. Jamšek, A. Stefanovska, P.V.E. McClintock and I.A. Khovanov, Time-phase bispectral analysis, Phys. Rev. E **68**, 016201 (2003).

2. J. Jamšek, A. Stefanovska and P.V.E. McClintock, Nonlinear cardio-respiratory interactions revealed by time-phase bispectral analysis, Physics in Medicine and Biology **49**, 4407 (2004).

Portions of this thesis were presented in the following scientific meetings:

1. J. Jamšek and A. Stefanovska, Bispectral analysis of cardiovascular signals, Nonlinear Seminar, Department of nonlinear physics, Lancaster University, United Kingdom (7.2. 2002).

2. J. Jamšek, A. Stefanovska and P.V.E. McClintock, Time-phase bispectral analysis, basic theory and applications, Nonlinear Seminar, Department of nonlinear physics, Lancaster University, United Kingdom (12.5. 2002).

3. J. Jamšek, A. Stefanovska and P.V.E. McClintock, Cardiovascular System, Cardiovascular system, time-phase bispectral analysis, basic theory and application, 2nd Slovenia-Japan Seminar, Center for Applied Mathematics and Theoretical Physics University of Maribor, Slovenia (28.5.-5.6 2003).

4. J. Jamšek and A. Stefanovska, Quadratic cardio-respiratory coupling?, INTAS international Workshop, Department of Physics, University of Pisa, Italy (22-24.4. 2003).

5. J. Jamšek, A. Stefanovska and P.V.E. McClintock, Nonlinear cardio-respiratory interaction, INTAS-ESF international Workshop, Ljubljana, Slovenia (10-13.11. 2003).

APPENDIX

A. Variance of the bispectrum estimate

B. Generation of harmonics

A. Variance of the bispectrum estimate

In order to interpret bispectral values from a finite length time series, the statistics of bispectrum estimates must be known [49]. To achieve statistical stability, the time series is divided into K segments for averaging. Phases of different segments are independent of each other and random variables over $[0, 2\pi)$. When there is a large number of segments, the estimate gains statistical stability at the expense of power spectral and bispectral resolution. For a real signal, with a finite number of points, the compromise between bispectral resolution and statistical stability may be expected at K approximately 30. Estimates are subject to statistical error, such as bias and variance. An estimate must be consistent, that is the statistical error must approach zero in the mean-square sense as the number of realizations becomes infinite. Here we neglect the effects of finite time series length, we assume that they are sufficiently long. Let us consider the bias and the variance of the bispectrum estimate $\hat{B}(k,l)$. The expected value of $\hat{B}(k,l)$ will be

$$\begin{aligned} E\left[\hat{B}(k,l)\right] &= \frac{1}{K}\sum_{i=1}^{K} E\left[X_i(k)X_i(l)X_i^*(k+l),\right] \\ &= E\left[X(k)X(l)X^*(k+l)\right] = B(k,l), \end{aligned} \tag{A1}$$

as K becomes infinite, X_i is the DFT of the i-th segment. Thus, $\hat{B}(k,l)$ can be taken as an unbiased estimate [14, 15, 25]. Its variance will be

$$\mathrm{var}(\hat{B}) = E\left[\hat{B}\hat{B}^*\right] - E\left[\hat{B}\right]E\left[\hat{B}^*\right] = \frac{1}{K}\left\{E\left[\left|X(k)\right|^2\left|X(l)\right|^2\left|X(k+l)\right|^2\right] - E\left|B(k,l)\right|^2\right\} \tag{A2}$$

Note that the variance is inversely proportional to K. From a mathematical statistics point of view, it is a nontrivial task to compute the quantity in the bracket in terms of low-order spectra, but one may write a good approximation [14, 15, 25]

$$\mathrm{var}(\hat{B}) = E\left[|X(k)|^2 |X(l)|^2 |X(k+l)|^2\right] = P(k)P(l)P(k+l), \tag{A3}$$

in which case the variance will be

$$\mathrm{var}(\hat{B}) = E\left[\left|\hat{B}(k,l)\right|^2\right] - E\left[\hat{B}(k,l)\right]^2 \approx \frac{1}{K} P(k)P(l)P(k+l)\left[1 - b^2(k,l)\right] \tag{A4}$$

Note that it is a consistent estimate in the sense that the variance approaches zero as K becomes infinite. The variance is proportional to the product of the powers ($P(k)$ = E[$X(k)X^*(k)$]) at the frequencies k, l and $k + l$. Consequently, a larger statistical variability is introduced in estimating larger values in the bispectrum. Finally, the variance is proportional to [1 - $b^2(k, l)$], where the bicoherence b^2 is a normalized bispectrum, $b^2(k, l)$ = E[$\hat{B}(k,l)$]^2 / [$P(k)P(l)P(k + l)$]. That is, when the oscillations at k, l and $k + l$ are nonlinearly coupled ($b^2 \sim 1$), the variance approaches zero, and when the components are statistically independent ($b^2 \sim 0$), the variance is proportional to the power at each spectral component [14, 15, 25].

Brillinger and Rosenblatt [11] have investigated the asymptotic mean and variance of Fourier-type estimates of high-order spectra and proved that under certain assumptions the k-th-order spectral estimate is asymptotically unbiased and Gaussian distributed and that estimates of different-order are asymptotically independent. The variances of the real and imaginary parts of the bispectrum are asymptotically (i.e., for large K) Gaussian and are equal, var{Re[$\hat{B}(k,l)$]} $\cong$ var{Im[$\hat{B}(k,l)$]}. For a perfect phase-coupled triplet, the variances of the real and imaginary parts are equal to zero. In the case of no coupling, there is an identical contribution to the variances from the real and imaginary parts of the estimate of the bispectrum.

The total variance is a sum of individual (i = 1,..., K) contributions, because different triplets are mutually statistically uncorrelated in the absence of phase coupling. Partial coupling can be expected to result in a combination of perfectly phase-coupled oscillations, and oscillations with randomly changing phases.

B. Generation of harmonics

In this appendix we show which harmonics appear in the spectrum of a weakly driven weakly nonlinear oscillator, and in particular we establish which harmonics correspond to quadratic coupling. The analysis that follows is for a Poincaré oscillator, but a similar result also follows for, e.g., a van der Pol or other oscillators of similar type.

Consider an oscillator of the form

$$\begin{aligned} \dot{x}_1 &= -x_1 r_1 - \omega_1 y_1 + Q(x_2, x_1), \\ \dot{y}_1 &= -y_1 r_1 + \omega_1 x_1, \\ r_1 &= \alpha(\sqrt{x_1^2 + y_y^2} - a), \end{aligned} \tag{B1}$$

where the term $Q(x_2, x_1)$ corresponds to a coupling of the main oscillator (x_1, y_1) to another one (x_2, y_2).

We seek a solution in the form

$$\begin{aligned} x_1 &= A\sin(\omega_1 t + \phi), \\ y_1 &= -A\cos(\omega_1 t + \phi), \end{aligned} \tag{B2}$$

and transform Eq. (B1) into amplitude/phase coordinates

$$\begin{aligned} \dot{A} &= -\alpha A(A-1) + Q(x_2, A, \phi)\sin(\omega_1 t + \phi), \\ A\dot{\phi} &= Q(x_2, A, \phi)\cos(\omega_1 t + \phi). \end{aligned} \tag{B3}$$

If there is no coupling ($Q(x_2, A, \phi) = 0$) this system has the simple solution

$$\begin{aligned} A &= A_0 = a, \\ \phi &= \phi_0 = \text{const.} \end{aligned} \tag{B4}$$

If the coupling is non-zero, the system cannot be solved exactly analytically. An approximate solution for small coupling and weak nonlinearity can, however, still be obtained. The amplitude and phase in this case vary only slightly and they can be expanded about (A_0, ϕ_0) as

$$A = A_0 + \beta,$$
$$\phi = \phi_0 + \gamma. \tag{B5}$$

For small β, γ, α the Eq. (B3) corresponding to those for $\dot{\beta}$ and $\dot{\gamma}$ can be solved approximately. For the simplest linear coupling of form

$$Q(x_2, A, \phi) = Q(x_2) = F\sin(\omega_2 t), \tag{B6}$$

one obtains

$$\beta \approx \frac{F}{2(\omega_1 - \omega_2)}\sin\big((\omega_1 - \omega_2)t + \phi_0\big) - \frac{F}{2(\omega_1 + \omega_2)}\sin\big((\omega_1 + \omega_2)t + \phi_0\big),$$
$$\gamma \approx \frac{F}{2a(\omega_1 - \omega_2)}\cos\big((\omega_1 - \omega_2)t + \phi_0\big) - \frac{F}{2a(\omega_1 + \omega_2)}\cos\big((\omega_1 + \omega_2)t + \phi_0\big). \tag{B7}$$

Then, in the spectrum of the variable

$$x = (A_0 + \beta)\sin(\omega_1 t + \phi_0 + \gamma), \tag{B8}$$

one observes the following harmonics: ω_1, ω_2, $2\omega_1 \pm \omega_2$. In the case of quadratic coupling

$$Q(x_2, A, \phi) = F(x_2 - x_1)^2 = F(A\sin(\omega_2 t) - x_1)^2, \tag{B9}$$

there appear additional harmonics: $2\omega_2$, $2\omega_1$, $2\omega_1 \pm 2\omega_2$, $\omega_1 \pm \omega_2$, $3\omega_1 \pm \omega_2$. In the limit under consideration, with small nonlinearity and weak coupling, the appearance of these additional combinational harmonics can confidently be associated with the presence of a nonlinear coupling.

It is of course the case that, for a nonlinear oscillator, all sorts of combinational harmonics can in principle appear even for linear coupling. However, the generation of these harmonics is a second-order effect which becomes significant only for large nonlinearity and large coupling coefficients. Under the latter circumstances, just the appearance of particular combinational harmonics cannot necessarily be related to a given type of coupling and some further analysis is then required.

Declaration

I hereby declare that the research described in this thesis, and the thesis itself, is the original, and sole work, performed by the author, under the guidance of doc. dr. Aneta Stefanovska, the mentor. The results which were done in collaboration with other colleagues are published in presented articles. Other assistance from colleagues is stated in the acknowledgments. The published results of other authors are presented in the references.

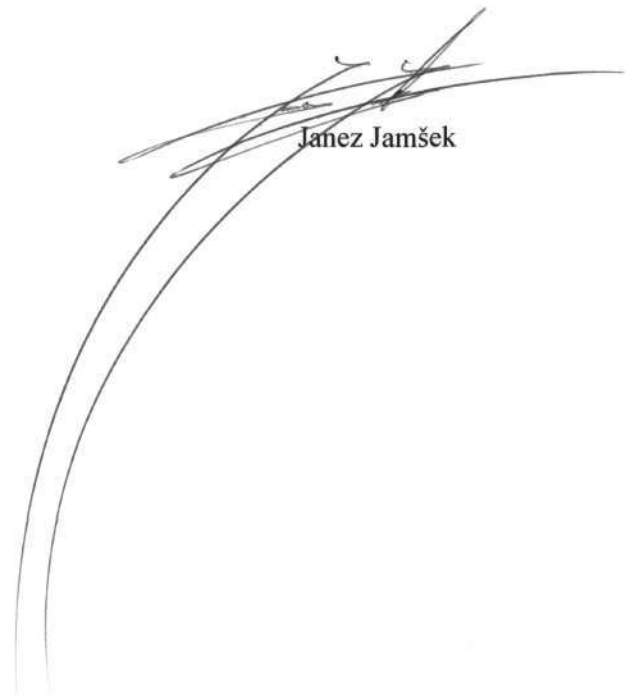

Janez Jamšek